10-25-2010

Consumable Process Development for Chemical Mechanical Planarization of Bit Patterned Media for Magnetic Storage Fabrication

Joseph T. Bonivel Jr.
University of South Florida

Consumable Process Development for Chemical Mechanical Planarization of Bit Patterned Media for Magnetic Storage Fabrication

by

Joseph T. Bonivel Jr.

A dissertation submitted in partial fulfillment
of the requirements for the degree of
Doctor of Philosophy
Department of Mechanical Engineering
College of Engineering
University of South Florida

Major Professor: Ashok Kumar, Ph.D.
Delcie Durham, Ph.D.
C. Fred Higgs III, Ph.D.
Garrett Matthews, Ph.D.
Geoffrey Okogbaa, Ph.D.
Frank Pyrtle, Ph.D.

Date of Approval:
October 25, 2010

Keywords: tribology, coefficient of friction, wear, superparamagentic limit, magnetic hard drive fabrication

DEDICATION

This thesis is dedicated to my family who has always lived by the mantra

“Do your very best”

I love you all my heart.

&

Thank you for everything you have done for me

ACKNOWLEDGEMENTS

First and foremost I would like to thank and acknowledge Jesus Christ, for without him none of this would be possible. I would like to thank my research advisors Dr. Ashok Kumar, and Dr. C. Fred Higgs III for their guidance, friendship, and counseling throughout this dissertation process. Without your guidance I would have not been able to complete this process I would also like to sincerely thank Mr. Bernard Batson who has been a cornerstone to my experiences at USF. I would like to thank the NSF-GK-12, NSF-Bridge to Doctorate, Sloan Foundation, and MRSEC-CMU, for funding my research. I would like to thank Dr. Garrett Matthews, Dr. Delcie Durham, Dr. Frank Pyrtle, Dr. Geoffrey Okogbaa for serving as my committee members for my dissertation and being patient with me through this process, your expertise is invaluable.

I would also like to thank Dr. Philip Voglewede, Dr. Philip LeDuc for their encouragement over the years. Thanks go to my CMU and NMRL USF labmates. I also thank my REU students Justin and Yusuf for their tireless work. To my colleagues, Alisha, Brandon, Boone, Frank, Eric, and Tarah thank you for your encouragement, support, and willingness to help me during this process. Lastly and most importantly I want to acknowledge and thank my friends and family who supported me during all of my schooling: my mother- Carolyn, father -Joe Sr, sister- Shon, brother -Marlon, Dennis, Bernie P, Marcus the "Shark", Eddie, Pat, Travis, Clint, Yazid, Alexis, Tiffany, Jennifer, Moiya, and the USC and USF members of Phi Beta Sigma fraternity Inc. I love you all.

TABLE OF CONTENTS

LIST OF TABLES

LIST OF FIGURES

ABSTRACT

As the superparamagnetic limit is reached, the magnetic storage industry looks to circumvent the barrier by implementing patterned media (PM) as a viable means to store and access data. Chemical mechanical polishing (CMP) is a semiconductor fabrication technique used to planarize surfaces and is investigated as a method to ensure that the PM is polished to surface roughness parameters that allow the magnetic read/write head to move seamlessly across the PM. Results from this research have implications in feasibility studies of utilizing CMP as the main planarization technique for PM fabrication.

Benchmark data on the output parameters of the CMP process, for bit patterned media (BPM), based on the machine process parameters, pad properties, and slurry characteristics are optimized. The research was conducted in a systematic manner in which the optimized parameters for each phase are utilized in future phases. The optimum results from each of the phases provide an overall optimum characterization for BPM CMP.

Results on the CMP machine input parameters indicate that for optimal surface roughness and material removal, low polish pressures and high velocities should be used on the BPM. Pad characteristics were monitored by non destructive technique and results indicate much faster deterioration of all pad characteristics versus polish time of BPM when compared to IC CMP. The optimum pad for PM polishing was the IC 1400 dual layer Suba V pad with a shore hardness of 57, and a k-groove pattern. The final phase of

polishing evaluated the slurry polishing properties and novel nanodiamond (ND) slurry was created and benchmarked on BPM. The resulting CMP output parameters were monitored and neither the ND slurry nor the thermally responsive polymer slurry performed better than the commercially available Cabot iCue slurry for MRR or surface roughness.

Research results indicate CMP is a feasible planarization technique for PM fabrication, but successful implementation of CMP for planarizing PM must address the high initial start up cost, increase in the number of replacement pads, and increase in polishing time to reach the required surface roughness for magnetic storage devices.

CHAPTER 1: MAGNETIC STORAGE DEVICES: PATTERNED MEDIA

1.1 Foreword

The hard disk drive is by far the most important member of storage hierarchy in modern computers[1]. The magnetic hard disk drive (HDD) currently plays the most influential role in the storage industry and this role is continually growing due to capacity, performance, and price. Areal density, also sometimes called bit density, refers to the amount of data that can be stored in a given amount of hard disk platter. Since disk platters surfaces are two-dimensional, areal density is a measure of the number of bits that can be stored in a unit of area [2]. Since the inception of the original RAMAC by IBM in 1956, a variation of scaling laws have been used to increase the areal density of HDD [1]. In current longitudinal magnetic recording media, high areal density and low noise are achieved by averaging several hundred weakly coupled ferromagnetic grains per bit cell [3]. The scaling laws that enable smaller bit and grain sizes will eventually prompt a spontaneous magnetization reversal process, which destroys the data, when the stored energy per particles competes directly with the thermal energy, at which point the maximum reliable areal density is reached, this point is the superparamagnetic limit. The growth rate of magnetic storage density has increased to compound growth rate of 100% per year. At this rate of areal density, the physical limit of areal density known as the superparamagnetic limit will soon be reached [4]. To elude the superparamagnetic limit new technologies must be developed in order to continue the increase in storage capacity or the risk of losing valuable data. The objectives for this chapter include:

1) Detailing the need for increasing the areal storage density for magnetic storage devices
2) Provide fundamental understanding on the feasibility of patterned media storage devices
3) Detail fabrication challenges in making patterned media storage devices and the need for chemical mechanical planarization as a fabrication step
4) Provide a systematic layout for this dissertation

1.2 Introduction

1.2.1 Fundamentals of Read/Write Magnetic Hard Drives

Data is read and written on magnetic disks due to the electromagnetic physics phenomena. In 1820 physicist Hans Christian Oersted, observed that an electrical current flowing in a wire moved the needle of a compass located near this wire. When the electrical current was shut down, the compass needle went back showing the location of Earth's magnetic north pole. Oersted concluded that all conductors (wires) create a magnetic field around them when an electrical current is flowing. When the direction (polarity) of this electrical current is reversed, so is the polarity of the magnetic field [5].

In 1831 another physicist called Michael Faraday found out that the inverse was also true, if a strong enough magnetic field was created near a wire, electrical current would be produced (inducted) in the wire. If the direction of this magnetic field was reversed, the direction of the electrical current was reversed as well [6].

To understand how data is read and written on hard disk drives (HDD) and other magnetic devices, it is important to note two electromagnetic properties:

1) All conductors create magnetic fields around them when there is an electrical current flowing

2) A strong magnetic field can generate (induct) electrical current on a wire.

The HDD read/write head is made up of a U-shaped conductive material with a coil wrapped around it. On the process of writing data to the hard disk drive, an electrical current is applied to the coil, creating a magnetic field around the read/write read. This field magnetizes the platter surface right below the head, aligning the magnetic particles to the left or to the right, depending on the polarity of the electrical current that was

applied. Reversing the electrical current polarity will also reverse the polarity of the magnetic field. A stored bit is a sequence of magnetized particles.

In the process of reading data from the hard disk drive, when the head passes on a magnetized area either a positive or a negative current will be inducted, allowing the drive control circuit to read the stored bits. Figure 1.1 contains a basic schematic of a read/write magnetic hard drive [7].

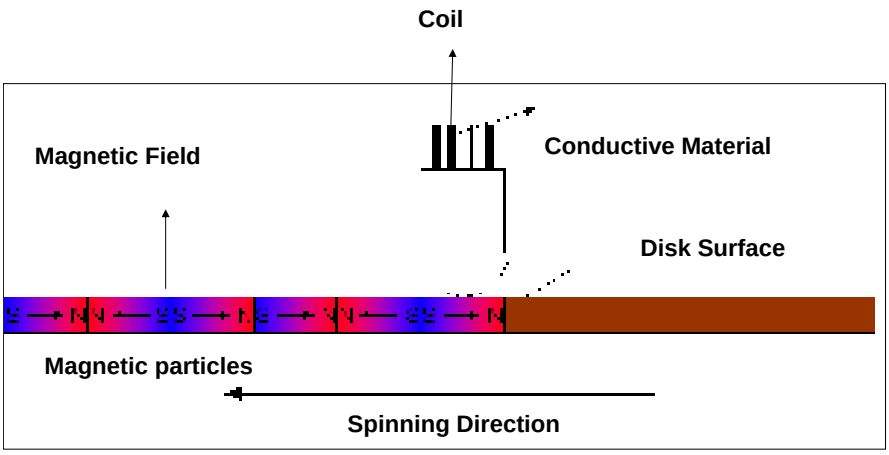

Figure 1. 1 Traditional longitudinal read/write hard drive

1.2.2 Magnetic Hard Drive Fundamentals

The history of hard disks is intertwined with the history of computing within the integrated circuit industry. The concept of storing large amounts of data on magnetic media was already in practice in the early 1950s with magnetic drum memories. However, the volumetric density was limited by the relatively low surface-to-volume ratio of such devices, meaning these drum memories could not hold much data [8, 9]. In a magnetic disk, data is stored on a recording medium (commonly referred to as media), which is responsive to the presence of strong magnetic fields, but stable in their absence. The storage density that a given medium can sustain is determined by a variety of factors:

1) Size and uniformity of the magnetic dipoles in the material
2) Orientation of the domains,
3) Coercivity
4) Temperature stability of the media.
5) Distance between the magnetic read/write head and the media.

Since the magnetic field drops off as the cube of the distance between the head and the media, writing and reading smaller spots depends on lowering the distance between the head and the magnetic media. Traditionally, the main component of this has been flying height [9]. This requires the read/write head to fly at nanometers above the surface in order for the HDD to be efficient.

The areal density, also sometimes called bit density, refers to the amount of data that can be stored in a given amount of hard disk platter. Since disk platters surfaces are two-dimensional, areal density is a measure of the number of bits that can be stored in a unit of area [2]. Since the inception of the original RAMAC by IBM in 1956, a variation of scaling laws have been used to increase the areal density of HDD, as shown in figure 1.2, and with a growth of 100% per year the limit to the scaling laws will soon be reached [1].

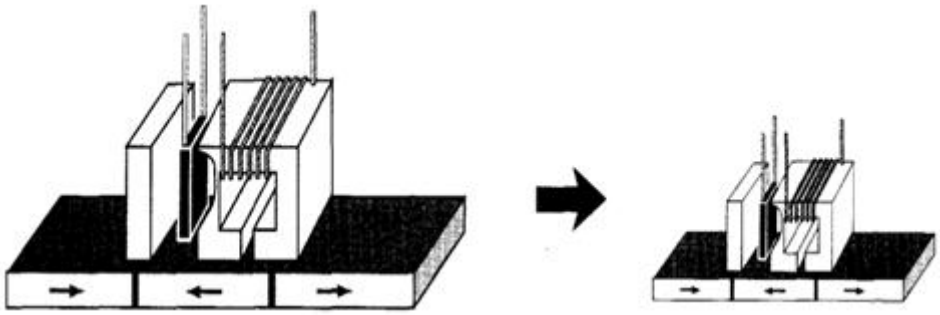

Figure 1. 2 Scaling factors used to increase areal density [10]

The latest push from the consumer market is to achieve 100 Gb/in^2 of areal storage and this storage density presents a fundamental processing issue. The problem with scaling down the feature size is fundamentally physics problem: decreasing bit size while achieving satisfactory signal-to-noise requires decreasing grain size. Grain size, however, cannot be shrunk significantly below its present state–of-the-art value, ~100 Angstroms (A^o), without the magnetization of the grains becoming thermally unstable or superparamagnetic [11].

The scaling laws that enable smaller bit and grain sizes will eventually prompt a spontaneous magnetization reversal process which destroys the data. When stored energy per particles competes directly with thermal energy, the maximum reliable areal density is reached. This point is the superparamagnetic limit. Details in the equations and boundary conditions of the superparamagnetic limit are beyond the scope of this dissertation but can be found in literature [4, 10-13].

1.3 Technologies to Avoid Superparamagnetic Limit

To circumvent this barrier, three major technologies are being proposed by magnetic storage experts. They include:

1) Perpendicular recording

2) Heat-assisted magnetic recording

3) Patterned media.

It is known that the thermal energy required to reverse the magnetization of a magnetic region is proportional to the size of the magnetic region and the magnetic coercivity of the material. This means the larger the magnetic region, the higher the coercivity of the material and the less likely the material will spontaneously demagnetize by local thermal fluctuations (avoidance of the superparamagnetic limit) [14].

1.3.1 Perpendicular Recording

Perpendicular recording uses a higher coercivity material through which the magnetic write head's penetration depth and geometry are enhanced [14-16]. Perpendicular recording represents the shortest technological leap as evidenced by the recent roll-out the world's first perpendicular hard disk drive by Toshiba [17]. In this method the magnetic domain is vertically aligned, shown in figure 1.3, so that more data can be stored but as storage growth increases this technology will ultimately succumb to the superparamagnetic limit.

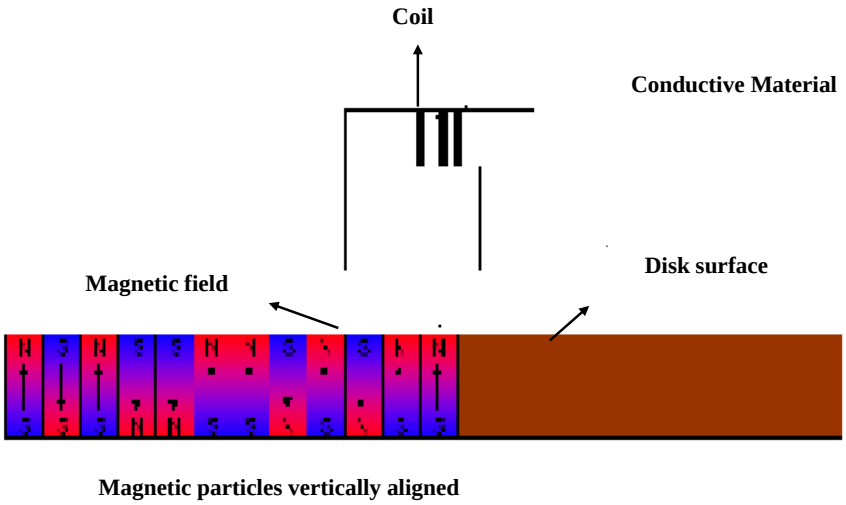

Figure 1. 3 Perpendicular recording

1.3.2 Heat Assisted Magnetic Recording

In heat assisted magnetic recording (HAMR), a laser is used to heat up the media to reduce its coercivity, thus sufficiently allowing switching of the field by the media head [18]. At almost the same instant as the laser is heating the media, the information is being written onto the media. HAMR takes advantage of high-stability magnetic compounds such as iron platinum alloy and these materials can store single bits in a much smaller area without being limited by the same superparamagnetic effect [19]. HAMR can theoretically create an areal density of 1 Tb/in^2 but requires a recorded mark size of approximately 25 nm. For this density the grain size in the recording medium must be less than approximately 5 nm to obtain a sufficient signal-to-noise ratio [18-20].

1.3.3 Patterned Media Data Storage

The concept of lithographically patterning a hard disk was originally introduced to improve head tracking and signal-to-noise ratio, but it is now clear that patterning offers the possibility of much higher areal densities than conventional hard disk media.

A patterned medium consists of an array of discrete elements or ‘‘nanomagnets.’ Each element is a single magnetic domain, with uniaxial magnetic anisotropy so that the magnetization points in one of only two directions at remanence, representing 1 bit of data as shown in figure 1.4.

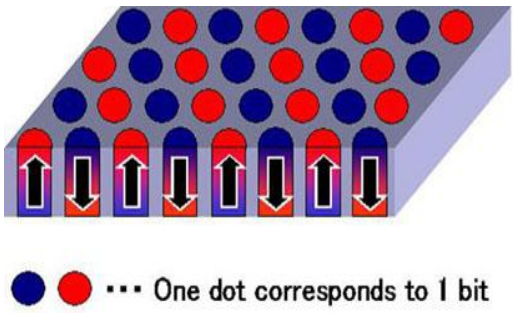

Figure 1. 4 Patterned media schematic[21]

The direction of magnetization in each dot (upward or downward) corresponds to the digital signal of "0" or "1". The patterned media’s advantage is that there is no transition noise in the read/write process. Additionally, the dot size, which determines the areal dot density, can be decreased ultimately to the critical grain size of thermal stability. An ultra high recording density beyond 10 Tbit/inch^2 is therefore expected to be achieved by applying the patterned media to the recording system.

1.3.3.1 Background on Patterned Media

The advantages of patterning recording media were recognized as early as 1963 by Shew et al. They showed that discrete patterned tracks on a hard disk platter could reduce the cross-talk and noise problems associated with head positioning errors and allow increased tracking tolerances [11]. More recently, Lambert et al. have used patterned magnetic films to explore narrow track recording [22]. It was shown that

patterned media can be used to provide feedback information to a head servomotor, and that M3 magnetized patterned media can be used as a read-only storage system [23].

The first studies of regular arrays of sub-micron patterned magnetic islands were presented in a series of papers by Smyth et al. The group investigated the collective switching properties of lithographically defined permalloy (NiFe) islands , and compared their results with micro-magnetic calculations [24].

Gibson et al. investigated the individual switching characteristics of similar permalloy particles using magnetic force microscopy (MFM) [25]. These permalloy particles behaved identically to single domain particles, and would reverse their magnetization under the influence of an MFM tip, The use of patterned magnetic islands as a single-bit-per-island discrete recording medium was not the focus of the aforementioned papers but the feasibility for such configurations is evident [11].

1.3.3.2 Patterned Media and Areal Density

Patterned media data storage technology aims to increase areal storage density by using advanced semiconductor processing techniques. This techniques are used to fabricate nanomagnetic structures for the purpose of isolating individual grains for magnetic domains into regular patterns [26, 27]. This technology would allow for storage of one bit per cell or grain, which is different from conventional drives where each bit is stored across a few hundred magnetic grains. Without the proper understanding of the prominent tribological issues that exist in the fabrication and successful operation of patterned media, this technology will remain in research laboratories. Conceivably, a patterned media disk drive will consist of a magnetic slider head that reads and writes information onto a spinning disk during flight. The disk will

be comprised of micro to nanoscale magnetic structures that must be planarized to prevent lateral collision between the slider and coarse topography on the disk surface. Figure 1.5 shows that the individual magnetic domains are initially rough after fabrication until a planarization step is employed.

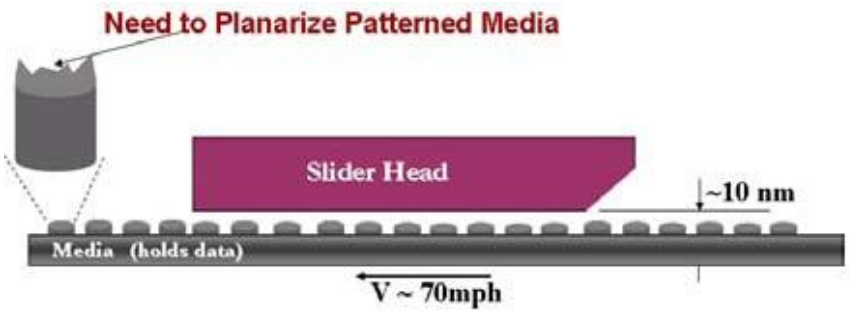

Figure 1. 5 Need for BPM planarization

1.3.3.3 Fabrication of Patterned Media

Some of the fabrication requirements for realizing the patterned media recording system include: highly ordered dot arrays with high aspect ratio, formation of the dot arrays in the desired position, mass productivity and low cost, and planarization techniques after fabrication for sufficient read/write clearance. The integrated circuit industry has tackled these fabrication limitations and the magnetic storage hard drive industry is utilizing those techniques to fabricate patterned media.

Fabrication of patterned media data storage devices utilizes semiconducting manufacturing techniques. These techniques include but are not limited to electrodeposition, evaporation and liftoff, etching processes, and chemical mechanical polishing (CMP) for planarization [26]. Figure 1.6 depicts an example of fabricated

columns (which consequently have an uneven surface due to the height differential of the columns and thereby need planarization) is shown.

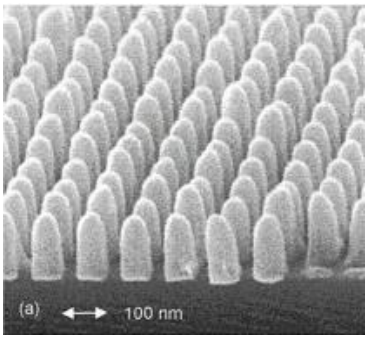

a) pillars diameter of 57 nm and height of 115 nm

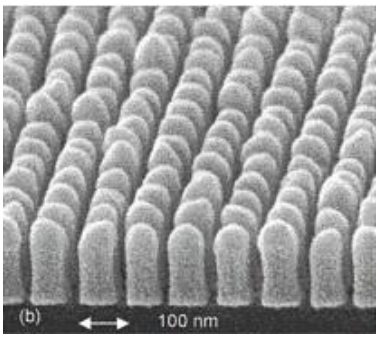

b) pillars diameter of 70 nm and height of 150 nm

Figure 1. 6 SEM of nanocolumns for patterned media [26]

There exists a need to understand the fundamental polishing mechanisms for planarization of PM. Optimization technique for planarization of the PM is needed to reduce waste and sustainability of consumables. The nanodots or squares fabricated for patterned media have the capacity circumvent the superparamagnetic limit but there exists little data that optimizes the parameters for polishing of these structures. CMP has been used since the 1920s for planarization of multiple materials and serves as a viable candidate to planarize these surfaces to the nanometer roughness they require for the read/write head fly height.

1.4 Outline of this Dissertation

This dissertation is divided into three main sections; the first phase of this dissertation is based on benchmarking the CMP machine process parameters on bit patterned matrix configurations. The second phase focuses on the consumables of the CMP process and their use for bit pattern matrix configurations. The last phase is a

completely separate study which is focused on modeling of the abrasive portion of the CMP process and detailing the change in mechanical properties as it affects the CMP process.

Chapter 2 explains the evolution of the CMP process from the integrated circuit (IC) industrial perspective. The chapter details the basic mechanisms of the CMP process from both a mechanical and chemical aspect, and present in detail the tribological mechanisms active during CMP. The chapter details the various models developed to predict the multi-physics phenomena of the CMP process. This chapter also serves to introduce the rest of the results for the phases studied during this dissertation after a full understanding of the process parameters and output from the CMP process is fully undertaken.

Chapter 3 focuses on benchmarking the bit patterned matrix data utilizing a multitude of metrology tools and analytical techniques. The chapter details the effects of the coefficient of friction, lubrication regimes, material removal rate, and resulting surface topographies from polishing the bit patterned media configurations. Finally the chapter offers a statistical analysis to determine the critical parameter in material removal from a statistical standpoint while evaluating the CMP process for bit patterned configurations versus stand copper thin film polishing.

Chapter 4 is the first of a two-chapter investigation in the consumables during the CMP process. This chapter deals with the CMP pad and compares three commercially popular pad architectures while detailing their material removal rates, surface qualities, and coefficient of friction during bit patterned media polishing. The pad life is characterized for bit patterned configurations and a novel non destructive technique

utilizing ultrasound detection is detailed and used to monitor pad material properties, while scanning electron microscopy is used to monitor the surface characteristics of the pad during polishing. The resulting surface qualities of the wafers are obtained through a surface profiler and a correlation between the pad characteristics and CMP output parameters is detailed.

Chapter 5 is the second half of the consumable process investigation for both bit patterned configurations. This chapter focuses on understanding the polishing phenomena of the slurry used during CMP and development of novel polymer-ND slurry to be used for either blanket or bit patterned copper CMP. The coefficients of friction, material removal rate, and surface quality are compared for three different slurries and an investigation into the abrasive polymer-ND slurry concentration is elucidated.

Chapter 6 reflects a separate modeling study which focuses the evolution mechanical properties during the CMP process. The deterministic microstructural variation during polishing is incorporated into a particle augmented lubrication model developed at Carnegie Mellon University and the results of the model are presented in this chapter.

Chapter 7 discusses the interaction between the consumables and the machine process parameters. The influence of the optimized bit patterned media CMP is discussed in detail. The chapter provides a detailed account how each parameter affects the output parameters of the CMP process.

Chapter 8 summarizes the work done in this dissertation along with suggestions for future work with bit patterned CMP process parameters and optimization techniques.

CHAPTER 2: CHEMICAL MECHANICAL PLANARIZATION

2.1 Foreword

CMP has been described as an enabling technology because the high degree of planarization generated with the CMP eases the burden of advanced lithography and etching techniques. The drawback to the CMP process is that it is not stable and well controlled and several issues ultimately affect the chip performance. The semiconductor device industry has been focused on implemented an increase in the number of transistors on a chip thereby increasing the device density.

This approach is emulated by the magnetic storage drive community for the aforementioned reasons of current areal density reaching the superparamagnetic limit. Both industries are striving to put greater numbers of features on a smaller area. For a complete and through historical development of the CMP process, the rest of the chapter explanations on CMP is based on the CMP approach from the semiconductor manufacturing industrial standpoint.

The research objectives of this chapter are:

1) Provide a fundamental background on the development of integrated circuit industry
2) Detail the fabrication steps of integrated chips
3) Detail the emergence of CMP as a planariazation step for many metals in particular for copper in integrated chips

4) Detail the fundamental removal mechanisms and the multi-physics phenomena of the CMP process
5) Outline and detail various models developed to predict the CMP process
6) Provide detail into the forthcoming chapters on CMP and its effect on bit patterned matrix configurations.

2.2 Introduction: Development of CMP

During the semiconductor fabrication and microelectronics revolution, the industry has been focused on rapidly increasing the number of devices per chip and shrinking the critical dimensions of these electronic components. According to "Moore's Law," the demand for the number of transistors per chip will double every 1.5 to 2 years in the semiconductor industry [28]. In conjunction with the demand for transistors from Moore, the microprocessor performance in terms of millions of instructions per second (MIPS) will also double in the same time frame [29]. Figure 2.1 gives a historical comparison of the trend of microprocessors according to the semiconductor industry performance [30].

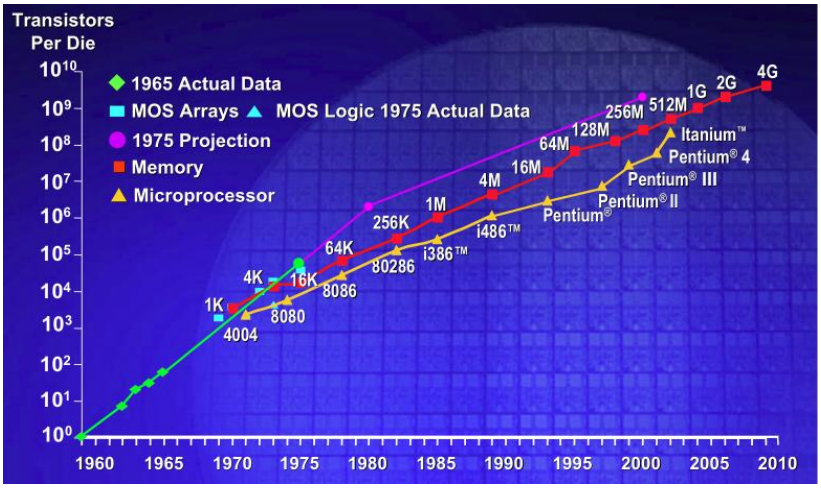

Figure 2. 1 Historical comparison of the trend of microprocessors [3]

The International Technology Roadmap for Semiconductors (ITRS) predicts that by 2011 over one billion transistors will be integrated on a single monolithic die [31]. Today's state-of –the-art integrated circuits (ICs) contain tens of millions of transistors, which are used to amplify and switch electronic signals, capacitors, that are used to block

direct currents and allow alternate currents to travel through the chip, and resistors, that are used to produce voltage, on a single chip. A transistor is typically a MOSFET (Metal-Oxide-Semiconductor Field Effect Transistor), which consists of a source, gate, and a drain. These devices can be made to operate faster by reducing the size of devices and having the devices packed densely into a given chip reducing the distance the carriers have to travel to interact [32, 33]. The minimum feature size decreases the size of the device itself, and this translates into reduction in intermediate pitch or spacing between features. Figure 2.2 is a basic schematic of the basic MOS capacitor.

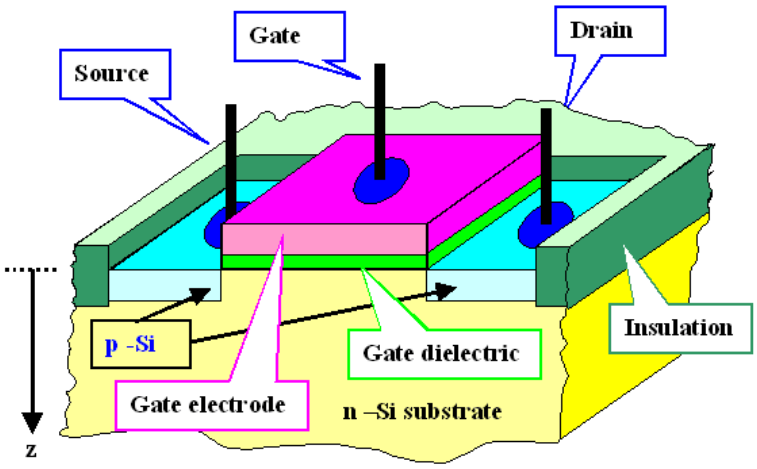

Figure 2. 2 MOS capacitor configuration

Shrinking of device dimensions has become a crucial caveat for both the semiconductor industries and the magnetic storage hard drive industry. However, the explosion in the number of transistors fabricated on a single IC has placed extreme demands on electrically interconnecting these devices in the manner necessary to perform the logical operations of a modern microprocessor. The transit time, (T_r), of electrons in a device with velocity (V) is directly proportional to the length of the gate (L_g). Transit

time is the ratio of gate length to velocity of the electron, and the transit times dictate the frequency of operation [33, 34]. Understandably, the efforts of the semiconductor industry are concentrated on reducing the gate length of the devices themselves with current devices having gate lengths on the order of nanometers [35].

2.2.1 Multilevel Metallization

For the past 40 years, relentless focus on Moore's Law on transistor scaling has provided ever-increasing transistor performance and density. Scientists and engineers have predicted the "end of scaling" for these devices, but each time the technology reached the predicted barriers, scaling did not stop. Instead, imaginative new solutions were developed to further extend Moore's Law [36].

The fabrication of these small devices faces several design, manufacturing, and process control challenges. Once the devices are fabricated on the silicon substrate in the preferred orientation, they need to be connected to a device network between each other and connected to the outside world via interconnect materials. Metallization is the fabrication step in which proper interconnection of circuit elements is made; it is the general name for the technique of coating metal on the surface of non-metallic objects. The metal layers deposited, typically copper, are vacuum deposited by one of four methods: filament evaporation, flash evaporation, electron-beam evaporation, or sputtering [37]. Details of the deposition process are outside the scope of the research for this dissertation; however, further details can be found within the references. The metals connecting the devices at the silicon substrate level are deemed contact or first-level metallization, and the metals that connect the devices to the outer world are the second level metallization [33, 34]. The materials required for metallization need to be selected

based on their mechanical, electrical, and chemical properties since these properties dictate the frequency of flow of the charge. The ITRS dictates that the minimum and maximum number of layers in a multi layer metallization (MLM) scheme needs to be 13 and 17 respectively. Figure 2.3 shows the cross-section image of a seven-level, multi layer metallization scheme with the silicon dioxide interlevel dielectrics (ILD) labeled [38, 39].

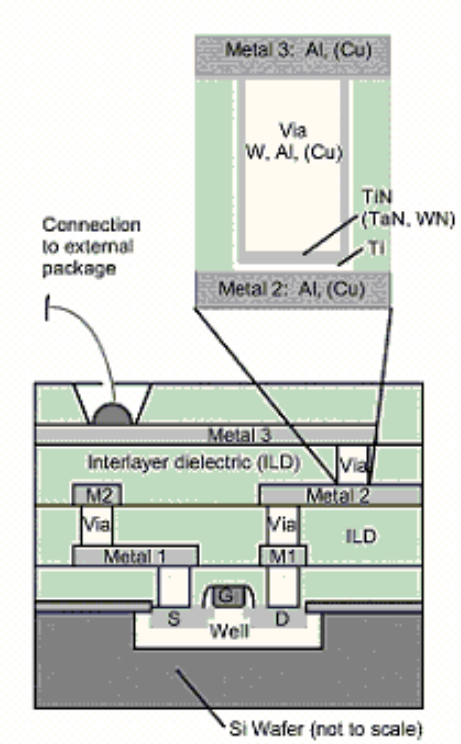

Figure 2. 3 MLM scheme [12]

As previously mentioned, chip manufacturers wanted to make chips with higher speed while simultaneously reducing the device dimensions. A single MOSFET is shown in figure 2.2, with gate (G), source (S), and drain (D) connections labeled. Interconnection of this MOSFET with other devices on the chip is not shown and is

accomplished through the polysilicon/metal alloy (silicide) gate level and several metal-SiO_2 ILD levels joined together by vertical vias [40]. Fabrication of interconnects was vital to the emergence of CMP and is briefly detailed in the following section.

2.2.2 Interconnect Fabrication

The relentless competitor- and customer-driven demand for increased circuit density, functionality, and versatility has led to evolutionary and revolutionary advances in the "front end" of the chip manufacturing line where the devices are fabricated, and the "back end" where these devices are appropriately wired within the integrated circuit (IC) [39]. Chip interconnections, or "interconnects," serve as local and global wiring, connecting circuit elements and distributing power [29]. In order to incorporate and accommodate the improvements in decreased feature size, increased device speed, and more intricate designs, the semiconductor industry increased research in the "back end of line" (BEOL) processes. This made BEOL processes equally as important as the development of the "front end of line" (FEOL) processes to reduce gate oxide thickness and channel length in the MLM layers [41].

In order to achieve high device frequency and low feature sizes of the devices, the interconnect delay had to be reduced so that the signals could pass faster through the metal layers, thus making devices function at greater speeds. The measure of the interconnect delay is the RC delay or the time delay (T_{RC}) in seconds, or the frequency of charge flow associated with the interconnect materials is computed as product of resistance (R) of the metal lines and the capacitance (C) of the insulating interconnects. Substituting for resistance in terms of wiring dimensions and material properties, *RC* time delay can be written as equation (2.1) [42]:

$$T_{RC} = R * C = 2\rho\kappa\varepsilon_0 L^2 \left[\frac{4}{P^2} + \frac{1}{T^2} \right] \quad (2.1)$$

where ρ is the resistivity of the metallic interconnect, *k* is the dielectric constant of the insulator, ε_o is the permittivity of vacuum, *L* is the length of the interconnect line, *P* is the pitch between interconnect lines, and *T* is the thickness of the line. Any changes in the variables will increase or decrease the interconnect delay. Reduction of the RC delay leads to an increase in the performance of ICs. Physically, a reduction in the RC delay translates to a reduction in the length of the interconnect wiring. This is why the IC fabrication industry has been increasing the number of metallization layers.

2.2.3 Multilevel Metallization Challenges

It can be seen from equation (2.1) that there is an increase in the RC delay with the decrease in interconnect wiring pitch. In order to decrease the RC delay several options were explored:

1) Cu has replaced Al as interconnect wiring materials due to its lower resistivity

2) Several novel low -k materials are being explored

3) Multilevel metallization scheme of wiring is being implemented.

Table 1 calculates the RC time constants calculated for a few metals of given R_s (sheet resistance) and 1 mm length on 1 μm thick SiO_2 [43].

Table 2. 1 Interconnection delay

Metal	**Bulk Resistivity** (μΩ-cm)	**Polycrystalline film resistivity** (μΩ-cm)	**Film Thickness** (A°)	**R_s** (Ω/square)	**Delay** (ps/mm)
Poly-Si	-	~100	5000	20	690
$CoSi_2$	10	15	2500	0.6	21
$MoSi_2$	~35	~100	2500	4	138
$TaSi_2$	45	55	2500	2.2	76
$TiSi_2$	13	15	2500	0.6	21
W	5.65	8-10	2500	0.32-0.4	11-14
Al	2.65	2.7	2500	0.11	4
Cu	1.67	2.0	2500	0.08	3

It is evident from table 2.1 that semiconductor manufactures would use Al or Cu as the interconnect material due to their low RC delay and advantageous material properties. In order to produce the multilevel metallization schemes in figure 2.3 for IC devices, the top most layer of the previous metallization layers must be optically flat, and in more recent devices, atomically smooth [44]. This is because if there exists any residual roughness at the previous layer, it will get compounded as the layers increase, and after a couple of compounded layers, the roughness will be so high that lithography (patterning) will experience issues with the depth of focus and any further processing will not be possible. To compound the problem of lithographic patterning, the irregular surface anomalies cause the variation of the thickness in fine line widths (sub 0.5 μm) depending upon photo resist thickness. An effectively planarized surface offers enormous benefits such as:

1) Higher photolithography and dry etch yields,

2) Elimination of step coverage concerns

3) Minimization of prior level defects,

4) Elimination of contact interruption, undesired contacts, and electro-migration effects

5) Reduction of high contact resistance and inhomogeneous metallization layer thickness

6) Limitation in the stacking height of metallization layers [45].

Figure 2.4 shows SEM images of a) unpolished and b) polished MLM schemes.

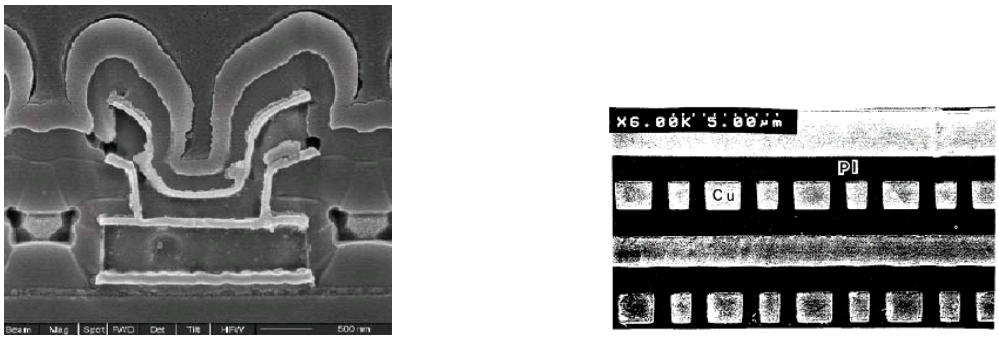

a) Roughness resulting from metallization

b) Post CMP global planarity for metallization

Figure 2. 4 SEM image MLM roughness [12,17]

2.2.4 Copper Emergence

It can be seen from figure 2.4 that it is not possible to proceed with further processing steps as depth of focus issues come up during photolithography. Several other subsequent processing challenges, such as voids within interconnect layers due to compounded roughness, also occur. Thus, the CMP process becomes a crucial

processing step in device fabrication in order to achieve successful fabrication of MLM structure. Besides increasing the number of metallization layers, reducing the resistance of the metal interconnects and the capacitance of the dielectric layer reduces the RC delay. Several electrical and mechanical properties are deemed optimal for selection of the correct materials for the metallic interconnects. For brevity the optimal properties for IC fabrication can be found in [46].

Based on the necessities of the IC industry, copper was chosen to replace aluminum as the material for metallic interconnects to further reduce RC delay for future application trends [47, 48]. Choosing electrically superior copper over aluminum comes with an inherent drawback. Due to the difficulty in dry etching fine line copper, the damascene approach was developed to make the metallization layers [49]. These layers are fabricated through two different BEOL processes: the subtractive process and the damascene process show in figure 2.5.

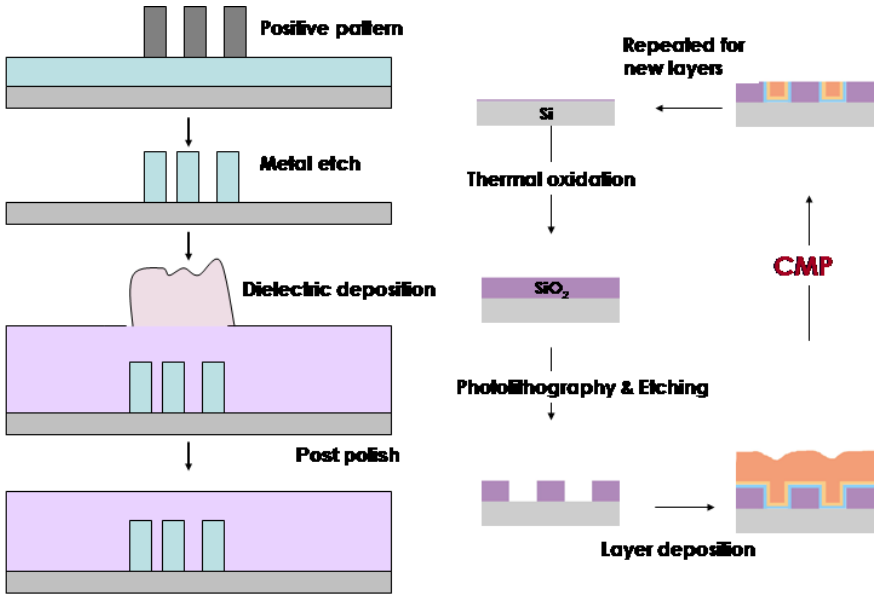

Figure 2. 5 BEOL IC fabrication

2.2.4.1 Subtractive Etch

In the subtractive process, the metal leads are patterned by subtractive etching followed by the deposition of an interlevel dielectric (ILD) to insulate and passivate the metal lines. This process was used for aluminum or tungsten interconnects.

2.2.4.2 Damascene Process

As Cu cannot be effectively etched due its ability to form non-toxic volatile byproducts and its property of diffusion in neighboring materials, present day MLM structures are fabricated using the damascene process. In the damascene process a thermal oxide layer is grown on the bare silicon in the preferred orientation. The oxide layer is then etched using photolithography techniques. A layer of metal is then deposited onto the etched dielectric and is polished to ensure planarity as the MLM scheme is complied (figure 2.5).

2.2.5 Options for Planarization

Several technologies exist that achieve local and global planarity and are utilized by the semiconductor and magnetic storage industry. Techniques such as spin on deposition (SOD), reflow of boron phosphorous silicate glass (BPSG), spin etch planarization (SEP), reactive ion etching, and etch back (RIE EB), SOD + EB have been discussed in detail by Zantye [45]. The different degrees of global and local surface planarity from each fabrication process can be seen from figure 2.7 [50]. These are the prominent output parameters of several competing technologies presently being used to achieve local and global planarization.

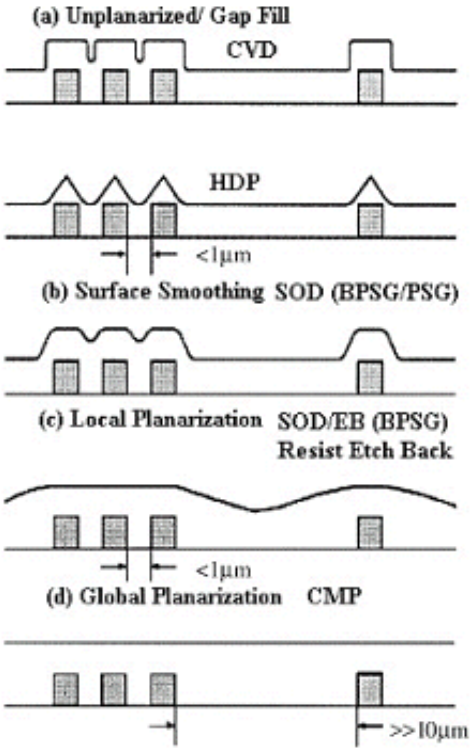

Figure 2. 6 Global and surface planarity for planarization processes [23]

2.3 Chemical Mechanical Planarization (CMP)

Chemical mechanical planarization (CMP) is the process of smoothing and polishing a surface by the aid of chemical and mechanical forces. Presently, CMP is the only technique that offers both local and global planarity on the surface of the wafer. The plasma-enhanced chemical vapor deposited oxides have limited capability of gap filling and are restricted in their gap filling ability below patterns having 0.3-μm feature size. High-density plasma deposited oxides have acceptable gap filling capabilities; however, they produce variation in surface topography on the local as well as global level. Even though spin on deposited (SOD) doped and undoped oxides and polymeric materials have acceptable ability for gap filling, the disadvantages and advantages of the CMP technique are listed in Table 2.2 and 2.3 respectively.

Table 2. 2 Disadvantages of CMP

Disadvantages	Comments
Multi-physics phenomenon	Poor control of process variables and variability in consumables leads to fine tuning for proper polishing parameters
New Defects	New defects from CMP can affect die yield (*crucial for sub 0.25 μ features)
Process developments	Endpoint detection difficult to control, therefore need for additional process control and metrology
High cost of ownership	Costly equipment and consumables with high turnover rate for consumables

Table 2. 3 Advantages of CMP

Benefits	Comments
Planarization	Global and local planarization
Material selection	Metals and non metals
Planarization of multi material services (MLM)	Achieves polishing of multiple materials on same polishing step (* polish rate varies)
High surface removal rate	Can removal extremely rough surfaces globally and locally for tight design restrictions and MLM
Metal patterning	CMP is an alternative means of patterning metal eliminating need to plasma etch difficult to etch metals and alloys
Metal step coverage	Reduction in surface topography reduces metal step coverage
Increased IC reliability	Contributes to increasing IC reliability, speed, yield (lower defect density) of sub 0.5µm and circuits.
Reduce defects	CMP is a subtractive process and can remove surface defects.
No hazardous gases	Does a not use hazardous gas common in dry etch process.

2.3.1 Applications of CMP

Historically CMP has been used to polish a variety of metals and was generally taken from nature as a polishing method used to produce beautifully finished stones from years of exposure to mild chemicals and mechanical forces of nature. Modern CMP originated from methods on polishing glass for optical devices [51]. Manufacture of telescopes, microscopes, eyeglasses, and various lenses was well understood and established prior to invention of transistors. IBM developed CMP for the semiconductor community during the 1980s. IBM initially applied the CMP process to the silicon dioxide inter-level dielectric planarization for the integrated circuit industry. CMP is now utilized in planarizing the interlayer dielectric (ILD) and metals used to form interconnections between devices [14].

With the successful implementation of CMP for local and global planarization of silicon dioxide (SiO_2), removal of excessive tungsten (interconnect) from the horizontal surfaces on the wafer pattern proved to be an asset for subsequent Al metallization [42, 52, 53]. CMP was developed with a two-fold approach of planarizing oxide and removing the via fill metal from the horizontal surfaces. The major applications of CMP are given in table 2.4 [45].

Table 2. 4 Applications of CMP technology

	Materials	Application
Metals	Al	interconnect
	Cu	interconnect
	Ta	diffusion barrier/adhension
	Ti	diffusion barrier/adhension
	TiN	diffusion barrier/adhension
	W	interconnection e- emitter
Dielectric	Cu-alloy	interconnect
	Al-alloy	interconnect
	PolySi	gate/interconnect
	SiO_2	ILD
	BPSG	ILD
	PSG	ILD
	Polymers	ILD
	Si_3N_4 or SiO_{xNy}	passivation layer
Other	Aerogels	ILD
	ITO	Flat panel
	High K dielectrics	packing
	High T_c Semiconductors	interconnect/packaging
	Optoelectronic materials	optoelectronics
	Plastics, Ceramics	packaging
	silicon on insulator (SOI)	advanced device/circuitry

The application of CMP in electronic device fabrication is significant in both memory and microprocessor device fabrication [46]. From table 2.4 it can be seen that CMP is emerging in all fields of study including microelectromechanical systems (MEMS) and various other electronic device fabrication. As devices continuously shrink with the technology advancement in device manufacturing, the output specifications of the CMP process have become more stringent.

2.3.2 History of CMP

Zantye et al. covered the basic history of CMP emerging as a technology from the an optical lens polishing technology to the modern day semiconductor multiphysics problem [41]. The first semiconductor CMP machine was an innovation of the optical

lens polishing machine. The proper polishing abrasives in presence of the slurry chemicals were used to achieve a superior degree of precision and flatness to meet the demands of the semiconductor industry. By supplementing mechanical polishing with high hardness abrasives, such as silica in an alkaline medium, there are significant gains in material removal and reduction in the process time.

A further improvement to the CMP process was made at IBM in the late 1970s and early 1980s. The new process was faster than the previous silica-based polishing method and resulted in ultra-flat, ultra-smooth surfaces to meet the stringent requirements of the IC industry [41]. The slurry was later tailored to reduce defects and surface non-planarity introduced by the etching and deposition processes. The IBM process was then applied for trench isolation in the late 1980s in Japan for various logic and DRAM devices. There was widespread industrial implementation of different variations of the CMP process by companies like NEC, Nation Semiconductor, Hitachi, etc. This led to the introduction of the first commercial polisher designed specifically for CMP by Cybeg in Japan in 1988. Later, International SEMATECH identified CMP as a technology critical for the future of IC manufacturing and launched a project to develop competitive, advanced CMP tools in the US [18].

Throughout the history of the CMP process there have been advances in the types and capabilities of each polisher. There have been a total of three different generations of polishers and each generation has improved upon the last generation's work based on the needs of the IC industry. The first generation CMP tools based on rotational platen had low throughput values of about 10–18 wafers/hour [54]. The second generation of CMP tools emphasized evolutionary improvements to the original designs and the second

generation of polishers included multi-wafer platen polishers and sequential rotational systems. The third generation equipment designs were modified to stay in production for long periods of time by giving them adaptability to future technology modifications. The third generation of polishers included sequential linear polishers, orbital polishers, rotary inverted polishers, and pad feed polishers [41, 45]. While the details of these polishers are not detailed in this dissertation, the evolution of these polishers has been critical in the variability of CMP to be utilized in many industries.

2.3.3 CMP Process

Wear is the phenomenon of material removal from a surface due to interaction with a mating surface, either through micro fracture, chemical dissolution, or melting the contacting surface [55]. CMP abrasive wear is usually divided into two types: two-body and three-body abrasion. The situation when exactly two bodies are involved in the interaction is known as two-body abrasion. Two-body abrasive wear is caused by the displacement of material from a solid surface due to hard particles sliding along the surface or when rigidly held grits pass over the surface like a cutting tool. Two-body abrasive wear is a complex process often involving high strain and plastic deformation and fracture of micro volumes of the material, which might be described as the removal of discrete surface by a harder substance which tends to gauge, score, or scratch. In the case of plastic contact between hard and sharp material and a relatively softer material, the hard material penetrates the softer one causing fracture (e.g., two-body abrasion). This fracture can lead to micro-cutting and ultimately material removal. In three-body abrasive wear the particles from two-body collisions or introduced wear abrasives are

free to roll as well as slide over the surface. It is through the wear process that raw materials can be turned into the electronic instruments used every day.

The CMP process shown in figure 2.7 involves mounting a wafer with a thin film of metal or oxide deposited on it onto a spindle. A downward force is exerted on the wafer pressing it onto a rotating polymer pad while a liquid containing colloidal abrasive particles and dissolved chemicals, labeled slurry, is introduced in the space between the pad and the wafer.

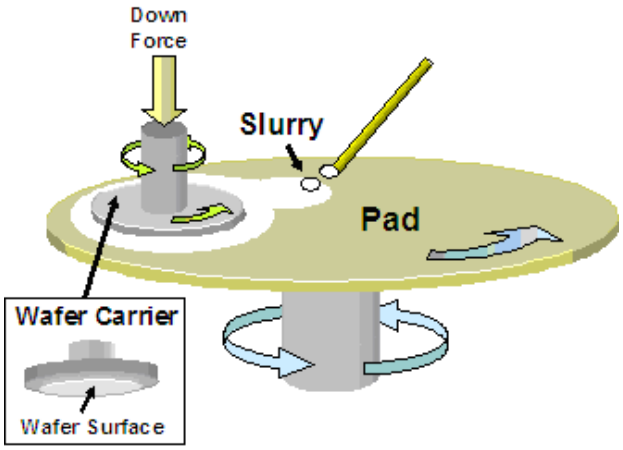

Figure 2. 7 Schematic of CMP process

This process employs both solid on solid (e.g., pad on wafer surface two-body abrasion) and solid on liquid (pad, wafer, with abrasive nanoparticles) three-body abrasion wear to polish the surface of thin films to atomic smoothness as shown in figure 2.8.

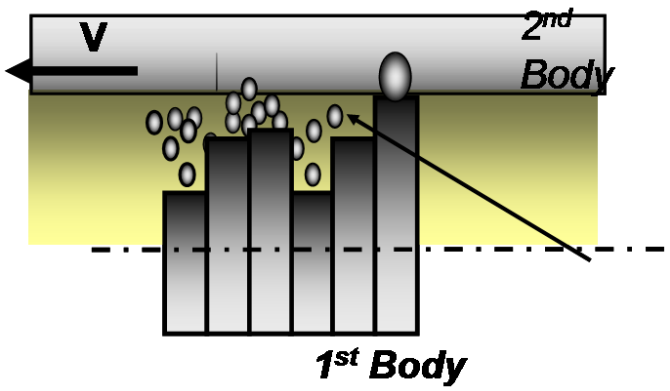

Figure 2. 8 Three body abrasion on CMP process

The slurry, which includes abrasive nanoparticles, polishes (or wears) the film surfaces by the combined action of chemical corrosion and mechanical removal. Therefore the CMP process can be described as a process which uses the combination of mechanical energy from the pad and abrasives and chemical energy from the slurry chemicals to polish and remove material from the wafer surface. The major consumables for bit patterned matrix configurations investigated in this dissertation are the polymer polishing pads and an initial investigation into the slurry abrasives with a novel slurry developed. Details for the pads and slurry will be discussed in subsequent chapters.

2.3.4 Material Removal Mechanism

As mentioned above, the CMP process involves both chemical and mechanical components acting in synergy to bring about removal of excess material as well as planarization of the surface topography. It is important to understand the mechanism of material removal during CMP. Studies by Ahmadi et al, have characterized removal during CMP into four different categories [56, 57]:

1) Abrasive wear

2) Adhesive wear

3) Corrosive wear

4) Erosive wear.

This section provides insight into the chemical and mechanical aspects of CMP, which are responsible for material removal.

2.3.4.1 Mechanical Aspects of CMP

The mechanical aspects of the CMP process deal solely in abrasive wear of the mating surfaces, whether it is wafer to pad abrasion or slurry abrasive to pad abrasion.

From figure 2.8, two body wear abrasion occurs when the abrasive particles from the slurry interact with the wafer surface, and also when the pad surface asperities (surface protrusions) slide against the wafer surface. As the roughness of the pad is on the order of microns and the size of the abrasive particles is on the order of nanometers, a significant amount of the two body abrasion takes place between the pad and the wafer asperities.

The interaction of the pad and wafer asperities, and the slurry abrasives leads to three body abrasion. Three body abrasions are much more complicated than the standard two body abrasion but results in lower removal rates and can lead to a reduction in surface defects. In three body abrasion the abrasive particles that come in contact with the wafer asperities, are held in place under a given pressure by the pad asperities. As the abrasive particles are dragged across the wafer surface under pressure applied, ploughing, and cutting processes occur simultaneously resulting in the material removal from the

wafer surface. Figure 2.9 is a simplified graphical representation of the interface during CMP.

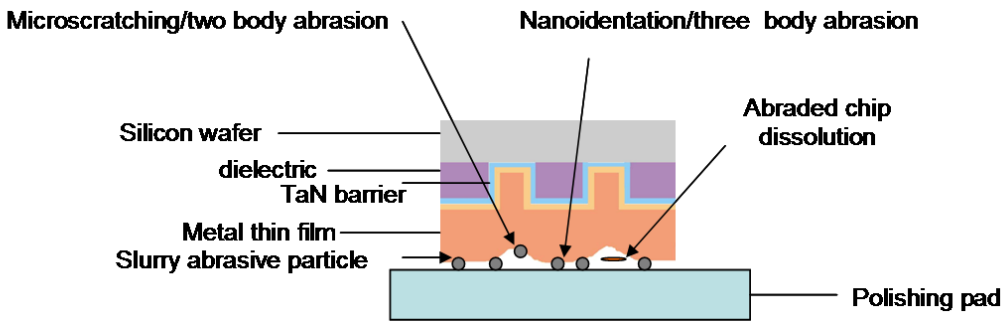

Figure 2. 9 Three body abrasion during CMP

The relative velocity of the wafer/pad interface aids in the removal process through the momentum transfer of abraded particles from the wafer and the abraded slurry particles as the centrifugal forces force these particles from the interfaces. This erosive wear is a function of the fluid motion which is covered in the fluid interfaces modeling section of this dissertation.

2.3.4.2 Chemical Aspects of CMP Material Removal

The "chemical" aspect of chemical mechanical polishing involves the slurry chemistry and the ability of the chemically enhanced slurry to modify the wafer surface through corrosive wear prior to abrasion by the particles. The slurry must be able to dissolve the abraded material, thereby avoiding re-deposition of the removed material onto the wafer surface. As CMP was initially developed to polish dielectrics (oxide layers in MOSFETS), the oxide layers were first hydrolyzed by the chemicals in the slurry and the abrasive particles abraded the surface. The same is true for metal polishing; the difference lies in the chemical make up for the slurries. The abrasives in the slurry

provide another mechanical abrasion to the surface, but also the abrasive particles bond themselves chemically to the wafers surfaces and remove material as they separate from the surface, through adhesive wear [41, 49]. Therefore the abrasives have a chemical role in removal to accompany their mechanical abrasion.

In the case of copper CMP, the slurries can be acidic and alkaline in nature [41, 58-61]. The metallic copper surface is modified by the active ingredients and pH of the slurry. The ingredients and the pH cause a reaction that dissolves the copper oxides and hydroxides and the rate of oxidation of the copper depends on the particular formulation of the slurry and concentration of oxidizers and complexing agents of the slurry. The formed surface copper compounds will then be abraded off the surface by the abrasive nanoparticles and the pad asperities. For copper CMP, the abrasive particles only provide mechanical action and the chemical nature of the particles plays no part in the material removal. The abraded copper compounds (from the dissolved oxides and hydroxides and the abraded particles) are carried away along with the dispensed slurry. The dissolution is very crucial to the removal process, as it avoids re-deposition of the material onto the wafer surface. The material removal rate (MRR) depends equally on the mechanical as well as chemical aspects during CMP.

2.3.4.3 Governing Factors of CMP Process

The CMP process is a multi-physics process with many factors governing the final material removal rate and surface quality. It is a process that is judged by its ability to have local and global planarity. Wafer planarization may be classified into three categories of planarity. These are summarized below and shown in figure 2.10:

1) Surface smoothing: feature corners are smoothed and high aspect ratio holes are filled
2) Local planarity: surfaces are flat locally, but the surface height may vary across the die
3) Global planarity: the surface is flat across the entire stepper field.

The requirement for surface smoothing and local planarity comes from metal step coverage, which is defined by the ratio of thinnest point in metal film to the thickest point in metal film [62]. The requirement for global planarity increases when the circuit dimensions reach sub-0.5µ.

Very few planarization schemes obtain the global planarity offered by CMP due to the stringent restrictions required to meet the depth of field requirements of lithography tools in the sub 0.5 micron regime. Planarization over many micrometers is needed to eliminate metal etch residuals, and planarization over several millimeters is required to alleviate photolithographic depth of focus limitations [53]. The varying degrees of planarity are shown in figure 2. 10.

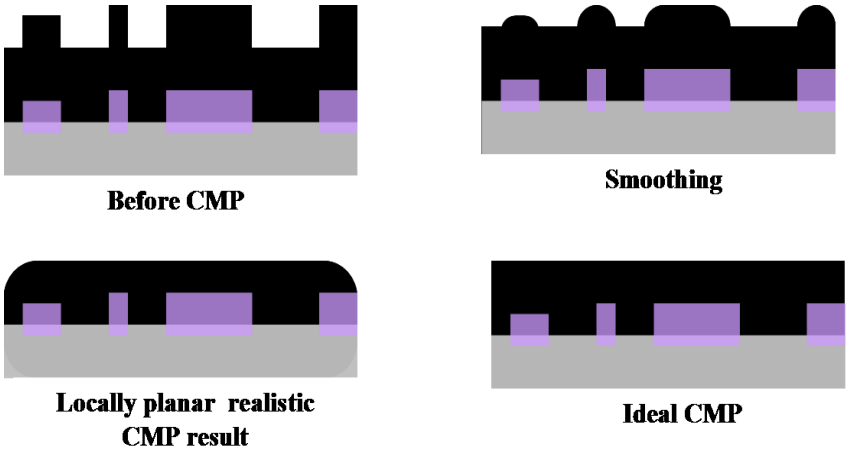

Figure 2. 10 Degrees of planarity in CMP process

The governing factors behind the planarity results and the multi-physics phenomenon can be categorized into process parameters and consumable characteristics. Table 2.5 gives an overall list of aspects that govern the output of the CMP process.

Table 2. 5 Factors governing output of CMP process

Process Parameters	Consumable Characteristics
1) Load applied (Psi) 2) Angular velocity - Polishing Pad - Wafer carrier 3) Slurry flow rate	1) Wafer - Contour and size - Bit pattern density - Pattern dimensions - Chemical compatibility of underlying layers to slurry components 2) Pad - Bulk characteristics - Surface characteristics - Groove design - Groove dimensions 3) Slurry - pH/ Zeta potential - Particle size and distribution - Additives - Oxidizer and concentration

2.3.5 Process Parameters

The applied pressure and velocities of the wafer carrier and polishing pad are the most crucial machine process input variables which impact CMP performance. From Preston's Law adopted from glass polishing, pressure and velocity during polishing dictate the removal rate during the process [51]. The pressure and velocity also dictate

the friction characteristics at the interface and determine the regime of lubrication as detailed by the Stribeck curve [63]. High pressure and velocities result in high shear forces applied on the wafer surface, which can induce delamination, or peeling of the deposition layer from the silicon substrate, at the weakly adhered surfaces involving ILDs [64]. The other process parameters that have an effect on the removal rate include slurry flow rate and pad surface temperature. These factors have been previously investigated by Mudhivarthi and Zantye [41, 46].

2.3.6 Consumable Characteristics

The characteristics of the wafer being polished have a significant effect on the CMP process. The size and shape of the wafer determines the contact area and the polishing uniformity across the wafer surface during polishing. The wafer shape also changes the interaction between pad and the wafer at different pressure settings resulting in a change in contact dynamics at the surface [65]. Looking at the die level, the pattern density and dimensions along with the layout of the pattern in a die affects the uniformity within the die resulting in change in uniformity of polish and generation of post CMP characteristics [66]. This process of pattern density and uniformity becomes important in the magnetic storage hard drive community as the flight height of magnetic head and the ability to access memory is dependent on the pattern density and planarity of the surface.

The polishing pad is consumable of CMP, which provides a major part of the mechanical component to polishing with a 550 million dollar economic impact. The asperities, or roughness of the pad surface, directly determine the contact area for material removal (this is also dependent on the pressure applied). A secondary function of the pad asperities is to prevent the abrasive particles of the slurry from sliding off the

pad due to centrifugal forces of rotation and to have an efficient pad-wafer contact. The abrasive particles, which are held at the contact by the pad asperities, are the only particles available to provide active mechanical component during CMP. Typically a polishing pad is constituted of two sections: the top section of the polishing pad, which consists of grooves and surface asperities, and the bottom bulk portion of the pad, which supports the upper portion and helps in achieving polishing uniformity [67]. The two sections of the pad are either fabricated together or applied together for specific CMP applications. The polishing pad is fundamental in material removal through two body abrasion and must also transport the slurry effectively to the polishing surface [68]. The dimensions of the pad groove, such as the width and depth of the groove, along with the groove pattern are also important to have a uniform slurry distribution on the pad surface.

Out of all the consumables the slurry and its chemical constituents have the most influential economic impact with profits and sells above two billion dollars a year [69]. CMP slurry is comprised of oxidizers, complexing agents, abrasive particles, and dispersants which all aid in the "chemical" part of the CMP process. The slurry plays a critical role in modifying the surface being planarized, abrading the surface, and also dissolving the abraded debris. The concentrations of its various constituents significantly influence the output of CMP. The particle size distribution, zeta potential, uniform dispersion, and other characteristics need to be maintained and monitored continuously to avoid formation of agglomerated particles or chipped particles. If the slurry characteristics are not closely monitored the wafer surface will end up being severely scratched, hampering the device yield and impacting the overall performance of the device. The slurry also acts as a barrier chemical selectivity layer for the different

underlying layers (ILD and barrier layers) that are not supposed to be polished. The barrier layer is created by utilizing suitable additives and pH conditions. Consequently this is where much of the research in polishing has been focused. Successful implementation of the CMP process significantly depends on optimizing the process parameters and selections of the consumables to ensure product performance and reliability.

2.4 Tribology of CMP Process

In order to truly understand the material removal mechanisms and the output during the CMP process, understanding of the tribological aspects of polishing is fundamental. Tribology is the science and engineering of interacting surfaces in relative motion. It includes the study and application of the principles of friction, lubrication, and wear. It is easy to ascertain that CMP is a tribology process from the applications of two-body and three-body abrasion, to the friction regimes during polishing, and the resulting material removal or wear during polishing.

2.4.1 CMP Process

CMP is an abrasion process which involves rubbing of wafer and pad surfaces in the presence of chemical slurry and abrasive particles. During the CMP process, low friction and efficient lubrication are desirable, but the optimization of the process focuses on highly controllable material removal as well as a great surface quality. Since the pressure and velocity are the major contributors to the removal process during CMP it is evident that the frictional forces would play a pivotal role in understanding and improving the CMP process. There are various analytical and theoretical models to predict frictional and removal characteristics during lubricating sliding contacts which is

closely related to the CMP process [70]. The interface during CMP process is much more complicated as compared to the studies on the frictional characteristics considered in the aforementioned models. The models fail to incorporate the abrasive particles for three-body wear and the chemical component of the slurry during polishing; therefore the applications of these models find minimal application in CMP predictions. The best way to understand the interfacial characteristics (dynamics, material removal, and surface tribology) is to study the frictional characteristics *in-situ* or during the process. One of the most influential parameters for the CMP process is the coefficient of friction during polishing.

2.4.2 Tribo-Metrology of CMP

The coefficient of friction (COF) and the contact acoustic emission signal (AE) are crucial in characterizing the friction characteristics of a system consisting of sliding surfaces. The study of these parameters along with the wear rate of the surfaces and pad wear are termed "tribo-metrology" by Li et al [71].

2.4.2.1 Coefficient of Friction

The coefficient of friction is the ratio of the tangential force that is resisting motion to the normal load [55]. The numerical coefficient representing the friction at the polishing interfaces reflects the nature of abrasive wear (two-body, three-body wear). The COF is influenced by several parameters including the material properties of the interacting surfaces, the shear force at the interacting surfaces, the pad's mechanical properties, the kinematic parameters of the polishing process, slurry viscosity, and chemical properties of the slurry and its ability to alter the surface.

As mentioned previously the COF is used to generate Stribeck curves which offer an efficient means to monitor tribological processes [63]. The Stribeck curves shown in figure 2.11 are generated using COF data and the Sommerfeld number.

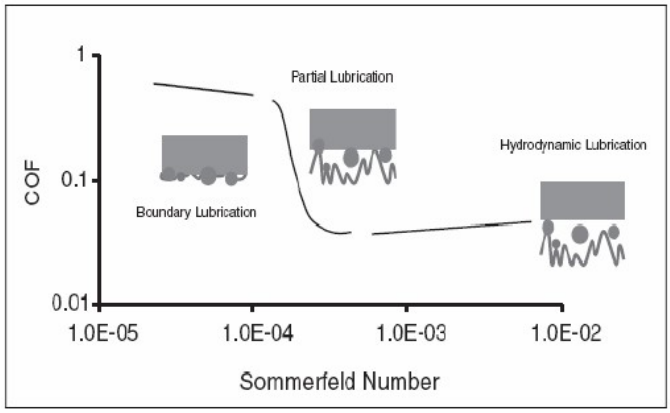

Figure 2. 11 Stribeck curves generated from COF data [33]

The COF and Sommerfeld number are used to determine the lubrication regime at the polishing interface. The Sommerfeld number is defined in equation (2.2),

$$S_f = \frac{\mu U}{p\delta_{eff}} \tag{2.2}$$

where μ is the viscosity of the lubricant, U is the relative velocity, p is the applied pressure, and δ_{eff} is the effective lubricant film thickness. The Sommerfeld number can be calculated since the process parameters dictate the pressure and velocity. The viscosity of the slurry is calculated based on the manufacturers' specifications, while the effective lubricant film thickness is the variable that does not remain constant and is estimated to be pad surface roughness based on literature [72]. To account for deviations of the slurry film thickness on different grooved pads, a dimensionless factor has also been suggested.

Based on figure 2.11 there are three different major regions of lubrication that can contribute or negate material removal, boundary lubrication, mixed or partial lubrication, and hydrodynamic lubrication at a lubricated frictional interface. Studies have shown that there are minor regimes such as hydrostatic and elastohydrodynamic lubrication regimes that are not investigated in this thesis due to their small contribution to the theory behind the removal rate [55, 73].

2.4.2.2 Boundary Lubrication

Boundary lubrication consists of two-body abrasion on solid-solid contact between the wafer and pad during boundary lubrication, where the removal process is dominated by surface abrasion. In this regime, polishing results in severe surface damage due to the aggressive abrasion by slurry particles and the polishing pad.

2.4.2.3 Mixed Lubrication

The mixed lubrication regime consists of a thin film of slurry which partially supports the applied pressure, and thus prevents the aggressive abrasion seen from boundary lubrication which has no lubrication. For optimization proposes the CMP process should be conducted in this regime to ensure reduction in surface damage.

2.4.2.4 Hydrodynamic Lubrication

The hydrodynamic lubrication regime is a mode of polishing resulting from the entire applied pressure being supported by the interfacial slurry fluid layer. This will result in a very low COF, and therefore a very low removal rate as there is little abrasion. Therefore knowledge of the polishing regime is highly beneficial to understanding the polishing process.

The importance of the process parameters becomes apparent based on the lubrication regimes for polishing. Too little slurry and the surfaces will be abraded with high COF and thermal stresses resulting in a highly polished material and high surface damage. If there is too much slurry they hydrodynamic lubrication regime will dominant and the result surface will have poor material removal. Optimization of the process parameters in patterned media configurations is detailed in Chapter 3.

2.4.3 Acoustic Emission

The AE signal is a caveat of the COF and can be monitored during the CMP process. The AE signal is an estimate of the acoustic energy dissipated at the interface due to the mechanical interactions of sliding surfaces and abrasive particles at the interface. The shear generated by the down pressure and platen rotation brings about a strain in the thin film that is being polished and thus is also responsible for material removal. If the shear force is sufficient enough to overcome the interfacial adhesion of the thin film and the buried layer, the interfacial adhesion energy is dissipated in the form of acoustic vibrations. Higher AE signals indicate intense mechanical interactions or aggressive abrasion at the interface and lower signal indicates a smooth, mild polishing resulting in lower shear forces and less damaged wafer surface. A noisy signal could indicate the presence of slurry agglomerates or delamination at the interface which is beneficial in knowing when to stop polishing.

2.4.4 End Point Detection

The end point detection parameters of the CMP process ensure that the goal of the process for wafer uniformity, removal rate, and removal stability are within process specifications. In line and/or in situ metrology that can assess the polish quality of the

CMP polishers and product wafers immediately can reduce the wafer test time (production time that ensures process specifications are met by polishing first few wafers empirically). There are numerous ways to determine the end point detection (EPD) of the CMP process. A summary of the end point detection methods is listed in the table 2.6.

Table 2. 6 End point detection methods

Methods To determine EPD	Techniques
Optical	Interferometry, reflectance, spectral reflectivity
Electrical	Friction sensing Impedance and conductance (non friction sensing)
Acoustic sensing	Generation of acoustic signal from abrasive grinding process

From table 2.6, most of the methods involve monitoring a signal which contains a signature indicative of an appropriate stopping point. The optical methods utilize a variation of techniques involving light to determine if process parameters are met. While the optical technique was the first utilized, it had the limitation of having to add an extra tool to the CMP process altering the overall effect of the CMP process to take measurements.

Electrical EPD systems fall into two subcategories, systems that monitor COF and those that do not. The systems that do not sense friction have typically been proven unsuccessful outside research premises [74]. The components for the systems that do not monitor COF are intrusive to the process and require electrical connections to the wafer during CMP or modifications to the platen/carrier which affect the performance of the

tool itself. The methods that measure the COF are passive and have provided solid reliable and viable data included in this dissertation.

2.4.4.1 EPD, COF, and AE Signal

During the process of CMP, work is done on the wafer by the pad and wafer carriers. This work is done by friction. As the two surfaces must pass across each other and friction is resisting that motion and causes material removal. In metal CMP, the material removal will eventually lead to the exposure of the underlying ILD which has a different COF than the metal. The EPD for these systems is based on monitoring the changes in the motor current to infer the state of the friction between the wafer and the pad [74].

As mentioned before, the concept behind the AE detection is that the grinding action that takes place during polishing generates an acoustic signal. The challenge in AE EPD is that the signal must be demodulated to yield information about the polishing process. The demodulating methods involve detecting and analyzing the amplitude and frequency of the spectral peaks or the acoustic wave velocity.

The COF and the AE can be constantly monitored and recorded to determine EPD of the polishing process [45]. Changes in the AE and COF are indications that a new polishing surface interface has been encountered due to the change in properties compared to the film that has been removed. Figure 2.12 is a graphical depiction of raw data acquired for copper CMP, the transition to the dielectric layer is shown as the signal increases.

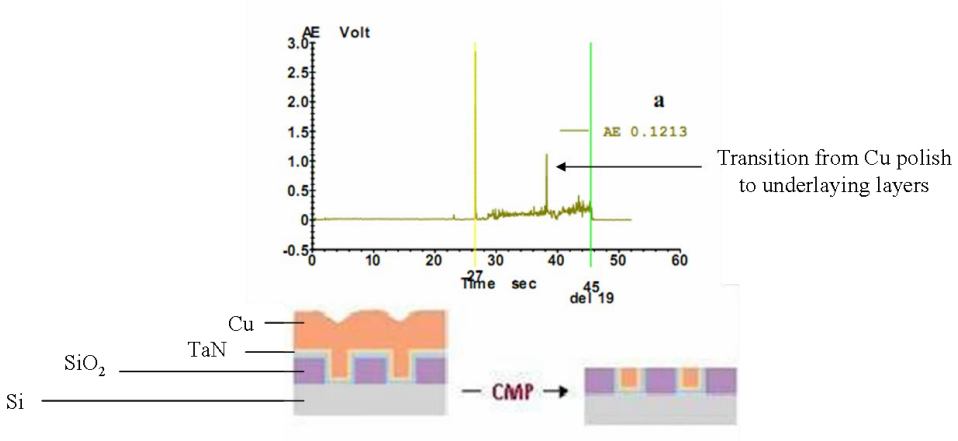

Figure 2. 12 AE signal to CMP polish layer change

From figure 2.12 the copper layer is deposited onto the barrier tantalum layer and then polished as the AE signal transitions the onset of polishing of the ILD-SiO_2 layer is evident. Either in-situ or post CMP analysis of the COF data allows for the calculation of the time to remove a particular layer such as copper, and allows for calculation of MRR [75]. Careful monitoring of these parameters can ensure that the samples are not over polished, and will avoid surface defects.

By running a variance sequential probability ratio test (SPRT) on the COF signal data, the EPD can be detected more effectively [75]. This will allow for not only the removal rate and EPD to be determined but also the uniformity of the polish can be estimated from the COF data. This can be done by monitoring the time for the COF transition from one end point to the next end point level. The longer the transition time, the higher the non-uniformity [76]. The same SPRT analysis can be done on the AE signal to determine process induced defects such as delamination and generation of micro scratches.

2.5 Modeling in CMP

It is evident from previous sections that CMP is a multi physics problem that incorporates multiple disciplines such as; chemistry, fluid mechanics, particle dynamics, solid mechanics, and physics which all combine to contribute to the removal at the wafer-pad interface. The lack of detailed knowledge on these effects on the 2 billion dollar semiconductor and magnetic hard drive industry has the driven industry to empirically tune the process. This has lead to several process models developed to help to optimize the process and predict the MRR and surface quality after polishing.

2.5.1 Preston Model

The most basic and referenced model to describe the CMP process was first proposed by Preston for glass polishing [51]. From section 2.3.1, the polishing of silicon dioxide, which is a form of glass, is approximated by Preston's equation, found in equation (2.3):

$$MRR = \frac{K_p * PV}{H} \tag{2.3}$$

where K_p is the Preston coefficient which incorporates several unknown variables such as chemistry effects in the CMP process, P is the pressure applied, V is the relative velocity of the wafer/pad interface, and H is the hardness of the wafer surface. The Preston's equation states that the material removal rate (MRR) is directly proportional to the pressure and the relative velocity and inversely proportional to the hardness of the wafer surface. Preston's wear equation has commonly been used as an approximation for global MRR [77]. From equation (2.3) the pressure applied is shown in equation (2.4):

$$P = \frac{L}{A} \tag{2.4}$$

where L is the load applied, and A is the contact area on the pad. The contact area is not necessarily the geometric area or the actual area surface, because wafer surfaces which are mostly patterned have severe topographies. In these cases the assumed contact area will not be the geometric area of the wafer being polished. This caveat has lead researchers to revise Preston's equation to account for variability in the surface topography based solely on the mechanical interactions of the wafer pad interface.

2.5.2 Mechanical Models

A number of sophisticated wafer surface wear models have been developed to account for various physical phenomena that take place during CMP. The mechanical models that have been developed can be broken into two major categories, empirical wear studies and contact mechanics models.

2.5.2.1 Empirical Wear Modeling Studies

The models that have employed an empirical wear modeling approach, typically account for the pressure and velocity components in the MRR and reference directly back to the Preston equation [77-82]. The empirical models do not often take into account all of the multiphysics phenomena in the process, and historically these models negate the slurry lubrication regime, the abrasive particle dynamics in the system, and the chemical effects of the slurry. Due to these limitations models developed for one tribosystem may not be applicable to a different tribosystem [77].

2.5.2.2 Contact Mechanics Modeling

The studies that have taken contact mechanics approach toward the CMP analysis assume that the wafer and pad surfaces are in direct sliding contact during the CMP process. These models predict that all MRR is due to the pressure and velocity process parameters. Several modifications to Preston's equation have been investigated to determine the wear parameters, and the equation has been proven to be non linear although the major parameters in the removal process remains unchanged [83-86]. Understanding of the contact models used in many approaches to CMP involves understanding of basic elastic contact.

Greenwood and Williamson provided a theory of elastic contact between two mating surfaces that a number of CMP mechanical models incorporate. The Greenwood and Williamson (GW) model and other statistical based models represent the contacting surfaces (pad or wafer) as a probability distributions function (PDF) of surface heights, and by using the PDF calculate the number of asperities contacting the surface. The reaction force (pressure) between the two forces is calculated and utilized to determine MRR.

The weakness of the statistical models is in the model's inability to accurately determine the contact area distribution as a PDF is used to estimate the surface topography [87-90]. To alleviate this approach researchers have used a deterministic approach in which the actual pad and surface topographies are found using metrology tools. Since the deterministic models are based upon the geometry of the contacting surfaces, it allows for both forces response and contact area distribution to be predicted [91-95].

Both methods of modeling exploiting only the mechanical aspects fail to incorporate the polishing regime, slurry abrasive particles and their interaction with the wafer surface, or the fluid mechanics that play a role in MRR.

2.5.3 Fluid Mechanics Models

A set of models has analyzed the CMP process based solely on fluid mechanics modeling of the wear. These approaches assume that the wafer and pad surfaces are completely separated by the slurry and fall into the hydrodynamic lubrication regime. Nanz and Camilletti, and Steigerwald et al. noted the importance of the slurry flow field in the overall CMP process as well as the need for in-depth understanding of the slurry flow at the wafer/pad interface [59, 92, 96]. Many of the fluid based models incorporate the GW model to solve for a contact stress distribution across the wafer and solve for the film thickness to input into the Reynolds equation, a simplified form of the Navier-Stokes equation 2.5. The Reynolds equation is used to relate the slurry pressure field, film thickness distribution, and shear rate to the CMP process. Reynold's 1-D equation shown in equation 2.6, is used to analyze film thickness and pressure distribution of viscous fluids through small gaps (e.g., wafer/pad interface). The full Navier–Stokes equation is shown in equation 2.5,

$$\rho \frac{Dv}{Dt} = -\nabla p + \nabla \bullet \Psi + f \qquad (2.5)$$

where v is the flow velocity, ρ is the fluid density, p is the pressure, Ψ is the deviatoric stress tensor, and f represents body forces (per unit volumes). Equation (2.5) is

simplified for Newtonian fluids, incompressible, constant viscosity, steady state flow, in one dimension to Reynold's equation shown in equation 2.6,

$$\frac{d}{dx}\left(h^3 \frac{dp}{dx}\right) = 6\mu U \frac{dh}{dx} \tag{2.6}$$

where p is the hydrodynamic pressure, h is the local film thickness, μ is the dynamic viscosity of the slurry, U is the relative velocity of the bottom surface (pad), and x is the downstream distance. The slurry pressure distribution is key parameter in the fluid mechanics modeling of CMP because it dictates whether the wafer and pad surfaces are in contact (negative pressure) or are completely separated by the fluid (positive pressure). Results from the solutions of the Reynolds equation are then combined with mass transport theory in order to predict the material removal rate distribution over the surface of the wafer.

Most of the aforementioned fluids modeling studies neglected the effect of the abrasive particles on the rheology of the slurry. Studies assumed that the wafer was fixed and the pad was the only rotating surface, which is not the case in the industrial process in which the pad and wafer rotate about different axes. These studies do not account for the wafer bending, pad deflection, slurry particle entrapment on the pad, or the corrosivity of the slurry on the surface as it "breaks down" the surface prior to polishing.

2.5.4 Hybrid Models (PAML)

In order to fully incorporate all of the physical aspects of the CMP process several hybrid models have been developed to try to successfully predict process outcomes. These models have combined the contact mechanics and abrasive particle into one model, while other studies have integrated the fluid mechanics and contact mechanics into their

predictions [78, 81, 82, 97-99]. While these studies included one or two of the main physical aspects the model by Terrell and Higgs captures all combinations of the physics of CMP. This model contains the fluid continuum modeling for the slurry flow and pressure distribution, the deterministic contact mechanics modeling allowing for true forces response and contact area distribution to be predicted, particle dynamics modeling of the abrasive particles in the slurry, and first principle wear modeling. This model was unique in the fact that it uses first principle approaches to model the CMP process, including the actual measured surface of the sample to be polished, the model has the variability to change the micro scale input parameters, and it is one the first models that allow for greater prediction of local wear phenomena. The model did not incorporate surface properties and characteristics and the analysis of the hardness variation within the PAML was investigated and discussed in subsequent chapters.

2.6 Challenges During the CMP Process

Although CMP has become the choice for local and global planarization, it also comes with its own inherent challenges as with any planarization process. The challenges for the process start with the number of materials utilized for copper/low k integration. Throughout this research project the challenges faced are:

1) Local and global non planarity
2) Etching and contamination
3) Microscratching
4) Delamination.

The following sections will detail the challenges faced when polishing bit patterned matrix configurations.

2.6.1 Non Planarity

The post polish planarity is a result of several factors and cannot generally be limited to one factor. The etch and dissolution rate of the slurry, pad asperities contact area, and non-uniform pressure distribution on the patterns with line width and density issue are a few of the issues [100, 101]. Figure 2.13 shows the various post CMP surface characteristics that result due to the factors at different pattern densities and line widths.

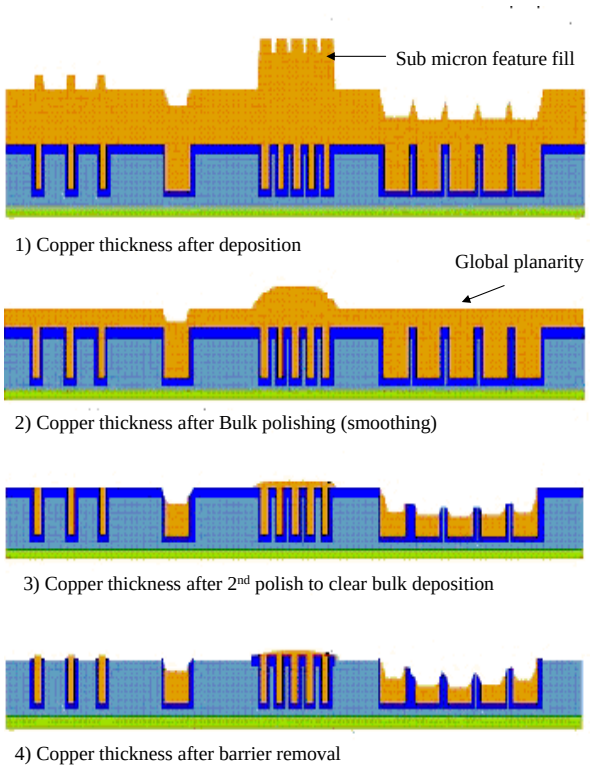

Figure 2. 13 Cu CMP surface characteristics

From the figure 2.13 the second and third step prove to be the most critical in compared to the global planarization step. There are four major surface defects that result in a surface that deviates from a planar surface:

1) Dishing
2) Erosion
3) Oxide loss
4) Metal loss.

2.6.1.1 Dishing and Erosion

A schematic illustration of dishing and erosion defects is shown in figure 2.14. The dishing effect is characterized by high polishing rates in localized regions where the pattern is significantly different from its surrounding. The formation of trough shaped dish has been attributed to excessive over polishing in these areas and an efficient EPD helps to prevent this defect.

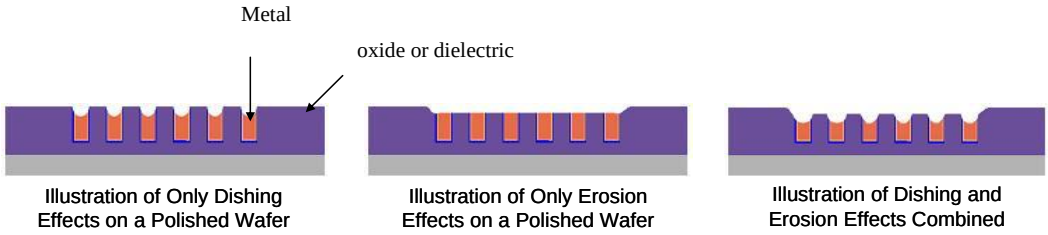

Figure 2. 14 CMP challenges

2.6.1.2 Oxide and Metal Loss

During copper CMP, a minuscule amount of over polishing is required to remove all metallic residues on the dielectric surface to ensure electrical or magnetic isolation between adjacent components. Oxide loss is the loss of the field oxide next to an array of

thin metal lines separated by a wide oxide pattern [102, 103].Metal loss is the total loss of thickness of metal lines separated by a thin oxide pattern.

All of these post CMP characteristics affect the electrical properties of the interconnect structure, chip reliability, and induce non planarity over the wafer surface, which in turn causes photolithography issues negating the initial use of CMP. The process parameters and consumables that cause these characteristics need to be understood in detail to avoid reduction in device yield.

2.6.2 Surface Scratches

The mechanical interaction of the abrasive particles within the surface of the wafer (two body abrasion) leads to plastic deformation and surface damage to the wafer surface. Although the plastic deformation is necessary to complete the fundamental job of CMP process, scratches, both macro and micro, can form due to the deep indentation and dragging of the abrasive particles as seen in figure 2.15.

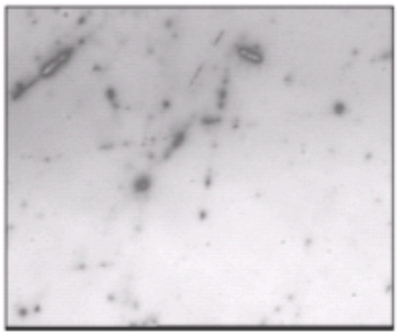

Figure 2. 15 Optical image of surfaces scratches from CMP

Many factors such as particle size, distribution, and formations of agglomerates due to slurry pH are possible factors contributing to surface scratches. A number of the surface scratches can be removed during the final buffer polishing, but the deeper

scratches are permanent and cannot be removed from the surface. As with dishing and erosion, the surface scratches reduce the usable yield of the wafers and impact electrical and magnetic schematic designs. Development of novel slurries to reduce scratches while maintaining performance continues to be a driving factor in research and is presented in chapter 5 of this dissertation.

2.6.3 Delamination

In conjunction with replacing aluminum with copper, another way to reduce RC delay is introduction of materials that have lower dielectric constant (low-k) than SiO_2. The drawback of introducing low-k materials is that they are mechanically weak materials [46, 104-109]. The low-k materials cannot withstand the shear forces applied by the shearing motions of the platen and wafer carrier during CMP. Their interfacial adhesion energies are low and even moderate frictional forces can induce failure of these interfaces [110]. The delamination shown in figure 2.16 has not been attributed to one factor but studies have proven that in order to reduce the delamination low pressures and velocities are ideal to during the CMP process.

Figure 2. 16 Delamination from copper CMP

Reducing the pressure and velocity leads to an increase in the number of polishes needed to complete a cycle for an individual wafer and an increase in processing time ultimately costing industry money. Therefore, fundamental studies are under current investigation to help understand the delamination phenomena.

The aforementioned defects destroy the devices and increase the cost of production. These defects along with post CMP characteristics such as dishing and erosion need to minimized if a successful implementation of the process is to be achieved [46]. Yield and throughput of the polishing process is highly dependent on the process parameters and consumable characteristics which is the focus of this dissertation.

2.7 Conclusion Research Objectives

The CMP process is a multidisciplinary problem in which the output metric are not directly tied with any one input metric. As shown in figure 2.17 the process must be broken into several sub factions and investigated individually in order to fully understand each parameter's contribution to the output.

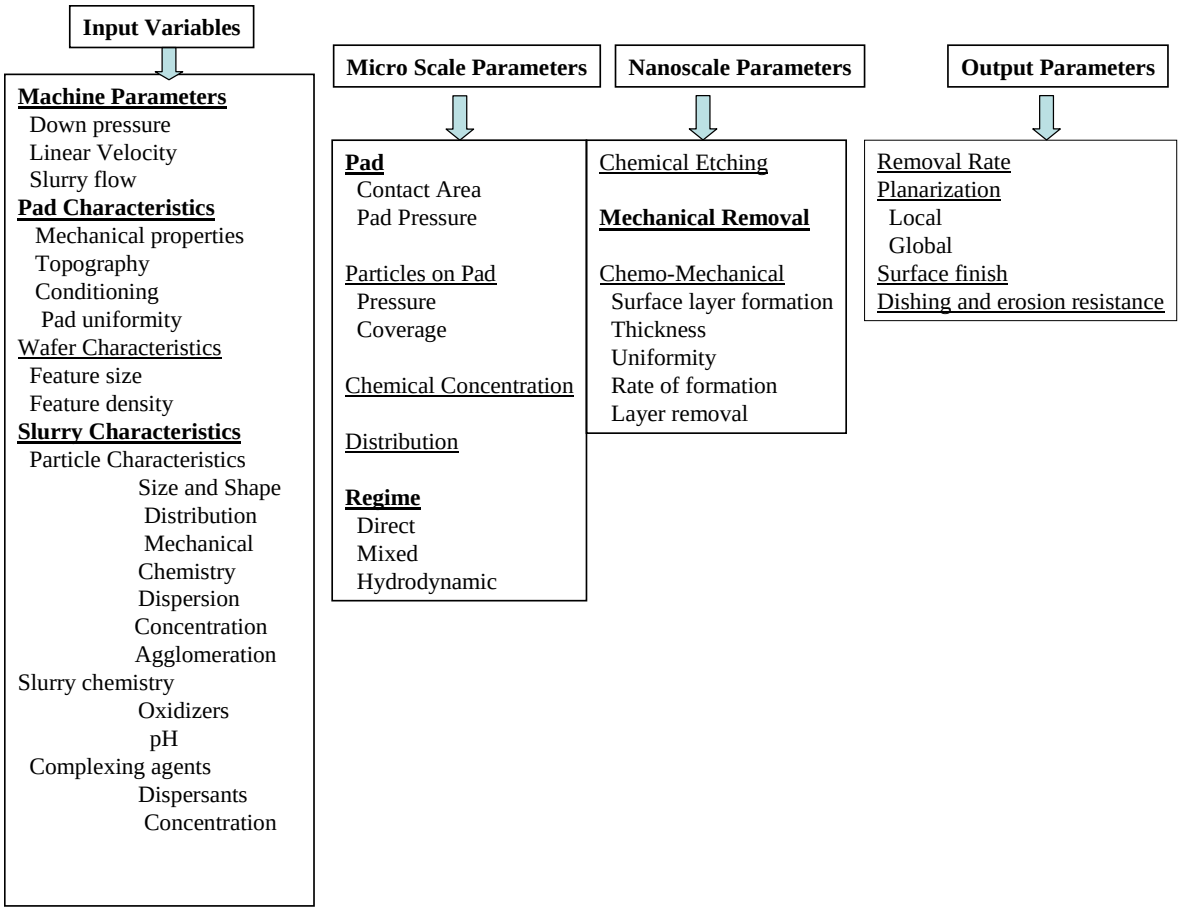

Figure 2. 17 CMP process factors

Figure 2.17 shows the CMP process broken into its individual subsections. The bolded subsections are detailed and outlined in this dissertation. All of the output factors are characterized based on the input parameters. The objectives of this research are to broken into phases and are as follows:

The first phase of this research will provide:

1) Provide benchmark data CMP on BPM configurations
2) To optimize the MRR and surface quality based on input parameters
3) Evaluate mechanical properties evolution during CMP of BPM

4) Complete a statistical analysis on the input parameters to determine which parameter in paramount in BPM CMP.

Following optimization of the machine parameters Phase II will:

1) Investigate pad wear on BPM CMP
2) Perform a parametric study of pad wear, pad roughness, COF, MRR, surface morphology
3) Give a qualitative analysis on the pad life, surface characteristics of the wafer, pad, and polishing regime
4) Determine optimal polishing pad for CMP of BPM from three commercially available pads.

Finally the optimized machine parameters and optimal pad are used in phase III which will:

1) Develop and investigate new nanodiamond (ND) slurry for BPM CMP
2) Determine the MRR and surface quality based on the new ND slurry.
3) Compare and contrast the novel ND slurry versus industrial slurry CMP.

This dissertation also contains a separate investigation into microstructural variation in mechanical properties during polishing and evolution of the MRR and surface roughness due to the variation. A model is developed to predict the evolution for standard abrasive grinding process and the resulting surface qualities and MRR are reported. The model uses deterministic pad and wafer surfaces to check validate the PAML model developed at CMU, based on incorporation of microstructural variation.

CHAPTER 3: CMP PROCESS MACHINE PARAMETER OPTIMIZATION

3.1 Foreword

Patterned media data storage technology aims to increase areal storage density by utilizing chemical mechanical planarization (CMP) as a planarization technique to create atomically smooth surfaces for the read/write head to fly across. Due to the novelty of the patterned media process there is limited data on the planarizing process of the patterned media (PM) structures. This phase of research focuses on improving the output parameters of material removal and local and global planarity, based on the machine input parameters of pressure and velocity from figure 2.17, and detailed in figure 3.1.

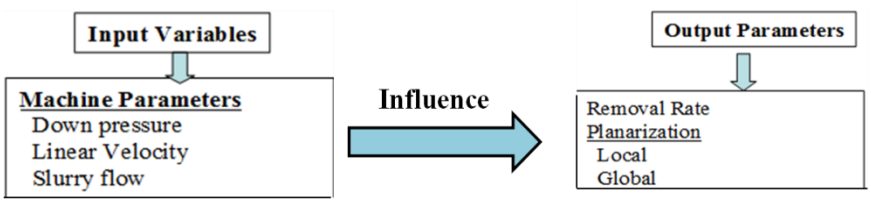

Figure 3. 1 Machine process parameters optimized for PM polishing

These machine parameters have been proven to be the main contributing factors in material removal and surface quality for integrated circuit CMP, and therefore shall be investigated in this chapter. A secondary analysis is performed based on the evolution of the mechanical properties during polishing, while a tertiary statistical analysis of variance (ANOVA) on the fundamental machine input parameters is analyzed and compared against Preston equation for MRR on patterned SEMATECH copper wafers.

In this research, bit patterned matrix (BPM) SEMATECH media samples of Cu are polished at various pressure and speeds and the material removal rate and surface quality are analyzed as an initial case study on the feasibility of CMP for patterned media fabrication. The pre-polishing and post-polishing hardness and elastic modulus were obtained through nanoindentation and discussed in further detail. The purpose is to optimize and benchmark data on CMP of patterned media configurations. In particular the goals of this research are as follows:

1) Provide benchmark data CMP on BPM configurations
2) To optimize the MRR and surface quality based on input parameters
3) Evaluate mechanical properties evolution during CMP of BPM
4) Complete a statistical analysis on the input parameters to determine which parameter in paramount in BPM CMP.

3.2 Patterned Media Data

As described in chapter 1, the data storage industry aims to increase areal storage density by using patterned media (PM) as a new storage technology. PM uses advanced semiconductor processing techniques to fabricate nanomagnetic structures for the purpose of isolating individual grains for magnetic domains into regular patterns [26, 27]. This technology would allow for storage of one bit per cell or grain as shown in figure 1.4 in chapter 1. PM is different from conventional longitudinal drives, shown in figure 3.1, where each bit is stored across a few hundred magnetic grains.

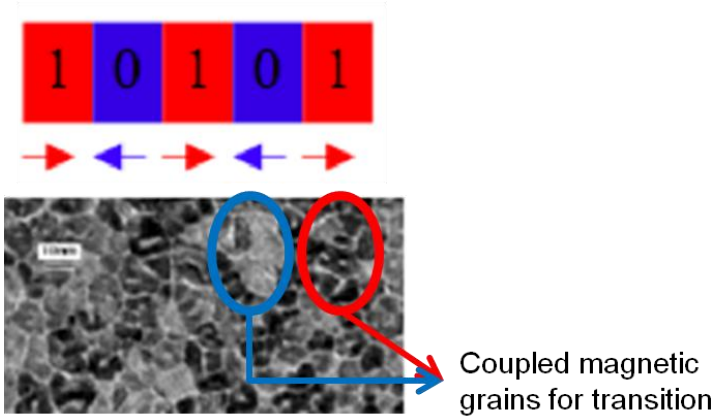

Figure 3. 2 Conventional longitudinal magnetic storage

As recently as August 2010, Toshiba successfully created a 2.5 Tbit hard disk using PM. The fabrication of the disk is the first successful PM hard disk created at the time, but it lacked the functionality of writing or reading data on the disk due to read/write head fly height issues [17]. Without proper understanding of the prominent tribological issues that exist in the fabrication and successful operation of the read/write head in patterned media, this technology will contain remain in research laboratories. Conceivably, a patterned media disk drive will consist of a magnetic slider head that

reads and writes information onto a spinning disk during flight. The Toshiba disk was comprised of micro to nanoscale magnetic structures that must be planarized to prevent lateral collision between the slider and coarse topography on the disk surface as shown in figure 3.3.

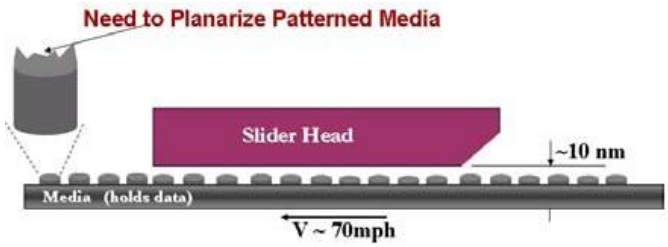

Figure 3. 3 Read/write slider head on PM

Fabrication of patterned media data storage devices utilizes semiconducting manufacturing techniques. These techniques include and are not limited to electrodeposition, evaporation and liftoff, etching processes, and chemical mechanical polishing (CMP) for planarization [26].

As discussed in chapter 2 the CMP process, shown in figure 3.4, is a vital interim fabrication step for integrated circuits (IC) and data storage devices where it is used to planarize thin film surfaces down to atomic smoothness.

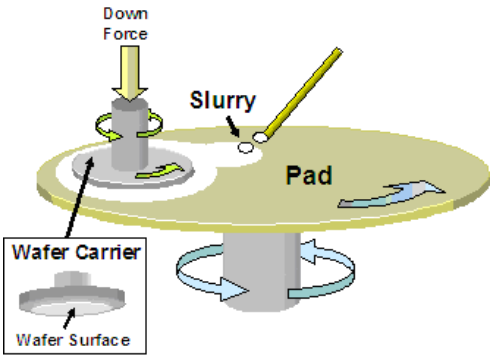

Figure 3. 4 CMP process

The material removal rate (MRR) affects the surface topography and thereby performance and reliability. The MRR corresponding to CMP is given by the rudimentary Preston equation, which contains the load applied, the relative velocity of the pad to the wafer carrier, the Preston coefficient that includes chemical dependencies, and the hardness of the material. Tribological MRR models mainly account for the mechanical removal [99, 111] and weakly account for the chemically-induced removal [66, 112] by using a sophisticated form of the well-known Preston equation (3.1)

$$MRR\,(x,y) = \frac{k \cdot P_{app}(x,y) \cdot U}{H} \tag{3.1}$$

where k is the Preston coefficient which accounts for the chemical and mechanical removal based on polishing experiments, P_{app} is the applied pressure on the wafer, U is the relative velocity between the wafer carrier and polishing pad, H is the hardness of the material being removed, and MRR is the material removal rate (typically in nm/min).

Since CMP is predominantly used for semiconductor IC applications, there is limited data available related to the polishing of thin films in PM configurations for

advanced data storage applications. Therefore, this effort will provide key benchmark data from CMP patterned media experiments that will answer questions about the viability of producing atomically smooth PM by CMP.

3.3 Experimental

3.3.1 Candidate Samples

Unless otherwise noted, all processing and characterization steps were completed in the Nanotechnology Research and Education Center (NREC) at the University of South Florida. The wafers unless otherwise noted were purchased from SEMATECH Inc. In order to fully characterize and optimize CMP on the 8" 1.012μ thick P-type copper patterned SEMATCH wafers, the wafers first had to be diced into their individual repeating patterns for polishing and mapping purposes. Prior to dicing a thin layer of SU-8 negative photoresist was deposited using the laurel spinner on the SEMATCH wafers in order to ensure no oxidation or mineral deposition on the wafers during the dicing process. The wafers were diced along the individual dicing axes and resulted in 1" by 1" wafer coupons. The photoresist was removed using acetone for characterization and experimentation. The wafers utilized a MIT 853 pattern developed and fabricated by Park et al. shown in figure 3.5 [113-115].

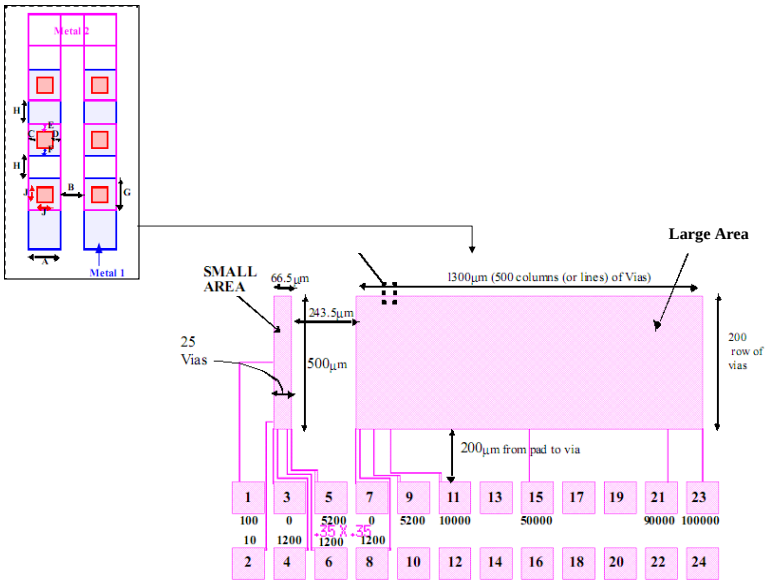

Figure 3. 5 MIT 854 pattern sublevel

The Cu/low-K CMP test mask set consists of three layers and thus three masks—M1 mask, via mask, and M2 mask enabling the study of multilayer issues in Cu CMP. However, the M1 mask itself is purposely designed to be efficiently used for characterizing single layer polishing behaviors. This M1 single mask contains all of the relevant structures for probing electrical or magnetic bond structures all within the same M1 layer [116]. Details of the pattern specifications and fabrication are not incorporated within this research but can be found in the references [116].

This test mask design is concerned with the following aspects of copper chemical mechanical polishing (CMP) with either conventional oxide (e.g., SiO2) or low-K dielectrics as the recession layer:

1) Intralevel Metal 1 (M1) polishing pattern effects resulting from various pattern factors created by combinations of different line widths and line spaces (e.g., density, pitch) and combinations of structures

2) Interlayer multilevel effects of polishing pattern effects with non-uniform topography on a layer below; effects on Metal 2 (M2) polishing of surface topography generated by M1 polishing

3) Intralayer (lateral) and interlayer capacitance and resistance variations from polishing non-uniformity (e.g., dishing and erosion) [116]

The MIT 854 samples are fabricated in a reversed patterned media configuration which is different from that of the patterned media configurations mentioned in chapter 1 as shown by the gold metal representation in figure 3.6.

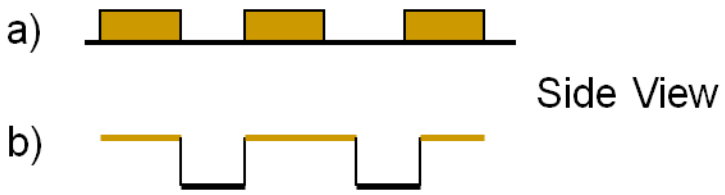

Figure 3. 6 Patterned media configurations

The planarization of repeating patterns on a Cartesian grid is fundamentally similar to conventional PM, and the interest of this dissertation lies in the fundamental science with CMP of these types of heterogeneous matrices. Therefore, through the remainder of the experimentation the reversed configuration will be notated as a bit patterned matrix (BPM) configuration. Table 3.1 gives the parameters for the BPM characterized samples.

Table 3. 1 Metrics for SEMATECH samples

Characteristic BPM SEMATECH Sample	Parameter Value: English (metric)
Diameter	6 in± .0009 (152.4 mm)
Length	1 in ± .0039 (25.4 mm)
Width	1 in ± .0039 (25.4 mm)
Initial film thickness	3.937E-05 (1.02 µm)

Figure 3.7 is an optical image of the BPM of the MIT 854 pattern at two different magnifications, and figure 3.8 is a focused ion beam (FIB) image of the patterned media configuration of the wafers.

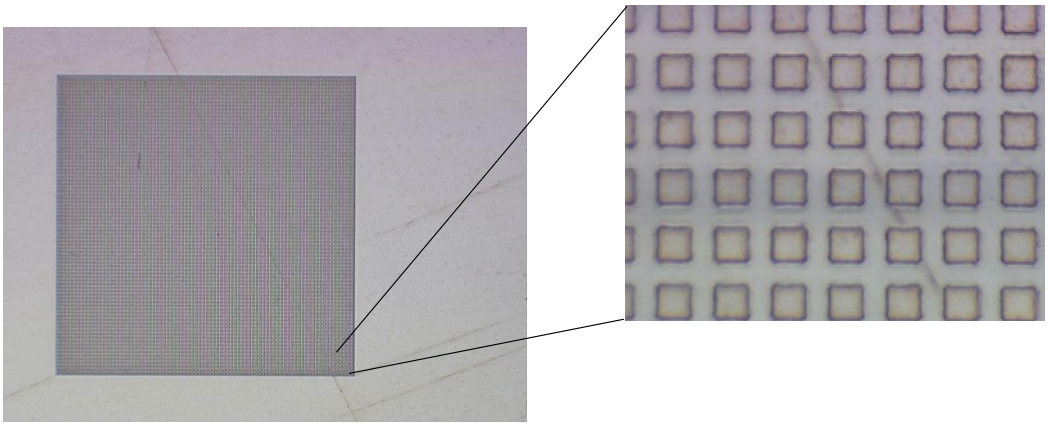

Figure 3. 7 Optical microscope images of BPM at 30x and 500x

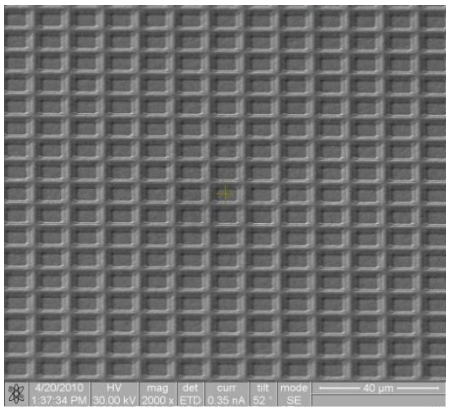

Figure 3. 8 FIB image of patterned media configuration

Figure 3.8 was taken at a magnification of 2000x with an accelerating voltage of 30 kV. From the figures above the individual bit pattern matrix (BPM) is shown in detail. This matrix configuration is analogous to the magnetic patterned media storage configurations utilized by the magnetic storage industry. The copper BPMs utilized throughout this dissertation were fabricated using some of the same semiconductor fabrication techniques as magnetic storage industry.

3.3.2 Mechanical Properties

The mechanical properties of the thin film being polished play an important role during CMP. The surface scratches, being one of the most critical aspects that determine polishing performance depend on the mechanical properties of the sliding surface. The harder the surface being polished, the harder the abrasive needed to polish the surface. This relationship can lead to scratches, cracking, dishing, and erosion of the underlying material during polishing. Following the removal of the photoresist, the mechanical properties of the BPMs were measured by nanoindentation using the Nano Indenter® XP (MTS System Corporation, Oak Ridge, TN) shown in figure 3.9. The elastic modulus and hardness were taken using a MTS Nano Indenter with Testworks 4 software.

Figure 3. 9 MTS Nano Indenter® XP

Nanoindentation is similar to conventional hardness tests, but is performed on a much smaller scale using very sensitive load and displacement sensing equipment. The force required to press a three-sided Berkovich-shaped diamond indenter into the candidate samples is recorded as a function of indentation depth. The load and unload displacement data obtained in the nanoindentation tests were analyzed according to the method of Oliver and Pharr [117, 118]. An example of a standard nanoindentation curve is shown in figure 3.10.

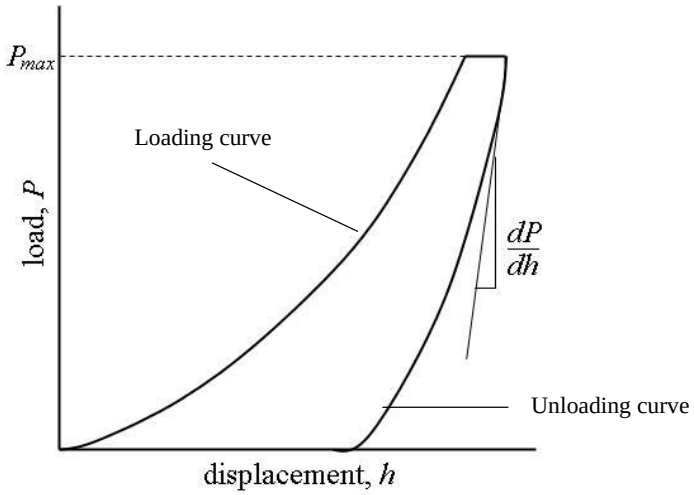

Figure 3. 10 Typical nanoindentation curve [119]

The stiffness and thereby modulus of elasticity is calculated from the unloading portion of the load displacement curve shown in figure 3.10. The continuous stiffness measurement (CSM) technique was used for measuring absolute and depth dependent hardness and modulus values. Equation 3.2 represents the equation utilized by most standard nanoindentors;

$$S = \frac{dP}{dh} = \frac{2\sqrt{A}}{\sqrt{\pi}} E_r \tag{3.2}$$

where S is the contact stiffness, and A is the contact area. In order to use equation 3.2 two keys assumptions are made:

1) Deformation upon unloading is purely elastic thus implying that the entire load is recovered and there is no plastic deformation into the wafer surface
2) Contact between the rigid indenter and the sample is modeled using Sneddon's equation.

The deformation of the sample and of the indenter tip can be combined and given as a reduced elastic modulus as shown in equation 3.3 [117, 119];

$$\frac{1}{E_r} = \frac{1-\nu_s^2}{E_i} + \frac{1-\nu_s^2}{E_s} \tag{3.3}$$

where E_r is the reduced modulus, υ is Poissons ratio, and the subscripts i and s represents indenter and sample respectively.

The hardness of the thin film being indented can be determined as the ratio of the maximum load, P, and the area of contact, A, equation 3.4 shown below.

$$H = \frac{P}{A} \tag{3.4}$$

The depth of penetration for the indenter was fixed at ~50% of the sample film thickness. The calculations of mechanical properties were performed at 50% of the indentation depth (e.g., ~25 % of the film thickness) [120-122]. At this depth the substrate effects as well as the effect of the surface oxide is avoided when calculating the mechanical properties [123]. Figure 3.11 shows an AFM image of the indented samples.

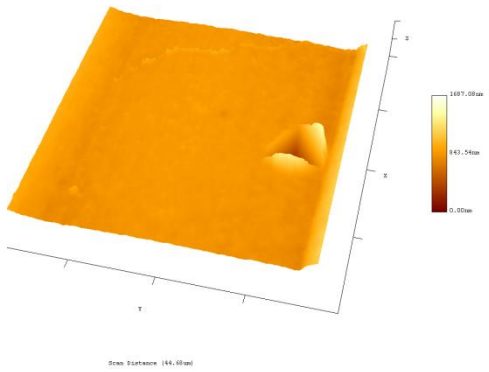

Figure 3. 11 Nanoindentation into BPM

Using the optical camera in the nanoindentor recognizable regions were chosen in the MTS nanoindentor for pre and post CMP measurements. A 40-micron by 40-micron indention square was created for statistical averaging of the nine indents done per sample. Mechanical property values were calculated by averaging a number of separate indentations at various depth specifications. Initially the instrument was calibrated with the standard sample (fused silica) provided by MTS along with other single crystal metal samples.

Values of the hardness and Young's modulus before and after CMP have been tabulated in table 3.2. Details of the mechanical properties impact on CMP will be discussed in later sections of this chapter.

Table 3. 2 Nanoindentation results of BPM copper

Patterned Copper Sample	Elastic Modulus (GPa)	Hardness (GPa)
Unpolished	121.657±3.152	1.249 ± 0.121
1 Psi	129.828±1.090	1.440±0.058
3 Psi	135.419±0.752	1.609±0.061
6 Psi	138.594 ± 1.292	1.962± 0.208

3.3.3 WYKO Surface Profiler

The surface topography and planarity of the wafers was measured using Wyko NT9100 surface profiler by Veeco Instruments Inc shown in figure 3.12.

Figure 3. 12 Wyko NT9100 surface profiler

Wyko surface profiler systems are non-contact optical profilers that use two technologies to measure a wide range of surface heights, phase-shifting interferometry and vertical scanning interferometry. Phase-shifting interferometry (PSI) mode allows you to measure smooth surfaces and small steps, while vertical scanning interferometry (VSI) mode allows you to measure rough surfaces and steps up to several millimeters high [124]. Phase-shifting interferometry (PSI) has typically been used to accurately measure previously smooth surfaces. In phase-shifting interferometry, a white-light beam is filtered and passed through an interferometer objective and onto the test surface. The interferometer acts as a beam splitter reflecting half of the incident beam onto the reference surface within the interferometer and the other half to the test surface. The beams reflected from the test surface and the reference surface recombine to form interference fringes. These fringes are the alternating light and dark bands that can be seen when the surface is in focus. Figure 3.13 shows a diagram of an interference microscope.

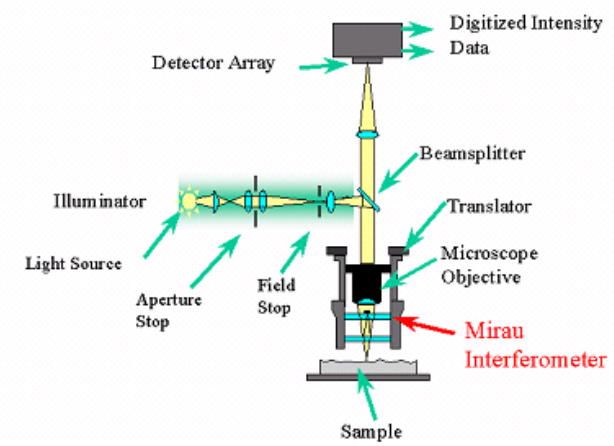

Figure 3. 13 Interference microscope [124]

During the measurement, a piezoelectric transducer (PZT) moves the reference surface a small, known amount to cause a phase shift between the test and reference beams. The system records the intensity of the resulting interference pattern at many different relative phase shifts, and then converts the intensity to phase data by integrating the intensity data.

The phase data is processed to remove phase ambiguities between adjacent pixels, and the relative surface height can be calculated from the phase data shown in equation 3.5;

$$h(x, y) = \frac{\lambda}{4\pi}\phi(x, y) \tag{3.5}$$

where λ is the wavelength of the source beam, and φ(x, y) is the phase data. This technique for resolving surface heights is reliable when the fringe pattern is sufficiently sampled. When the surface-height difference between adjacent measurement points is greater than λ/4, height errors in multiples of λ/2 may be introduced and the phase data

cannot be reliably reconstructed [124]. Thus, conventional phase-shifting interferometry is limited to fairly smooth, continuous surfaces and due to the rougher BPM surfaces encountered during polishing the vertical-scanning interferometry (VSI) technique is employed.

The basic interferometric principles are similar in both techniques: light reflected from a reference mirror combines with light reflected from a sample to produce interference fringes, where the best-contrast fringe occurs is typically at the best focus. However, in VSI mode, the white-light source is filtered with a neutral density filter, which preserves the short coherence length of the white light, and the system measures the degree of fringe modulation, or coherence, instead of the phase of the interference fringes [125]. The system scans through focus (starting above focus) as the camera captures frames of interference data at evenly-spaced intervals. As the system scans downward, an interference signal for each point on the surface is recorded. The system uses a series of advanced computer algorithms to demodulate the envelope of the fringe signal. Finally the vertical position corresponding to the peak of the interference signal is extracted for each point on the surface. Table 3.3 has a comparison of both modes and the resolutions ranges for scans.

Table 3. 3 Comparison of VSI and PSI modes in Wyko surface profiler

Process Parameter	VSI	PSI
Light	Neutral Density filter for white light	Narrow bandwidth filtered light
Scanning and Focus	Vertically scans the objective actually moves through focus	phase-shift at a single focus point the objective does not move
Data processing	Processes fringe modulation data from the intensity signal to calculate surface heights	Processes phase data from the intensity signal to calculate surface heights
Vertical Resolution	3nm single scan <1nm scans averaged	3 A° single scan 1 A ° scans averaged
Range	2 mm	160 nm

From table 3.3 the range refers to the greatest vertical distance the profiler can accurately measure. Given the high initial roughness of the BPM configurations from the MIT 854 pattern the VSI mode was chosen as the mode used in the WYKO NT9100.

The Wyko NT9100 has several outputs for the roughness of the surface being examined, the average roughness, R_a, and the root mean squared (RMS) roughness, R_q, are both displayed in the results throughout this dissertation. R_a represents the two-dimensional roughness average, the arithmetic mean of the absolute values of the surface

departures from the mean plane. R_a is normally used to describe the roughness of machined surfaces. The effect of a single spurious, non-typical peak or valley will be averaged out and have only a small influence on the value. This statistic cannot detect differences in spacing or the presence or absence of infrequently occurring high peaks and deep valleys; therefore, it gives no information as to the shape of the irregularities or surface [124]. The R_a value is useful in determining the global planarity of the surface as it is an average of the hills and valleys of the surface.

R_q represents the root mean square (RMS) roughness, obtained by squaring each height value in the dataset, then taking the square root of the mean. RMS roughness is generally used to describe the finish of optical surfaces. It has statistical significance because it represents the standard deviation of the surface heights. RMS roughness cannot detect differences in spacing or the presence or absence of infrequently occurring high peaks and deep valleys; therefore, these statistics give no information as to the shape of the irregularities or surface. A surface with a high spatial frequency may have the same Rq as a surface with a low spatial frequency, but may behave radically differently. Because height values are squared in the calculation, the RMS roughness statistics are more sensitive to peaks and valleys than average roughness statistics [124]. The RMS roughness will be utilized for local planarity and is also insightful for the global planarity of the surface.

Prior to taking any measurements the VSI mode is calibrated against a 10μm step height standard that is supplied by VEECO. This calibration was done daily and the system would only allow further measurements if the calibration was within ± 0.5% of the calibration sample.

3.3.4 CETR Benchtop Chemical Mechanical Polishing Tester

All of the CMP tests ran on BPM in this dissertation were done with a benchtop CMP tester (CETR Inc, Ca) shown in figure 3.14. The machine process parameters discussed in the chapter are inputs for the CMP process on the CMP tester.

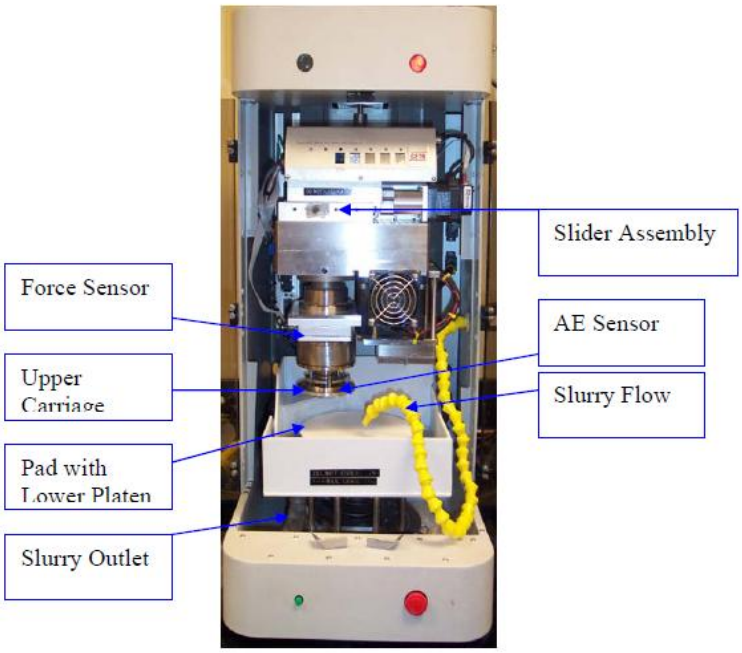

Figure 3. 14 CETR benchtop tester

The CMP tester has several sensors (force sensor, acoustic emission (AE) sensor, and electrical sensor), which are used for in-situ monitoring and optimizing of the CMP process. A strain gauge force sensor (0–200 N) can record both vertical and frictional force and the coefficient of friction (COF) is monitored during the process.

The system is also equipped with a high-frequency acoustic emission (AE) sensor, which can detect the delamination, endpoint, and debris during polishing. As mentioned in chapter 2 the AE analysis is a powerful technology that can be deployed within a wide

range of usable applications of non-destructive testing. The AE sensor works on the basis of elasticity of the materials. All solid materials have certain elasticity and they become strained or compressed under external forces and spring back to original form (given no plastic deformation) when released. Higher input forces and, thus, the elastic deformation, results in higher elastic energies. If the elastic limit is exceeded a fracture occurs immediately given it is a brittle material, otherwise fracture will occur after a given amount of plastic deformation in ductile materials like copper. If the elastically strained material contains a defect, e.g. a welded joint defect, a non- metallic inclusion, incompletely welded gas bubble or similar, cracks may occur at heavily stressed spots, rapidly relaxing the material by fast dislocation motion. This rapid release of elastic energy is what we call an AE event. It produces an elastic wave that propagates and can be detected by appropriate sensors and analyzed. The impact at its origin is a wideband movement (up to some MHz). The frequency of AE testing of metallic objects is usually between 100 and 300 kHz, typical values for ultrasound. The acoustic emission sensor employed in this tester has a frequency range between 0.5 to 5 KHz. The AE sensor, in conjunction with COF, has been used to detect the delamination, endpoint, and debris during polishing.

The CMP tester can hold a pad up to 15.24 cm diameters. The upper carriage can hold sample wafers up to 40mm X 40mm. The upper carriage is connected to a vertical linear motion system that has a travel length of 150mm and can oscillate on the pad during polishing.

The CMP tester is a testing tool and thus the following assumptions are made when different pads, slurries and materials were evaluated;

1) Due to the lack of uniformity on the surface of the coupon, an average of the material removal rate measured at different points from the center to the edge of each BPM coupon and was assumed to be the MRR.

2) During the in-situ detection of MRR using COF the non uniformity of the sample surface brought about gradual tapering of the signals even for blanket samples. The end point was assumed to have occurred when more than 70 % of the material was removed from the surface and further material removal brought significant change in the COF signals.

Further details of the CMP benchtop tester are found in previous literature on the tester [126, 127].

3.3.4.1 Experimental Procedure: Process Parameters

Influence of machine parameters such as down force, relative velocity, coefficient of friction (COF) and material removal rate (MRR) were observed. Based on previous studies and models of the CMP process, relative velocity and pressure were chosen as the influential parameters to vary for the BPM copper CMP [78, 79, 84, 85, 96, 104, 128, 129]. The initial downward force applied to wafer from the CETR tester is calculated using this equation (3.6):

$$F= (P*A)/2.2046 \quad (3.6)$$

where P is the pressure in Psi and A is the estimated contact the area (in^2). The forces applied to the wafers ranged from 1-6 pounds per square inch (Psi). After polishing the wafers are cleaned with acetone and blown dry with compressed nitrogen, to avoid any surface deposition from the slurry or oxidation of the newly polished copper surfaces

(although the oxidation is inevitable to avoid, reducing the oxidation is the closest solution for wear, surface quality, and mechanical property measurements). Table 3.4 shows the variation in process parameters for the polishing experiments.

Table 3. 4 Process parameters for CETR tests

#	Process Parameter	Metric
1.	Pressure	1, 3, 6 Psi
2.	Platen speed	50-300 RPM *$_{\text{increments of 50 RPMs}}$
3.	Wafer carrier speed	50-300 RPM *$_{\text{increments of 50 RPMs}}$
4.	Slider movement	3 mm/s
5.	Slurry flow rate	75 ml/min
6.	Time	120 sec
7.	Pad	Rodel IC 1000 Suba IV k-groove
8.	Specimen	MIT 854 BPM 1”x 1” copper coupons

The polishing experiments were run for 120 seconds and all experiments were repeated five times with a statistical average shown in the results section.

3.3.4.2 Experimental Procedure: Material Removal Rate

The initial thickness of the Cu films were obtained using three different methods to ensure that the beginning thickness was accurate as shown in table 3.1. Initially the copper mask was etched using hydrofluoric acid to the silicon substrate, and then the step edge was measured using a Dektak 150 stylus profilmentor by Veeco. A second

measurement was taken by a Cascade 4 Point Probe Station, with a Keithley current source, and a HP digital multimeter shown in figure 3.15.

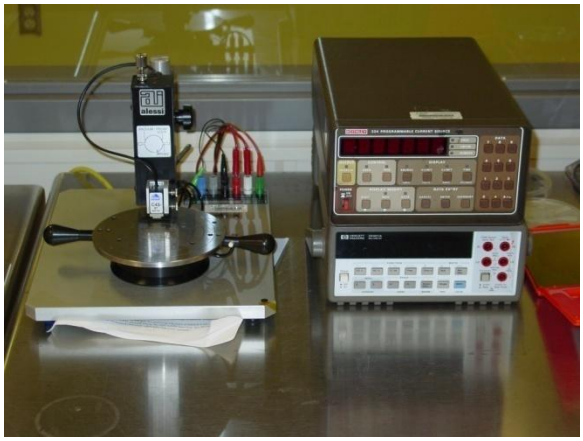

Figure 3. 15 Four point probe station

The second measurement captured the sheet resistance at six fixed points on the diced wafer in the specified patterned region. Equation 3.7 contains the sheet resistance equation used for calculation of the sample.

$$R_s = \frac{\rho}{t} = 4.53\frac{V_m}{I_s} \tag{3.7}$$

where R_s is the sheet resistance, ρ is the resistivity, t is this thickness, V_m is the voltage, and I_s is the current. The value of 4.53 is a constant that is equal to the pi divided by the logarithm of 2. This value is derived from equation 3.8 which is the resistivity of thin film layers [130].

$$\rho = (\frac{\pi}{\ln 2})\frac{t * V_m}{I_s} \tag{3.8}$$

The bulk resistivity of copper is 1.68e-6 ohm-cm and knowing this resistivity the thickness can be solved for given that all other parameters are inputs. During experimentation the average of nine tests is taken for the final thickness measurement with the error shown accordingly in the graphs. The final thickness measurements of the samples were further verified by a Quanta 200 3D dual beam focused ion beam (FIB) by FEI. The procedures for these measurements are detailed below in the transmission electron microscopy (TEM) section. The FIB measurements were taken after individual sections to be analyzed by the TEM were "lifted out" of the sample. It should also be noted that in later chapters the use of the COF for EPD is used to determine the final MRR and by knowing the initial thickness a removal rate can be calculated.

3.3.4.3 Transmission Electron Microscopy (TEM)

With the decrease in feature size below the sub-micron range, transmission electron microscopy (TEM) has become the most important tool for detailed physical failure analysis and material analysis. The focus ion beam (FIB) has become a necessary tool utilized for TEM sample preparation. The samples were prepared using the FIB "lift-out" technique detailed by Overwijk. [131]. The technique involves generally no sample preparation as long as sample sizes are able to fit inside the FIB specimen chamber. A metal line of platinum is deposited over the area of interest and a large stair-step FIB trench is cut on one side of the area of interest and a rectangular FIB trench is cut on the other side of the area of interest. Prior to final thinning the sample is tilted to >45° and then the bottom, left side, and a portion of the right side of the are cut free [132]. Then the sample is tilted back to its starting position and the specimen is thinned to electron transparency. Since the specimen is to be used for high resolution electron

microscopy (HREM), a final FIB cut is performed ~1–2° with respect to the plane of the specimen surface, therefore the thinnest portion of the specimen lies in the area of interest [132]. The finalized sample is imaged using a Technai F20 TEM by FEI Inc, with an accelerating voltage of 200kV. Results from the TEM imaging are discussed in subsequent sections of this chapter.

3.3.4.4 Consumables

A six-inch circular portion of a Rodel, Inc IC 1000 Suba IV A-4 perforated pad was used for polishing. Table 3.5 contains the properties of the pad tested for the experiments.

Table 3. 5 CMP pad material properties

Rodel IC 1000 Suba IV A-4 Parameter	Value: English (metric)
Diameter	32" (81 cm)
Specific gravity	630-800 (kg/cm^3)
Thickness	50 mils (1270µm)
Hardness	57 (Shore D)
Compressibility	2.25%

The pad is conditioned for 20 minutes followed by 1 minute of polishing on a dummy sample, then another 20 minutes of conditioning, followed by another 1 minute of polishing on a dummy sample, and then the final 10 minutes of conditioning of the pad followed by the actual experiments with copper slurry. The conditioning of the pad is used to increase the roughness of the pad to help in the material removal process and reduce glazing of the pad. The fundamentals of the conditioning process are further

explained in chapter 4. During conditioning and dummy polishing deionized (DI) water is used as the lubricant instead of the slurry mixture used in the actual experiments.

The slurry used in these experiments was Cabot iCue 5001which contains 500 nm precipitated alumina oxide abrasive nanoparticles. Nine hundred milliliters of Cabot slurry was combined with 100ml of hydrogen peroxide during polishing of the BPM. A magnetic stirrer was utilized to disperse the mixture and particles in the slurry. The abrasive particles are amorphous in nature and the hardness of the alumina oxide particles can lead to scratches on the surface as discussed in chapter 2. The Cabot iCue slurry is developed for copper CMP and has a low selectivity and etch rate on the silicon dioxide dielectric layer. Due to priority reasons the distribution, shape, and mechanical properties of the abrasive silica particles are not disclosed but the pH of the slurry is maintained at 7.64. Further details on the slurry as a consumable and their interactions during CMP are detailed in chapter 5.

3.3.4.5 Optimization of CMP Experimentation

A statistical analysis of variance (ANOVA) was done with two factors and three levels as the experimental design. The factors analyzed are the pressure and velocity to test the effect these factors had on the MRR during CMP. Table 3.6 described below contains the specifications for polishing of the wafer.

Table 3. 6 Statistical ANOVA table

#	Factor	Level
1.	Pressure	1, 3, 6 Psi
2.	Relative Velocity	0.2, 0.8, 1.2 m/s
3.	Time	120 seconds

Each test was completed three times giving a total of 27 total experiments and values were averaged when completing the ANOVA. The levels chosen were based on IC CMP for the CMP benchtop tester in order to compare the values to previously attained values blanket materials. These factors were chosen to optimize the CMP process for BPM fabrication.

3.4 Results and Discussion

The results from benchmark experimentation on CMP of BPM are detailed below. Analysis on the MRR, lubrication regime, mechanical properties, and a statistical analysis is presented below.

3.4.1 CMP of the Patterned Media Surface

Results of the CMP of the BPM surface are detailed below. The interactions of the output parameters are discussed in the conclusion. Results have an indication on the feasibility of CMP as a fabrication technique.

3.4.1.1 MRR and Pressure

As the pressure is increased and the velocities of pad and carrier are held constant the MRR is also increased, shown in figure 3.16, and this directly correlates to the material removal from Preston's equation.

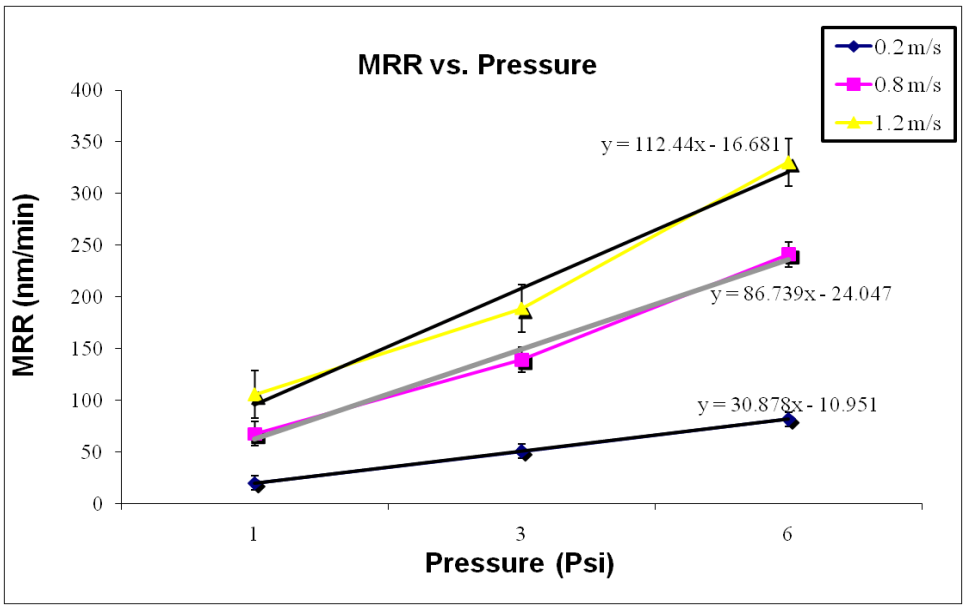

Figure 3. 16 Pressure vs MRR for BPM CMP

As the pressure increases the number of asperities from the pad and abrasive particles that come into contact with the wafer surface asperities increases, causing an increase in the MRR. Consequently the increase in pad to wafer surface contact pushes the polishing regime closer to the boundary lubrication regime which is characterized by high MRR and high surface defects due to lack of a lubricating fluid during polishing. It should be noted that similar tests done on blanket copper wafers at 3 Psi and 1.1 m/s relative velocity yields a MRR from 135 nm/min to 200 nm/min which is on the higher end of the BPM CMP MRR.

3.4.1.2 MRR and Velocity

Similar to section 3.4.1.1 the pressure values are held constant and the velocities are increased to determine the effect of velocity change on BPM CMP. Figure 3.17 shows that as the velocity is increased and pressure is held constant the MRR are also increased.

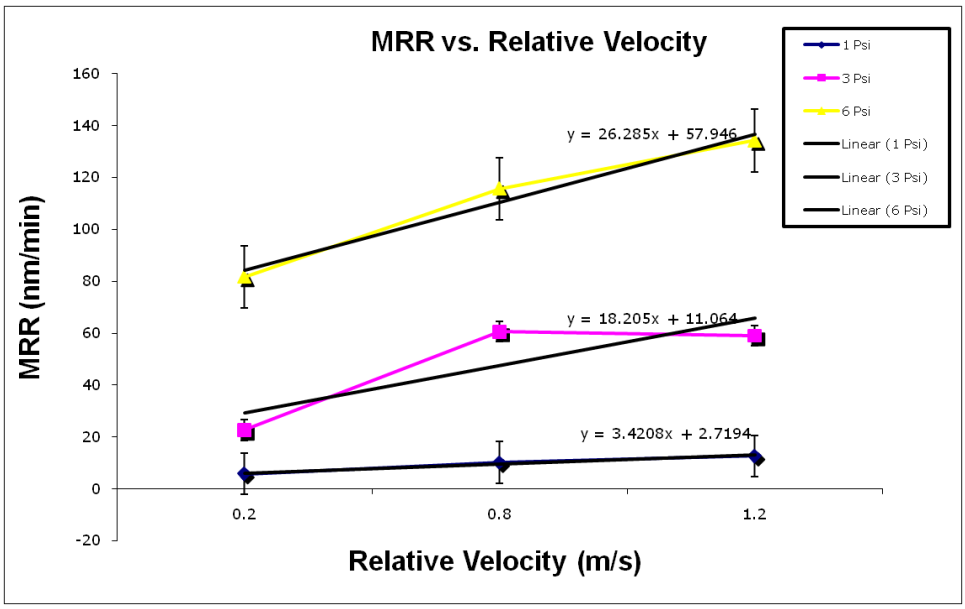

Figure 3. 17 MRR vs. relative velocity

The increase in velocity introduces more abrasive particles from the slurry into contact with the wafer surfaces and pad asperities leading to a higher removal rate [84]. The increase in the velocity does not have the large increases in MRR as with the pressure increase and this can be attributed to the fact that as the velocity increase the number of particles interacting with surface will plateau depending on the concentration of particles in the slurry and further increase in the speed yields little to no effect on the MRR. It should be noted that the both the 1 Psi and 6 Psi curves are linear in fashion with respect to the MRR, while there is a decrease in the MRR at high speeds of the 3 Psi polish.

It is also interesting to note that for the relative velocity plots the linear trend approximation for Preston's equation holds close to the actual MRR, but these estimations are not exact. The relationship is not a linear relationship and this fact has been determined by several other authors [56, 83, 133-135].

Quantitative results indicate that the pressure increase has a more pivotal impact on the MRR than the velocity based on the increases in the values for the MRR from figures 3.16 and 3.17.

3.4.1.3 Stribeck Curve

The COF at the interface is a function of various factors such as surface topography of the pad and wafer and the machine process parameters. The Stribeck curve can be calculated by first calculating the Sommerfeld number shown in equation 2.2 and reproduced below;

$$So = \frac{\mu U}{p\delta} \tag{2.2}$$

In the above equation μ is the slurry viscosity, U is the relative pad-wafer average linear velocity, p is the applied wafer pressure, and δ is the effective slurry thickness in the pad-wafer region. Determination of U and μ are fairly straightforward as the latter can be measured experimentally for a given slurry, while the former depends on tool geometry and angular velocities of the wafer and the platen [136].

Based on knowledge of the Cabot iCue 5001 slurry the viscosity ranges from 1-3 cP, and the average value of 2 cP is used for calculation of Sommerfeld number. This number will shift the Sommerfeld number to the left or right based on the other parameters but will not affect the overall importance of the regime.

Previous dual emission laser induced fluorescence (DELIF) experimental results by Coppeta and Lu have shown that the slurry film thickness in the pad-wafer region ranged from 20 to 40 μm [137, 138]. Li et al. proposed using the surface roughness of

the pad to estimate the δ in the Sommerfeld equation as their results indicated a pad roughness form 20 to 50 μm [136]. In this study through WYKO surface profiler the pad roughness was found to be closer to ~10 μm and will be used as an estimate of the slurry thickness. This approximation resulted in the calculated Sommerfeld number to shift to the right or to the left, in the data but had no effect on the trends of the Stribeck curves [136]. The film is considered to distribute the pressure and eliminate the effect caused by different grooves. Therefore the wafer pressure is defined as the applied down force divided by the wafer area [136]. Figure 3.18 is the Stribeck curve for the polishing parameters for experimentation in table 3.4.

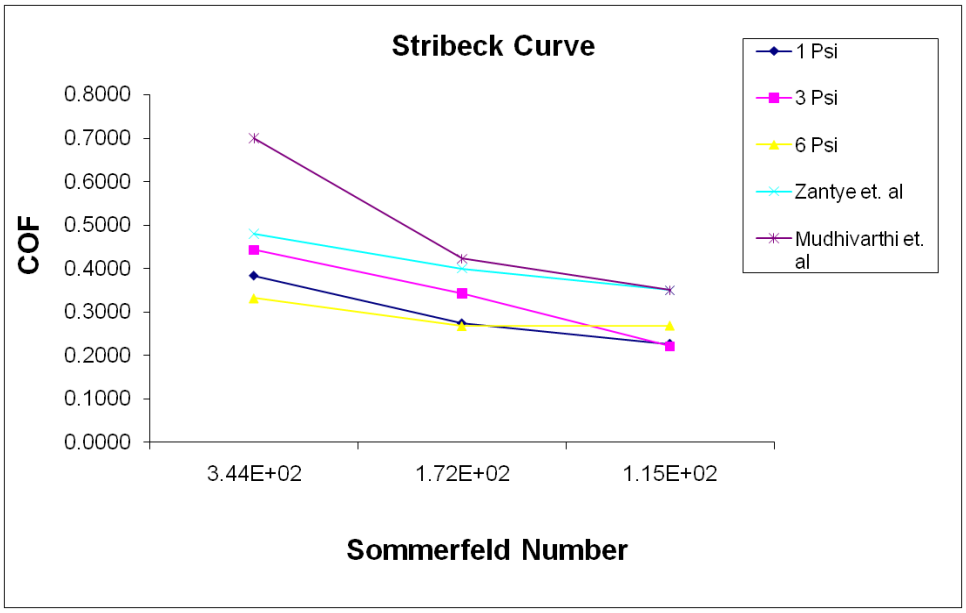

Figure 3. 18 Stribeck curve

From figure 3.18 it is evident that all three polishing pressures undergo transitions into all three lubrication regimes. All of the process start with the boundary lubrication regime in which the fluid carries little or none of the pressure applied. In this regime the

pad asperities and the wafer asperities are in direct contact and all of material removal is due to mechanical interactions of the pressure and velocity. Consequently due to the lack of slurry lubrication the COF is highest in this regime and the thermal energy dissipated in the case must be very high resulting in non uniform and inconsistent material removal. All curves then transition to the hydrodynamic or partially lubricated regime, in which the pad to wafer contact and the slurry interaction play a role in MRR. The slurry along with the abrasive nanoparticles within slurry interacts with the wafer surface causing chemical corrosion and mechanical removal. This regime has high MRR and low surface defects; the longer a process is in this regime the better the results for the output parameters. The final transition occurs at the end of polishing to the fully lubricated regime in which the slurry contributes to all of the MRR, because the pad and wafer are not in contact. Polishing in this regime results in smooth surfaces but to increase the MRR, the velocities of the pad and wafer must be increased up to a threshold value.

These regimes from the Stribeck curve are consistent with the calculated Stribeck curves from literature but for the BPM wafers the COF values are all larger than standard copper CMP [45, 46]. The blanket copper wafers have a greater decline in the COF over the course of polishing and this fact could be due the planarization of the thin film in blanket copper CMP, whereas the BPM configuration polishing is not fully planarizing the surface but rather a smoothing surface as seen in figure 2.13. This leads to a fairly constant value of the COF during polishing. The COF also gives a measure of polishing intensity at the interface which would result in heat dissipation generation of thermal energy from mechanical interaction [126, 139]. Thus, measure of the COF at the

interface during CMP gives vital information about the polishing and removal mechanism. Figure 3.19 gives the MRR versus the COF for the three-recorded pressures.

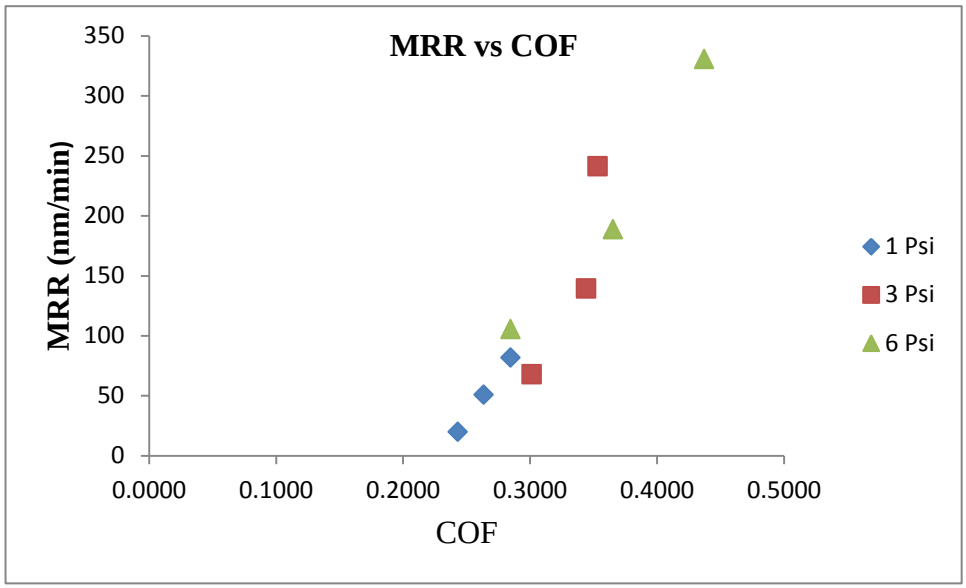

Figure 3. 19 MRR vs. COF

The trend from figure 3.19 indicates that the lower the COF the lower the MRR during polishing. The MRR and COF values indicate that as the pressure is increased the MRR and COF are also increased. Utilizing the fact that the COF can be monitored in-situ a qualitative model can be developed for the BPM CMP based on these results. The results do not indicate the overall surface quality but the trend followed for material removal. CMP of BPM follows closely to experimentation by Zantye for COF and MRR trends done on silicon dioxide and other ILDs [45].

3.4.2 BPM Pre/Post CMP Mechanical Properties

Table 3.8 below gives the pre and post CMP mechanical properties evolution during the CMP process for the increases in pressure.

Table 3. 7 Nanoindentation results of BPM copper

Patterned Copper Sample	Elastic Modulus (GPa)	Hardness (GPa)
Unpolished	121.657±3.152	1.249 ± 0.121
1 Psi	129.828±1.090	1.440±0.058
3 Psi	135.419±0.752	1.609±0.061
6 Psi	138.594 ± 1.292	1.962± 0.208

Table 3.7 shows the results from the nanocharacterization of the BPM CMP experiments. From the table it is evident that as pressure increases during polishing the elastic modulus and the hardness increase as well. Increase in the mechanical properties arises from two possible reasons. The number of dislocations is increased as the abrasives particles permanently deform particles and then are removed due to the velocity and removal of the slurry. As the dislocation density is increased, the surfaces become harder to indent and permanently deform.

Another possible reason is due to the multigranular structure. Focused ion beam (FIB) and TEM images clearly depict several grains within the patterned structure. Orientation of these grains plays a role in the hardness due to several crystallographic effects. The critically resolved shear stress (CRSS) required to cause slip in a crystal (grain) depends heavily on the orientation of that grain. Within the multigranular structure seen during polishing several orientations exists and as the BPM is polished through shearing of the surface the resulting surface will have an orientation different from the previous grain. The new grain orientation along with the dislocation motion to

the grain boundaries increases the mechanical properties of the material through work hardening. These enhanced mechanical properties are advantageous for the BPM ability to withstand down pressure and shear during CMP.

3.4.2.1 Slurry Chemistry Characterization

To ensure that the slurry chemistry did not have strengthening effect on the copper surfaces, each BPM sample was allowed to sit in the Cabot iCue slurry and nanoindentation was done on each sample to determine the effects of the slurry on the mechanical properties of the samples. Table 3.9 shows the results from the experimentation.

Table 3. 8 Mechanical properties from the slurry

BPM Sample	Elastic Modulus	Hardness (GPa)
Unpolished	121.657±3.152	1.249 ± 0.121
5 minutes slurry	120.921±2.758	1.228± 0.221
30 minutes in slurry	119.241 ± 3.56	1.256± 0.48
1 hour in slurry	118.441 ± 4.21	1.205± 0.19
10 hours in slurry	117.021 ± 1.51	1.18± 1.13
24 hours in slurry	113.231± 1.93	1.17 ± 0.59

Based on table 3.8, the effect of the slurry alone has as detrimental effect on the mechanical properties of the BPM wafer coupons. The data in table 3.8 is based on nine indents averaged from the MTS indenter. It is evident that the Cabot iCue slurry weakens the copper on the silicon substrate and this is beneficial from a commercial aspect to

increase the MRR during CMP, but this does not account for the increase in the properties seen in table 3.7.

3.4.2.2 TEM Analysis

Prior to polishing the a TEM image was taken using the Technai F20 TEM shown in figure 3.20 shows that the patterned wafers are multi-granular. The two major factors that affect the mechanical properties of a metal are the size of the grains coupled with the grain boundaries and grain orientation [140-142].

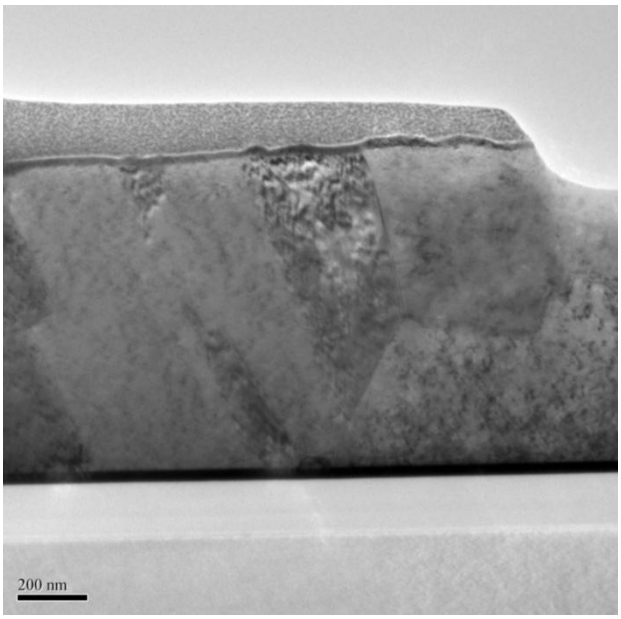

Figure 3. 20 Initial multigranular cross section of copper BPM

Given that the act of polishing is mechanical work on the metals, the increase in mechanical properties is produced by work hardening and plastic deformation of the metal. For copper with large grains (micron size), the plastic yielding occurs by generation of dislocations from internal sources. The increase in stress results from the pile-up of dislocations causing the activation of sources in the adjacent grains and the

resulting strain hardening arises from the accumulation of dislocations as seen in figure 3.21[143, 144].

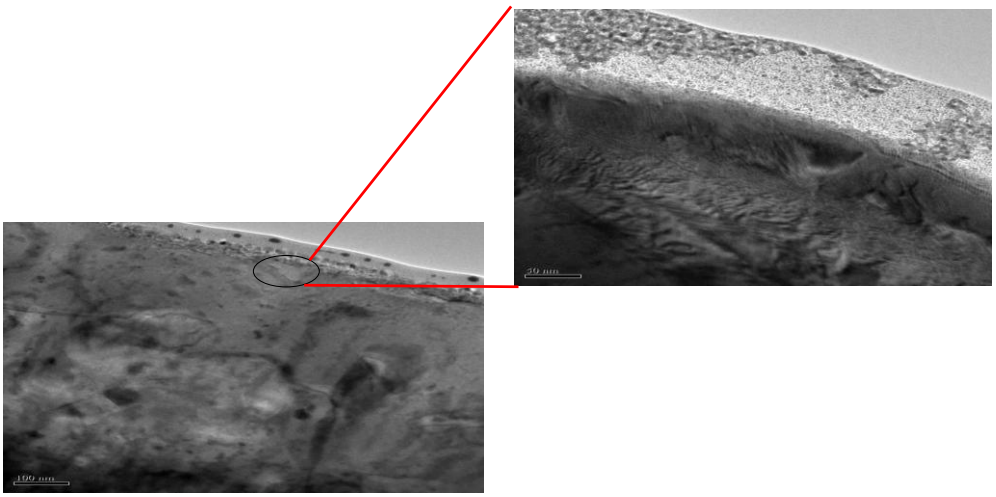

Figure 3. 21 Post polish TEM of Cu BPM

The increase in the theoretical shear strength of metals from shearing or indentation has been reported in literature and the dislocation motion has been documented accordingly [145]. Minor et al, provided evidence of the dislocation motion and increase in shear strength as shown in Figure 3.22.

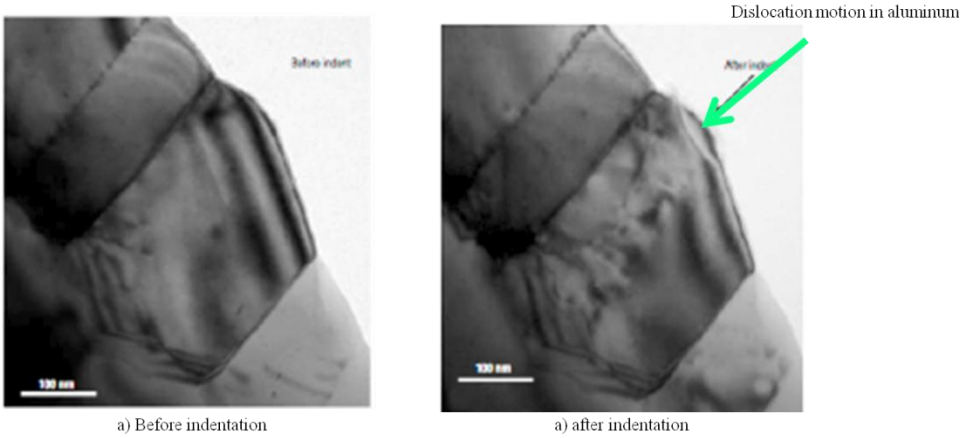

Figure 3. 22 Dislocation motion in aluminum [145]

The grain boundaries disrupt the movement of dislocations in a crystal and the disruption leads to larger applied forces need to cause the crystal to deform and lead to micro-cracks as seen in figure 3.23.

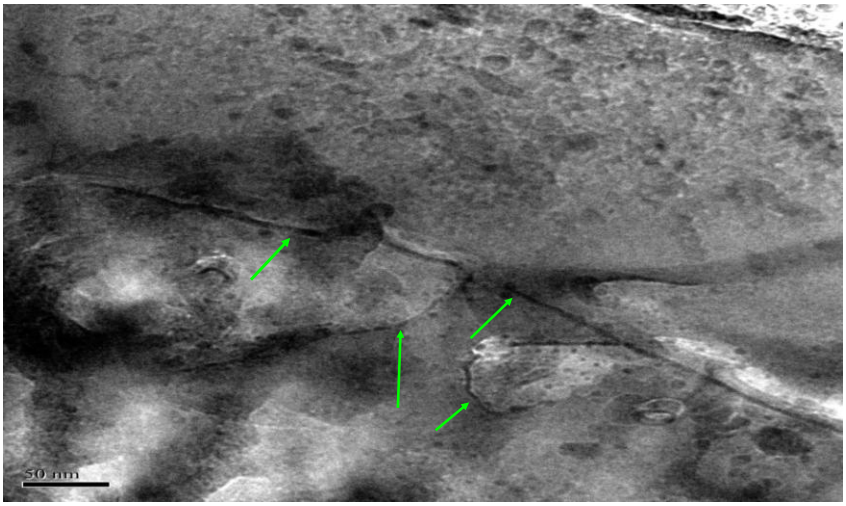

Figure 3. 23 Microcrack formations after polishing

The micro-cracks seen below the surface in figure 3.19 was witnessed in all cases of polishing in the samples, even at the optimized polishing parameters. The formation of these cracks will cause the PM to lose any data written on it and future research will

have to investigate either a means to reduce and remove the cracks or stronger materials to circumvent cracking.

3.4.3 Surface Roughness Characterization

Surface roughness and the overall surface quality play vital roles in the performance of the magnetic devices. It is imperative that the devices have atomically smooth surfaces so that the slider and magnetic head does not crash into the data on the devices. Table 3.9 contains the final average surface roughness values after CMP, the initial surface roughness, RMS, for the BPM configurations was 352.73 ± 1.24 nm.

Table 3. 9 RMS surface roughness for CMP process parameters

Relative Velocity (m/s)	1 Psi	3 Psi	6 Psi
0.2	336.88 ± 1.95 nm	322.34 ± 3.24 nm	339.00 ± 6.96 nm
0.8	334.04± 0.86 nm	201.00± 0.38 nm	222.42± 4.95 nm
1.2	304.17 ± 10.98 nm	195.88 ± 0.32 nm	195.57± 2.57 nm

From table 3.9, the polishing parameters for 3 Psi had the least amount of standard deviation. Figures 3.24 contain the initial 3D surface topography taken by the Wyko NT 9100 by Veeco, Inc. Figures 3.25-3.27 contain the final characterization images taken by white light interferometry using the VEECO NT-9100 surface profiler for the optimum polishing conditions using the polishing parameters from table 3.4. The images for each polish are contained in the appendix of this dissertation but the optimum images for each pressure are shown below.

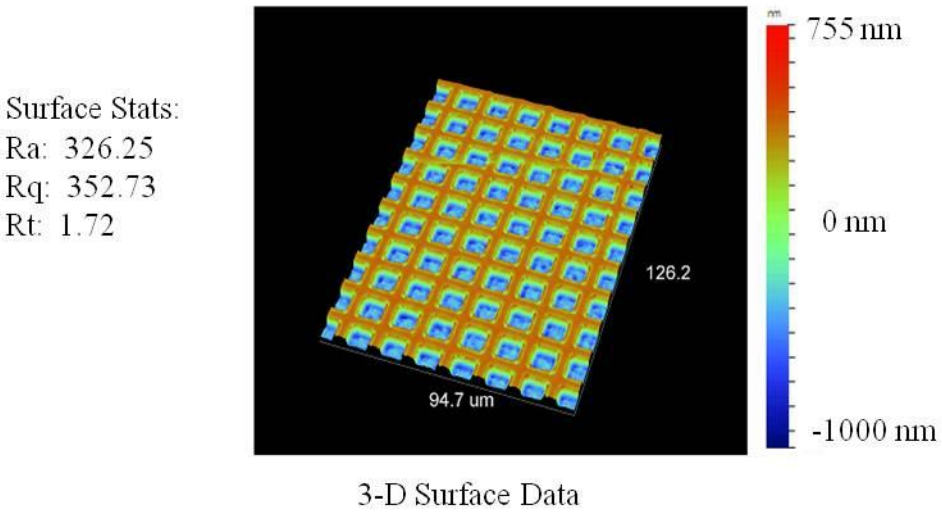

Figure 3. 24 Initial surface roughness for BPM prior to polishing

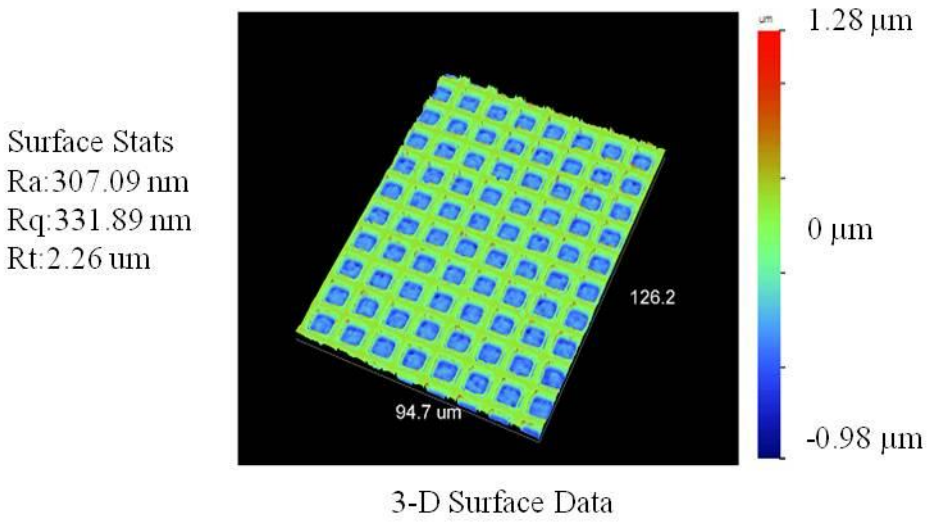

Figure 3. 25 1 Psi post CMP surface roughness

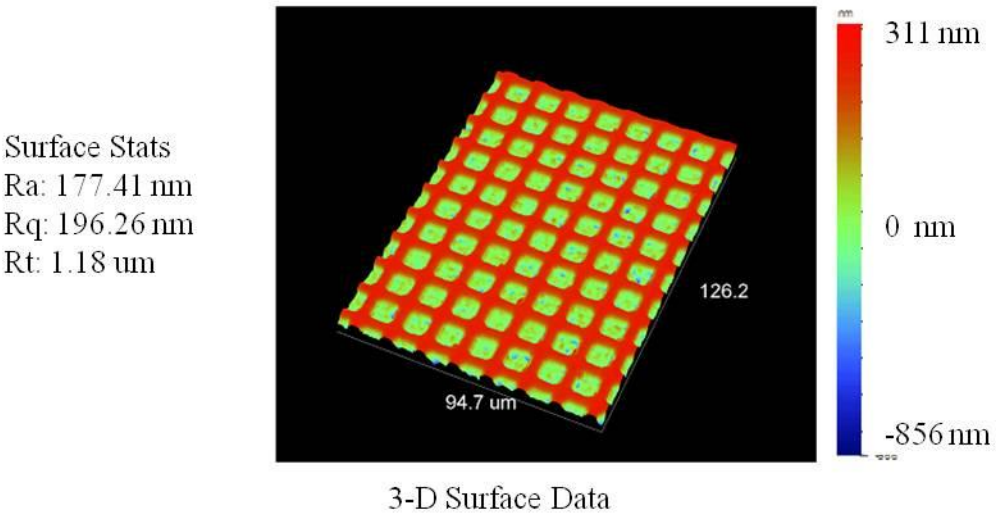

Figure 3. 26 3 Psi post CMP surface roughness

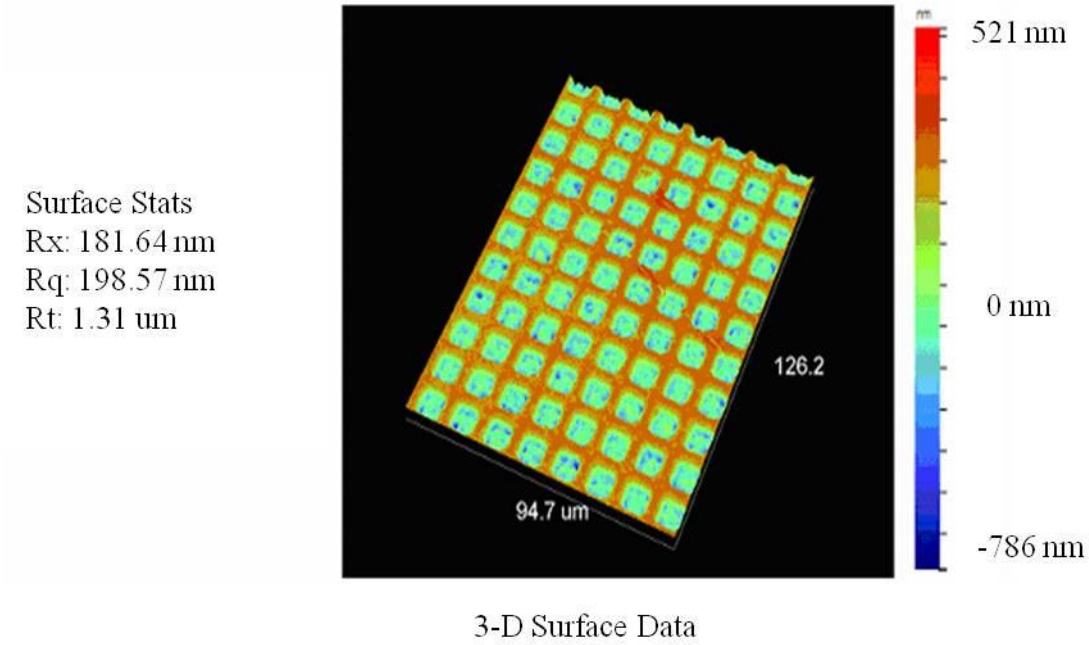

Figure 3. 27 6 Psi post CMP surface roughness

The final RMS surface roughness, Rq, from the 3 Psi, 1.2 m/s polishing is of 196.26 nm after polishing 120 seconds. This median pressure and highest velocity

yielded the optimal surface roughness for polishing at 120 seconds using the parameters for standard polishing in the IC industry. It should be noted that the 6 Psi polishing parameters had the highest MRR but the surface roughness was contaminated with debris from surface scratches and delamination at the edges due to over polishing. Figure 3.28 shows the delaminated SEM images after polishing at 6 Psi and 1.2 m/s.

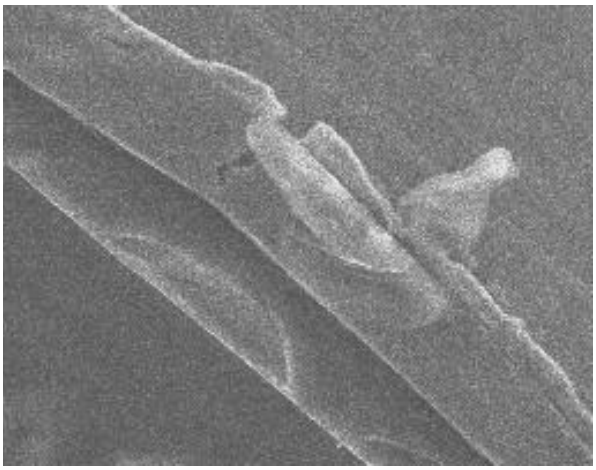

Figure 3. 28 Delaminated edge SEM image

After determining optimal machine input parameters for the surface roughness and MRR for BPM CMP, a statistical analysis was conducted to determine the importance of each parameter.

3.4.4 Statistical Analysis of Variance (ANOVA)

Table 3.10 contains the results from the ANOVA done on the 3^2 factorial test design on patterned media CMP using an alpha of 0.5.

Table 3. 10 ANOVA table for pressure and velocity of BPM CMP

ANOVA SOURCE	SS	Df	MS	F	F-Critical
A	323210.5	2	161605.2	1141.19	3.354141
B	8609.056	2	4304.528	30.39682	3.35414
AB	3984.611	4	996.1528	7.034425	2.727765
Error	3823.5	27	141.6111		
Total	339627.6	35			

Factor A is the pressure and factor B is the velocity, the statistical analysis also accounts for the interaction between the two variables (namely the multiplication of AB) as a further factor for analysis. The results indicate that the pressure is the dominant factor in the MRR as the experimental results have proven. The velocity plays a less significant role in the MRR and these results were also reported by Tseng et al. [84]

The results indicate that the interaction of the pressure and velocity plays a significant role but is simplified to a linear relationship as reported by [83, 134, 135]. A residual versus fitted values graph is show in figure 3.29 to ensure there were no compounded errors in the calculations.

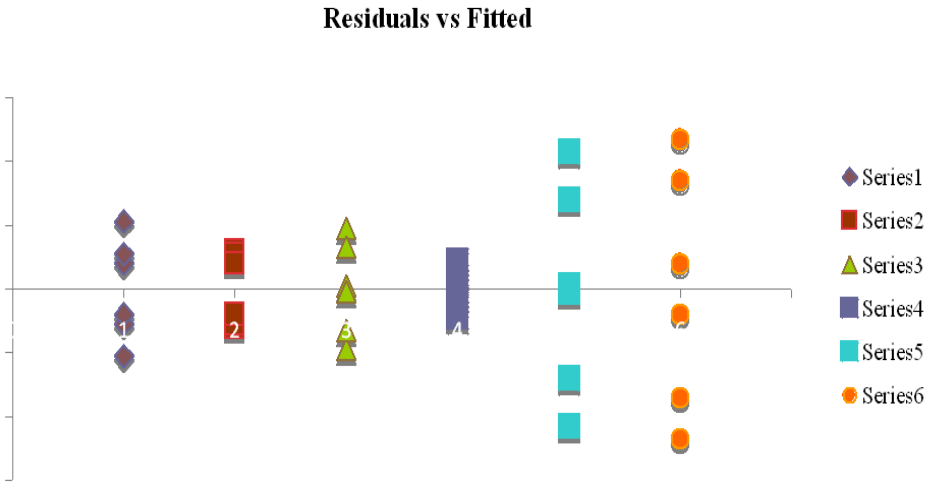

Figure 3.29 Residuals plot

From figure 3.25 since there is not a "cone shape" the values are taken to be true. And the statistical analysis is verified for the process parameters. Based on the values for the inputs of pressure and velocity and the resulting value of the MRR a linear regression model was developed as shown in equation 3.9;

$$Y = 489.74 + 53.31X1 + 4.65E-10\,X2 + 0.16X \qquad (3.9)$$

where Y represents the MRR, and X1 and X2 represent the pressure and the velocity respectively. This equation does not take into the account the slurry chemistry or the Preston coefficient and is detailed here as an accompaniment to the statistical analysis.

3.5 Conclusion and Remarks

CMP tests were run on copper bit patterned media in magnetic data storage device configurations, in order to understand the viability of CMP as the planarization technique on the new data storage configuration. The data on the CMP of BPM copper wafers was presented and detailed aspects of the MRR were determined. The pressure and velocity

were optimized to determine the parameters to induce the best surface quality and repeatability and the Preston's equation for material removal based on pressure and velocity was verified through statistical analysis.

Results indicate the best surface roughness of 196.26 nm occurs at polishing at 3 Psi, 1.2 m/s, and for the duration of 120 seconds. The highest MRR of 320 nm/min occurs at the highest pressure of the experiment of 6 Psi, 1.2 m/s, and 120 second polishing time. The values of the MRR for BPM are considerably lower for the same process parameters of blanket copper wafers with a percent difference for the low end of polishing of 3.11%-40% difference in the overall MRR. At all three velocities for the 6 Psi polishing test resulted in delamination of the patterned media from the substrate, indicating that this polishing pressure should be avoided. Polishing at 6 Psi will result in failure of the magnetic hard drive to the magnetic read/write head crashing while trying to access a grain or from crashing into the delaminated edges of the PM surface.

The overall low surface roughness and repeatability of the low polishing pressures and high velocities indicate that the required atomic surface roughness can be achieved on the PM configurations.

The mechanical properties were characterized before and after polishing and results indicate an increase in mechanical properties with no depreciable change in grain size. The cause for the increase in mechanical properties is linked to work hardening through the plastic deformation from the mechanical work done during polishing as evidenced through metallurgical studies [145, 146]. TEM analysis shows dislocation motion and pile up at grain boundaries further verifying that the metallic copper is reaching the theoretical shear strength through the dislocation pile up [145].

Optimization based on a statistical analysis, mechanical properties, and metrology studies provided results that yield promising initial ramifications on the feasibility of using CMP as a planarization technique. The machine parameters have been optimized based for BPM CMP based on IC CMP. This chapter serves to be the foundation for polishing BPM as literature has proven that the machine input parameters provide the greatest influence on the output parameters for polishing [42, 59, 84, 85].

The consumables utilized in the CMP process must next be optimized based on the machine input optimization in this chapter. The next phase characterizes the pads used for the BPM CMP process as detailed in figure 2.17.

CHAPTER 4: BIT PATTERNED MATRIX CMP PAD CHARACTERIZATION

4.1 Foreword

A stable and predictable CMP process requires full control of the consumable parameters shown in figure 2.17. Luo argues that based on his particle scale model, the micro-scale polishing pad topography, and nano-scale abrasive size distribution in the slurry are the two most important parameters for the CMP process (consequently the slurry size distribution is covered in chapter 5 of this dissertation) [147]. The polishing pad is arguably the most important component of the CMP system and has an economic impact of 550 million dollars annually [148]. The pad plays a crucial role in both the mechanical and chemical aspects of the polish. The mechanical properties of the pad will determine the polish rates and planarization ability of the process. The surface of the polishing pad, with its pores, grooves, and compressibility play an important role in the mechanical removal of the reaction products from the wafer surface [149]. The pad also carries the slurry on top of it, executes the polishing action, and transmits the normal and shear forces during polishing. At the pad/wafer interface, the slurry acts on the wafer and forms a compound with the material that is being polished. This compound is removed when the abrasive particles collide with pad and wafer asperities. The material removed, is then washed away due to the constant slurry flow on the pad.

This chapter serves to focus on characterization of the pad and pad life in comparison to the material removal and resulting surface quality of the BPM wafer

surface, based on the optimized parameters from chapter 3, the machine input parameters are used for pad characterization as shown in figure 4.1.

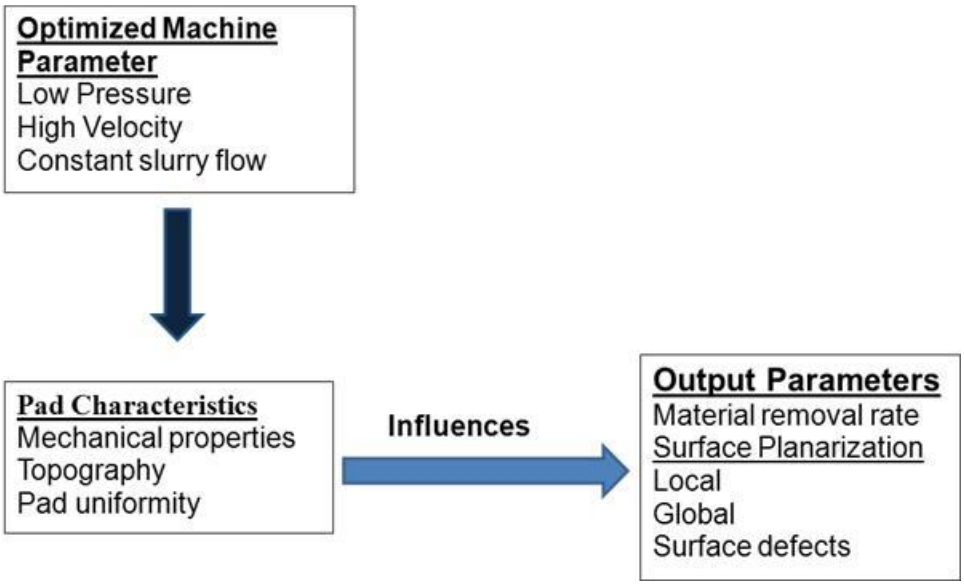

Figure 4. 1 Pad characterization based on optimized machine input parameters

The objectives for this chapter are:

1) Investigate pad wear on BPM CMP
2) Perform a parametric study of pad wear, pad roughness, COF, MRR, surface morphology
3) Give a qualitative analysis on the pad life, surface characteristics of the wafer, pad, and polishing regime
4) Determine optimal polishing pad for CMP of BPM from three commercially available pads.

4.2 Introduction: CMP Pads

Polishing pads are major consumables affecting the within-wafer and wafer-to-wafer non-uniformity (WIWNU and WTWNU respectively) in planarization technology. WIWNU is where there is non-homogeneity of polishing at different areas of the same wafer, and WTWNU occurs when there is non-homogeneity of polishing when one wafer is compared to another [150]. Polishing pads are composed of either a matrix of cast polyurethane foam with filler material to control hardness or polyurethane impregnated felts [42]. The role of the pad is to transport media of slurry to the polishing reaction point and to support polishing pressure derived from down force to the wafer [151-154]. The pad also transfers the shear force of the slurry to the wafer surface and eliminates polishing residue from the polishing point to allow new polishing reactions [153]. The combination of the many duties of the pad results in the properties and behavior of the pads directly affecting the CMP output parameters. Unfortunately pad fabrication technology has not kept pace with the continual progress of device fabrication processes. Specific problems include short pad life, inconsistent process results and extreme variability within each pad and from pad-to-pad; this requires costly adjustments of the CMP system and process parameters [154].

4.2.1 Pad Materials

Based on the microstructure, pads can be divided into four categories [155]. Type (1) pads typically are polymer impregnated felts. The microstructure of a pad of Type (2) is characterized by non-woven polyester fibers infused with polyurethane. Porometrics form the Type (3) pads and pads of this type display a porous layer on a substrate. Type (4) pads are filled polymer sheets and have a closed foam structure with macro pores.

For any polishing technique the choice of pad depends on the nature of the material to be polished and polishing output requirements [156]. Most commercial polishing pads for metal or oxides are of viscoelastic nature and, are mostly of type (1) [93, 157].

Polyurethanes are condensation polymers prepared by reaction of isocyanate and a polyol in the presence of a catalyst and a foaming agent [158]. The intrinsic polymer properties, like glass transition temperature (Tg) and mechanical properties like elastic modulus, compressive strength, shear modulus etc., are strongly dependent on the molecular structure of the isocyanate and polyols. A large selection of commercially available isocyanates and polyol combinations, along with very versatile chemistry of urethanes, makes it possible to synthesize polymers with specifically tailored properties [159]. Synthesis of the pads is not specifically covered in this dissertation but can be found in literature review [159-163].

4.2.2 Effect of Pad Geometry

The polishing process involves, intimate contact between the asperities on the wafer surface and the pad material, in the presence of slurry. The mechanical properties of both surfaces play a significant role in the final planarity and polishing rate. The wafer surface is hard and brittle, while pads tend to be made of relatively softer materials for optimal polishing.

4.2.2.1 Effect of Pores

The polyurethane pad consists of pores within the pad. These pores can be either closed or open pore systems. In either case the pores on the pad surface aid in slurry transport, to all parts of the wafer surface thereby ensuring chemical erosion. The cell walls of the foam mechanically remove the reaction products from the wafer surface and

the pores of the pad enable transport of the reaction products from the interior of the wafer surface to outside as seen in figure 4.2 [159].

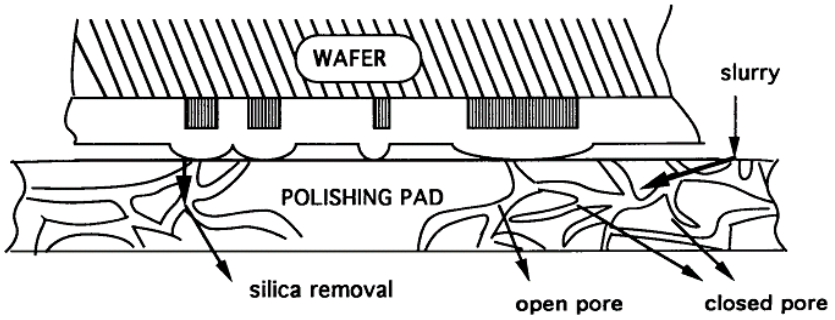

Figure 4. 2 Schematic of CMP polyurethane pad pores [159]

The pores on the pad surface enhance both the chemical and mechanical aspects of the process [159]. For a pad with an open pore structure, increasing the number of pores increases the cell wall scraping and henceforth the mechanical abrasion. Alternatively the closed pad structure is not interconnected to the wafer surface and therefore does not aid in the mechanical abrasion. The closed pore structures (pores that have a dead end) cannot aid slurry transport and/or product removal, but assists in supporting the pressure applied to the pad for stability. It is important to know the total pore volume as well as the fraction of open cells. The pad design should involve optimization of both to aid in support of the pad structure, the slurry movement through the pad, and mechanical abrasion [159].

4.2.2.2 Effect of Grooves

The grooves or perforations on the polishing pads have a significant impact on the polishing mechanism and outcome parameters [164, 165]. Grooves on the pad allow for effective slurry flow under the wafer surface and thus are very crucial for an effective

CMP process. Phillipossian et al. carried out fundamental tribological studies on CMP of pads with different groove types at various slurry abrasive concentrations [166]. The COF data was fitted as a function of Sommerfeld number and a tribological mechanism indicator "β" was developed to index and describe the change in COF. Stribeck curves were generated using the friction data for a variety of groove and pad types. From the shapes of individual curves, the authors hypothesized that some of the pads polished in partial lubrication regime and some in boundary lubrication at lower Sommerfeld numbers and transitioned to partial lubrication regimes. Consistent removal rates and uniformity were observed as long as the polishing regime is in boundary lubrication regime, although polishing in the boundary lubrication regime is aggressive and may induce delamination of the surface.

4.3 Pad Characterization

There is ongoing research to investigate the dependence of various pad material properties on the CMP process. Various researchers have focused on the macro effect of the wafer shape, mechanical properties, and polishing pad profile on the MRR, and findings include that there is a drop in the MRR as a function of time due to varying the mechanical response under conditions of critical shear [167]. During the CMP process the surface of the CMP pad gets loaded with debris from the polishing operation, which leads to "glazing" on the surface. This means that there are no asperities to hold the abrasive grits, which leads to inefficient polishing and possible micro-scratching on the surface wafer. The phenomenon of pad "glazing" is also attributed to the mechanical response under conditions of shear. Other researchers have focused on the wafer planarity and determined that the wafer planarity is a function of pad stiffness, which is

determined by the elastic properties of the pad material [167, 168]. As previously stated it has been shown that the pad may be directly responsible for several process defects like WIWNU and WTWNU and the techniques used for characterization of the CMP polishing pads such as, dynamic mechanical analysis (DMA) are destructive and therefore do not yield ex-situ information on the pads which requires a new and novel way to analyze the pad characteristics, properties, and life. This chapter serves on qualitative characterization of pad properties through a novel nondestructive technique and their effect on the output parameters. Secondly this research aims to predict pad life for BPM configurations to reduce waste and increase the sustainability of the pads.

4.3.1 Ultrasound Transmission

A novel non destructive ultrasound transmission system (UTS) developed at USF has been effectively used for evaluation of the CMP pads [169] . This technique works on the principle of ultrasound permeability through absorbing viscoelastic medium. The transmitted ultrasound signal is used to determine how the material properties of the pad vary over its geometry [170]. By sending an ultrasonic wave through the pad and measuring the change in transmitted signal at different spots, one can create a UTS map of the underlying pad structure. The UTS amplitude can be monitored as a function of time, height above pad and depth below its surface application of compression at different transmitted frequencies [170]. The regions of polishing pad having variations in specific gravity transmit different amplitudes of UTS at a same frequency. The amplitude of the ultrasound permeability with in a pad obtained as a result of UTS is normalized to against the average UTS amplitude to estimate the comparative variations in specific gravity in the different regions of the same polishing pad. The output of the

measurement is a Doppler diagram in which different colors correspond to different amplitudes of UTS within the pad. This picture may be correlated with the pad life and performance in order to predict these variables. This could increase yield by reducing the number of rejected wafers as the pad ages prematurely or lengthen production time by indicating which pads have more desirable properties.

The UTS system developed at the Center for Microelectronics Research (U. South Florida) is comprised of two key elements; a resonance circular piezoelectric transducer as an emitter of acoustic vibrations of selected amplitude and frequency, and an acoustic probe as a receiver of ultrasonic vibrations. A schematic diagram for the UTS system is shown in Figure 4.3 with the transducer and acoustic probe labeled respectively.

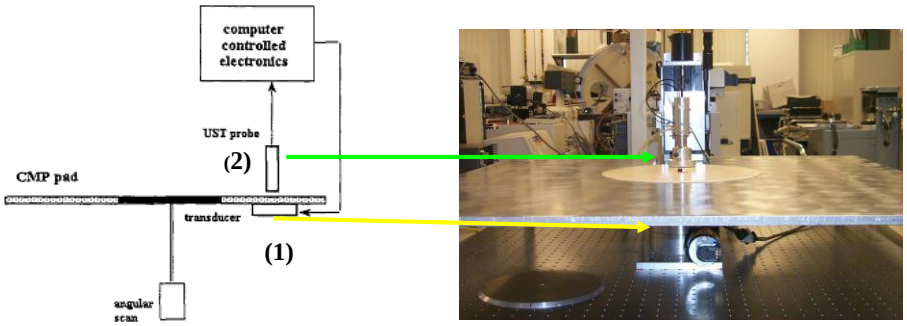

Figure 4. 3 UTS schematic for CMP pads [138]

4.3.2 Surface Characterization

The surface morphology of the pads was characterized using a JEOL JSM6490 scanning electron microscope (SEM) shown in figure 4.4.

Figure 4. 4 Jeol JSM6490 SEM surface morphology tool

The SEM supports ultrastructural analyses of surfaces, 3D organization, and has a 3.0 nm resolution. Prior to SEM, the polyurethane pads were coated with a thin layer, ~10 nm, of gold using the HUMMER X sputtering system at the Nanomaterials and Research Engineering Center (NREC) at the University of South Florida (USF). The SEM is used to investigate the surface morphology, cross section of the pads, and the effect of polishing on the pores and grooves of the pads.

4.3.3 Wafer and Pad Surface Roughness

As detailed in chapter 3 section 3.3, the WYKO NT9100 surface profiler is used to determine the surface profile roughness in three dimensions for the pad surfaces and the BPM wafer surfaces detailed in chapter 3 section 3.3.1. Knowledge of the resulting roughness parameters wafer will lead to conclusions about how the wear life of the pads affects the overall surface roughness of each wafer. Optimization of this parameter can lead to predetermination of unusable pads which can reduce WTWNU thereby decreasing waste.

During polishing pad roughness is expected to decrease along with the MRR during polishing. The removal of the pores and grooves significantly reduces the ability of the pad to remove material and a prediction of the pad life is therefore vital for sustainability. The decrease in the roughness of the pad is detailed by the WYKO NT9100. A statistical WTWNU measurement is calculated by dividing the standard deviation of the wafer surface roughness by the average surface roughness of each polish. This value will indicate how repeatable the polish parameters are for each pad and polish set.

4.3.4 Ex- Situ and In-Situ CMP Pad Characteristics

As described in chapter 3 section 3.3.4 the CETR benchtop tester allows for in-situ monitoring of the forces applied for polishing. The F_x, F_z forces are utilized to determine the COF during polishing of all pads and wafers. Knowledge of the COF and the polishing parameters along with the pad roughness allows for calculation of the Sommerfeld number during pad wear. This calculation allows for elucidation on the lubrication regime and thereby the polishing mechanism during the CMP process.

4.3.5 Material Removal

The material removal on the BPM copper wafers was determined using the technique described in chapter 3 section 3.3.4.2. The four point probe was used to determine the thickness of the wafers before and after polishing and this change over time was deemed the material removal rate. A second method was also used when the BPM wafers were polished to the silicon substrate. Figure 4.5 shows the initial thickness measurement done by the FIB machine described in chapter 3.

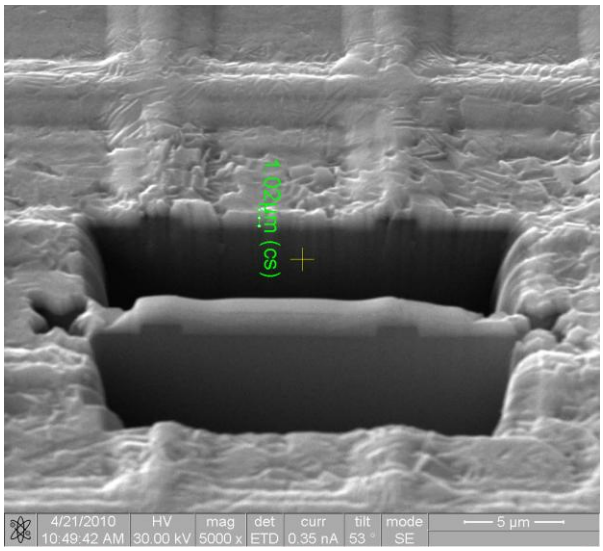

Figure 4. 5 FIB image of initial thickness of BPM

By knowing the initial thickness of 1.02 µm from the wafer substrate to the top level of the BPM the amount of time used to polish to the substrate can also be used to determine the MRR.

4.4 Experimental Set Up

Details on the experimental set up for characterization of the CMP pads are described below. All experimentation was done on a statistical analysis with testing done a minimum of five times for each pad and experiment.

4.4.1 CMP Pads

Three different CMP pads were tested for experimentation. These commercial pads are all utilized in either copper or other metal polishing. The MRR and pad wear is characterized by the techniques mentioned in section 4.2 of this dissertation. Details of each individual pad are shown in table 4.1 (note k-grooves are concentric pores).

Table 4. 1 CMP pad characteristics

CMP Pad Type	Diameter	Specific Gravity	Thickness	Hardness	Compress-ibility	Groove type
(1) Rodel-dual layer IC 1000	81 cm	630-800 (kg/cm^3)	1270µm	55-59 shore D	2.25%	k-groove
(2) Rodel dual layer IC 1400 Suba V	81 cm	$0.75g/cm^3$	1270µm	57 shore D	0.7-6.6%	k-groove
(3) RD-2003 matrix foam	57.15 cm	n/a	~2500 µm	~10 shore D	n/a	xy-groove

It should also be noted that discussions of the pads will be noted by the numerical value assigned in table 4.1 (e.g. Rodel IC 1000 will be referred to as pad (1), etc). The shore-D value of pads (1) and pad (2) are much greater than pad (3) for the same scale. The shore A value of hardness was converted to shore D value based on literature [171].

Prior to polishing experiments all commercial pads had to be conditioned for polishing. Pad conditioning is an important process to restore the pad properties that deteriorate over time from stagnant pads. The surface interactions involved in the process of polishing are influenced by the pad texture resulting from conditioning. The process of conditioning is used to:

1) Maintain the roughness of the pad and promote effective slurry distribution
2) Remove unwanted products after polishing (glazing).

Various pad conditioning methods have been used to improve the pad properties and stabilize the removal rates. The most effective method found was using diamond as the abrasive material [149]. The properties of the conditioner such as diamond density and diamond mounting play a major role. The other input variables for the conditioning process include parameters such as the conditioning down force and relative speed of rotation (rpm) of the pad platen and the conditioner. The process of conditioning can be quantified in terms of MRR, pad roughness, and wear of pad. It has been found that a pad conditioned before the first polished wafer doubled the removal rate compared to the unconditioned pads. Conditioning maintains the removal rate by maintaining the asperity height and density on the pad surface. Uneven pad wear results in uneven distribution of the pressure affecting the planarization uniformity and removal rate.

During the process of conditioning, the conditioner disk rotates about its axis and simultaneously moves linearly towards and away from the center of the pad for a uniform conditioning of the pad surface. All pads were conditioned with TBW grid-abrade 2µ diamond pad conditioners, for 20 minutes followed by 1 minute of polishing on a dummy sample, then another 20 minutes of conditioning, followed by another 1 minute of polishing on a dummy sample, then the final 10 minutes of conditioning of the pad followed by the actual experiments with Cabot iCue 5001 copper slurry (details of this slurry are in chapter 3 section 3.3.4.4).

4.4.2 Ultrasound Transmission Testing System (UTS)

The UTS system consists of a flat square table that can accommodate polishing pads as big as 32” in diameter. The center of the table has a circular hole that allows the two screws that holds the pad to pass through. One side of the table has a slot which

enables the transverse movement of a 3" Valpey Fisher piezoceramic transducer along the radial direction of the polishing pad. The transducer has a hole in the center and has trenches in the sides which help in generation of the vacuum which is used to hold the pad on the surface during UTS measurement. The piezoceramic transducer emits resonance ultrasound vibrations at 26 KHz (first resonant frequency of the piezoceramic transducer), while a 7 mm diameter quartz rod or a pinducer housed in aluminum casing aligned directly above the transducer acts as the receiver. The received ultrasound frequency is then converted in to electrical energy and the raw output is seen on the oscilloscope. The signal from the probe and reference input are both sent to a lock-in amplifier which records the amplitude of the received signal at the same frequency as the emitted signal. Different sections of the polishing pad are scanned be rotating the pad using the mounting screws by a step motor with 2 degrees angular steps, and moving the emitting piezoceramic transducer and the aligned receiver with another step motor at 7mm radial steps with help of a threaded spindle and screw. There is a provision for vertical movement of the receiving pinducer with the help of a vertically positioned spindle and screw.

The measurements are taken at a distance of 100 μm below the pad surface to eliminate the presence of possible "air pockets". Due to the viscoelastic nature of the cross linked polymer material of the polishing pad, all measurements taken are "curve fitted" taking the effect of measurement stress and temperature on the material into consideration. The details of the UTS set up, measurement techniques, characterization procedures and operation have already been published in literature [169, 170]. The UTS experiments were performed on the "as received" polishing pad with the plastic release

liner below it. It is assumed that the bottom PSA and the plastic liner are uniform and will have a similar effect on the ultrasound transmission. These effects could then be filtered out when the entire data is normalized against the mean UTS. The areas of interest (e.g., showing the highest or lowest ultrasound transmission over the entire pad was designated as "high transmission" or 'HT', while the lowest ultrasound transmissions were designated as "low transmission" or 'LT'). These areas were imaged under high magnification in the SEM to look at the surface characteristics of the pads.

4.4.3 CETR CMP Polishing

In order to fully understand and characterize the pad, the process machine input parameters are kept constant during polishes of the pad. The input parameters are based on the optimized data from chapter 3. Table 4.2 contains the process input parameters for pad characterization.

Table 4. 2 Process parameters for pad characterization polishing

#	Parameter	Conditions
1.	Pressure applied	2 Psi
2.	Platen rotation	200 RPM
3.	Carrier rotation	200 RPM
4.	Slider movement	3 mm/s
5.	Slurry flow rate	75 mL/min
6.	Time	120 Seconds
7.	Pad	Varying
8.	Specimen	MIT 854 BPM 1"x 1" copper coupons

The pads undergo a design of experiments that consists of:

1) Ultrasound testing of the pad at each polish
2) SEM of the pads HT and LT sections based on the UTS output for surface morphology
3) If needed the pads are conditioned and steps (1) and (2) are repeated
4) The pad then polish the specimen using the process parameter in table 4.2
5) Steps 1- 4 are repeated for each pad up ~ 100 polishes or 200 minutes.

This process described above begins with the as received pads and completed after all polishes on the BPM are completed. For benchmarking purposes the tests are run until a) the BPM is fully removed from the silicon substrate or b) the pad life has been exceeded without conditioning (e.g., the pad is visibility wore or the thickness is half of the initial thickness of the pads based on micrometer readings) [42, 168, 172].

4.5 Results and Discussion

For each polish and pad including the conditioning of the pads, the average COF, MRR, wafer surface roughness, and pad surface roughness are recorded at 20 minute intervals. Wyko surface profile images of the wafer and pad surface roughness, 2-D profile, surface data including any scratches or delamination, a histogram of the height distribution, and a 3-D image were recorded for all polishes, this data is presented in this dissertation for pad (2), the images for the other pads is referenced in the appendix of this dissertation. A table of the graphical values is shown in the conclusions section.

4.5.1 COF and Pad Polishing

The importance of the COF during all polishing process was detailed in chapter 3 and verified by literature [73]. During characterization of the pad, the COF helps to

determine the polishing regime, as well as gives an indication of the MRR, and pad life for each of the pads tested.

4.5.1.1 Stribeck Curve

The Stribeck curves were calculated for the three pads for values of the COF from 10 polishes to 100 polishes (20 minutes to 200 minutes). The COF was monitored in-situ and the average value was taken for calculation. The Sommerfeld number was calculated using equation 2.2 and the input parameters from table 4.2, along with using the Cabot Microelectronics value for the viscosity of the slurry and a slurry film thickness approximation based on the pad roughness. The Stribeck curve is plotted in figure 4.6 for changes pad roughness during polishing to locate the polishing regime.

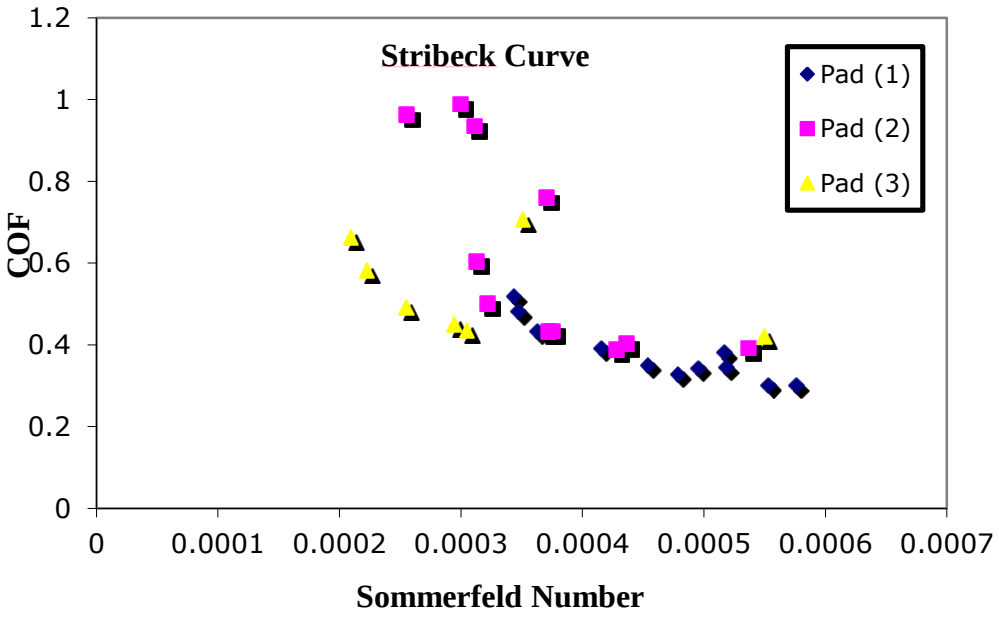

Figure 4. 6 Stribeck curve for pad polishes

The lubrication regimes and characteristics for each regime during polishing were covered in chapter 2. Based on figure 4.6, it can be seen that pad (1) operated predominately in the fully lubricated regime; and this regime has the lowest MRR along

with the least amount of surface defects. Pad (2) polished in the partial lubrication regime, and this regime's properties designate it as the most preeminent for CMP because it allows for high MRR along with low surface defects. Pad (3) borders the boundary lubrication regime as well as the partial lubrication regime. The boundary lubrication regime is good for the material removal rate but because of the two body abrasion has high surface defects. It should be noted that for BPM the least amount of surface defects does not equate to the lowest RMS surface roughness. This is due to the face that the patterned surface is only planarized for each high asperity leaving the differential between the remaining asperity heights and valleys high and therefore leaving the root mean square surface roughness high.

4.5.1.2 COF and the MRR

A model between the COF and the MRR for composite non heterogeneous materials has not been developed due to the changes in pads, material properties, process parameters, and slurries (which includes chemistries and abrasive particles). During polishing a correlation was investigated to find a relationship that can be used as a parameter to optimize the MRR and COF. Figure 4.7 has the MRR versus the COF data.

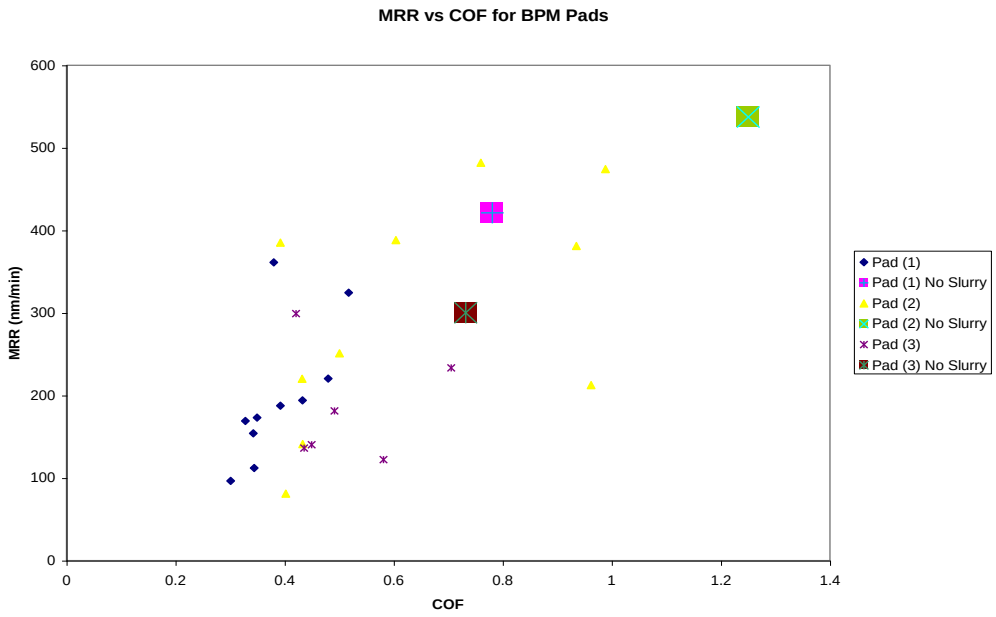

Figure 4. 7 MRR vs COF for CMP of BPM pads

Although a predicting model cannot be drawn from figure 4.6, there does exist a relationship between the COF and the MRR. The higher the COF the greater the MRR for all three pads, regardless of layering, groove type, or polishing parameters. This relationship could be described by the action of mechanical polishing during CMP. As the high asperities come into contact with the pad there is two-body abrasion that happens and during this interaction between the pad/wafer surfaces the COF is highest.

Alternatively, the three body abrasion system inherently cannot have a value as high for COF as the two body abrasion due to the lubricating fluid as a medium. The regime with the highest COF would be boundary lubrication and this regime has the highest MRR while also producing the greatest surface defects. This fact is further proven by the high material removal during polishing without slurry and the higher COF value, the lack of lubrication shows that the boundary lubrication regime dominates with

high material removal and high COF, but his regime has the highest amount of surface defects.

4.5.1.3 COF and Polish Time

The COF is a direct corollary to the MRR during polishing and in-situ measurements of the COF during polishing lends to predictable determination of the MRR during polishing. Figure 4.8 details the COF versus polish time for the pads.

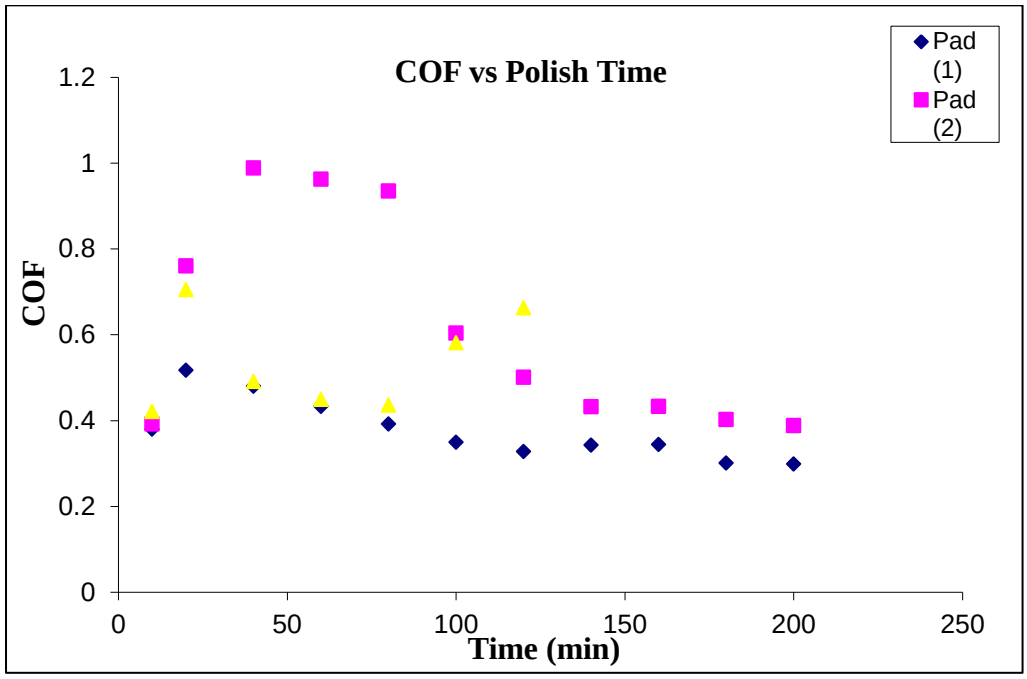

Figure 4. 8 Polish time versus COF for BPM CMP pads

The initial value for the COF for all three pads is roughly 0.4 based on figure 4.8. All pads are still in the break-in portion of polishing and no difference in COF is appreciable (although the MRR is different for all pads). After 20 minutes of polishing all pads exhibit an increase in the COF and this corresponds to increase in the MRR during polishing for all pads seen in section 4.5.2.1. After break-in for pad (1) the decrease in the COF remains study during polishing for 200 min. This correlates to a

steady and repeatable polishing regime for pad (1). Pad (2) has another COF increase in polishing between 40 and 50 polishes, due to introduction of a new wafer coupon for polishing. Pad (2) then has the same decrease in COF as seen in pad (1) only shifted for higher COF values. The COF values for pad (3) follow the same pattern as the other two pads for the but as the pad deteriorates there is no relationship to be determined for COF and polish time for pad (3), and the introduction of pad particles into the wafer/pad interface causes anomalies in the COF values.

4.5.1.4 BPM Surface Roughness and COF

The ability to determine the output parameters by monitoring in-situ parameters is paramount for BPM CMP. It has been shown the COF is an indicator of several process parameters such as the MRR and lubrication regime. Figure 4.9 contains the plot of the BPM surface roughness versus the COF.

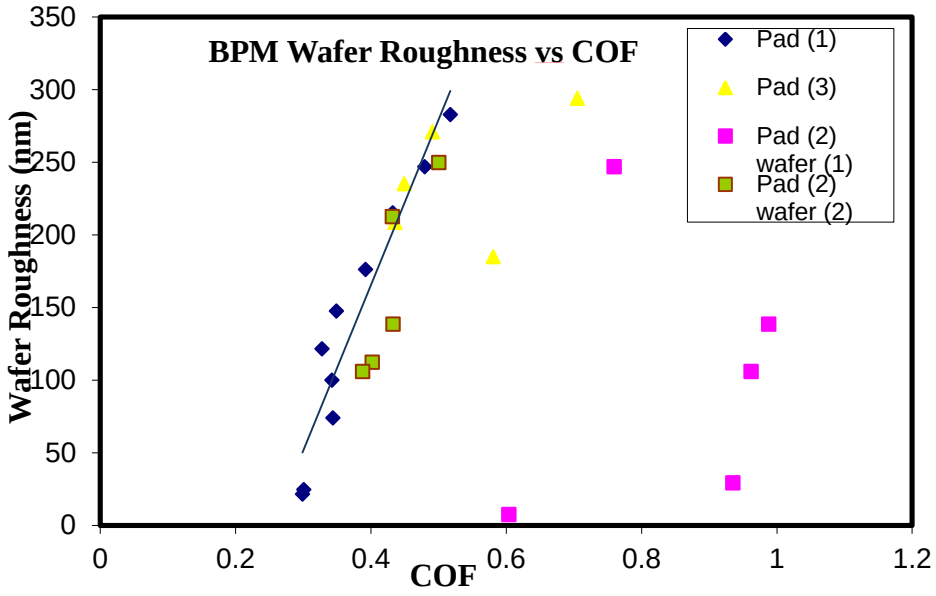

Figure 4. 9 BPM wafer roughness vs. COF

Based on figure 4.9, as the COF is decreased the wafer surface roughness is also decreased for pad (1) and pad (2). As the pads polish the surface the number of contacting asperities becomes worn and the contact area is decreased. As the contact area is decreased the COF decreases and the worn surfaces become smoother. The trend does not hold for pad (3) and again this is linked to the deterioration of the pad. Pad (1) has the lowest COF values and the gradual increase in polish time results in a lower COF, and thereby wafers roughness. Pad (2) follows this same trend but broken into two separate wafer coupons. The consistently higher values of COF seen from pad (3) arise from the abraded pad particles becoming trapped in the wafer/surface interface instead of being removed by the angular velocity. These particles lead to a stagnant value COF during polish time.

4.5.2 Polish Time Metrics

The amount of time required to polish the BPM to atomic roughness based on IC CMP elucidates the overall efficiency of the process. Pad characterization will serve to dictate the output parameters during polishing. The data reported in this chapter for the pads is based on only initial conditioning of the pad. Standard CMP practices reconditions the pads throughout the process cycle, but for benchmarking purposes the pad is conditioned only that the onset of utilization.

4.5.2.1 Material Removal

The CMP process is employed to remove unwanted material from surfaces to ensure local and global planarity during polishing. The MRR is plotted versus the polish time in figure 4.10.

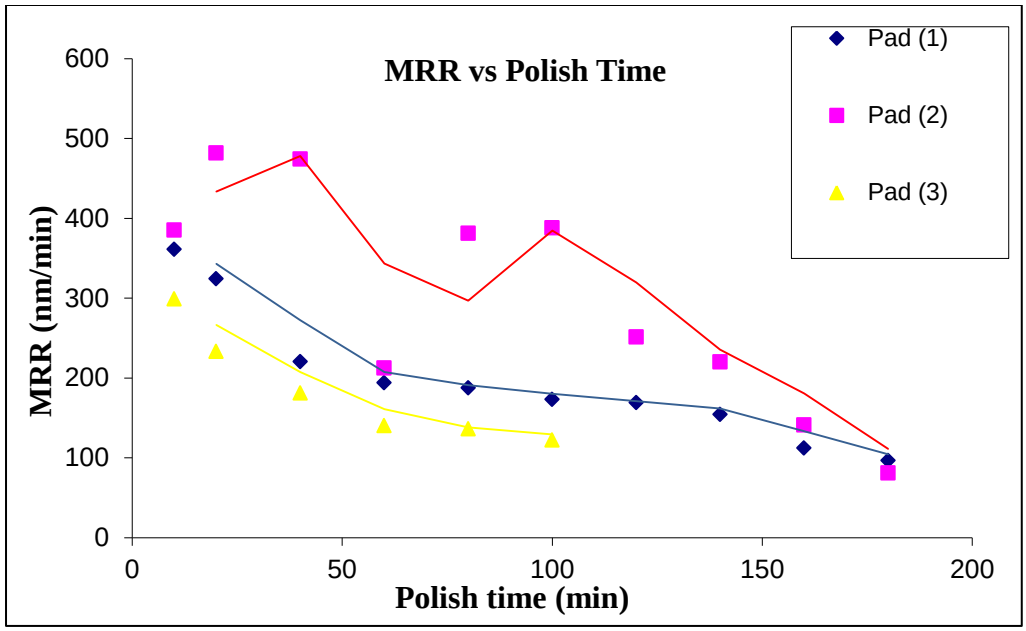

Figure 4. 10 MRR vs. polish time

From figure 4.10, the polish rate decreases with time for polishing of BPM. Based on the Stribeck curve, pad (1) operated in the fully lubricated regime which was distinguished by low material removal but extremely smooth resultant surfaces. Although lower MRR than pad (2), pad (1) showed a linear decrease in MRR over the 200 minute polish time. Pad (2), which operated in the partial lubrication regime, had the highest MRR of the three pads. It should be noted that pad (2) polishes two different wafer coupons; the first coupon reached the atomic surface roughness within 75 minutes of polishing and was subsequently replaced with a new coupon for pad (2) to polish. Pad (3) operated on the border of the boundary lubrication regime (wafer to pad contact) rapidly deteriorates due to the low Shore hardness value of the pad and possibly the groove pattern and after 100 minutes of polishing the pad no longer removes appreciable material.

4.5.2.2 BPM Surface Roughness

The second overall goal for CMP is to polish surface to an atomic smoothness. Figure 4.11 contains the resulting BPM surface roughness versus polish time for the pads tested.

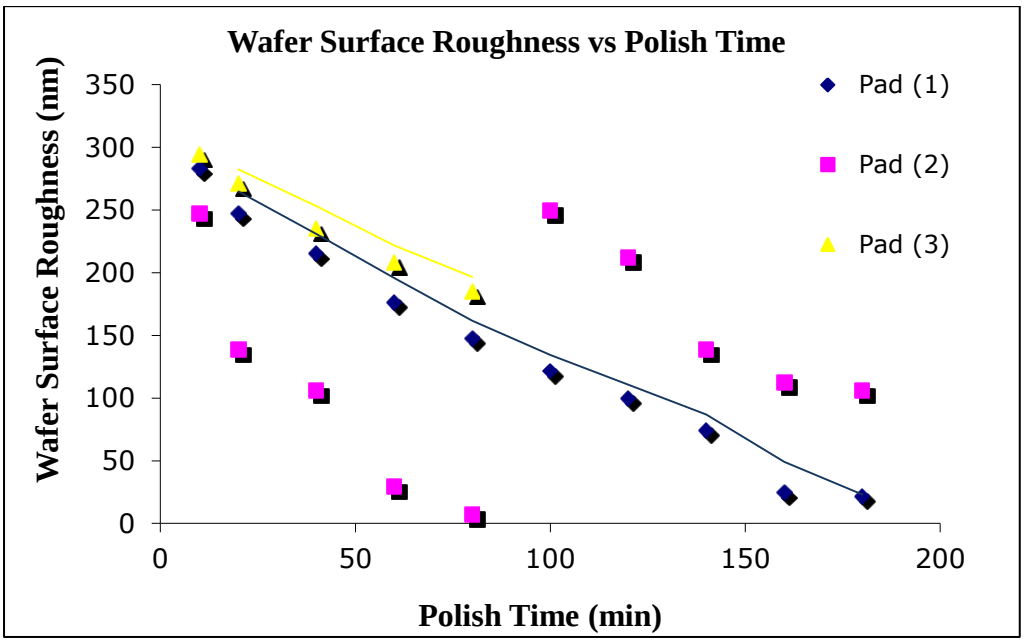

Figure 4. 11 BPM surface roughness vs. polish time

From figure 4.11, as polish time increases the BPM surface roughness decreases. This is expected and follows the trend from figure 4.9 in which the MRR rate is initially very high and as the BPM becomes planarized the MRR decreases as there is less material to remove. Pad (1) takes the longest time to polish the wafer to atomically smooth surfaces requiring at nearly 200 minutes. Pad (2) completed polishing to the required 10 nm surface roughness in roughly 75 minutes, after which a second coupon was polished to try and determine if a second BPM could be polished to the required roughness value. This resulted in the second coupon reaching a surface roughness of

roughly 125 nm, far below the initialized value of 352 nm. Pad (3) was unable to polish the surfaces below 200 nm roughness and as mentioned previously deteriorated rapidly during polishing.

4.5.2.3 Pad Roughness

The relation of the pad roughness to the resulting surface roughness provides valuable data into the regime and how the pad is actually polishing the material. The pad roughness will ultimately determine how smooth the BPM surface will be due to the pad/wafer interface asperities dominating the MRR as shown in chapter 3. As mentioned previously the pad roughness has been directly linked to the material removal rate and efficiency of the pad. The pad roughness is plotted versus the polish time in figure 4.12.

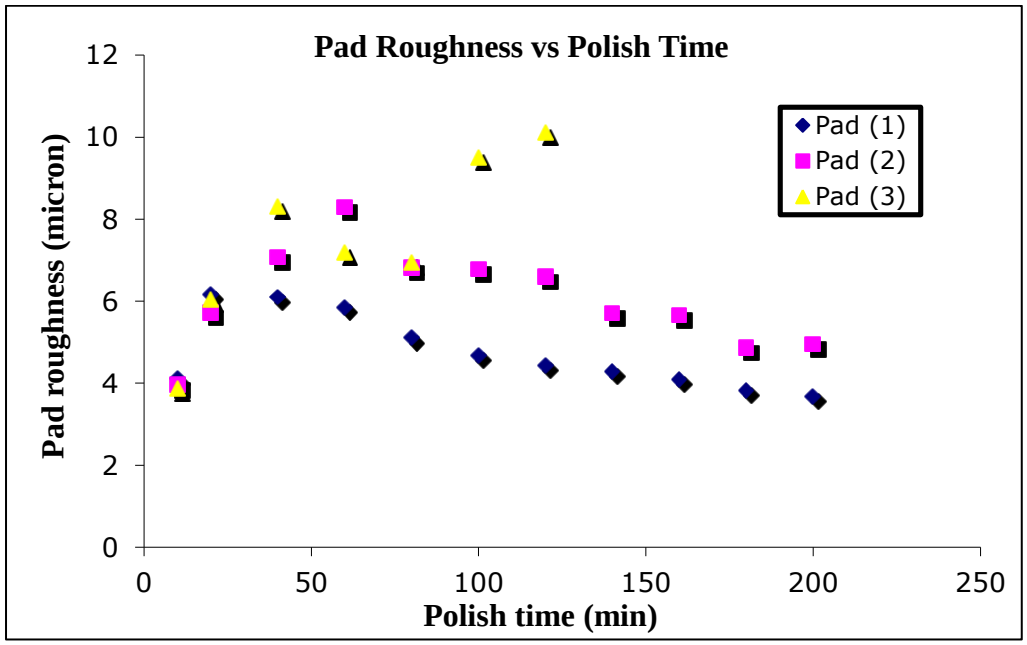

Figure 4. 12 Pad roughness vs. polish time

For pads (1) and (2) there is a direct relationship between the pad roughness and polishing time. As the pads continue to polish the BPM the glazing effect reduces the pad roughness and thereby the MRR and resulting BPM surface roughness. The increase in pad roughness seen in figure 4.12 for pad (3) results from deterioration of pad (3) during polishing. The abraded pad particles were embedded on the surface of the pad during polishing and the resulting imaging seen in the appendix reflects this embedment. A secondary indicator for pad (3) roughness phenomena arises from the fact that the MRR did not increase for pad (3) as would be seen if the imaging were a correct representation of the pad surface without deterioration.

4.5.2.4 Pad Thickness

Industrial standards indicate that once the pad has reached half the original thickness the pad must replaced in order to reduce cost of losing useable wafer coupons. Replacing the pads is a costly procedure and benchmark evidence on the life of the pads for BPM is critical to reduce waste. Figure 4.13 shows the reduction in pad thickness over time.

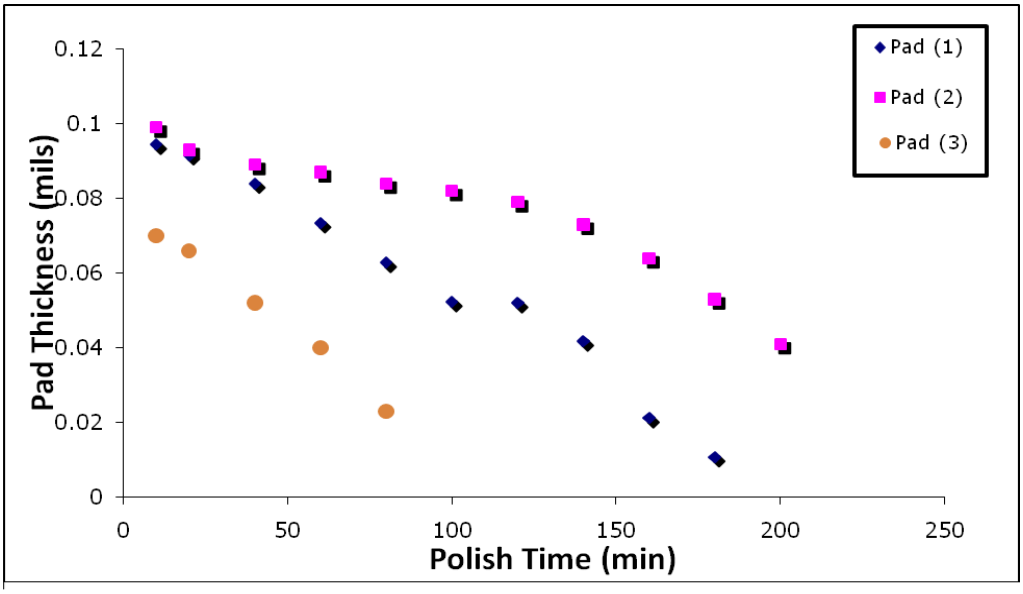

Figure 4. 13 Pad thickness vs. polish time

The initial thickness is seen as the first data point on figure 4.13 for each pad. The pad thickness decreases with polish time as would be expected. The rate at which the pads lose thickness is much faster than would be expected from IC CMP. The pads tested have a pad life from 400-700 minutes and results indicate replacement of the pads at 100 minutes, 200 minutes, and 50 minutes for pads (1-3) respectively. This dramatic change in pad life must be taken as a cost for polishing BPM and is due to the high initial roughness of the BPM surfaces when polishing as opposed to the relatively smooth surfaces for IC CMP.

4.5.3 Metrics Discussion

It has been shown in the previous sections that the rougher the pad, the higher the COF, and the higher the COF, the higher the MRR, and pad roughness to the MRR. This knowledge can prove beneficial from an economic standpoint because optimal pad

roughness for BPM is essential for polishing regimes and vendors can specifically supply pads with the required roughness values to improve sustainability and reduce polishing times. For the pads testing and utilized to polish BPM configurations the highest removal rate was obtained by the k groove pad along combined with the highest surface roughness. All three trends are linear in fashion and the values for polishes rates are presented in the appendix. Pad (2) obtained the highest MRR with a value of 480.27 ± 16.7 nm/min.

4.5.4 Surface Morphology Characterization

A qualitative understanding of the surface morphology evolution during polishing is needed to predict pad life and wear characteristics; this is paramount for sustainability and process optimization during the CMP process. The UTS and SEM machines were utilized to characterize each polish for the BPM from table 4.2. Figures 4.10-4.15 show the representative surface evolution of pad (2) during polishing for 80 minutes of polishing (time required to polish wafer coupon to atomic roughness). Pads (1) and pad (3) images are depicted in the appendix of this dissertation.

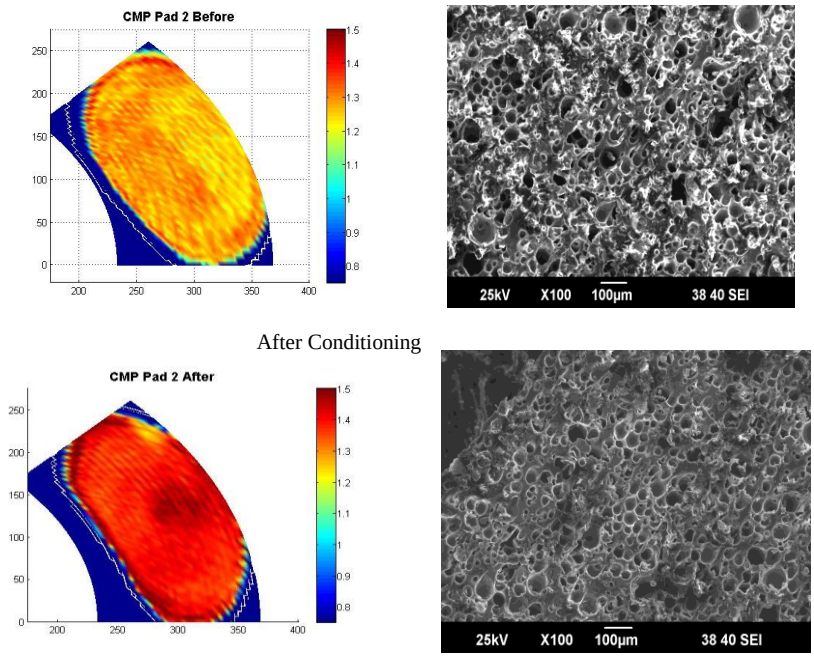

Figure 4. 14 As received and conditioned UTS and SEM images of pad (2)

The UTS amplitude is monitored as a function of height above pad and depth below its surface application of compression at different transmitted frequencies. The normalized UTS figures are pictorial representation of the changes in specific gravity (which can be related to the density) during polishing, with the darker red areas deemed HT and the lighter colors deemed LT. From figure 4.14, after conditioning the pad the as received pad the specific gravity increases along with the viscoelastic properties. The surface characteristics from the SEM follow the UTS images.

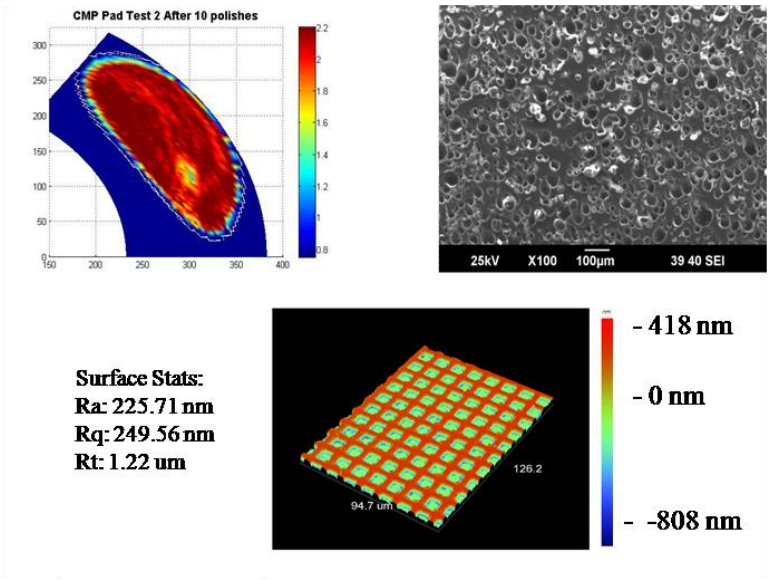

Figure 4. 15 UTS, SEM, and BPM surface roughness of pad (2) 10 polishes

In comparison to figure 4.14, figure 4.15 shows a representation of the UTS value increase in the number of areas of HT. This increase in HT corresponds to the increase in pad roughness as seen in section 4.5.2. The SEM images show a rougher morphology of the polishing surface while the WYKO images indicate the surface roughness from the BPM wafer being polished.

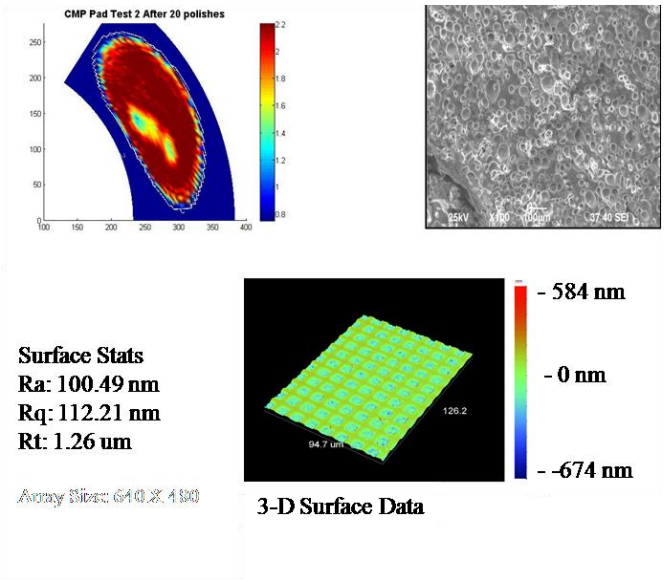

Figure 4. 16 UTS, SEM, and BPM surface roughness for pad (2) 20 polishes

After 20 polishes as seen in figure 4.16, the UTS graph indicates that the pad continues to become denser during polishing and the compression properties increase while the SEM morphology reflects the change in the surface characteristics. It should be noted that the pad has a reduction in roughness, and the surface can be seen to contain slurry remnants and partial glazing of the surface. The wafer surface continues to become further planarized and the results match well with the data from section 4.5.2. This trend is continued below in figure 4.17 and a summary of the results is described after figure 4.18.

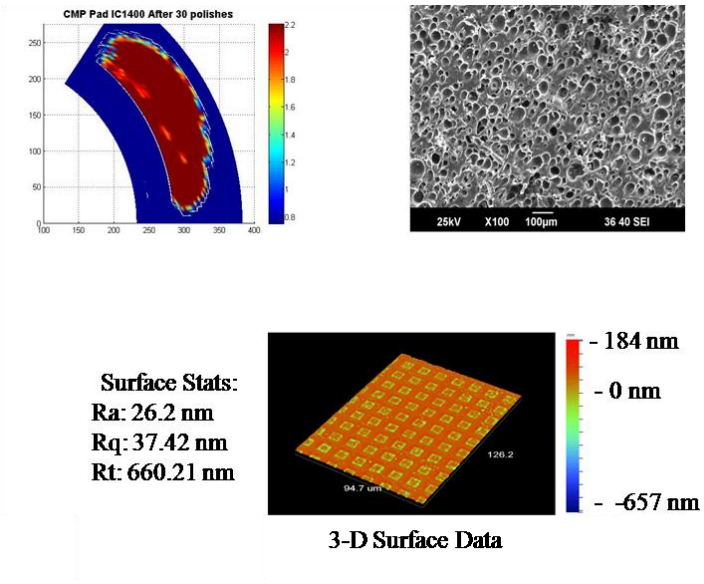

Figure 4. 17 UTS, SEM, and BPM surface roughness of pad (2) 30 polishes

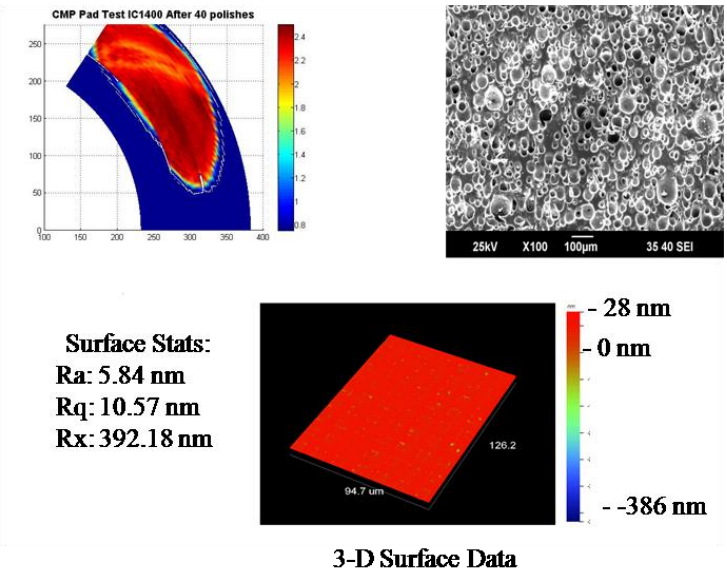

Figure 4. 18 UTS, SEM, and BPM surface roughness of pad (2) 40 polishes

The material properties of the pad begin to deteriorate after 40 polishes for pad (2) based on figure 4.15. This decrease is also characterized by the SEM picture, and the overall surface quality for 40 polishes of pad (2) has reduced the BPM wafer surface down to approximately 10 nm. The SEM images of the pad clearly depict slurry

remnants, pad glazing, and changes in the pore sizes and grooves due to the polishing of the rough BPM surface. There remain a number of good HT regions in the pad after 40 polishes therefore the pad is still suitable for polishing and therefore a new coupon was polished utilizing this pad.

4.5.4 Pad Morphology Discussion

The optimal polish time to planarize the BPM wafers for pad (2) was discovered to be 75 minutes for the process parameters in table 4.2. A parametric study was conducted to determine how each output parameter would affect each other to determine other methods for EPD and polishing requirements. The next step in determining the pad wear and polishing (beyond the UTS and SEM as these characterization techniques are costly and require the machine to be shut down in order to process this information).

4.5.5 WTWNU

The ability to detect the amount of variation that a particular pad will yield on the wafer surface is paramount and the ability to have accurate and repeatable results for given process conditions reduces cost and waste to the fabrication industry. A statistical WTWNU measurement is calculated using by dividing the standard deviation of the wafer surface roughness by the average surface roughness of each polish. This value will indicate how repeatable the polish parameters are for each pad and polish set. Table 4.3 contains the WTWNU values for each polish set (in increments of 10), up to the deterioration point of the pad or the planarity of the wafer.

Table 4. 3 WTWNU percentage based on BPM wafer CMP

WIWNU	10	20	30	40	50	60	70
Pad (1)	19.79%	27.48%	8.7%	6.87%	4.47%	11.32%	10.99%
Pad (2)	14.32%	16.39%	8.54%	3.34%	11.47%	16.42%	13.47%
Pad (3)	10.49%	9.61%	27.21%	28.01%			

From table 4.3, pads (1) and (2) follow a trend in which increase the polish time results in the surfaces having a lower WTWNU measurement. Pad (3) had the highest WTWNU and this could be due to the rapid decline of the pad, as indicated by the steady WTWNU up to 30 polishes. This table indicates that pad (2) produces the greatest number of repeatable results for polishing the copper BPM wafers.

4.6 Conclusion and Remarks

A benchmark parametric study on CMP pads for BPM copper wafers was completed to determine the effect on output parameters during the CMP process based on optimization of the machine parameters from chapter 3. Results indicate that as the pad is polished over time the MRR, COF, BPM surface roughness, pad thickness, and pad roughness are decreased. The process input parameters were held constant for polishing and a Stribeck curve was created for the pads based on the change in slurry thickness during polishing. An analysis of the lubrication regime which helps dictate polishing output parameters indicate that pad (1) operates mostly in the full lubrication regime, pad (2) operates in the partial lubrication regime, and pad (3) operates in the boundary regime.

Results also show that a force sensor is easily implemented into most standard polishing systems and can be used to determine the COF and analyze the pad life, MRR, and surface quality based on the COF during polishing.

The pad life, pad material removal, and pad roughness are characterized for 100 200 minutes of polishing at the process parameters in table 4.2) for each of the three commercially available pads and results indicate that for BMP copper CMP, the Rodel dual layer IC 1000 Suba V k-groove pad provides superior MRR, wafer roughness, and pad life for polishing with Cabot iCue 5001 and Cabot iCue 5003 slurries.

The surface morphology evolution of the pad was characterized using a novel non destructive ultrasound technique and scanning electron microscopy. The UTS readings are crucial indicators of the pad life and provide critical insight into the evolution of this morphology through a cost effective means. The UTS characterization and SEM characterization were able to detect that the pad material properties are inversely proportional to the porosity of the pad. This means that as the pads are polished over time the pores in the pad are worn away, and the lower material characteristics of the pad lead to a lower porosity and henceforth a lower MRR and COF. Several other researchers have found this aspect true for blanket copper and dielectric polishing, but the novelty in this research is in proving that the BPM wafers pad life is much lower than pad life for blanket wafers, with an average percent difference of 63.63% [167, 168]. The experimental pad morphology lifetime without reconditioning was characterized for all three pads with images from the SEM, UTS, and WYKO in the appendix of this dissertation.

A statistical WTWNU measurement is calculated by dividing the standard deviation of the wafer surface roughness by the average surface roughness of each polish. This value will indicate how repeatable the polish parameters are for each pad and polish set. Pad (1) provided the lowest WTWNU measurement, indicating that the repeatability of the process is optimal utilizing pad (1), although not optimal for MRR and surface roughness characteristics. Results for the optimal machine parameters and pad are next utilized in the slurry characterization seen in the forth coming chapter.

CHAPTER 5: SYNTHESIS OF NOVEL CMP SLURRY

5.1 Foreword

The economic impact of the slurry during CMP for the semiconductor industry rises over 2 billion dollars a year. There is significant research into manufacturing new slurries that have the capability of high removal rate, excellent global planarization, corrosion prevention (in case of metal, especially copper), good surface finish, low probability of defects and high selectivity. The chemical and mechanical interactions of the slurry is the least understood mechanism during the CMP process and ongoing research has yet to adequately explain these mechanisms. CMP is a process that is influenced by numerous slurry parameters such as pH, solution chemistry, charge type, concentration and size of abrasives, complexing agents, oxidizers, buffering agents, surfactants, corrosion inhibitors, etc [42, 173, 174]. The specific and proprietary nature of slurry manufacturing makes it difficult to elucidate the exact effects of slurry on the particular thin films that are polished by it. The slurry interactions at the pad wafer interface are probably therefore, the least understood mechanisms in entire semiconductor fabrication process technology [154]. Due to lack of understanding of the mechanisms for polishing and the economic impact the slurry has, CMP slurry has continued to be a catalyst for research and development. The ability to chemically etch a specific material and polish that material while essentially leaving the underlying material alone are interests of both the industrial and academic relevance. Based on the

optimized machine parameters and pads the output parameters based on the slurry interaction are investigated as shown in figure 5.1.

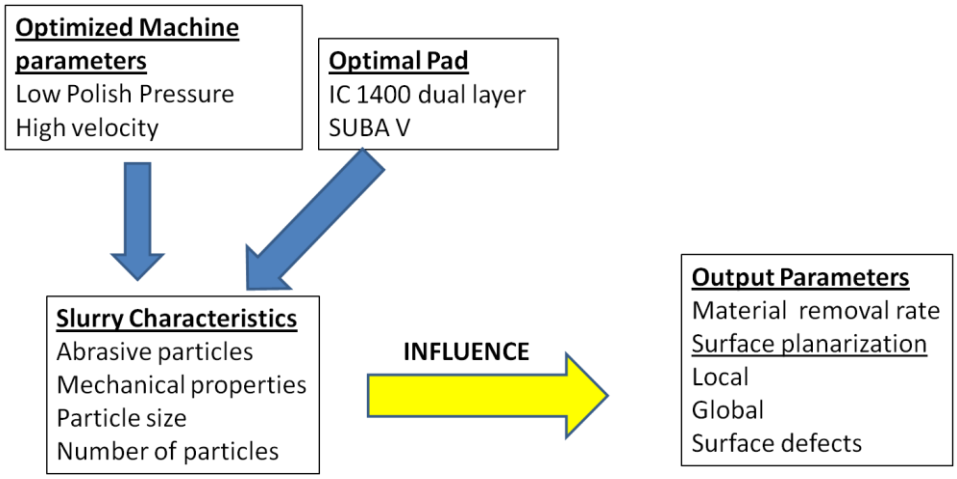

Figure 5. 1 Slurry optimization schematic

The research objectives of this chapter are:

1) Develop and investigate new nanodiamond (ND) slurry for BPM CMP
2) Determine the MRR and surface quality based on the new ND slurry.
3) Compare and contrast the novel ND slurry versus industrial slurry CMP.

5.2 Introduction

In order to create slurry that is novel in use and effective for the CMP process, an investigation into the most important aspects of the slurry is given in the following sections. While not all of the chemical aspects are investigated for this slurry, this research is a feasibility study in utilizing nanodiamond (ND) particles in polymer matrix as a polishing solution or a final buffing solution for the CMP process.

5.2.1 Effect of Slurry on Planarization (Surface Quality)

In order to achieve the strict requirements of the magnetic storage and semiconductor industries on the removal rate and surface roughness during CMP, the effects of the slurry must be investigated. Table 5.1 lists the output parameters for global planarization and the mechanisms by which these parameters are achieved by the slurries [175]. The slurry parameters must be optimized so that the mechanical removal of the material is minimized because excessive mechanical removal produces high frictional forces and can thus damage the surface topography. An initial study into the surface characterization of new and novel slurry was undertaken based parameters in the table below.

Table 5. 1 CMP process output and slurry mechanisms [175]

Global planarity	Removal Rate	Surface defectivity	Selectivity	Slurry handling
Formation of thin passivation layer	Rapid formation of thin surface layer	Rapid formation of thin surface layer	Top layer chemomechanical polishing	Formation of stable slurries
Minimize chemical etching	Control of mechanical/interfacial properties of the surface layer	Minimize mechanical polishing	Bottom layer mechanical polishing	Control of interparticle and particle surface interactions
Minimize mechanical polishing	Stress induction by abrasion to remove surface layer	Control of particle size and hardness	Reduction of mechanical component in slurry	Steric force based repulsion in ionic systems
	Indentation based wear	Control of particle size distribution		
	Fracture/delamination-based removal			

In order to make effective slurry for CMP there are several issues that must be considered before specific slurry design, the slurry must:

1) Minimize the frictional forces

2) Maintain constant local polishing pressure

3) Reduce excess chemical etching

The frictional forces must be minimized in order to ensure that the amount of surface defects is reduced. High frictional forces indicate that polishing is going in boundary lubrication regime which is a two body abrasion mode in which the pad and wafer are in direct contact; consequently this would indicate that the slurry is not contributing to material removal. Lowering the pressure and increasing the polishing

times helps to lower the COF and increases global planarity [175]. Ensuring that the local pressure is constant is paramount because variable pressure leads to variable polishing rates and non uniformity in the wafer surface. Excessive chemical etching adversely affects surface planarity and induces defects on the surface such as corrosion [175, 176]. The novel slurry developed in this chapter seeks to lower the COF as compared to industrial slurry, while reducing the chemical etching on BPM matrices.

5.2.2 Chemical Effect of Slurry of Material Removal Rate

The reaction of the slurry chemicals on the metal to be polished, the mechanical abrasion of the particles, the interplay of the different complexing agents, oxidizers, and corrosion inhibitors are all intertwined into one process during polishing. There have been numerous studies on the effect of the chemicals in the slurry on the wafer surface. It has been concluded that the reaction rate and the creation of a passivation layer on the surface can be increased up to a limit by adding oxidizers and corrosive inhibitors [78, 153]. Creation of a passivation layer weakens the metal surface allowing for the abraded particles to strike the surface and cause material removal. Figure 5.2 is a diagram of these interactions.

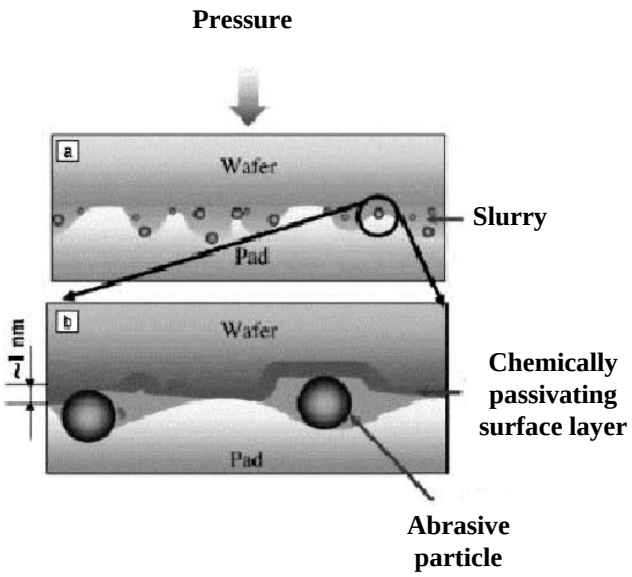

Figure 5. 2 Pad/wafer interface reactions with the slurry

5.2.3 Mechanical and Material Properties

The particle concentrations all play a role in the overall material removed during polishing. The generalized abrasive material removal rate (MRR) for CMP has been modeled in the literature and is shown in equation 5.1 [153].

$$MRR = nVol_{removed} \tag{5.1}$$

The variable n is number of active abrasives taking part in the process and $Vol_{removed}$ is the volume of material removed by each abrasive. To estimate the total volume of material removed, it is necessary to estimate the total area of the pad/wafer and wafer/abrasive contact. The area of active abrasive contact is given by equation 5.2,

$$A = \pi x \delta \tag{5.2}$$

where A is the area of contact, x is diameter of abrasive, and δ is the depth of indentation on the passivating film made by the abrasive particle [129]. Based on the above equations many models have been created that suggest the influence of the abrasive particle size on the material removal rate and surface finish. Jairath et al. and Xie et al. observed that the polishing rate increases with both particle size and concentration [177, 178]. Contrary to these findings, Bielmann et al. have found that decreased particle size led to higher polishing rates or no effect on the MRR [179, 180]. Mahajan, Lee, and Sign have proposed that the CMP process is based on two removal mechanisms: an indentation based wear which dominates for large abrasive particles and a contact based mechanism which dominates for small abrasives [181]. In either case there is a saturation point for abrasives in which an increase the amount of particles and/or the particles size results in there no longer being an increase in the amount of material removed. A qualitative explanation for this was given by Luo, the total contact area between the wafer and pad surface asperities is occupied by the active abrasives when saturation occurs, and a further increase in concentration cannot increase the number of abrasives in the contact area, as shown in figure 5.3 [147].

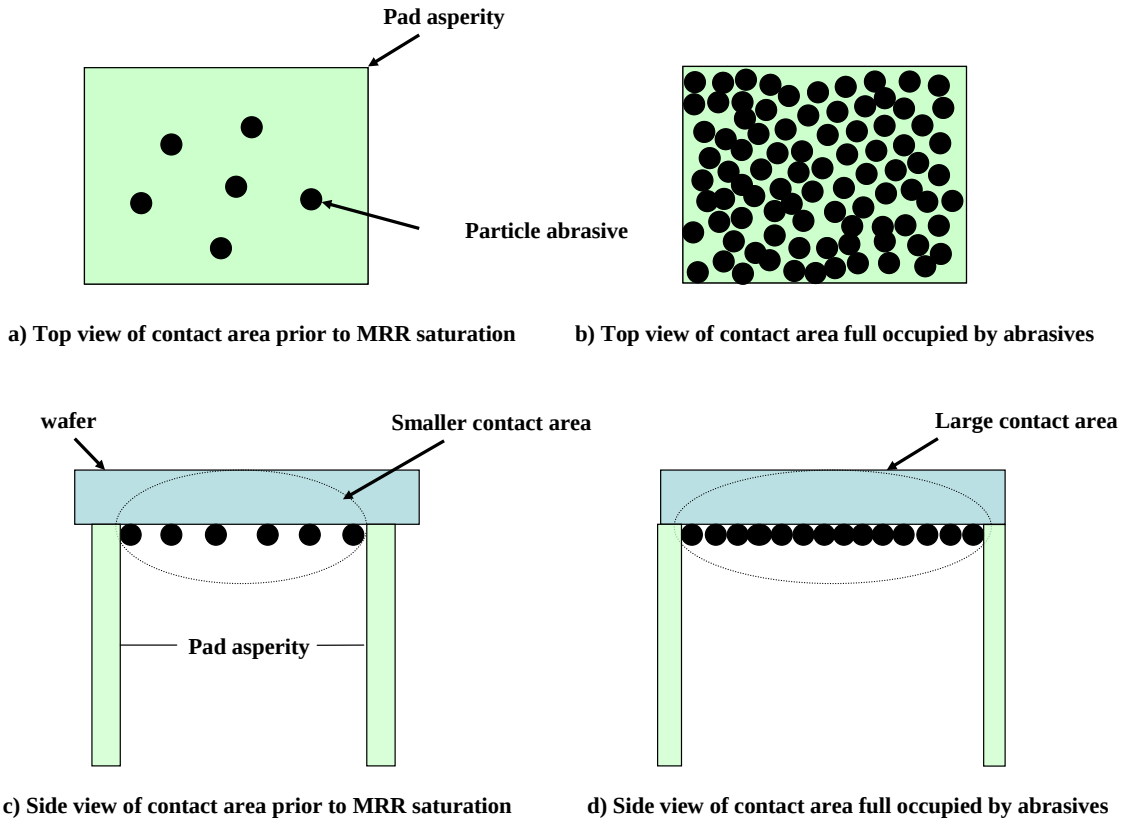

Figure 5. 3 Contact modes with abrasive weight concentrations

From figure 5.3, an increase in particle size as well as concentration will lead to the same effects from the saturation of the contact area. Therefore there are two transitions of material removal regions with the increase in abrasive weight concentration or size. First the transition from a rapid increase at a small abrasive concentration to a slower linear increase region. The second transition is from the linear increase region to the saturation region at larger abrasive concentrations. This example is shown in figure 5.4.

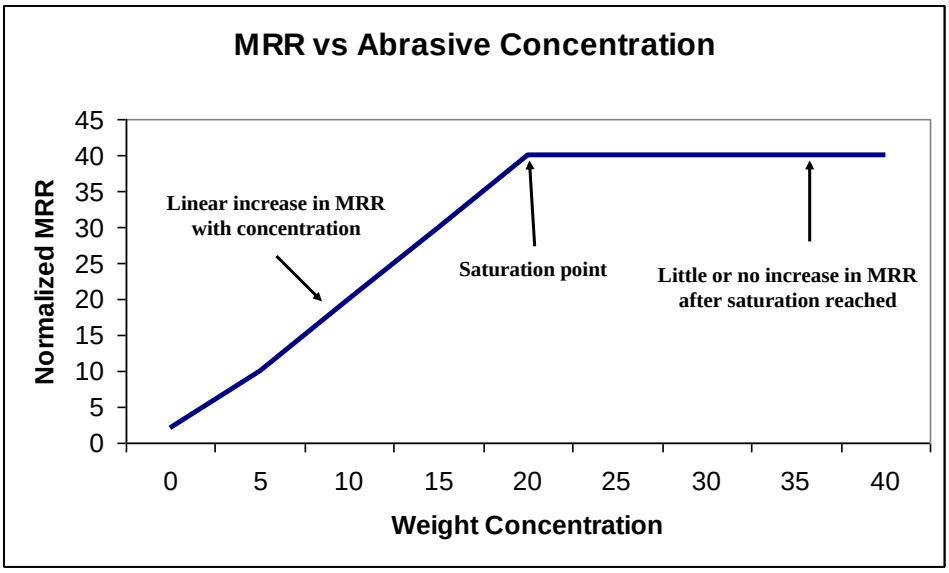

Figure 5. 4 Example of saturation for MRR

The figure gives an example of the effect seen in literature for increase the particle concentration, is this effect shown for polishing on SiO2 by Singh et al [175].

As shown by Singh, Bajaj and, Mahajan et al., the removal rate of the silica increases with increase in particle size and concentration at low particle concentrations, however after a particular threshold for every given particle size the mechanism of removal changes and there is considerable decrease in removal rate with increase in particle concentration [181] . This effect will be investigated for the novel slurry created in this chapter.

5.2.4 Particle Size and Hardness

As mentioned in section 5.2.3, the particle size has the same effect as the concentration on the removal rate during CMP, and a similar figure to figure 5.2 could be drawn for particle size. The particle size also has effects on the overall surface quality after polishing. An increase in particle size or hardness also gives rise to surface defects

such as micro-scratches that cause fatal long-term device failure. Bigger and harder particles would cause deeper micro-scratches, which will be very difficult to eliminate even by the final buffing CMP step. Therefore in the creation of the ND slurry, the particle size is kept small. Although diamond is the hardest natural material, the inclusion of the softer polymer matrices helps to reduce the effects after polishing of the harder abrasive particles.

5.2.5 Abrasive Particle

The abrasive particle in the CMP slurry serves as the mechanical mechanism for abrasion during polishing. Without the abrasive particles, the slurry would only aid in chemical corrosion of the surfaces. Selection of the correct abrasives requires knowledge of the mechanical properties, hardness, and fabrication of the nanoabrasives.

5.2.5.1 Commercial Slurry Abrasive Synthesis

The quality of the post CMP wafer surface is significantly dependent on the characteristics of the abrasive particles present in the slurry. There are several abrasive particle type options and the table below outlines the abrasives and the synthesis technique.

Table 5. 2 Slurry abrasive characteristics

Slurry Abrasive	Synthesis Type Fumed (F), colloidal (C), Sol (S)	Abrasive Use	Characteristics	Remarks
Silica	F,C,S	Oxides: F,C Cu: C W: F, C	Sizes vary, of medium hardness Low selectivity	Polishes vast number of materials, low selectivity
Alumina	F, C	Dielectrics Copper	Strong Lewis-acidic surface Very Hard Amorphous	Low MRR on dielectrics, Hardness can lead to surface scratches
Ceria		SiO_2	Low scratches and high MRR Lewis-acidic surface	Expensive High selectivity for SiO_2
Titania, Zirconia	C, S	FRAM, dielectrics , oxides	Additives have high hardness and selectivity abrasives	High selectivity Low MRR Used with other abrasives

The synthesis method determines the size of the abrasive particles. Fumed abrasives tend to be chained particles that are larger in size than colloidal abrasives, which consist of discrete particles in dispersion that precipitate from a solution. For the

same solids concentration, the removal rate using a fumed abrasive is higher than that using a colloidal abrasive due to larger particle size. For this reason the defect density using a fumed abrasive is also higher and the colloidal abrasive having a uniform particle size is preferred. However, to achieve the same removal rate as using a fumed abrasive, the solids concentration of colloidal slurry must be almost three times higher, thereby increasing the cost of the slurry.

5.2.5.2 Surface Quality Based on Abrasives

The generation of surface scratches depends on a wide variety of factors such as the process conditions as mentioned in previous sections of this chapter. Of particular interest in the present research are the characteristics of the abrasive particles and their effect on the surface quality. A comparison of ND polymer slurry synthesized to the abrasives used for commercial copper CMP helps to evaluate the surface quality and feasibility of the ND polymer slurry during polishing. Several other commercial abrasives have been detailed in literature and are not characterized in this dissertation [136, 156, 176, 182, 183]. Alumina particles have been used for copper CMP due to their low selectivity and material removal of the dielectric layer below copper, but the high hardness value has lead to severe surface scratches. These particles typically have a Mohns hardness value of 9, which is only below the hardness of diamond which values at 10.

The alumina abrasive particles can agglomerate in the slurry. The effective size of the particles can be much higher than the specification of the slurry and the agglomerated particles can make deep scratches in the surface. The deep scratches result in defects that cannot be removed by any other post processing techniques. Commonly

used ceramic abrasive particles are much harder than the low dielectric constant materials and copper. These particles can easily scratch the surface and, if agglomerated, can result in permanent scratch defects. Thus, the inherent nature of the particle plays a significant role.

The abrasive particles that result in low friction at the interface are beneficial to the process due to the fact that lower friction helps reduce surface damage during CMP [184]. The particle residue encountered after polishing along with post CMP cleaning are parameters that must also be investigated for any slurry fabricated[135, 185].

5.3 Novel Nanodiamond (ND) Slurry Synthesis

Knowledge of the slurry chemistry, particle size, particle concentration, and hardness are properties that must be investigated in order to create any new or novel slurry. The slurry developed in this dissertation contains composite particles that are inherently soft due to the presence of polymer. This alternative approach involves using responsive polymer microgels to entrap the ND particles and utilize the new slurry for CMP. In this approach, the ND particles will on the surface of the polymeric microgel (hybrid composites) and will conceivably prevent aggressive abrasions of the ND on the wafer surface resulting in smoother surfaces and reduced surface damage. The ND slurry composite is hypothesized to provide a cushioning effect to the wafer due to the soft nature of the polymer and yet achieve appreciable CMP material removal due to the abrasion of the hard ND particles. The polymer particles exhibit controllable surface hardness and chemical nature and hence are hypothesized to prevent aggressive scratching, particle residue, and apply high mechanical stress during polishing. The incorporation of functional groups onto polymer latex surfaces to form new hybrid

materials represents an emerging discipline for the synthesis of novel materials with diverse architectures. Polymer particle synthesis and characterization was initially conducted and verified by Dr. Cecil Coutinho under the guidance of Dr. Vinay Gupta in the Department of Chemical Engineering at the University of South Florida.

5.3.1 Hybrid Particle Synthesis

Unless otherwise noted, all chemicals were purchased from Sigma-Aldrich (WI) and used without further purification. The monomer nisopropylacrylamide (NIPAM TCI) was recrystallized from hexane before use. With the goal of developing novel slurry for CMP applications, polymer-siloxane (hybrid) microgels were formed by the surfactant free precipitation polymerization of NIPAM (5g) in aqueous media (800 ml) using N,N' methylenebisacrylamide (0.2g) as the cross-linker. Following purging with N_2 for 1h, the reaction mixture was heated in an oil bath to 75°C and the ionic initiator potassium persulfate (0.1g) was added to instigate polymerization. After an initial polymerization of 2 hours, 3-(trimethoxysilyl) propyl methacrylate (1g) was added to the reaction mixture and the polymerization continued for a further 90 minutes. The microgels formed were collected and purified by repeated centrifugation (7800g, 30minutes) and re-dispersed with deionized water [186-188].

The nanodiamond (ND) particles were acquired from International Technology Center (ITC Raleigh, NC). The particles were suspended in a water solution with 1 wt% concentration. The ND particles are 98% pure and are all in cubic phase and were measured to be 5 ±3 nm.

The ND slurry was composed of the softer NIPAM microgel matrix and the harder fused ND particles. For characterization of the slurry, 500 µl of the ND particles

were immersed in 4 ml of deionized water. The solution was put into an ice bath and was allowed to chill for twenty minutes. In conjunction with the ice bath, 250 µl of NIPAM was immersed in 2 ml of deionized waters and the solution was put on a hot magnetic stirring plate and heated and stirred at 40°C for twenty minutes. Heating NIPAM allows the thermally responsive polymer to denature the polymeric chains that create the spheres seen from TEM imaging. Once the NIPAM is receptive to the ND particles the two solutions are mixed together on the stirring plate for 30 minutes. The solution is then centrifuged at 5000 RPM for an additional 30 minutes. The new slurry labeled NIPAMND is settled and dispersed in 3ml of deionized water.

5.3.2 Particle Characterization

The NIPAM particles along with the ND particles were characterized to ensure synthesis and fabrication of the particles was successful. Dr. Coutinho completed the dynamic light scattering characterization of the NIPAM particles while the rest of the characterization was completed during the research of this dissertation.

5.3.2.1 NIPAM Dynamic Light Scattering [188]

Microgel sizes and polydispersities were determined via dynamic light scattering (DLS) using a Zetasizer Nano-S (Malvern, PA). Samples were sonicated prior to analysis. A 1ml of the microgel solution was placed into a cuvette and allowed to thermally equilibrate to a certain temperature for 10 minutes before each measurement. Data fitting was done using a multi-modal algorithm supplied by Malvern. The collected correlelograms were fitted to diffusion coefficients and converted to a hydrodynamic diameter using the Einstein-Stokes equation [186-188].

5.3.2.2 Transmission Electron Microscopy (TEM)

The NIPAMND composites were examined using TEM to visually determine the extent of ND loading and dispersion within the polymer matrix. A drop of the sample solution was diluted with ethanol and then was placed on a Formvar-coated Cu TEM grid that was examined using a FEI Morgagni 268D.

5.3.2.3 Post CMP Surface Characterization

Qualitatively, the surface quality of the BPM and blanket copper surfaces post CMP was examined by WYKO NT 9100 and a Leitz Ergolux optical microscope. The resulting surface roughness was measured from the WYKO NT 9100. The removal rates were calculated from four point probe measurements on the sample and details of those calculations are in chapter 3, section 3.2.4.2. The initial and final thickness measurements were calculated as an average after nine different readings were taken. The benchtop CMP tested provided real time measurements of the friction coefficient during polishing and the average value after the process had reached state has been reported.

5.4 Experimental Conditions for ND Slurry and Particle Slurry Testing

Three different slurries were used as a comparison for testing the validity of the NIPAMND slurry. The slurries were tested on the MIT 854 BPM copper wafer and a blanked wafer of copper. The blanket wafer was fabricated at University of South Florida, NREC and is a silicon substrate with, a 5nm layer of barium on top of the silicon substrate, as well as a 10 nm layer of tantalum, and finally electrodeposited with 10µm thick copper. The Cabot iCue 5001 colloidal alumina commercial slurry, the NIPAM polymer matrix, and the developed NIPAMND slurry have their properties displayed in

table 5.3. All the slurries formulated were to have an equal amount of weight percentage of abrasive particles.

Table 5. 3 Slurry details

Slurry Name	Particle type	Particle Size (nm)	Hardness (Mohrs)	Wt%
Cabot iCue 5001	Alumina	20 ± 6 nm	9	1.5
NIPAM	Hybrid polymer	500 ± 20 nm	0	1.5
NIPAMND	Hybrid-ND	500 ± 40 nm	ND-10	1.5

The slurries were then employed for performing CMP on the BPM copper wafer mentioned in chapter 3, section 3.2.1, they were also used on blanket 1" blanket copper wafers. The testing of the slurry samples was carried out at the process conditions summarized in table 5.4.

Table 5. 4 Process conditions for slurry testing

#	Parameter	Value
1.	Pressure	4 Psi
2.	Platen speed	200 RPM
3.	Carrier speed	200 RPM
4.	Slider movement	3 mm/s
5.	Slurry flow rate	75 mL/min
6.	Time	60 seconds
7.	Pad	Rodel IC 1400 Suba K-groove pad
8.	Specimen	MIT 854 BPM 1"x 1" copper coupons

5.5 Results and Discussion

As with chapter 4, the amount of data acquired for analysis through the WYKO NT9100 greatly exceeds the amount of reasonable space in this dissertation therefore images and characterization for the surface profile presented in the section are the images

that reflect the most important information of all the data. Additional data is presented in the appendix of this dissertation. The blanket copper polish experimentation was done to compare to the IC industry to determine if the ND slurry was a feasible means for either IC fabrication or BPM fabrication. The blanket results due not elucidate any information on BPM CMP.

5.5.1 TEM Imaging

The hybrid particles were synthesized using precipitation polymerizations, and all three slurries were characterized using TEM, and the average size from the TEM calculations is shown in table 5.3. Figure 5.5 contains the image for the three abrasive particles from the TEM imaging.

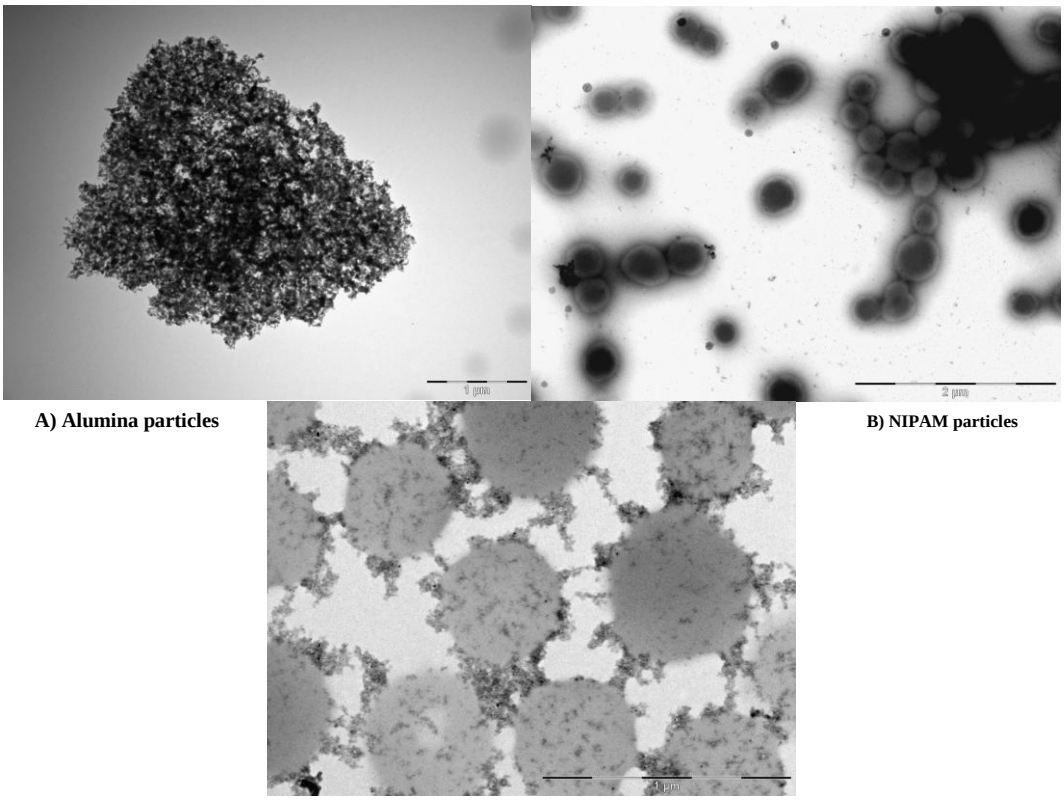

A) Alumina particles

B) NIPAM particles

C) NIPAMND particle

Figure 5. 5 Slurry particles

The agglomeration for the particles in all three figures seen in above is cause for concern for the result surface quality. The massive agglomeration of the Cabot slurry particles helps further validate the necessity of new and novel slurry.

5.5.2 COF of the Slurry Abrasives

The values from the CMP benchtop tester for COF during polishing for the abrasives against the BPM and blanket copper wafers are shown in figures 5.6 and figure 5.7 respectively.

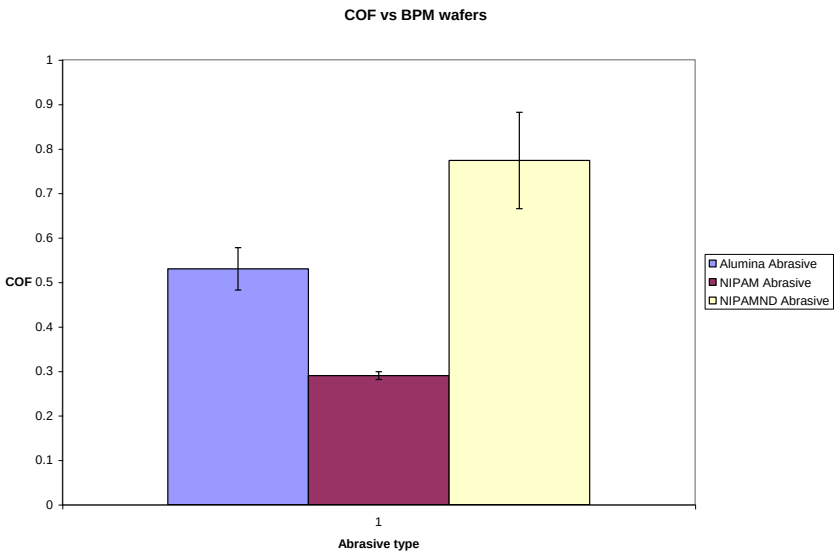

Figure 5. 6 COF vs. BPM wafers

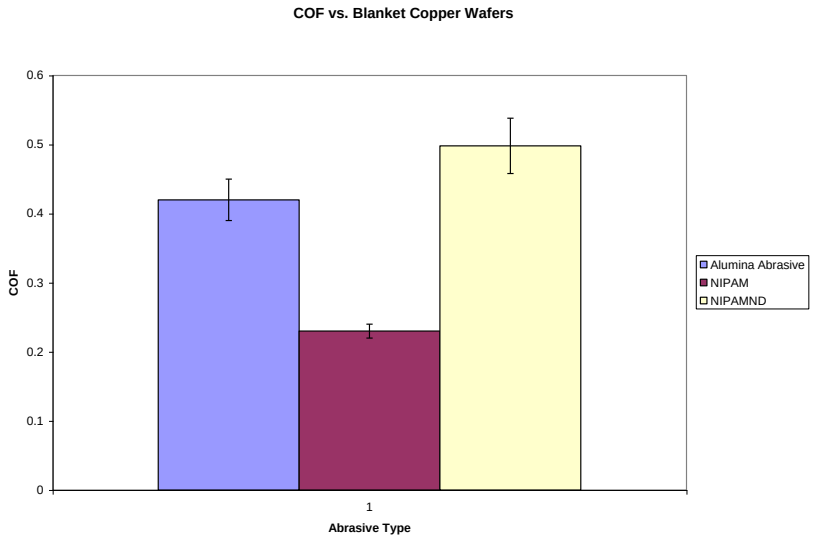

Figure 5. 7 COF vs. blanket copper wafers

From the figures above, it is evident that the softer NIPAM particles have the lowest COF, whereas the Cabot and the NIPAMND particles have coefficients that are similar. This is to be expected since the hardness values (e.g., the amount each particle will indent into the surface and possibly abrade the material) are larger than that for the

NIPAM alone. Hardness is the ability for a surface to resist plastic deformation, and this resistance can be linked to the COF. The hardness of the NIPAM lends to the indentation based wear regime developed by Mahajan et al., but the size leads to the contact based wear, and this is optimal for the polishing regimes of the NIPAMND. The fact that the alumina particles have a higher COF than the NIPAMND even though the NIPAMND has harder abrasives than the alumina particles is promising and elucidates further research into the NIPAMND slurry as a technique for CMP.

5.5.3 MRR Versus the Abrasive Particle

The MRR for the slurries must be known in order to determine the feasibility of the process. Figure 5.8 contains the MRR versus the various slurries for the polishing parameters in table 5.4.

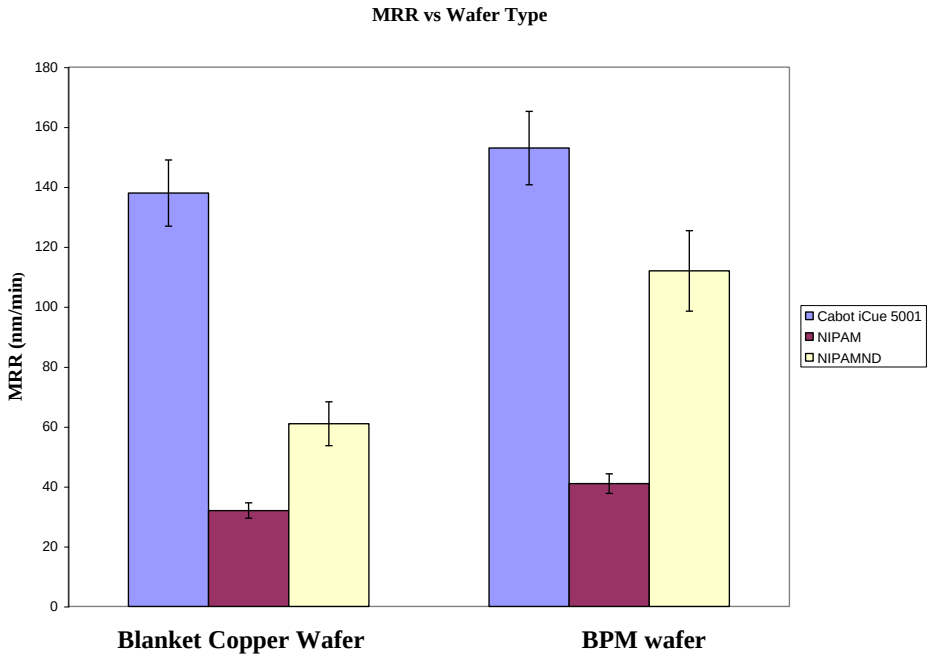

Figure 5. 8 MRR vs. wafer type for analysis of slurry abrasives

Figure 5.8 details the interactions of the slurry with the wafer surfaces. The NIPAM slurry achieves the lowest MRR, and this is expected due to the inability of the particles to impinge upon the harder copper surface and remove material. The removal mechanism during this polishing is solely due to the asperities of the pad and the wafer asperities. The NIPAMND slurry has a significantly higher MRR than the NIPAM alone, but this value still falls short of the Cabot slurry MRR. The difference in the MRR for the Cabot slurry and the NIPAMND cannot be explained solely by the hardness of the abrasive as it can with the COF data. The Cabot slurry has a chemical aspect that both the NIPAM and NIPAMND slurry do not contain, as this commercial slurry has oxidizers and passivating agents in order to further break up the copper surface to help the abrading particles. In order to develop fully commercialized NIPAMND slurry the chemical aspects of the slurry and the interacting surface must be fully understood and investigated.

5.5.4 Surface Quality and Roughness

The resulting surface roughness (RMS) values from polishing of the blanket copper wafers and the BPM wafers are shown in table 5.5. The initial roughness value for the BPM is 352.73 ± 1.24 nm and for the blanket copper wafers the initial value is 50.92 ± 2.46 nm.

Table 5. 5 Surface roughness for slurries

Slurry	BPM Roughness (RMS)	Blanket Cu (RMS)
Cabot iCue 5001	308.23 ± 3.45 nm	27.37 ± 3.16 nm
NIPAM	343.07 ± 2.21 nm	41. 75 ± 2.08 nm
NIPAMND	344.25 ± 2.72 nm	38.18 ± 2.31 nm

From the table above, the Cabot and the NIPAM ND slurries result in very similar surfaces although the MRR is much greater with the Cabot slurry. The surface roughness of the blanket copper wafer with respect to the NIPAM slurry is defect free but the MRR and the resulting RMS values indicate that the NIPAM slurry is ineffective without a harder abrasive agent for copper CMP. The WYKO images of three slurries for the BPM matrix and blanket copper wafers are shown in figures 5. 9 and 5.10 respectively.

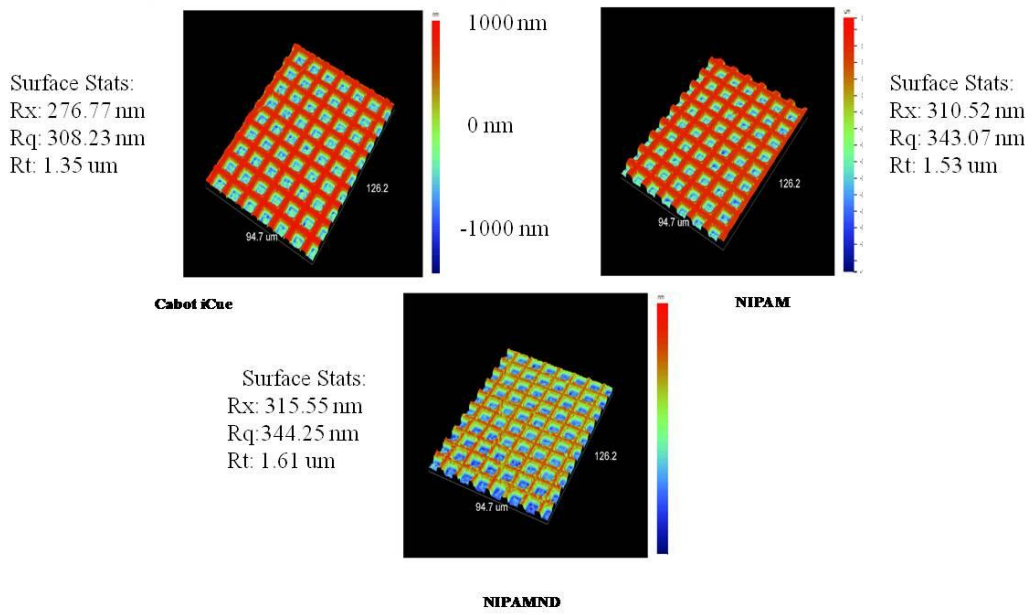

Figure 5. 9 WYKO surface profiler images for BPM polishing

From figure 5.9 the NIPAM and the NIPAMND had very similar surface roughness values for the BPM wafer polishing although the MRR for the slurries differed. The theory behind the matching surface roughness values arises from the ND particles that were not removed during post CMP clean up. These particles embedded themselves in the BPM configurations and continued to cause scratches on the surface or were embedded in the matrix configurations themselves.

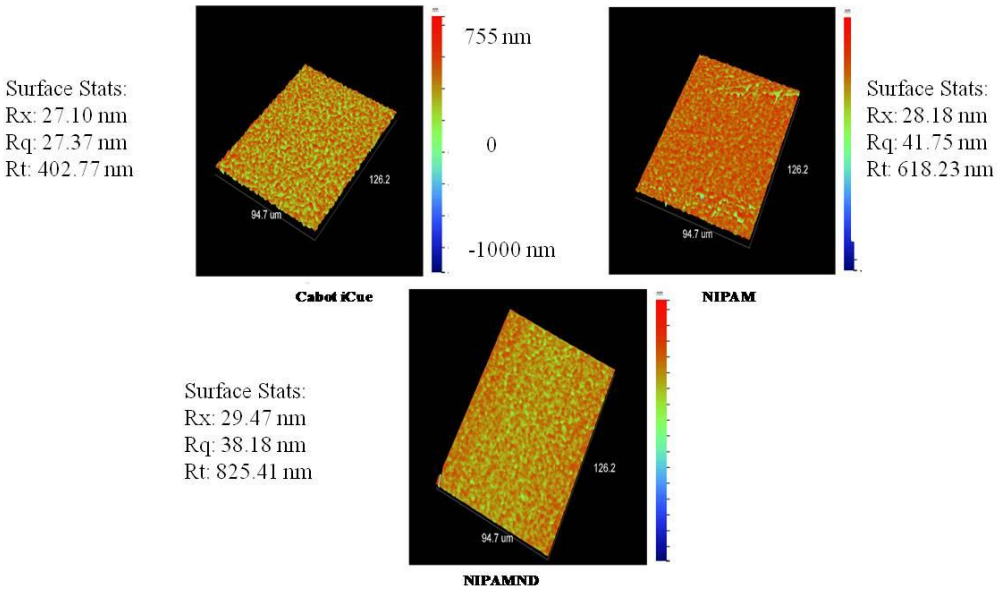

Figure 5. 10 WYKO images of slurry polishing of blanket copper wafers

From figure 5.10, the results are indicative of the MRR results. The NIPAMND slurry achieves greater local and global planarity then the NIPAM particles themselves while still lacking in overall polish quality of the commercially available Cabot slurry. The NIPAMND surface was further hampered by ND embedment in the surface and this is an issue to address in the post CMP cleanup process.

5.6 Analysis of NIPAMND Abrasive Concentration

With a successful synthesis and polishing using the NIPAMND slurry, an initial investigation into two different abrasive concentrations and the saturation point is studied. Due to the success of the blanket copper wafer CMP, only these wafers are included in the study of the saturation point and the process outputs. The nomenclature used for the number of abrasive particles is as follows:

1) Particle (1): 6.07x 10^{19} ND particles in the solution

2) Particle (2): 1.21x10^{20} ND particles in the solution

3) Particle (3): 1.81x10^{20} ND particles in the solution

4) Particle (4): 3.642x 10^{20} ND particles in the solution.

The values for the number of ND particles in the solution were arbitrarily chosen. The novelty of the slurry requires inherent baseline testing for the number of abrasives. The same synthesis technique of the NIPAM slurry as mentioned in section 5.3 is done for this research parameter. The amount on ND concentration is varied. The same process parameters and characterization techniques as table 5.4 are investigated.

5.6.1 COF and the Abrasive Particle Concentration

Figure 5.11 shows the variation in the COF with the different abrasive concentrations used in parametric study.

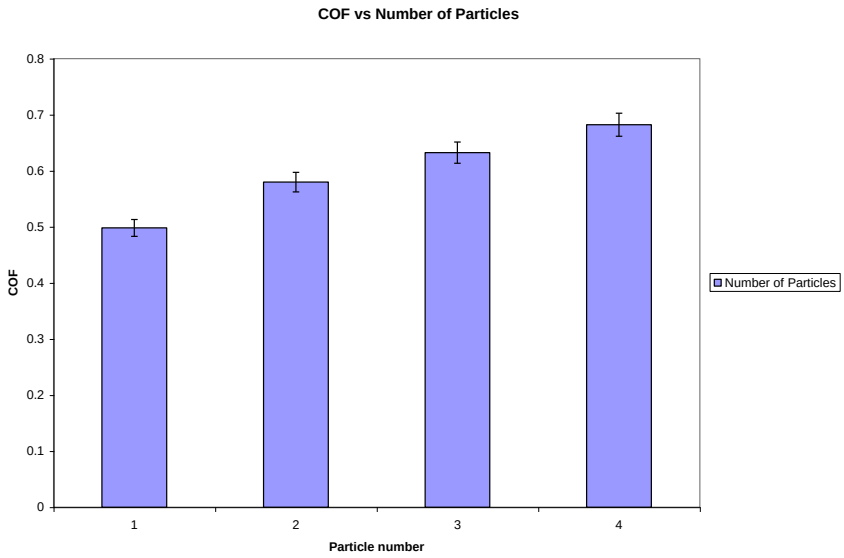

Figure 5. 11 COF vs. number of particles for NIPAMND slurry

Figure 5.11 details that the COF value does not significantly increase for the parameters from table 5.4, above particle (3) number. This could be due to saturation of the particles on the contact area of the wafer, with full coverage increasing the number of particles impinging the surface will not increase active particles in the polishing region and thereby the COF.

5.6.2 MRR and Abrasive Particle Concentration

Figure 5.12 shows the MRR versus the abrasive particle concentration for both the blanket copper wafers and the BPM wafers.

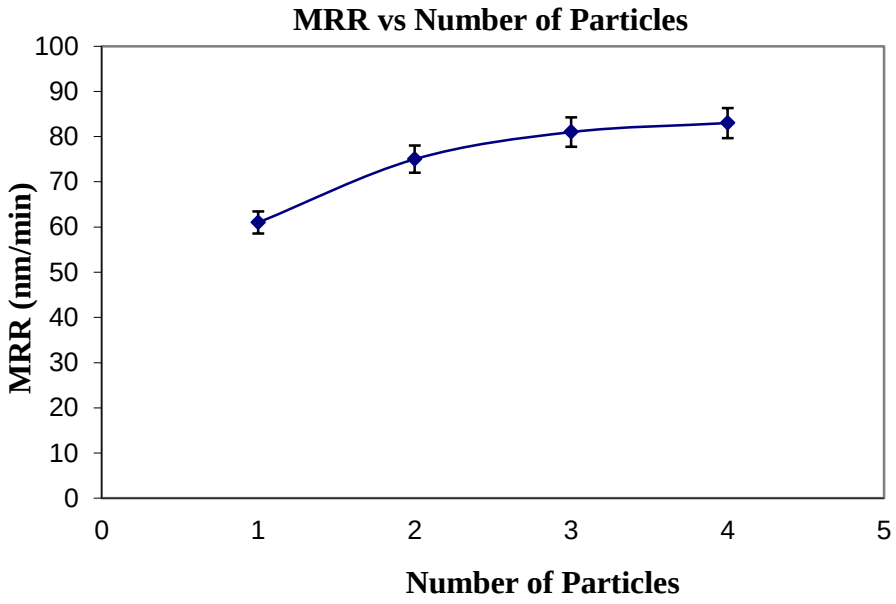

Figure 5. 12 MRR vs. number of abrasive particles for NIPAMND slurry

Figure 5.12 indicates that the saturation point for the number of particles that are active in the contact area during polishing is at particle number (3). Above this number of particles the MRR no longer increases linearly and the resulting slurry particle concentration is not advantageous for polishing.

5.6.3 Surface Roughness and Abrasive Particle Concentration

Table 5.6 contains the surface roughness values for the abrasive concentrations used during experimentation.

Table 5. 6 WYKO surface profile data for number of particles

Number of Abrasive Particles	Surface Roughness (RMS)
Particle (1)	38.18 nm
Particle (2)	34.17 nm
Particle (3)	31.21 nm
Particle (4)	30.54 nm

From table 5.6 and the data from figures 5.11 and 5.12 increasing the number of particles and thereby the cost of the slurry does not significantly increase the output of the deliverables of the slurry (e.g., MRR and surface roughness). For the NIPAMND slurry the optimal number of particles for copper CMP remains between particle number (2) and (3).

5.7 Conclusions and Remarks

There has been tremendous amount of research and development of novel slurries funneling from the 1 billion dollar economic impact that the slurries have on CMP. Although there is a multitude of slurries for various applications no slurry exists that has been able to polish several different materials locally and globally without a detrimental effect to the surface finish. In this chapter new novel hybrid polymer based ND slurry were developed for polishing on both BPM copper wafers and blanket copper wafers. The process parameters remained constant during polishing and the resulting COF, MRR,

and surface roughness were monitored. The particles were characterized by DLS and TEM. The NDs were suspended within the thermally responsive NIPAM polymer matrix and provided better results for polishing the then previously published NIPAM polishing results because the hard ND particles were a better abrasive for wear than the softer NIPAM slurry [186]. Consequently the NIPAMND slurry contained a higher COF than the NIPAM slurry and was comparable to the commercial slurries in the COF. This higher COF may be attributed to the hardness value of the ND particles. Upon successful synthesis and testing of the NIPAMND slurry, two different concentrations were created to test the saturation limit for the ND particles and the removal rate. It was determined that beyond particle number (3) the MRR and surface roughness outputs remain nearly constant for polishing of the blanket wafers. Discussion of future work will be in chapter 7.

CHAPTER 6: CMP MODELING OF MICROSTRUCTURAL VARIATION

6.1 Foreword

With the rapid change of materials systems and decreased feature size, thin film microstructure and mechanical properties have become critical parameters for microelectronics reliability. This requires inherent knowledge of the mechanical properties of materials and an in depth understanding of the tribological phenomena involved in the manufacturing process. CMP is a semi-conductor manufacturing process used to remove or planarize ultra-thin metallic, dielectric, or barrier films (copper) on silicon wafers. The material removal rate (MRR), which ultimately effects the surface topography, corresponding to CMP is given by the standard Preston equation, that contains the load applied, the velocity of the pad, the Preston coefficient which includes chemical dependencies, and the hardness of the material. Typically, the hardness, a bulk material constant, is taken as a constant throughout the wafer and thereby included in the Preston coefficient. Through metallurgy studies (on the micro and nano scale) it has been proven that the hardness is dependent upon grain size and orientation.

This research served to first relate the crystallographic orientation of a crystal to a hardness value. The second objective of this chapter is to use the hardness variation in the previously developed particle augmented mixed-lubrication (PAML) model to verify the surface topography and MRR during CMP.

6.2 Introduction

Wear is the phenomenon of material removal from a surface due to interaction with a mating surface either through micro fracture, chemical dissolution, or melting the contacting surface. In the case of plastic contact between hard and sharp material and a relatively softer material the hard material penetrates the softer one causing fracture; this fracture can lead to micro-cutting and ultimately material removal.

As mentioned above CMP is utilized in the semiconductor industry for planarization of thin film metal layers on a silicon substrate. For most reliability and performance tests, knowledge of the thin film constitutive mechanical behavior is required. Mechanical properties of thin films often differ from those of the bulk materials due to the small grain sizes attributed to the deposition methods. Small sized grains typically contain high grain boundary volume fractions that can lead to an increase or decrease in resulting hardness dependent on the volume fraction [189]. This can also be partially explained by the nanocrystalline structure of thin films and the fact that these films are attached to a substrate. Most research on mechanical properties has concentrated on measurements of hardness as function of grain size; however this relationship has not been extensively investigated in relation to CMP and the resulting MRR. Thin film mechanical properties can be measured by tensile testing of freestanding films and by the micro-beam cantilever deflection technique, but the easiest way is by means of nanoindentation (chapter 3, section 3.2.2), since no special sample preparation is required and tests can be performed quickly and inexpensively. For most reliability and performance tests, knowledge of the thin film constitutive mechanical behavior is required. Mechanical properties of thin films often differ from those of the

bulk materials, due to the small grain sizes attributed to the deposition and various annealing methodologies [105, 110].

6.3 Crystallography

There are two major factors that affect the hardness of a material; the size of grains coupled with types of grain boundaries and the individual grain orientation, (e.g., the crystallography). The grain boundaries disrupt the movement of dislocations in a crystal and the disruption leads to larger applied forces required to cause the crystal to deform. This leads to a larger yield stress for plastic deformation and the smaller the grains the harder the material, this relationship is known as the Hall-Petch relationship which relates grain size to yield strength, however there is a limit to dependence on size of the grain on a micro nano-scale as the relationship begins to break down for grains smaller than 1 micron and the hardness to grain size relationship on the scale has yet to be completely investigated [190, 191].

The orientation of the grain will determine how a dislocation will move. The presence of dislocations strongly influences many of the properties of real materials. The critically resolved shear stress (CRSS) is a characteristic property of a material. The slip system that it is activated under CRSS and can be measured by orienting a single crystal sample with respect to the applied stress and calculating the yield stress. Copper is a face centered cubic (FCC) structure which contains 12 different slip systems. The CRSS effects the yield stress of the material thereby affecting the hardness, the predominant slip plane for copper is [111]. Values of CRSS for FCC metals range from 0.34 MPa to 0.69 MPa. The material slip system for copper is {111} <110> and the CRSS for copper is 0.64.

The orientation variation is dependent on the deposition method and more specifically, the time and temperature at which the target is deposited on the substrate. Sputtering copper directly onto silicon wafer leads to less variation while electroplating copper yields a greater variation in orientations. Annealing the wafers after the deposition process causes the variation in grain size to decrease and the predominant orientation <111> results [8].

6.4 Experimental Design

A blanket set of polished orientation (100) 1-10 ohm-cm SSP 4850um Prime silicon wafers were deposited with .75 μm of copper using the Materials Research Science Engineering Center (MRSEC) at Carnegie Mellon University. One set was electroplated and the other set utilized sputtering as the deposition method. Both sets were then annealed at 450 degrees centigrade for 13 hours in order to allow the grains to grow on the order of several microns.

Following annealing, the sample was then polished using the Strabraugh chemical mechanical polisher in order to remove any oxide layers that may have formed from the annealing process.

A Hysitron triboindentor shown in figure 6.1 was then used in order to obtain the deterministic surface topography of the sputtered and electroplated surface. X-Ray diffraction and orientation imaging microscopy (OIM) were utilized after annealing to determine the orientations of the grains in the sample, these were found to be the predominant <111> orientation. A raster can was implemented in order to scan a 30-μm by 30-μm area and provide the profilometry of that surface. Figure 6.2 shows the surface topography of the wafer.

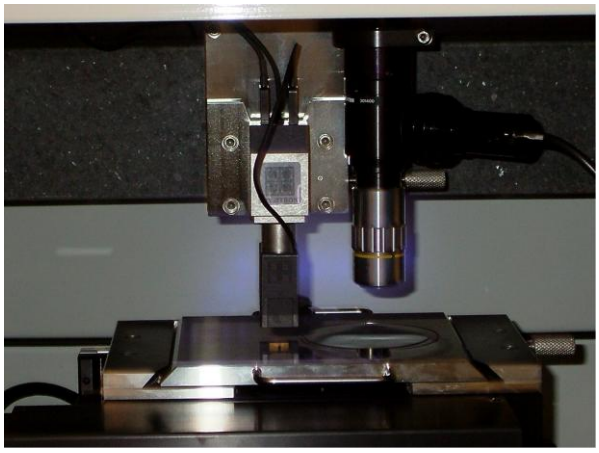

Figure 6. 1 Hysitron nanoindenter

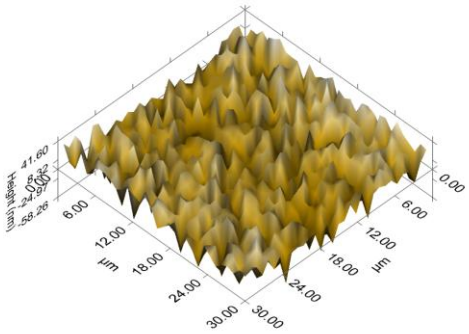

Figure 6. 2 Deterministic surface topography

A nanoindentation method was utilized to determine the hardness variation throughout the 30-µm by 30-µm sample and a contour plot of the hardness versus (x,y) position is shown in figure 6.3 along with a hardness grid corresponding to the gray scale on the plot. An indentation depth less than 10% of the film thickness was done to avoid indentation size effects (ISE).

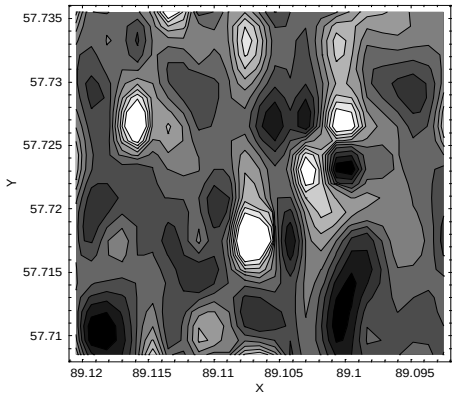

Figure 6. 3 Contour map of hardness

The gray scale shown here has hardness values of 1.2 GPa, the white correspond to values in the range of 2.0 GPa, and the black with values ranging near 1.75 GPa. Elastic modulus variation was shown to range from 115 GPa to 132 GPa.

6.4.1 CMP Simulation

The coefficients of load, P_{app}, equal to 100 microNewtons, U_{pad} and U_{wafer} equal to 10 RPMs, and Preston coefficient, k equal to 1, are all initialized in the PAML model. The Preston coefficient is set to 1 therefore the effects of the slurry are negated for this simulation. The authors determined a thorough understanding of the mechanical abrasion and the resulting effect from variable hardness is a first case scenario. Future simulations will incorporate slurry chemistry and colloidal particle effects. The experimental surface topography was imported and a technique developed by Dickerell et al., is utilized to convert the experimental data into volume pixels (voxels). Each voxel, shown in figure 6.4 contains the x-y and z position in three-dimensional space of each grain along with the corresponding value of hardness from experiments. A random pad surface topography is generated and contact is initiated with the wafer surface. The stress on individual voxels is calculated and these stresses are used to calculate individual and

cumulative wear rates on the wafer surface. The wear distance from each voxel is calculated and then subtracted from the wafer surface.

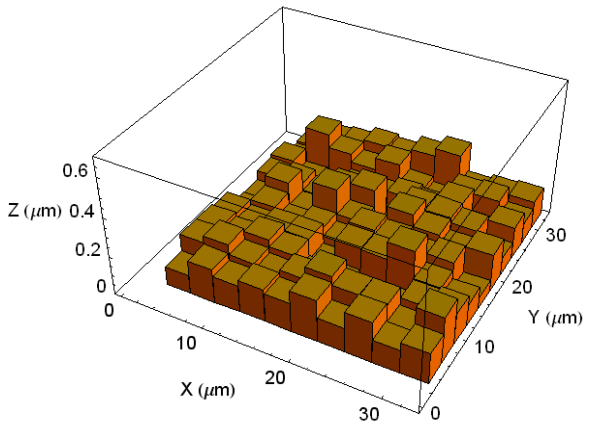

Figure 6. 4 Voxelized surface topography

6.5 Simulation Results

The results from the numerical simulation are shown in figure 6.5.

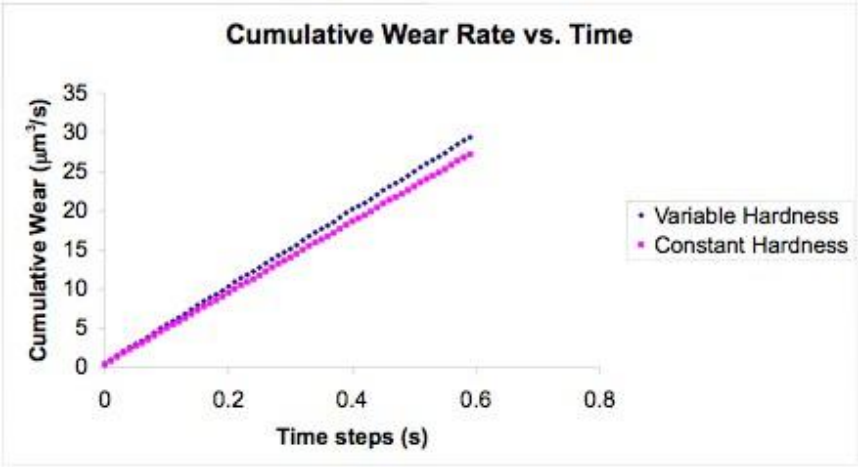

Figure 6. 5 Cumulative wear rate simulation of CMP

The MRR difference between the variable hardness and bulk modulus value (constant hardness) is 2.17 $\mu m^3/s$. Although this value is not large the chemical effects and particle dynamics of the slurry have not been incorporated in this initial investigation. This wear is calculated by the aforementioned numerical simulations. Of greater importance is the resulting surface topography as this relates directly to the viability of the integrated circuit or media storage device fabrication. Incorporation of the variation of hardness resulted in a surface topography with a difference in roughness from the bulk constant hardness value of 6 nm.

6.6 Conclusions and Remarks

A two-part investigation was conducted in order to determine if a previously developed chemical mechanical polishing (CMP) model, PAML, could be enhanced through further experimental validation. The first part involved relating the critically resolved shear stress (CRSS) of a single crystal to an individual hardness value. An investigation relating the CRSS to the hardness value was conducted based on the orientations and hardness values from experimentally found properties. Currently there is not an empirical model or equation to relate the CRSS to the hardness value. The second part of this investigation utilized the variation in hardness values from the initial study and incorporated these results into a particle augmented mixed-lubrication (PAML) numerical model that incorporates all the mechanical physics of chemical mechanical polishing (CMP). Incorporation of the variation of hardness resulted in a surface topography with a difference in roughness from the bulk constant hardness value of 6nm. The MRR of the process differs by 2.17 $\mu m^3/s$.

CHAPTER 7: MULTIPHYSICS DISCUSSION OF BPM CMP

7.1 Foreword

The feasibility of utilizing the CMP process for planarizing patterned media has been investigated and benchmark data has been reported. The CMP process is a multi-physics process in which the machine inputs, pad, and slurry characteristics affect the output parameters as shown in figure 2.16 and repeated below.

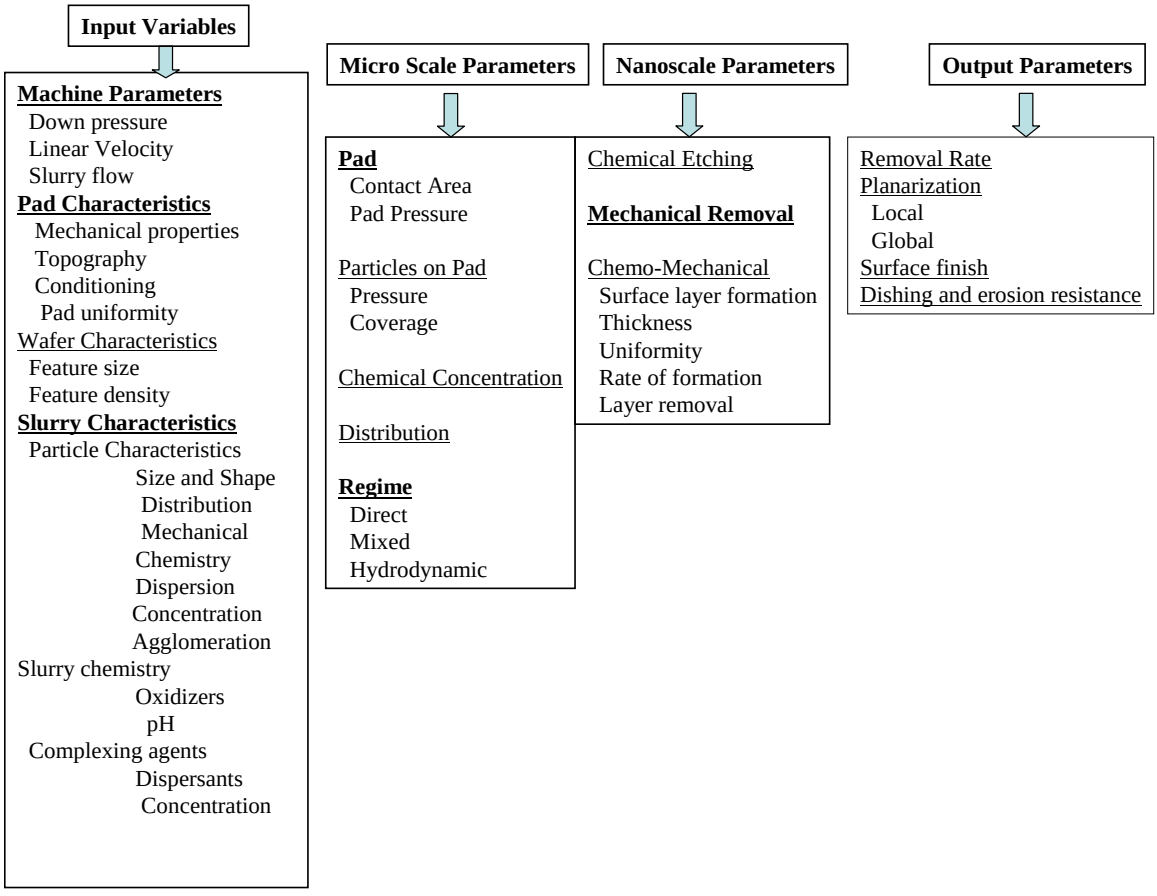

Figure 7. 1 CMP process parameters

Based on figure 7.1, the machine input parameters, pad characteristics, and slurry characteristics were evaluated to help determine the optimum polishing pressure, pad and wafer velocities, and CMP pad. A separate evaluation on the role of the CMP slurry based on the characteristics of the aforementioned parameters was also conducted. During the CMP process the machine input parameters dictate the removal mechanism, resulting MRR, surface roughness, and surface defects. The inputs for pressure and velocity are the key parameters which determine the outputs. Due to the complexity of the process, the relationship between each parameter and resulting output is not straightforward and this chapter discusses the interactions between all of the parameters and introduces a conclusion on the feasibility of using CMP for the PM planarization process.

7.2 Pad Based Wear

From chapter 3, it has been reported that as the pressure is increased and the velocity is held constant, the MRR increases at a faster rate than if the pressure is held constant and velocity is increased. The resulting MRR from the two cases offers insight into the fundamental science of CMP polishing, namely, pad based wear versus slurry based wear as the main polishing theory.

For the case of increasing pressure and constant velocity the main polishing mechanism is the pad, and is deemed pad based wear. The increase in pressure causes an increase in two body abrasion as the wafer and pad are forced into contact due to the high pressures. Figure 7.2 shows the schematic of two body abrasion during polishing.

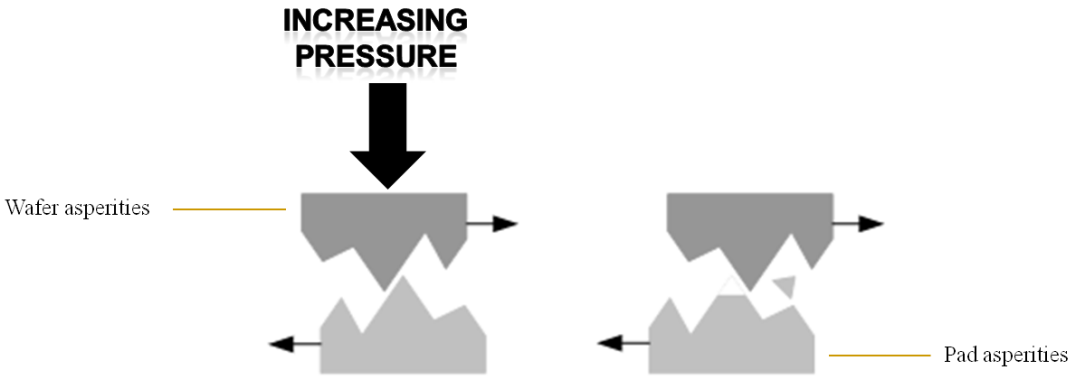

Figure 7. 2 Pad based wear

Two body abrasion results in a high COF, high MRR, high surface defects, and the boundary lubrication regime (from the Stribeck curve). It is useful to note that in the calculation of the qualitative Sommerfeld number during polishing, increasing the pressure decreases the overall Sommerfeld number shifting the curve further into boundary lubrication which was detailed in chapter 2.4.2.1. Pad based wear also results in microcrack formation during polishing as seen and explained in chapter 3. For the case of BPM, the high pressures and fatigue of polishing the metal causes shearing of the crystals, causing work hardening on the BPM and thereby causing an increase in the mechanical properties during polish. This increase is only momentary as the crack propagation occurs through the fatigue of the metal during polishing. The cracks formed during polishing weaken the material and also reduce the reliability of the BPM in magnetic storage hard drive use.

Pad based wear also results in the highest pad wear during polishing as evidenced in chapter 4 through pad thickness and pad roughness studies. The rougher pads initially start in the boundary lubrication regime and result in higher MRR. The pads then slowly

transition into the partial lubrication and finally full lubrication regimes during polishing (based on Sommerfeld number and COF). The high pad wear reduces the pad roughness and pad life but also plays a vital role in reducing the wafer surface roughness due to the high MRR. During the CMP process the two body wear is most beneficial at the start of the process due to the high wear rates but is also detrimental to the pad life.

There is little slurry interaction with pad based wear, due to increase in pressure the entrenched fluid (slurry) is "pushed" out to the edges of the polishing pad. Therefore interaction of the wafer surface and slurry only results from the chemical corrosion of the wafer surface and not from the abrasive particles.

7.3 Slurry Based Wear

The opposite is true as the velocity is increased and pressure is held constant during CMP. The increase in the relative velocity which is correlated to the angular velocities of the pad and wafer carrier increases the entrenchment of the slurry to the wafer surface. As velocity is increased the Sommerfeld number is increased shifting the polishing regime further to the hydrodynamic lubrication or full lubrication regime. This regime has the slurry fluid supporting the entire load (pressure) with little or no wafer to pad contact. This regime is also two body abrasion, but the abrasion occurs between the abrasive nanoparticles and the wafer surface as shown in figure 7.3.

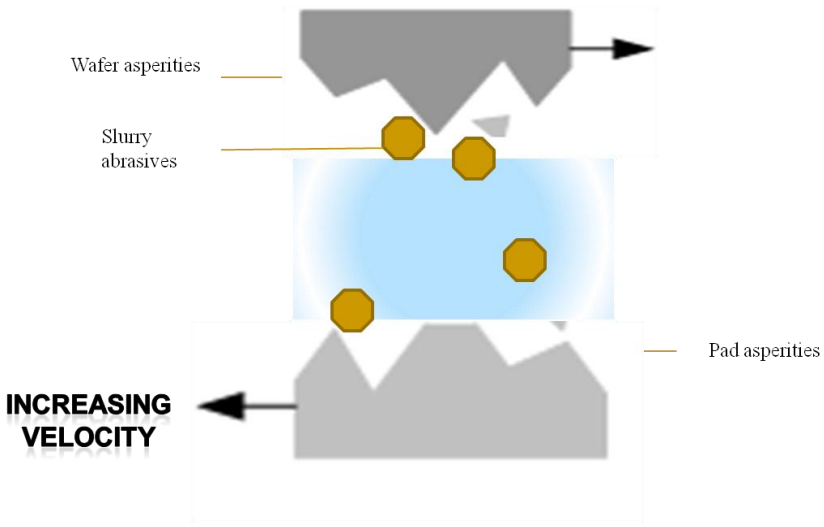

Figure 7. 3 Slurry based wear

The full lubrication regime results in lower MRR but less surface defects and lower surface roughness values. The wear from the abrasive particles is based on indentation or ploughing. During ploughing the slurry abrasives are harder than the wafer surface being polished. The harder slurry abrasives such as alumina, silica, Titania, zirconia, or nanodiamond plastically plough through the surface during polishing by striking the surface causing the surface to plastically deform. The material removal is completed through the angular velocities of the pad and wafer carrier during which the ploughed wafer surface particles are removed from the surface through centripetal acceleration. Increasing the velocity during CMP of BPM increases the number of collisions between the slurry abrasives and the wafer surface, thereby increasing ploughing. This serves to also remove the abraded material more quickly than at slower speeds. The evidence of the ploughing surfaces can be seen in chapter 3 for the high polish pressures in which the harder alumina particles leave "streaks" from where the abrasive particle has ploughed through the surface causing surface defects. The slurry

based wear has lower MRR than the pad based wear but the resulting surface defects and roughness values are better.

The slurry interaction during slurry based wear is pivotal as the wafer surface is only in contact with the slurry during polishing. The chemistry, particle size, particle distribution, and particle material properties all contribute to the MRR and resulting wafer surface. An important caveat of the slurry chemistry and particles is the abrasive agglomeration during polishing. In both cases of polishing for NDs and alumina abrasive the particles agglomerated to form larger particles which are detrimental to the CMP process. As the larger particles interact with the surface the ploughing of these particles has two effects on the surface:

1) The bigger particle removes a greater amount of material then the non agglomerated particles resulting in a reduction in the surface quality of the surface
2) As the particles plough the surface the bigger agglomerated particles begins to deposit particles onto the BPM during polishing consequently both effects are undesirable for BPM CMP.

During polishing of the BPM the MRR was increased with an increase in the hardness of the abrasive particle and an increase in the number of particles in a solution. Due to the regime of polishing, low MRR, and high initial surface roughness of the BPM, the amount of slurry required to polish the surface to an atomically smooth surface is increase thereby increasing cost. As the slurry is the most expensive consumable conducting polishing in this regime of low pressure and high velocity is not cost-effective for all materials.

During slurry based wear the pad lifetime is decreased through "glazing" of the pad surface even though the pad is not in direct contact with the wafer surface and not being worn away (allowing for softer and less expensive pads). Glazing is a CMP phenomenon in which the slurry abrasive become entrapped in the pad surface along with chemical etchants and wafer surface particles. The glazing effect reduces the surface roughness of the pad through the two body abrasion of the pad surface by abrasive particles (akin to the wafer surface). Results from the nanoparticle deposits on the pad surfaces were characterized in the SEM images in the appendix of this dissertation. The glazing effect decreases the pad thickness over time and reduces the number of usable pads during polishing.

7.4 Mixed Polishing

The final set of parameters that produce an overall effect on the output parameters of figure 7.1 was a variation in the pressure and the velocity during polishing. The elastohydrodynamic regime or partial lubrication regime combines the optimum settings of pressure and velocity to ensure a balance between pad based wear and slurry based wear or the boundary lubrication regime and the full lubrication regime respectively. The mixed lubrication regime combines the contact of the pad based wear with the entrenchment of the slurry during polishing. The resulting wear is based on three body wear shown in figure 7.4.

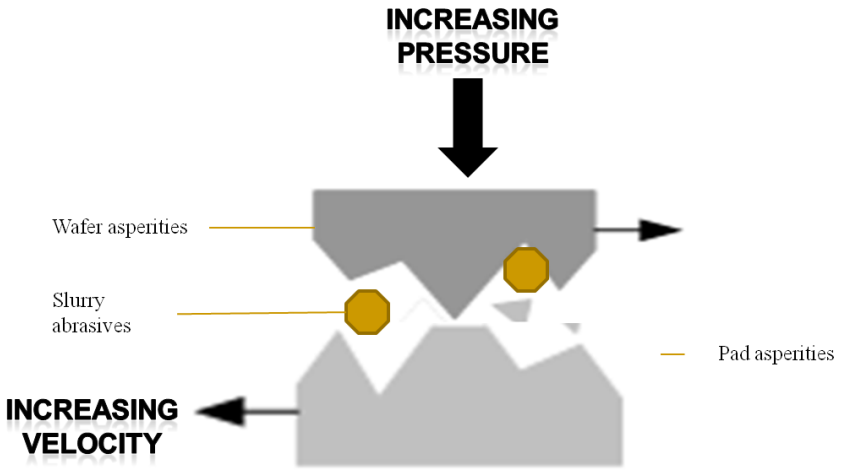

Figure 7. 4 Three body wear

Based on this research the optimal input polishing parameters for the BPM matrices result from using relatively low polish pressure and high velocities. The Stribeck curve from these parameters on BPM CMP results in the partially lubricated polishing regime (as the Sommerfeld number is optimized for the input parameters and the in-situ COF is monitored). This regime results in a median MRR from the pad based contact and atomic surface roughness of the BPM from the slurry chemistry and nanoparticle abrasive interaction.

As with the slurry based wear the slurry nanoparticles must be harder than the surface they are polishing in order to ensure ploughing the wafer surface. The surface chemistry must etch the surface to weaken the surface during polishing to aid in the MRR. Characteristics of the slurry for the partial lubrication regime remain unchanged from the fully lubricated regime in part because the overall task to be completed by this type of wear remains the same, namely reducing the surface roughness during polishing.

During polishing of the partially lubricated regime the pad and wafer surface are in direct contact in combination with entrenchment of the slurry particles ploughing the surfaces of the wafer and the pad during CMP. This is the optimal configuration for BPM polishing. The pad based wear and slurry based wear interactions were coupled during polishing of the BPM and reduction of the pad lifetime was evident as the pad lifetime for BPM CMP falls below the IC-CMP industry average of 400-700 minutes of polishing for each pad. Typical lifetimes for the commercial pads tested ranged from 80-200 minutes, far below the industry average. SEM and UTS results indicate the glazing effect during polishing which is indicative of slurry based wear, while the reduction in pad thickness and pad roughness coupled with the decrease in MRR are indicators of pad based wear. Due to the atomic surface roughness required, high initial surface roughness of BPM, and the entrenchment of the slurry into the medium between the pad and the wafer during polishing, the glazing onset was much earlier than for typical IC-CMP pads dictating the need for new fabrication technology for polishing pads of BPM configurations.

In order to incorporate CMP as the main planarization technique for the PM configurations several process advantageous and limitations must first be well understood. CMP is able to polish the PM configuration, on both a local and global planarization scheme, to the required surface roughness values for the read/write head to work efficiently, but the drawback of the process comes at the high cost of this planarization. The lower pressures and high initial surface roughness of the PM result in a higher number of polishing steps to reach required outputs. The increase in process steps arises from the need to begin polishing based on pad based wear, where the contact

mechanics of the pad and wafer dominate polishing to wear down the high surface roughness. The pad needs to transition to the partially lubricated regime in which the process still maintains an appreciable MRR but the PM surface begins to become smoother through the entrenchment of the slurry as an additional removal mechanism utilizing both chemical and mechanical effects. The final polish should be maintained in the full lubrication regime in which is dictated by a low MRR and a lower surface roughness. The final polish results in slurry based wear. It should be noted that during the course of the transitions to polish to atomically smooth surfaces the pads will need to be replaced depending on the groove type and hardness value (k-groove and shore hardness about 55 shore D for the optimized pad utilized in this experiment) for optimal output parameters. The slurry will also be a provide high cost for PM CMP as the abrasive for polishing must be harder than the wafer surface (Mohrs hardness of 9-10) and the slurry chemistry for the material must be customized for the PM. CMP is a viable and feasible process for planarization of the surface if there is no other methodologies are available but the magnetic storage industry must be willing to incur the initial high start up cost to utilize this technology.

CHAPTER 8: CONCLUSION AND FUTURE WORK

8.1 Conclusions

As the superparamagnetic limit is reached, the magnetic storage industry looks to circumvent that barrier by implementing polymer and patterned media (PM) as a viable means to store and access data [26, 27]. The issue with PM is the ability of the magnetic read/write head to "fly" over the data without crashing into the rough PM surfaces. Chemical mechanical planarization (CMP) is a semiconductor fabrication technique used to planarize surfaces in the multi-level metallization schemes for the integrated circuit (IC) industries. The CMP technique is thereby employed to ensure that the PM is polished to surface roughness requirements of the magnetic storage industry that will allow the magnetic read/write head to move seamlessly across the PM.

Due to the novelty of PM fabrication, data on the output parameters of the CMP process based on the machine process parameters, pad properties, and slurry characteristics is extremely limited, and therefore benchmark data on a specific reversed patterned matrix was conducted and compared to standard IC fabrication CMP. A reverse bit patterned media (BPM) matrix is tested in this research for benchmarking purposes. The BPM is fabricated with silicon as the substrate, followed by barium and tantalum adhesion layers, and silicon dioxide with copper in the PM configuration. The planarization of repeating patterns on a Cartesian grid in the reverse BPM configuration is fundamentally similar to PM configurations, and the interest of this dissertation lies in the fundamental science with CMP of these types of heterogeneous matrices (assuming

another material is the recession). The research was conducted in a systematic manner shown in figure 8.1 [192-194].

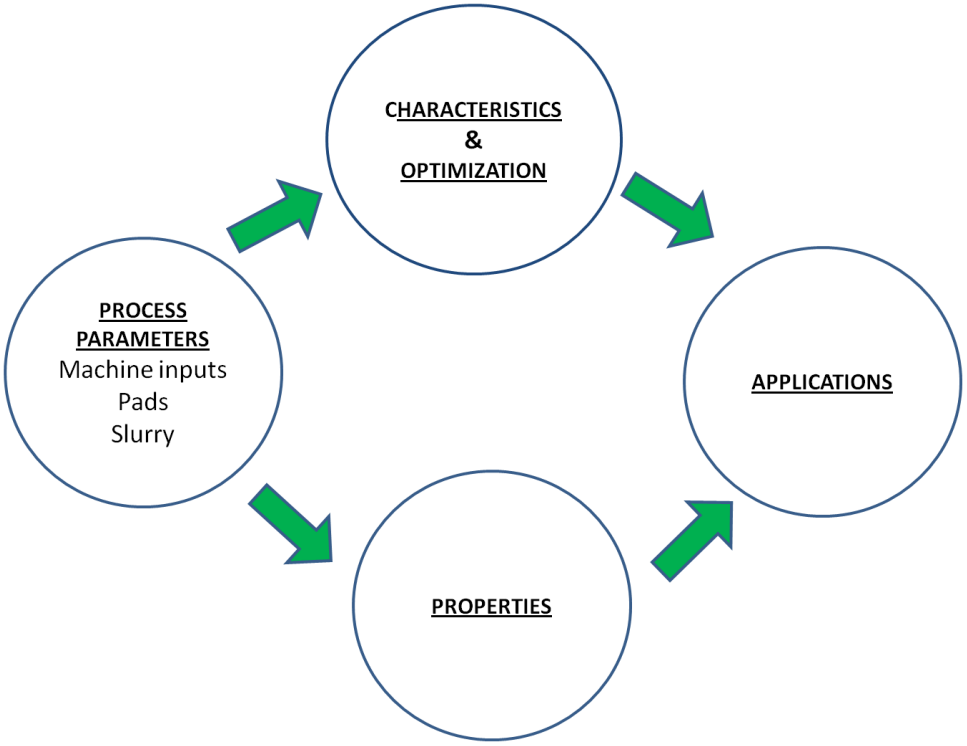

Figure 8. 1 Process schematic for BPM CMP

Based on figure 8.1, the process parameters were first determined for BPM CMP. These parameters include the machine parameters, pad characteristics and slurry characteristics. The parameters were then characterized individually and optimized based on the previous integration of parameters. The machine process parameters were first investigated, followed by the pad characteristics during polishing, and finally investigation into the slurry characteristics on BPM was conducted.

Following the characterization of the process, the quantitative and qualitative data from the experiments was then interpreted to determine the best applications for CMP on

BPM based on the systematic approach utilized in solving the problem. Results from this research has implications in feasibility studies of utilizing CMP as the main planarization technique for PM magnetic hard drive fabrication, sustainability in the consumables of the CMP process for fabrication, and practicability of different slurry designs to polish BPM.

A separate investigation was conducted which modeled the evolution of the mechanical properties during CMP process to determine the importance of microstructure during polishing. This investigation looked at the process parameters and evaluated the mechanical properties to determine the best set of applications utilizing a simulation. It should still be noted that the input parameters for both sets of experiments was based on IC CMP.

The input parameters for pressure and velocity dictate the resulting material removal and surface roughness of the CMP process [41, 42, 59, 83, 85, 178]. Results from a two factor-three level statistical analysis of variance, quantitative data are reported, and Stribeck curves of polishing of the BPM indicate that pressure is major driving factor in the material removal during polishing. The optimal machine parameters for the surface roughness and material removal are at low polish pressures and high relative velocities. These parameters ensure there is three-body abrasion between the pad, wafer surface, and abrasive particles in the slurry and polishing remains in the partial lubrication regime [55]. The mechanical properties during polishing were monitored and an increase in the shear strength during polishing is attributed to dislocation motion toward grain boundaries during polishing. This phenomenon has been reported in previous literature for metal nanoindentation and polishing [145, 146, 195]. The

dislocation motion also leads to micro-cracks in the BPM and future research will address this problem.

Using the machine parameters from previously mentioned optimization, the consumables were characterized to determine their effect on polishing of BPM. The MRR, COF, wafer surface roughness, pad roughness, and pad thickness were monitored and results indicate a deterioration of all the parameters versus polish time. This deterioration is directly linked to the sustainability life of each pad. A new non destructive ultrasound technique for evolution of the pad properties during polishing followed closely to quantitative data and this technique can be utilized to test future pads for enhanced pad life. The optimum pad for BPM polishing was the IC 1400 dual layer Suba V pad with a shore hardness of 57, and a k groove pattern. The softer, polyurethane matrix foam pad with x-y groove pattern was inadequate to polish PM configuration and should not be utilized in future PM fabrications. The resulting pad life for PM polishing indicates a dramatic decrease is pad life for polishing of PM when compared to the IC CMP pads. The feasibility of the magnetic storage industry utilizing CMP as the planarization process must incorporate the increase in costs for pad replacement.

The final consumable analyzed was the slurry for CMP of BPM. Again, using the optimized machine parameters and optimized pad for polishing, the slurry polishing properties were evaluated and a novel nanodiamond (ND) slurry was created to benchmark the data on BPM and blanket copper polishing. The process parameters remained constant during polishing and the resulting COF, MRR, and surface roughness were monitored. The particles where characterized by DLS and TEM. The NDs were suspended within the thermally responsive polymer matrix and provided better results for

polishing than the previously published polymer polishing results because the hard ND particles were a better abrasive for wear than the softer polymer slurry. Upon successful synthesis and testing of the ND slurry, four different concentrations were created to test the saturation limit for the ND particles and the removal rate. It was determined that beyond inclusion of $1.81x10^{20}$ ND particles in the solution, there is not an appreciable increase in the output metrics for polishing. Neither the ND slurry nor the polymer slurry performed better than the commercially available Cabot iCue slurry for MRR or surface roughness, partially due to the chemical effects of the Cabot slurry on the surface of the BPM. Although the commercially available slurry outperformed the ND slurry, the new ND slurry offered an improvement in MRR and surface roughness for blanket copper wafers when compared to polishing with the patented thermally responsive polymer [186-188]. Based on a cost-benefit analysis to incorporate the ND slurry to current CMP process metrics, the ND slurry is not cost effective for BPM CMP, but could be potentially used as a buffer step in the final polish of the PM.

A separate study on the importance of microstructure was conducted to determine how microstructural variation affects the polishing output metrics. A two-part investigation was conducted in order to determine if a previously developed particle augmented mixed lubrication (PAML) model could be enhanced further through experimental validation. The first part involved relating the critically resolved shear stress (CRSS) of a single crystal to an individual hardness value, and results indicate that currently there is not an empirical model or equation to relate the CRSS to the hardness value. The second part of this investigation utilized the variation in hardness values from the initial study and incorporated these results into the PAML simulation. Incorporation

of the variation of mechanical properties resulted in a surface topography with a difference in roughness from the bulk constant hardness value of 6nm, while the MRR of the process differs by 2.17 $\mu m^3/s$.

8.2 Future Work

The benchmarking of the data for BPM CMP involves a systematic approach to solving for the optimized input parameters enhance the output parameters. The approach utilized in this dissertation took a methodical approach in which variations in each process parameter were tested individually, an optimization was found, and that optimized factor was imparted into the next phase as seen by the arrows in figure 8.1. This approach did not take into account a reversal in the input parameters and how the metrics would affect each other. This means that the selection of the Rodel IC1400 pad as the optimized pad is a consequences of the optimized machine parameters of low polish pressure and high velocity. A design of experiments which incorporates the effects of the individual pads or slurry on the different machine input parameters would increase the knowledge on the interactions CMP process properties. Figure 8.2 depicts a schematic of the current and future work for the process.

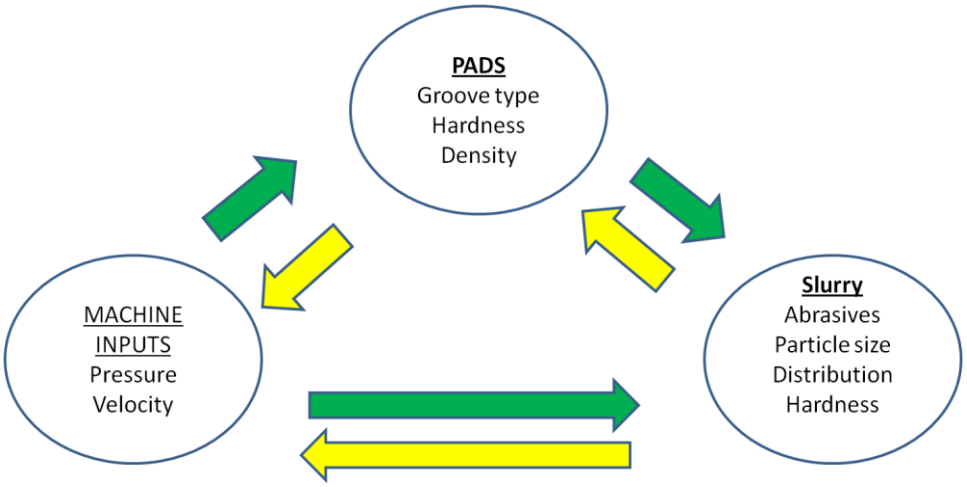

Figure 8. 2 Future work

The green arrows represent the work and path currently taken in this research. The yellow arrows represent the interaction of the process parameters on each other and the resulting optimization that needs to be undertaken to gain further knowledge on the process.

Research conducted was based on CMP of copper PM. While this is an option the magnetic storage industry has investigated most of the PM fabrication technology utilizes $Co_{70}Cr_{18}Pt_{12}$, nickel ferrite, or other polymer or highly magnetic metal films [11, 23, 26, 196]. It should be noted that copper PM offers a worst case scenario for PM CMP, as the copper is the hardest material utilized for BPM out of the choices currently used. This worst case scenario will ultimately result in a decrease in the pressures applied and number of polishing steps required for other materials in PM configuration, as copper has the highest mechanical properties and therefore greatest resistance to plastic deformation. Consequently since the polishing steps would be decreased, the pad life would be increased based on replacing the copper with less hard and less stiff polymers and metals. The slurry interaction cannot be fully understood for other materials as the slurry

chemistry utilized in experiments was specifically designed for copper CMP, although the abrasives in the slurry would remain effective.

Research in this dissertation is a benchmark study on the CMP for PM as a intern fabrication step, due to the novelty of the project, the amount of future work described herein is extensive and the interactions between the phases and parameters warrants future work that may not be fully understood in this dissertation. Future work for the process optimization of BPM CMP would include indexing the geometrical shape of the PM being polished. The shapes of the PM, columns or bit pattern matrix form, have an effect on the tribological interaction during CMP. The PM shape determines the area of contact between the wafer and pad along with the abrasives. Thus, the amount of surface asperity interaction and the particle wafer interaction depends also on the PM shapes. The fluid film that is in contact with the wafer surface also is dependent on the PM shape. Scarfo et al., conducted polishing tests at different process conditions on different wafer samples with concave, convex and intermediate surface contours [65]. The study determined that the change in coefficient of friction is directly linked to changes within the shape. The variability in the shape leads to a change in the Sommerfeld number due to changes in the process conditions because of the resulting contact area and pressure changes [65]. This study did not take into account shapes other than BPM configuration, based on the assumption that BPM wafers are single level wafers and the variability could be negligible. Future studies should incorporate any PM shape variability.

Future work for pad characterization would incorporate the mechanical property evolution of the pads during BPM polishing. Characterization and evaluation of the elastic modulus, shear modulus, and pad hardness during each polish step along with

results from ultrasound system would lead to a better model for prediction pad life for BPM CMP.

The commercial slurry performed better than the ND slurry created in this research, due to the effects of the slurry chemistry on the surface. Future work for the slurry would incorporate an etchant and oxiders in the slurry chemistry to help weaken the surface prior to polishing. The interaction of the thermally responsive polymer and ND particles with the slurry chemistry must be fully understood to optimize material removal. This would require inherent knowledge of chemistry and surface mechanics making it a multidisciplinary problem to be solved.

The simulation work done in chapter 6, took into account only the mechanical interactions of the polishing process. It is a mechanical polishing simulation with the evolution of microstructure displayed during abrasive polishing. The abrasive module predicted that the MRR during polishing changes as each copper grain is sheared away and a new grain is revealed which may have a different orientation resulting in a different hardness value. Further studies into the grain boundary interaction during polishing warrants research for future work. Most grains will get harder due to the dislocations piling up at the grain boundaries while others will become weaker as they are removed from the polishing surface. This evolution of the mechanical properties due to grain boundary orientation parameters needs to be properly understood and implemented in the PAML simulation. Future work for the simulation would also incorporate the slurry chemistry interaction with the surface to accurately predict the MRR and surface roughness.

Based on the benchmark data on the three phases of this research, CMP is a feasible process to planarize the BPM to atomically smooth surfaces. In order to incorporate the CMP process the magnetic storage industry must understand the tribological issues that must first be overcome:

1) In order to polish the PM to atomic smoothness, low polish pressures and high velocities need to be incorporated. This will result in multiple polish steps (increasing cost) to insure local and global planarity.
2) The CMP pads utilized to polish the PM will have a much shorter pad life than the IC CMP and this will result in an increase in the number of replacement pads as the optimal pad for polishing will last roughly half of the pad life for IC CMP.
3) The commercial slurry for copper CMP is an adequate substitute for PM CMP, but a change in the material for polishing results in further research in the slurry chemistry for multiple materials.

Successful implementation of CMP for the planarization step in PM fabrication must address the high initial start up cost, increase in the number of replacement pads, and increase in polishing time to reach the required surface roughness for magnetic storage devices.

REFERENCES

1. Thompson, D. and J. Best, *The future of magnetic data storage technology.* IBM Journal of Research and Development, 2000. 44(3): p. 311-322.

2. Grochowski, E. and R. Halem, *Technological impact of magnetic hard disk drives on storage systems.* IBM Systems Journal, 2003. 42(2): p. 338-346.

3. Weller, D. and A. Moser, *Thermal effect limits in ultrahigh-density magnetic recording.* IEEE Transactions on Magnetics, 1999. 35(6): p. 4423-4439.

4. Skumryev, V., et al., *Beating the superparamagnetic limit with exchange bias.* Nature, 2003. 423(6942): p. 850-853.

5. Dibner, B., Oersted and the Discovery of Electromagnetism. 1962.

6. Faraday, M., Experimental researches in chemistry and physics. 1859: Taylor & Francis.

7. *How Perpendicular Recording works*. 2006 [cited 2010 September 15]; Available from:http://www.hardwaresecrets.com/article/347.

8. Daniel, E., C. Mee, and M. Clark, *Magnetic recording: the first 100 years*. 1999: Wiley-IEEE Press.

9. Abramovitch, D. and G. Franklin, *A brief history of disk drive control.* Control Systems Magazine, IEEE, 2002. 22(3): p. 28-42.

10. Thompson, D. and J. Best, *The future of magnetic data storage technology.* IBM Journal of Research and Development. 44(3): p. 311-322.

11. White, R., R. Newt, and R. Pease, *Patterned media: a viable route to 50 Gbit/in< sup> 2</sup> and up for magnetic recording?* Magnetics, IEEE Transactions on, 2002. 33(1): p. 990-995.

12. Majetich, S. and Y. Jin, *Magnetization directions of individual nanoparticles.* Science, 1999. 284(5413): p. 470.

13. Weller, D. and A. Moser, *Thermal effect limits in ultrahigh-density magnetic recording.* Magnetics, IEEE Transactions on, 2002. 35(6): p. 4423-4439.

14. Piramanayagam, S., *Perpendicular recording media for hard disk drives.* Journal of Applied Physics, 2007. 102: p. 011301.

15. Khizroev, S. and D. Litvinov, *Perpendicular magnetic recording*. 2004: Kluwer Academic Publishers.

16. Hoagland, A., *History of magnetic disk storage based on perpendicular magnetic recording.* IEEE Transactions on Magnetics, 2003. 39(4): p. 1871-1875.

17. Merritt, R. *Toshiba Ships "Perpendicular " Disk Drive*. 2005; Available from: http://informationweek.com/story/showArticle.jhtml?articleID=169300286.

18. Challener, W., et al., *Light delivery techniques for heat-assisted magnetic recording.* Jpn. J. Appl. Phys., Part, 2003. 1(42): p. 981–988.

19. Rottmayer, R., et al., *Heat-assisted magnetic recording.* IEEE Transactions on Magnetics, 2006. 42(10): p. 2417-2421.

20. Gavrila, H., *Heat-assisted magnetic recording.* Journal of Optoelectronics and Advanced Materials, 2008. 10(7): p. 1796.

21. *Fabrication of magnetic nanodot arrays by using electrochemical deposition process*. [cited 2010 August 12]; Available from: http://www.ec.appchem.waseda.ac.jp/research/rese05.htm.

22. S. E. Lambert, I.L.S., A. M. Patlach, M. T. and M. Krounbi, IEEE Trans. Mag, 1987. MAG-23,(3690).

23. Lambert, S., et al., *Beyond discrete tracks: Other aspects of patterned media.* Journal of Applied Physics, 2009. 69(8): p. 4724-4726.

24. J. F. Smyth, S.S., D. R. Fredkin, D. P. Kern, and H.S. S. A. Rishton, M. Cali, T. R. Koehler, J. Appl. Phys, 1991. 69(5262).

25. G. A. Gibson, J.F.S., S. Schultz, D. P. Kern, IEEE Trans. Mag. , 1991. MAG-27(5187).

26. Ross, C., et al., *Fabrication of patterned media for high density magnetic storage.* Journal of Vacuum Science & Technology B: Microelectronics and Nanometer Structures, 1999. 17: p. 3168.

27. Terris, B., T. Thomson, and G. Hu, *Patterned media for future magnetic data storage.* Microsystem technologies, 2007. 13(2): p. 189-196.

28. Moore, G., *Cramming more components onto integrated circuits.* Proceedings of the IEEE, 1998. 86(1): p. 82-85.

29. Yu, A., *Future of microprocessors.* IEEE Micro, 1996. 16(6): p. 46-53.

30. Gordon, M., *Solid-State Circuits Conference, Digest of Technical Papers.* ISSCC., IEEE International, 2003. 1: p. 20-23.

31. Davis, J. and J. Meindl, Interconnect technology and design for gigascale integration. 2003: Kluwer Academic Pub.

32. Sze, S. and K. Ng, *Physics of semiconductor devices*. 2007: Wiley-Blackwell.

33. Mayer, J. and S. Lau, *Electronic Materials Science*: Macmillan Press.

34. Thompson, S., et al., 130nm logic technology featuring 60nm transistors, low-k dielectrics, and cu interconnects. Intel Technology Journal, 2002. 6(2): p. 5-13.

35. Chau, R., et al. 30nm Physical Gate Length CMOS Transistors with 1.0 ps n-MOS and 1.7 ps p-MOS Gate Delays. 2000: IEEE; 1998.

36. Kuhn, K. CMOS scaling beyond 32nm: challenges and opportunities. 2009: ACM.

37. Ghate, P., J. Blair, and C. Fuller, *Metallization in microelectronics.* Thin Solid Films, 1977. 45(1): p. 69-84.

38. Quirk, M. and J. Serda, *Semiconductor manufacturing technology*. 2000: Prentice Hall Upper Saddle River, NJ.

39. Ryan, J., et al., *The evolution of interconnection technology at IBM.* IBM Journal of Research and Development, 1995. 39(4): p. 371-382.

40. Hopwood, J., Ionized physical vapor deposition of integrated circuit interconnects. Physics of Plasmas, 1998. 5: p. 1624.

41. Zantye, P., A. Kumar, and A. Sikder, *Chemical mechanical planarization for microelectronics applications.* Materials Science and Engineering: R: Reports, 2004. 45(3-6): p. 89-220.

42. Steigerwald, J., S. Murarka, and R. Gutmann, *Chemical mechanical planarization of microelectronic materials*. 1997: Wiley-Interscience.

43. Murarka, S., et al., Advanced multilayer metallization schemes with copper as interconnection metal. Thin Solid Films, 1993. 236(1-2): p. 257-266.

44. Xuan, Y., et al., Atomic-layer-deposited nanostructures for graphene-based nanoelectronics. Applied Physics Letters, 2008. 92: p. 013101.

45. Zantye, P., Processing, reliability and integration issues in chemical mechanical planarization. 2005, University of South Florida.

46. Mudhivarthi, S., Process optimization and consumable development for Chemical Mechanical Planarization (CMP) processes. 2007.

47. Bakli, M., et al., *Materials and processing for 0.25 [mu] m multilevel interconnect.* Microelectronic Engineering, 1997. 33(1-4): p. 175-188.

48. Stavreva, Z., et al., *Chemical-mechanical polishing of copper for interconnect formation.* Microelectronic Engineering, 1997. 33(1-4): p. 249-257.

49. Zantye, P., et al., *Metrology and characterization of application specific chemical mechanical polishing pads.* Journal of Vacuum Science & Technology A: Vacuum, Surfaces, and Films, 2005. 23: p. 1392.

50. Shon-Roy, L., A. Wiesnoski, and R. Zorich, *Advanced Semiconductor Fabrication Handbook.* Integrated Circuit Engineering Corporation, Scottsdale, AZ, 1998: p. 5-58.

51. Preston, F., *The theory and design of plate glass polishing machines.* J. Soc. Glass Technol, 1927. 11: p. 214ñ256.

52. Stein, D., J. Cecchi, and D. Hetherington, Atomic force microscopy, lateral force microscopy, and transmission electron microscopy investigations and adhesion force measurements for elucidation of tungsten removal mechanisms. J. Mater. Res, 1999. 14(9): p. 3696.

53. Landis, H., et al., Integration of chemical-mechanical polishing into CMOS integrated circuit manufacturing. Thin Solid Films, 1992. 220(1-2): p. 1-7.

54. Li, S. and R. Miller, Chemical mechanical polishing in silicon processing. 2000: Academic Pr.

55. Bhushan, B. and P. Ko, *Introduction to tribology.* Applied Mechanics Reviews, 2003. 56: p. B6.

56. Ahmadi, G. and X. Xia, A model for mechanical wear and abrasive particle adhesion during the chemical mechanical polishing process. Journal of the Electrochemical Society, 2001. 148: p. G99.

57. Mazaheri, A. and G. Ahmadi, *Modeling the effect of bumpy abrasive particles on chemical mechanical polishing.* Journal of the Electrochemical Society, 2002. 149: p. G370.

58. Luo, Q., D. Campbell, and S. Babu, *Chemical-mechanical polishing of copper in alkaline media.* Thin Solid Films, 1997. 311(1-2): p. 177-182.

59. Steigerwald, J., et al., *Chemical processes in the chemical mechanical polishing of copper.* Materials Chemistry and Physics, 1995. 41(3): p. 217-228.

60. Li, Y., M. Hariharaputhiran, and S. Babu, *Chemical-mechanical polishing of copper and tantalum with silica abrasives.* Journal of Materials Research, 2001. 16(4): p. 1066-1073.

61. Ein-Eli, Y., M. Auinat, and D. Starosvetsky, Electrochemical and surface studies of zinc in alkaline solutions containing organic corrosion inhibitors. Journal of power sources, 2003. 114(2): p. 330-337.

62. Wolf, S. and R. Tauber, *Silicon Processing for the VLSI Era, Volume 1, Process Technology*. 1986: Lattice Press, Sunset Beach, CA., USA.

63. Stribeck, R., Characteristics of Plain and Roller Bearings (in German), Zeit. VDI, 1902. 76: p. 1341-1432.

64. Hosali, S. and E. Busch, *Analyzing damage from ultralow-k CMP.* Solid State Technology, 2005. 48(11): p. 33.

65. Scarfo, A., et al., *In situ measurement of pressure and friction during CMP of contoured wafers.* Journal of the Electrochemical Society, 2005. 152: p. G477.

66. Luo, J. and D. Dornfeld, *Optimization of CMP from the Viewpoint of Consumable Effects.* Journal of the Electrochemical Society, 2003. 150: p. G807.

67. Li, W., et al., The effect of the polishing pad treatments on the chemical-mechanical polishing of SiO2 films. Thin Solid Films, 1995. 270(1-2): p. 601-606.

68. Nishioka, T., K. Sekine, and Y. Tateyama. Modeling on hydrodynamic effects of pad surface roughness in CMP process. 1999.

69. Micheal Fury, R.R., Steven Holland, *CMP consumables market reaches middle age.* 2008.

70. Ludema, K., Friction, wear, lubrication: a textbook in tribology. 1996: CRC.

71. Li, Y., Microelectronic applications of chemical mechanical planarization. 2007: Wiley-Interscience.

72. Philipossian, A. and S. Olsen, *Effect of slurry flow rate on pad life during interlayer dielectric CMP.* Journal of the Electrochemical Society, 2004. 151: p. G436.

73. Ludema, K. and W. Friction, *Lubrication: A Textbook in Tribology*. 1996, CRC Press, Boca Raton.

74. Bibby, T. and K. Holland, *Endpoint detection for CMP*. Journal of Electronic Materials, 1998. 27(10): p. 1073-1081.

75. Das, T., et al., *Online end point detection in CMP using SPRT of wavelet decomposed sensor data.* IEEE Transactions on Semiconductor Manufacturing, 2005. 18(3).

76. Gitis, N., Tribology issues in CMP. 2007.

77. Terrell, E., Application of a particle augmented mixed lubrication model to chemical mechanical polishing: Modeling and experimentation. 2007, University Microfilms International, P. O. Box 1764, Ann Arbor, MI, 48106, USA.

78. Luo, J. and D. Dornfeld, *Material removal mechanism in chemical mechanical polishing: theory and modeling.* IEEE Transactions on Semiconductor Manufacturing, 2001. 14(2).

79. Chekina, O., L. Keer, and H. Liang, *Wear Contact Problems and Modeling of Chemical Mechanical Polishing.* Journal of the Electrochemical Society, 1998. 145: p. 2100.

80. Seok, J., et al., Multiscale material removal modeling of chemical mechanical polishing. Wear, 2003. 254(3-4): p. 307-320.

81. Castillo-Mejia, D. and S. Beaudoin, *A locally relevant wafer-scale model for CMP of silicon dioxide.* Journal of the Electrochemical Society, 2003. 150: p. G581.

82. Fu, G., et al., *A plasticity-based model of material removal in chemical-mechanicalpolishing (CMP).* IEEE Transactions on Semiconductor Manufacturing, 2001. 14(4): p. 406-417.

83. Tseng, W. and Y. Wang, Re examination of Pressure and Speed Dependences of Removal Rate during Chemical Mechanical Polishing Processes. Journal of the Electrochemical Society, 1997. 144: p. L15.

84. Tseng, W., J. Chin, and L. Kang, A comparative study on the roles of velocity in the material removal rate during chemical mechanical polishing. Journal of the Electrochemical Society, 1999. 146: p. 1952.

85. Zhao, B. and F. Shi, *Chemical mechanical polishing: Threshold pressure and mechanism.* Electrochemical and Solid-State Letters, 1999. 2: p. 145.

86. Wei, C. and R. Harrington, *Computation of the parameters of multiconductor transmission lines in two dielectric layers above a ground plane.* Department of Electrical and Computer Engineering, Syracuse Univ., Tech. Rep. TR-82-12, 1982.

87. Jiang, B. and G. Muldowney. Computational Solid Mechanics Modeling of Asperity Deformation and Pad-Wafer Contact in CMP. 2007: Warrendale, Pa.; Materials Research Society; 1999.

88. Põdra, P. and S. Andersson, *Wear simulation with the Winkler surface model.* Wear, 1997. 207(1-2): p. 79-85.

89. Sawyer, W., Surface shape and contact pressure evolution in two component surfaces: application to copper chemical mechanical polishing. Tribology Letters, 2004. 17(2): p. 139-145.

90. Feng, C., et al., A Contact-Mechanics-Based Model for General Rough Pads in Chemical Mechanical Polishing Processes. Journal of the Electrochemical Society, 2009. 156: p. H601.

91. Terrell, E., M. Kuo, and C. Higgs. *An approach to modeling particle-based and contact-based wear in CMP*. 2007: Warrendale, Pa.; Materials Research Society; 1999.

92. Terrell, E. and C. Higgs III, A particle-augmented mixed lubrication modeling approach to predicting chemical mechanical polishing. Journal of Tribology, 2009. 131: p. 012201.

93. Johnson, K., *Contact mechanics. 1985*. Cambridge Uni.

94. Johnson, K., *Contact mechanics*. 1987: Cambridge Univ Pr.

95. Johnson, K., *Contact mechanics and the wear of metals.* Wear, 1995. 190(2): p. 162-170.

96. Nanz, G. and L. Camilletti, *Modeling of chemical-mechanical polishing: a review.* IEEE Transactions on Semiconductor Manufacturing, 1995. 8(4): p. 382-389.

97. Tichy, J., A.A.L.D.D. G. Dalmaz, and M. Priest, Contact mechanics and lubrication hydrodynamics of chemical-mechanical planarization, in Tribology and Interface Engineering Series. 2001, Elsevier. p. 63-68.

98. Zhao, Y. and L. Chang, A micro-contact and wear model for chemical-mechanical polishing of silicon wafers. Wear, 2002. 252(3-4): p. 220-226.

99. Higgs III, C., et al., *A mixed-lubrication approach to predicting CMP fluid pressure modeling and experiments.* Journal of the Electrochemical Society, 2005. 152: p. G193.

100. Chang, S., et al., *Pattern effects on planarization efficiency of Cu electropolishing.* Jpn. J. Appl. Phys., Part, 2002. 1(41): p. 7332.

101. Nguyen, V., H. VanKranenburg, and P. Woerlee, *Dependency of dishing on polish time and slurry chemistry in Cu CMP.* Microelectronic Engineering, 2000. 50(1-4): p. 403-410.

102. Pan, J., et al. Copper CMP integration and time dependent pattern effect. 1999.

103. Li, S. and R. Miller, *Chemical Mechanical Polishing in Silicon Processing, vol. 63*. 2000, Academic Press, New York.

104. Borst, C., et al., Chemical mechanical polishing mechanisms of low dielectric constant polymers in copper slurries. Journal of the Electrochemical Society, 1999. 146: p. 4309.

105. Volinsky, A., J. Vella, and W. Gerberich, Fracture toughness, adhesion and mechanical properties of low-K dielectric thin films measured by nanoindentation. Thin Solid Films, 2003. 429(1-2): p. 201-210.

106. Yang, L., et al., Improving electrical performance of Cu= porous ultra-low k dielectrics single damascene lines. Electronics Letters, 2004. 40: p. 12.

107. Balakumar, S., et al., *Peeling and delamination in Cu/SiLK (TM) process during Cu-CMP*. Thin Solid Films, 2004. 462: p. 161-167.

108. Shen, L., et al., Determination of the hardness and elastic modulus of low-k thin films and their barrier layer for microelectronic applications. Microelectronic Engineering, 2003. 70(1): p. 115-124.

109. Wang, Y., et al., The mechanical properties of ultra-low-dielectric-constant films. Thin Solid Films, 2004. 462: p. 227-230.

110. Volinsky, A., N. Moody, and W. Gerberich, *Interfacial toughness measurements for thin films on substrates.* Acta Materialia, 2002. 50(3): p. 441-466.

111. Shan, L., S. Danyluk, and J. Levert. *Interfacial Pressure Measurements at Chemical-Mechanical Polishing Interfaces*. 1999: Warrendale, Pa.; Materials Research Society; 1999.

112. Sundararajan, S., et al., Two-dimensional wafer-scale chemical mechanical planarization models based on lubrication theory and mass transport. JOURNAL-ELECTROCHEMICAL SOCIETY, 1999. 146(2): p. 761-766.

113. Park, T., T. Tugbawa, and D. Boning. Pattern dependent modeling of electroplated copper profiles. 2002: IEEE.

114. Park, T., T. Tugbawa, and D. Boning. Overview of methods for characterization of pattern dependencies in copper CMP. 2000: Citeseer.

115. Park, T., et al. Pattern and process dependencies in copper damascene chemical mechanical polishing processes. 1998: Citeseer.

116. Tae Park, T.T., Duane Boning (MIT); Steve Hymes, Konstantin Smekalin and (SEMATECH) (2000) *MIT/SEMATECH 854 AZ Copper on Low-K Chemical Mechanical Polishing (CMP) Characterization Test Chip*. International SEMATECH Technology Transfer.

117. Oliver, W. and G. Pharr, Improved technique for determining hardness and elastic modulus using load and displacement sensing indentation experiments. Journal of Materials Research, 1992. 7(6): p. 1564-1583.

118. Taylor, C., et al. Investigation of ultralow-load nanoindentation for the patterning of nanostructures. 2002.

119. Pharr, G., *Measurement of mechanical properties by ultra-low load indentation.* Materials Science and Engineering A, 1998. 253(1-2): p. 151-159.

120. Nix, W., *Mechanical properties of thin films.* Metallurgical and Materials Transactions A, 1989. 20(11): p. 2217-2245.

121. Cammarata, R., et al., Nanoindentation study of the mechanical properties of copper nickel multilayered thin films. Applied Physics Letters, 2009. 56(19): p. 1862-1864.

122. Fang, T. and W. Chang, Nanomechanical properties of copper thin films on different substrates using the nanoindentation technique. Microelectronic Engineering, 2003. 65(1-2): p. 231-238.

123. Suresh, S., T. Nieh, and B. Choi, *Nano-indentation of copper thin films on silicon substrates.* Scripta Materialia, 1999. 41(9): p. 951-958.

124. Zecchino, C.L.a.M., *WYKO Surface Profilers Technical Reference Manual*. 1999, Veeco Metrology Group: Tuscon, Arizona. p. 1-3.

125. Amstutz, H., *Surface Texture: The Parameters*, Warner & Swasey, Sheffield Measurement Division).

126. Sikder, A. and A. Kumar, Mechanical and tribological properties of interlayer films for the damascene-Cu chemical-mechanical planarization process. Journal of Electronic Materials, 2002. 31(10): p. 1016-1021.

127. Ronay, M., Second-order normal force brought about by polishing with a polyurethane pad. Journal of the Electrochemical Society, 2004. 151: p. G847.

128. Vijayakumar, A., et al., *Polishing mechanism of tantalum films by SiO2 particles.* Microelectronic Engineering, 2003. 70(1): p. 93-101.

129. Jeng, Y. and P. Huang, *Impact of abrasive particles on the material removal rate in CMP*. Electrochemical and solid-state letters, 2004. 7: p. G40.

130. Fuchs, K. The conductivity of thin metallic films according to the electron theory of metals. 1938: Cambridge Univ Press.

131. Overwijk, M., F. Van den Heuvel, and C. Bulle-Lieuwma, *Novel scheme for the preparation of transmission electron microscopy specimens with a focused ion beam.* Journal of Vacuum Science & Technology B: Microelectronics and Nanometer Structures, 1993. 11: p. 2021.

132. Giannuzzi, L. and F. Stevie, A review of focused ion beam milling techniques for TEM specimen preparation. Micron, 1999. 30(3): p. 197-204.

133. TSENG, W. and Y. WANG. The Intercorrelation Between Microstructure and Chemical-Mechanical Polish of Metal Thin Films. 1999: Materials Research Society.

134. Shi, F. and B. Zhao, *Modeling of chemical-mechanical polishing with soft pads.* Applied Physics A: Materials Science & Processing, 1998. 67(2): p. 249-252.

135. Zhang, F. and A. Busnaina, *Submicron particle removal in post-oxide chemical–mechanical planarization (CMP) cleaning.* Applied Physics A: Materials Science & Processing, 1999. 69(4): p. 437-440.

136. Li, Z., et al., Determining the effects of slurry surfactant, abrasive size, and abrasive content on the tribology and kinetics of copper CMP. Journal of the Electrochemical Society, 2005. 152: p. G299.

137. Coppeta, J. and C. Rogers, Dual emission laser induced fluorescence for direct planar scalar behavior measurements. Experiments in Fluids, 1998. 25(1): p. 1-15.

138. Lu, J., et al., *Measurements of slurry film thickness and wafer drag during CMP*. Journal of the Electrochemical Society, 2004. 151: p. G241.

139. Sikder, A., et al. Delamination studies in Cu–ultra low-k stack. 2003.

140. Bonivel, J., et al. The Effect of Microstructure on Chemical Mechanical Polishing Process of Thin-Film Metals. in Proceedings of the STLE/ASME International Joint Tribology Conference. 2007: ASME.

141. Fracassi, F., *R. d'Agostino, P.* Favio J. Electrochem Soc, 1992. 139(9): p. 2636-2643.

142. Bonivel, J., et al. THE Effect of Microstructure on Chemical Mechanical Polishing Process of Thin-Film Metals. in Materials Research Society 2009. San Francisco.

143. Cottrell, A., *Theory of brittle fracture in steel and similar metals.* Trans. Met. Soc. AIME, 1958. 212(192): p. 56.

144. Ebrahimi, F., et al., *Mechanical properties of nanocrystalline nickel produced by electrodeposition.* Nanostructured Materials, 1999. 11(3): p. 343-350.

145. Minor, A., et al., A new view of the onset of plasticity during the nanoindentation of aluminium. Nature Materials, 2006. 5(9): p. 697-702.

146. Shan, Z., et al., Mechanical annealing and source-limited deformation in submicrometre-diameter Ni crystals. Nature Materials, 2007. 7(2): p. 115-119.

147. Luo, J., Integrated modeling of chemical mechanical planarization/polishing (CMP) for integrated circuit fabrication: from particle scale to die and wafer scales. 2003, UNIVERSITY OF CALIFORNIA.

148. Kim, I., *The semiconductor industry.* Chemical Engineering Progress, 2002. 98(7): p. 12-14.

149. Hooper, B., G. Byrne, and S. Galligan, *Pad conditioning in chemical mechanical polishing.* Journal of Materials Processing Technology, 2002. 123(1): p. 107-113.

150. Zantye, P., et al. Investigation of mechanical integrity and its effect on polishing for novel polyurethane polishing pad. 2004.

151. Wang, D., et al., *Von Mises Stress in Chemical Mechanical Polishing Processes.* Journal of the Electrochemical Society, 1997. 144: p. 1121.

152. Srinivasa-Murthy, C., et al., *Stress distribution in chemical mechanical polishing.* Thin Solid Films, 1997. 308: p. 533-537.

153. Runnels, S. and L. Eyman, *Tribology Analysis of Chemical Mechanical Polishing.* Journal of the Electrochemical Society, 1994. 141: p. 1698.

154. Sikder, A., et al. Evaluation of mechanical and tribological behavior and surface characteristics of CMP pads. 2001: Warrendale, Pa.; Materials Research Society; 1999.

155. Oliver, M., Chemical-mechanical planarization of semiconductor materials. 2004: Springer Verlag.

156. Manocha, C., Chemical mechanical planarization: Study of conditioner abrasives and synthesis of nano-zirconia for potential slurry applications. University of South Florida, 2008.

157. Hepburn, C., *Polyurethane elastomers.* C. Hepburn, Applied Science Publishers, Barking(Essex) 1982, 402, 1982.

158. Saunders, J. and K. Frisch, *Polyurethanes: chemistry and technology*. Interscience, New York, 1962. 1.

159. Bajaj, R., et al. Effect of polishing pad material properties on chemical mechanical polishing (CMP) processes. 1994: MATERIALS RESEARCH SOCIETY.

160. Szycher, M., Szycher's handbook of polyurethanes. 1999: CRC.

161. Wolf, R., et al., Polyurethane pad covering for gel filled articles. 1997, Google Patents.

162. Cruz, J., et al., *Composite polish pad for CMP*. 1999, Google Patents.

163. Sperling, L., *Introduction to physical polymer science*. 2001: Wiley Online Library.

164. Doy, T., et al., Impact of novel pad groove designs on removal rate and uniformity of dielectric and copper CMP. Journal of the Electrochemical Society, 2004. 151: p. G196.

165. Muldowney, G. and D. James. Characterization of CMP pad surface texture and pad–wafer contact. 2004.

166. A. Philiposian , S.O., *Chemical Mechanical Planarization.* Japan Journal of Applied Physics, 2003. 42: p. 6371.

167. Lu, H., Y. Obeng, and K. Richardson, *Applicability of dynamic mechanical analysis for CMP polyurethane pad studies.* Materials Characterization, 2002. 49(2): p. 177-186.

168. Lu, H., et al., Quantitative analysis of physical and chemical changes in CMP polyurethane pad surfaces. Materials Characterization, 2002. 49(1): p. 35-44.

169. Totzke, D.G., Ultrasound of chemical mechanical planarization pads, in Electrical Engineering. 2000, University of South Florida: Tampa.

170. Totzke, D., et al. Non-destructive characterization of CMP pads using scanning ultrasonic transmission. 2001.

171. Performance Plastics Shore Conversions: Brokenhurst. p. 2.

172. Stein, D., et al., *Optical interferometry for surface measurements of CMP pads.* Journal of Electronic Materials, 1996. 25(10): p. 1623-1627.

173. Kondo, S., et al., *Abrasive-free polishing for copper damascene interconnection.* Journal of the Electrochemical Society, 2000. 147: p. 3907.

174. Tsai, T. and S. Yen, Localized corrosion effects and modifications of acidic and alkaline slurries on copper chemical mechanical polishing. Applied Surface Science, 2003. 210(3-4): p. 190-205.

175. Singh, R., et al., Fundamentals of dielectric and metal chemical mechanical planarization (CMP). MRS Bull, 2002. 27: p. 752.

176. Tsai, T., Y. Wu, and S. Yen, A study of copper chemical mechanical polishing in urea-hydrogen peroxide slurry by electrochemical impedance spectroscopy. Applied Surface Science, 2003. 214(1-4): p. 120-135.

177. Jairath, R., et al. Consumables for the chemical mechanical polishing (CMP) of dielectrics and conductors. 1994: Materials Research Society.

178. Xie, Y. and B. Bhushan, Effects of particle size, polishing pad and contact pressure in free abrasive polishing. Wear, 1996. 200(1-2): p. 281-295.

179. Bielmann, M., U. Mahajan, and R. Singh, *Effect of particle size during tungsten chemical mechanical polishing.* Electrochemical and solid-state letters, 1999. 2: p. 401.

180. Cook, L., *Chemical processes in glass polishing.* Journal of Non-Crystalline Solids, 1990. 120(1-3): p. 152-171.

181. Mahajan, U., S. Lee, and R. Singh. Effect of slurry abrasive size on polish rate and surface quality of silicon dioxide films. 2000: The Electrochemical Society.

182. Basim, G. and B. Moudgil, *Effect of soft agglomerates on CMP slurry performance.* Journal of Colloid and Interface Science, 2002. 256(1): p. 137-142.

183. Basim, G. and B. Moudgil, Slurry design for chemical mechanical polishing, KONA Power Technol. Jpn, 2003. 21: p. 178.

184. Choi, W., et al., *Effect of slurry ionic salts at dielectric silica CMP.* Journal of the Electrochemical Society, 2004. 151: p. G185.

185. Zhang, F., A. Busnaina, and G. Ahmadi, *Particle adhesion and removal in chemical mechanical polishing (CMP) and post-CMP cleaning.* Journal of Electrochemical Society, 1999. 146(7).

186. Coutinho, C., et al., *Novel ceria-polymer microcomposites for chemical mechanical polishing.* Applied Surface Science, 2008. 255(5): p. 3090-3096.

187. Coutinho, C. and V. Gupta, Formation and properties of composites based on microgels of a responsive polymer and TiO2 nanoparticles. Journal of Colloid and Interface Science, 2007. 315(1): p. 116-122.

188. Coutinho, C., Multi-Functional Composite Materials for Catalysis and Chemical Mechanical Planarization in Chemical and Biomedical Engineering. 2009, University of South Florida: Tampa.

189. Volinsky, A., et al. *Microstructure and mechanical properties of electroplated Cu thin films*. 2001: Warrendale, Pa.; Materials Research Society; 1999.

190. Hall, E., *The deformation and ageing of mild steel: III discussion of results.* Proceedings of the Physical Society. Section B, 1951. 64: p. 747.

191. Petch, N., *The cleavage strength of polycrystals.* J. Iron Steel Inst, 1953. 174(1): p. 25–28.

192. Carney, C. and D. Durham, Optimization of hardness by the control of microwave power in TiN thin film deposited by electron cyclotron resonance assisted sputtering in a nitrogen plasma. Journal of Vacuum Science & Technology A: Vacuum, Surfaces, and Films, 1999. 17: p. 2535.

193. Carney, C. and D. Durham, Establishing the relationship between process, structure, and properties on titanium nitride films deposited by electron cyclotron resonance assisted reactive sputtering. II. A process model. Journal of Vacuum Science & Technology A: Vacuum, Surfaces, and Films, 1999. 17: p. 2859.

194. Kim, S. and D. Durham, *Microscopic studies of flank wear on alumina tools.* Journal of Tribology, 1991. 113: p. 204.

195. Gane, N., *The direct measurement of the strength of metals on a sub-micrometre scale.* Proceedings of the Royal Society of London. Series A, Mathematical and Physical Sciences, 1970. 317(1530): p. 367-391.

196. Albrecht, M., et al., *Magnetic coercivity patterns for magnetic recording on patterned media.* Applied Physics Letters, 2003. 83(21): p. 4363-4365.

APPENDIX A: PHASE I MACHINE PARAMETERS

A.1 Machine Parameters WYKO Images

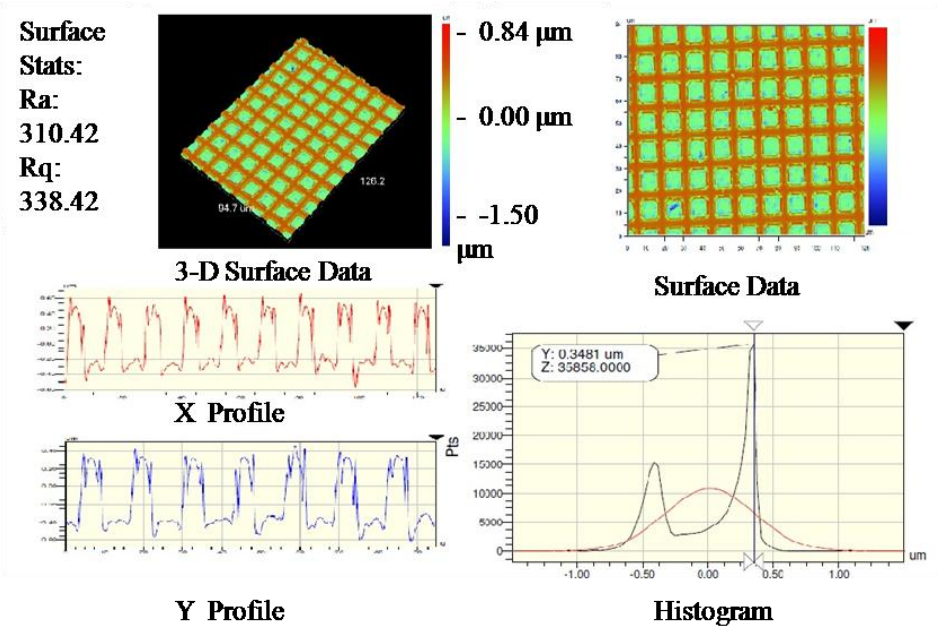

Figure A. 1 1 Psi 0.2 relative velocity

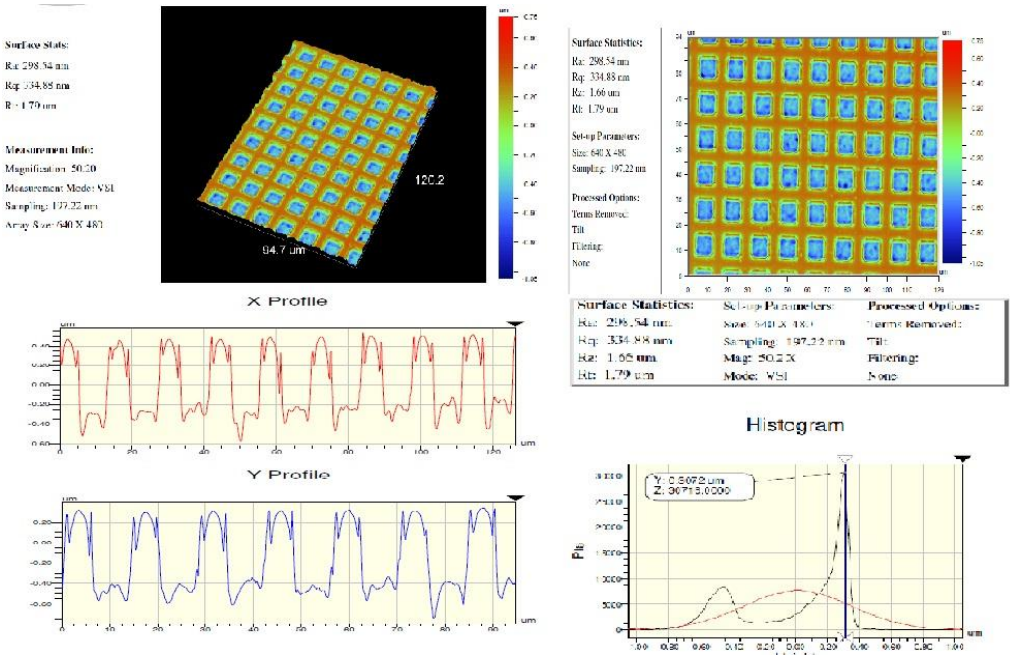

Figure A. 2 1 Psi 0.8 relative velocity

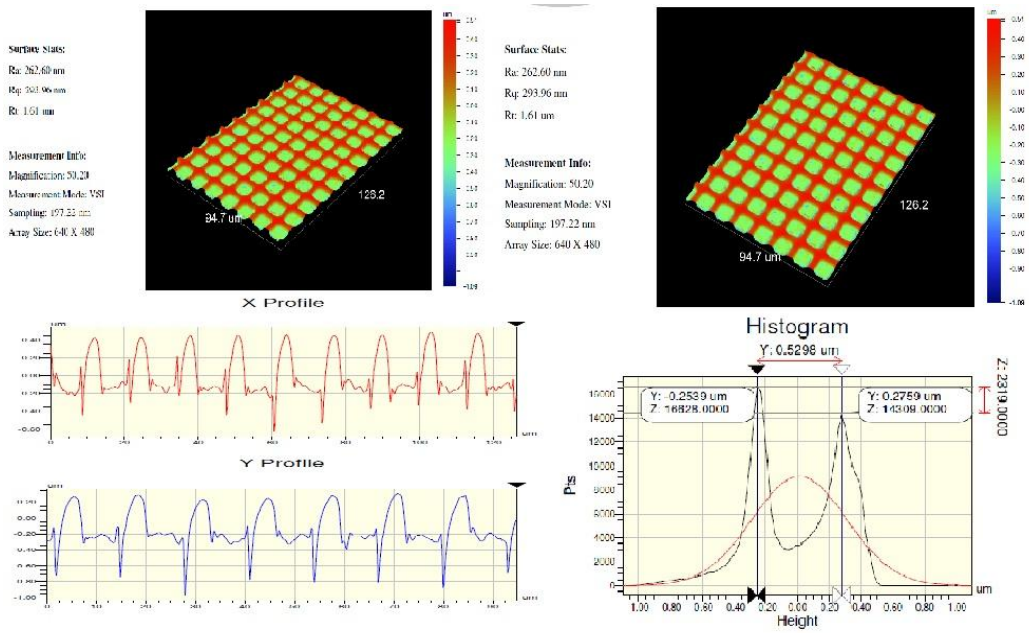

Figure A. 3 1 Psi 1.2 relative velocity

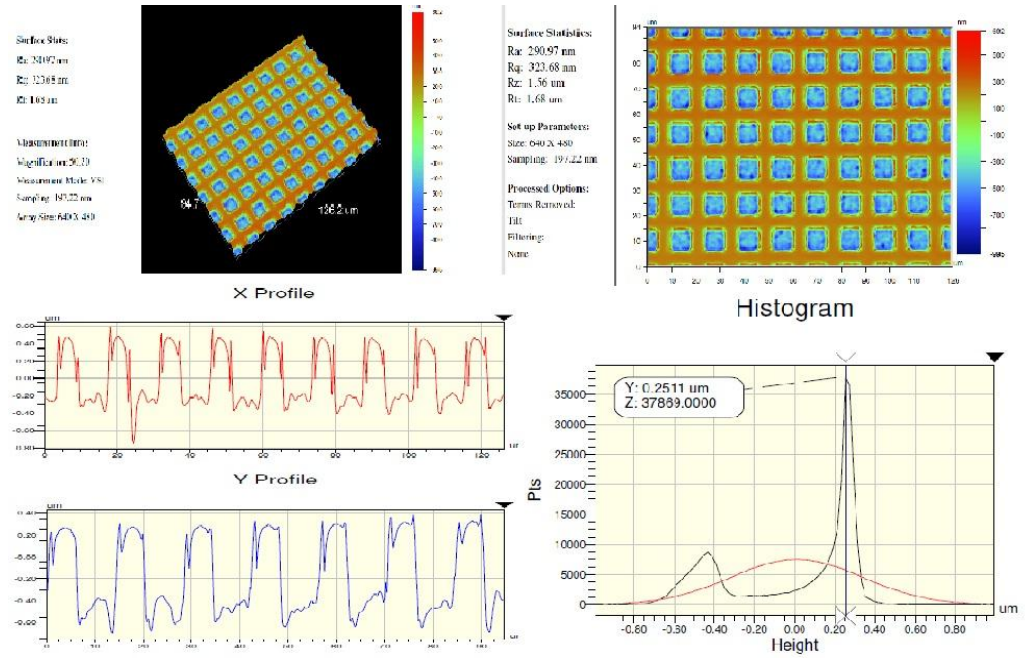

Figure A. 4 3 Psi 0.2 relative velocity

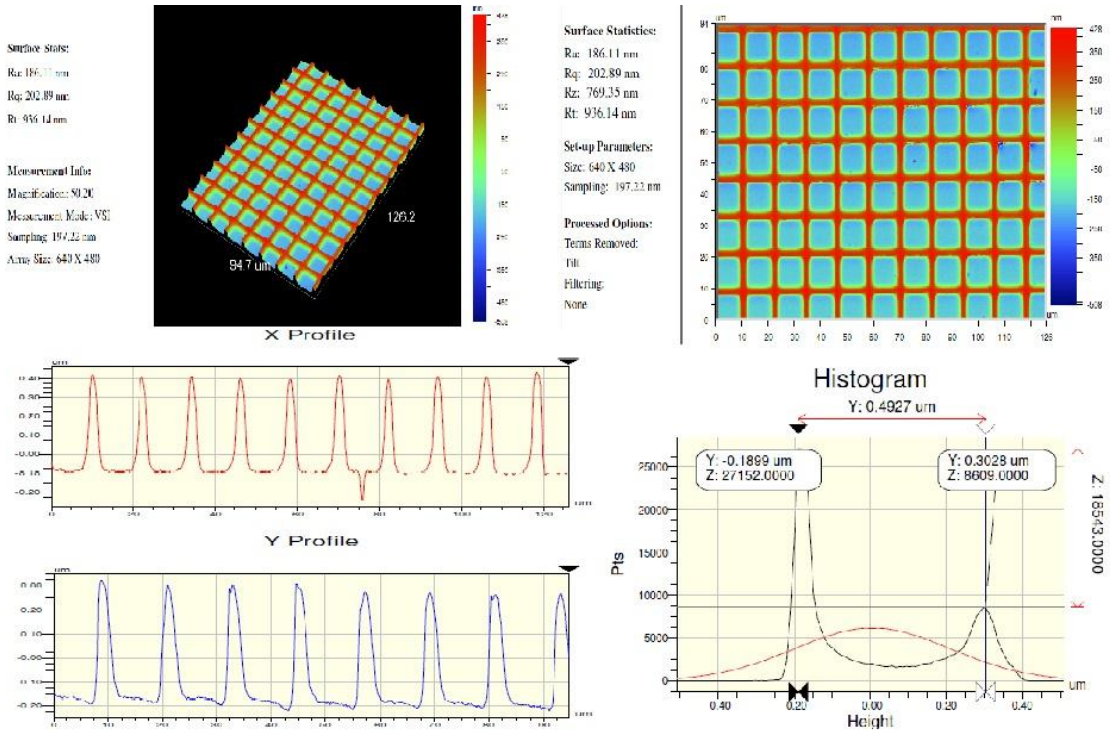

Figure A. 5 3 Psi 0.8 relative velocity

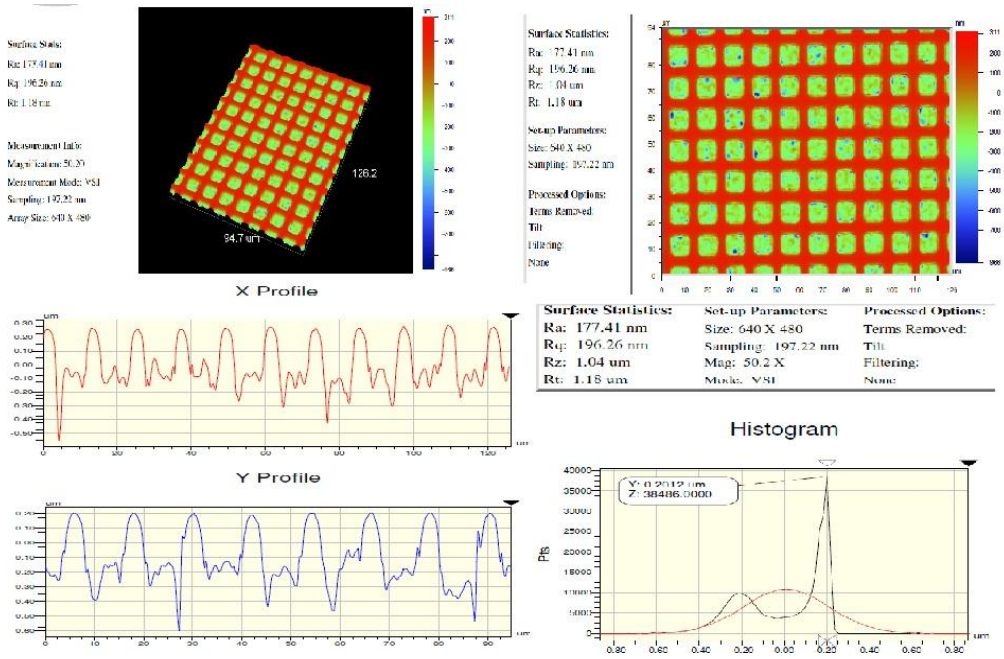

Figure A. 6 3 Psi 1.2 relative velocity

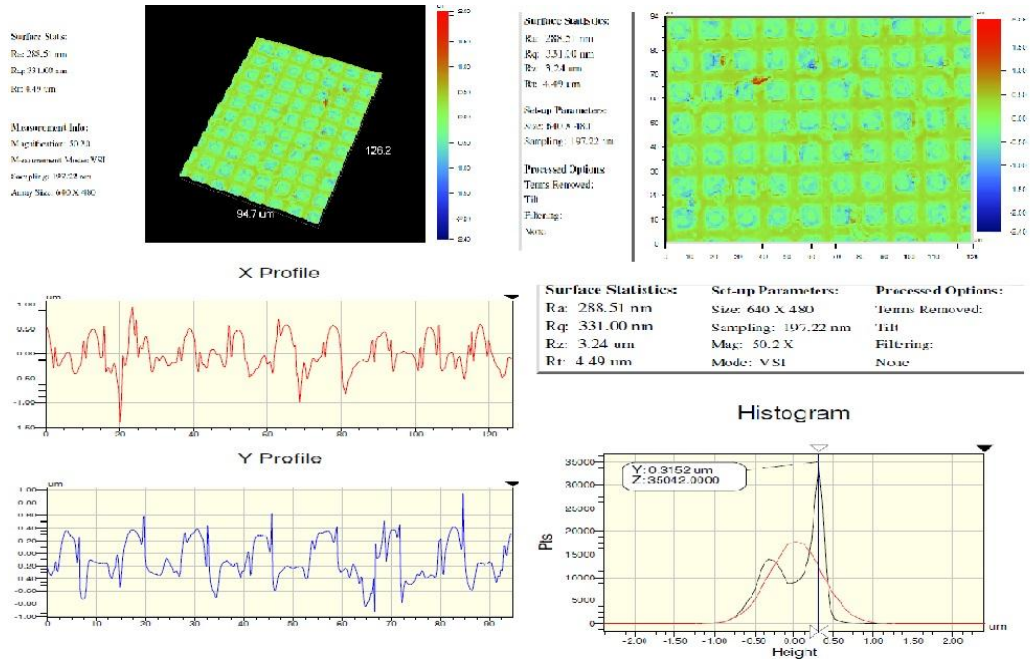

Figure A. 7 6 Psi 0.2 relative velocity

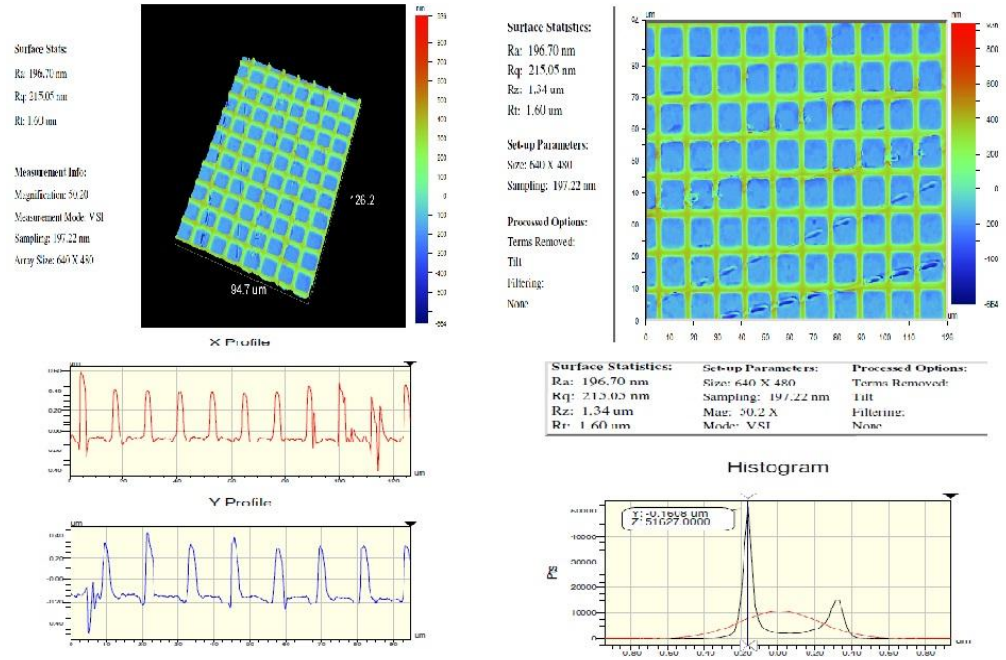

Figure A. 8 6 Psi 0.8 relative velocity

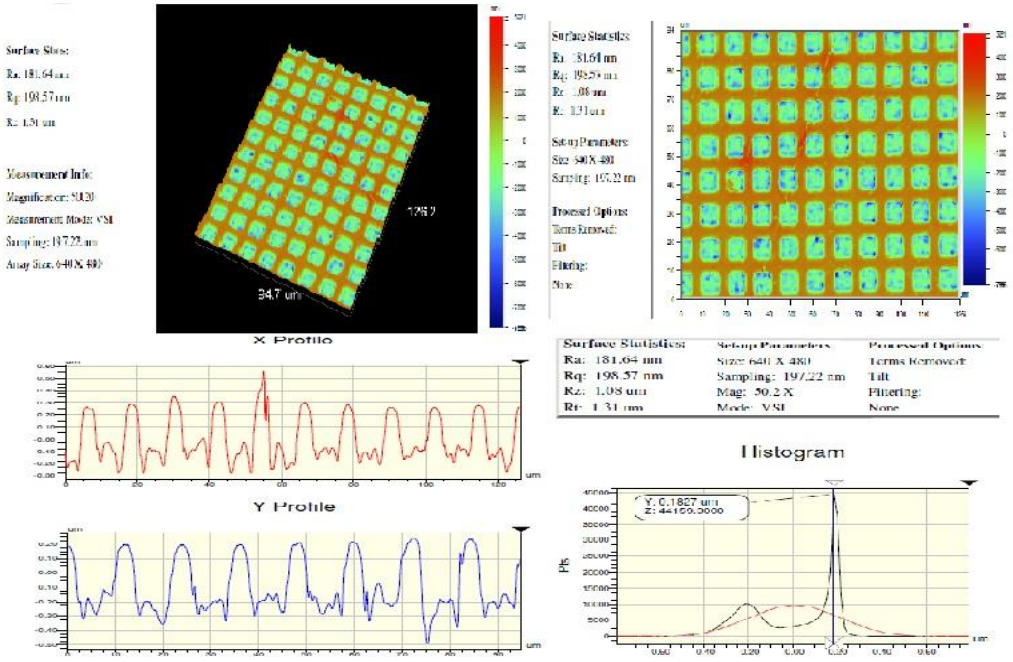

Figure A. 9 6 Psi 1.2 relative velocity

A.2 COF Versus MRR

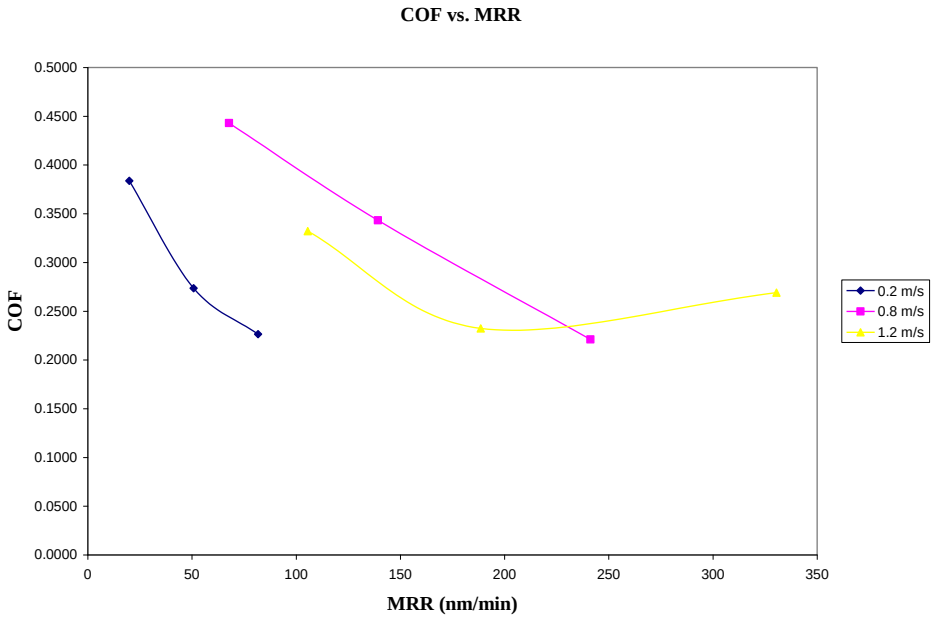

Figure A. 10 COF vs. MRR for BPM

A.3 SEM Characterization of BPM Surfaces

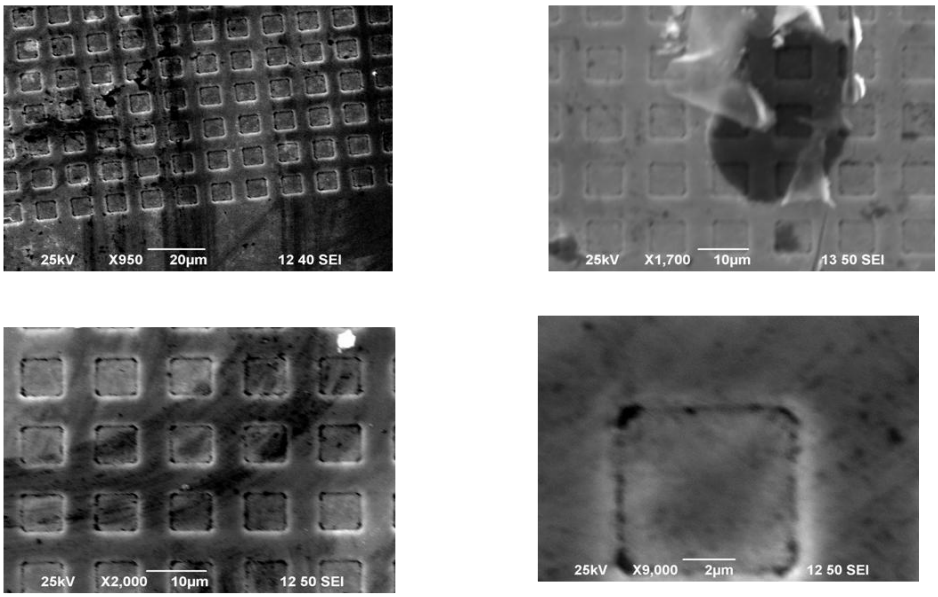

Figure A. 11 SEM of BPM delamination at 6 Psi

APPENDIX B: PHASE II: PAD CHARACTERIZATION DATA

B.1 Pad Roughness Evolution

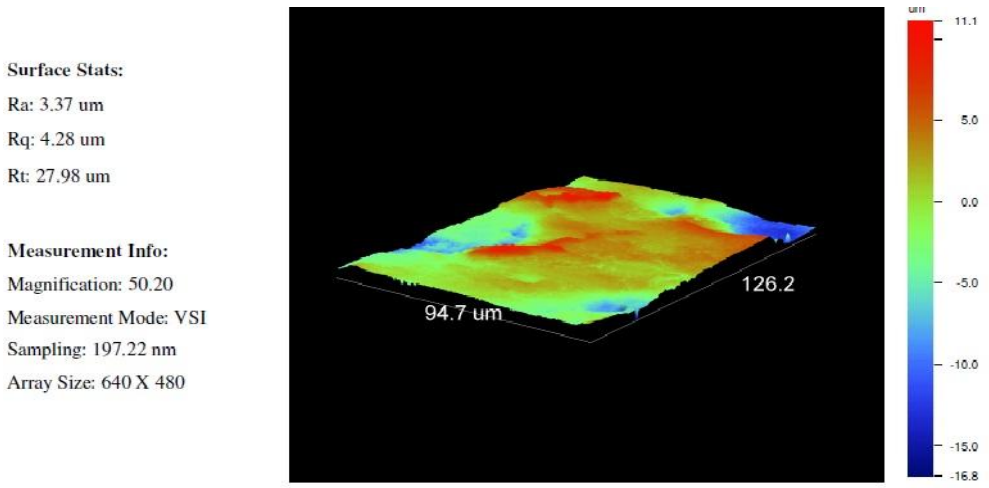

Figure B. 1 Pad 1 (10 polishes)

Surface Stats:
Ra: 4.73 um
Rq: 6.17 um
Rt: 29.44 um

Measurement Info:
Magnification: 50.20
Measurement Mode: VSI
Sampling: 197.22 nm
Array Size: 640 X 480

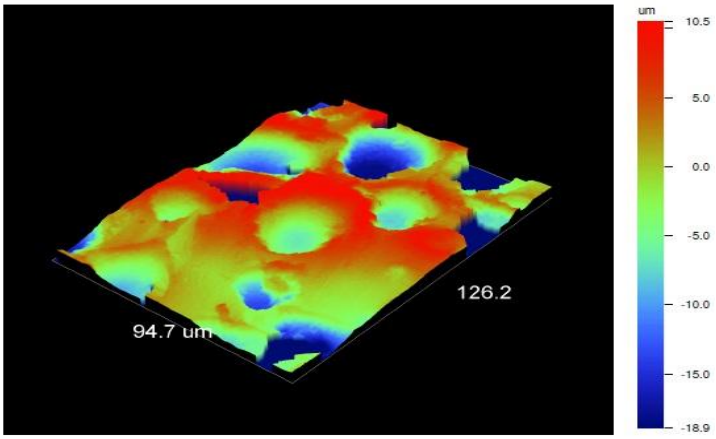

Figure B. 2 Pad 1 (20 polishes)

Surface Stats:
Ra: 4.99 um
Rq: 6.10 um
Rt: 33.92 um

Measurement Info:
Magnification: 50.20
Measurement Mode: VSI
Sampling: 197.22 nm
Array Size: 640 X 480

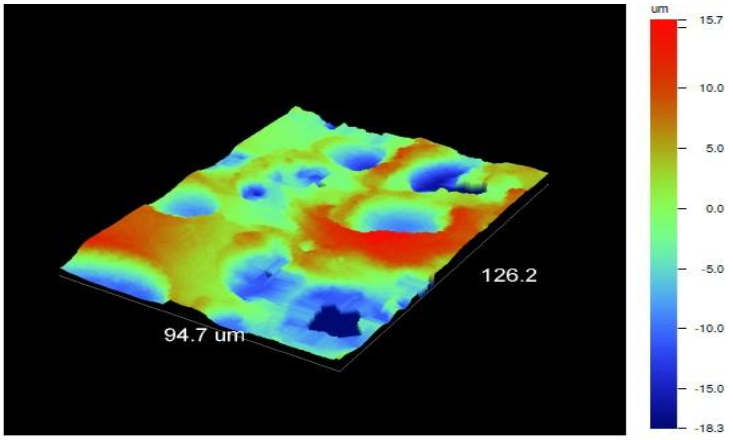

Figure B. 3 Pad 1 (30 polishes)

Surface Stats:
Ra: 3.54 um
Rq: 4.43 um
Rt: 21.15 um

Measurement Info:
Magnification: 50.20
Measurement Mode: VSI
Sampling: 197.22 nm
Array Size: 640 X 480

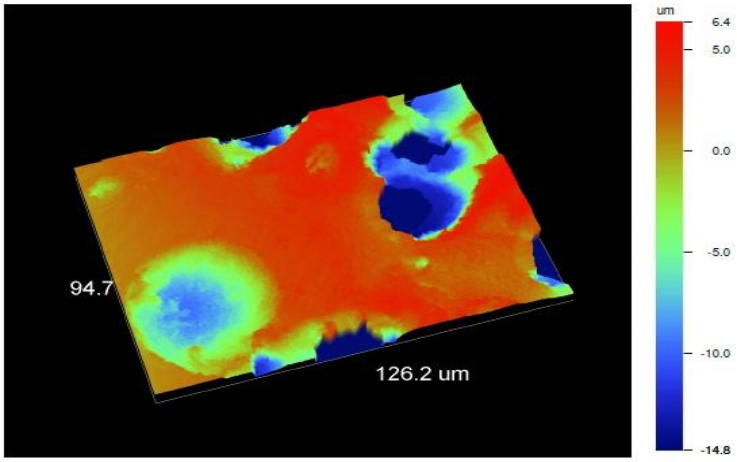

Figure B. 4 Pad 1 (40 polishes)

Surface Stats:
Ra: 4.05 um
Rq: 5.53 um
Rt: 26.09 um

Measurement Info:
Magnification: 50.20
Measurement Mode: VSI
Sampling: 197.22 nm
Array Size: 640 X 480

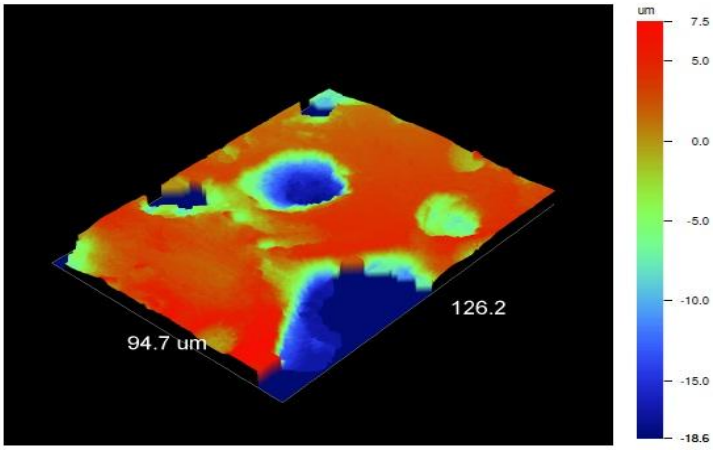

Figure B. 5 Pad 1 (50 polishes)

Surface Stats:

Ra: 4.44 um

Rq: 5.70 um

Rt: 32.04 um

Measurement Info:

Magnification: 50.20

Measurement Mode: VSI

Sampling: 197.22 nm

Array Size: 640 X 480

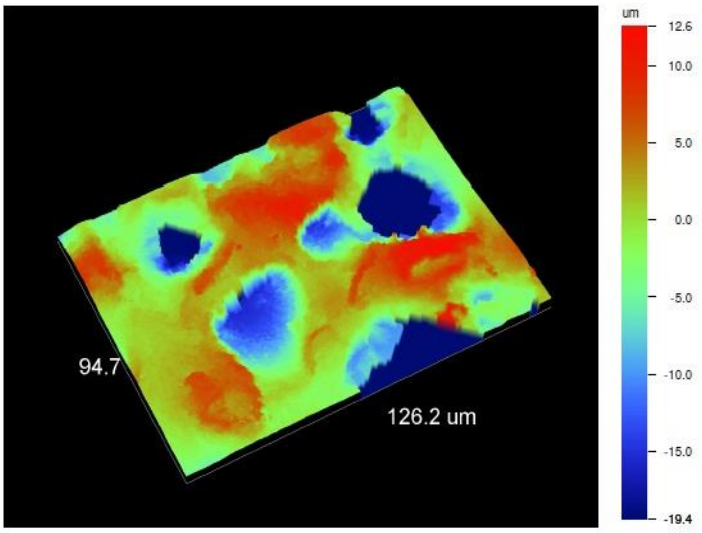

Figure B. 6 Pad 2 (10 polishes)

Surface Stats:

Ra: 5.34 um

Rq: 6.78 um

Rt: 40.00 um

Measurement Info:

Magnification: 50.20

Measurement Mode: VSI

Sampling: 197.22 nm

Array Size: 640 X 480

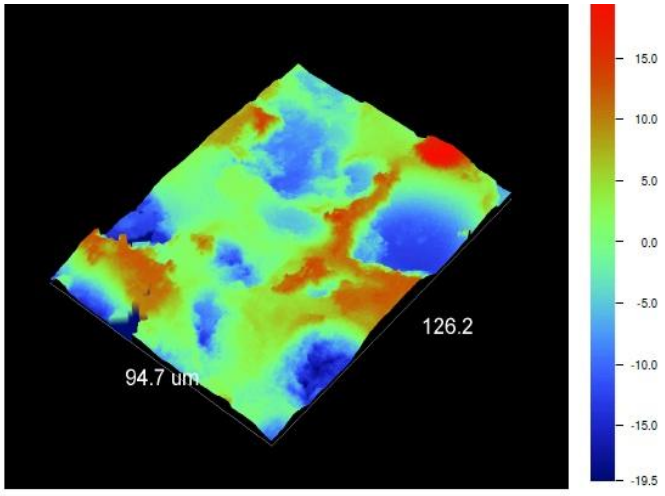

Figure B. 7 Pad 2 (20 polishes)

Surface Stats:

Ra: 5.56 um

Rq: 6.81 um

Rt: 37.10 um

Measurement Info:

Magnification: 50.20

Measurement Mode: VSI

Sampling: 197.22 nm

Array Size: 640 X 480

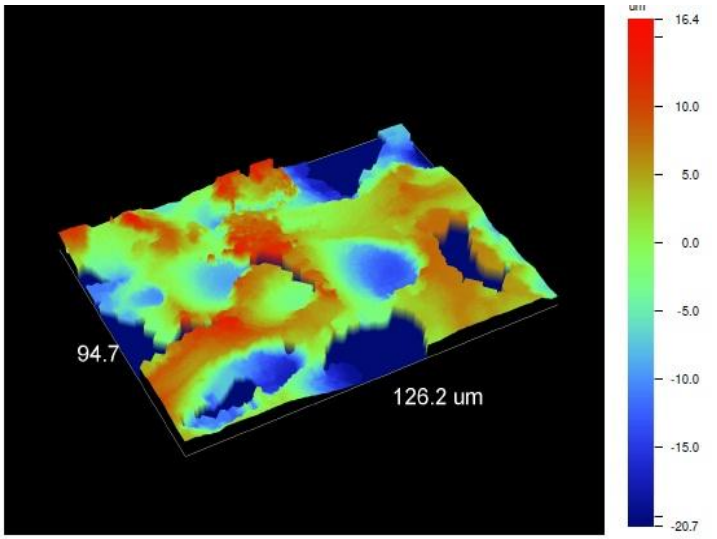

Figure B. 8 Pad 2 (30 polishes)

Surface Stats:

Ra: 6.57 um

Rq: 7.97 um

Rt: 31.22 um

Measurement Info:

Magnification: 50.20

Measurement Mode: VSI

Sampling: 197.22 nm

Array Size: 640 X 480

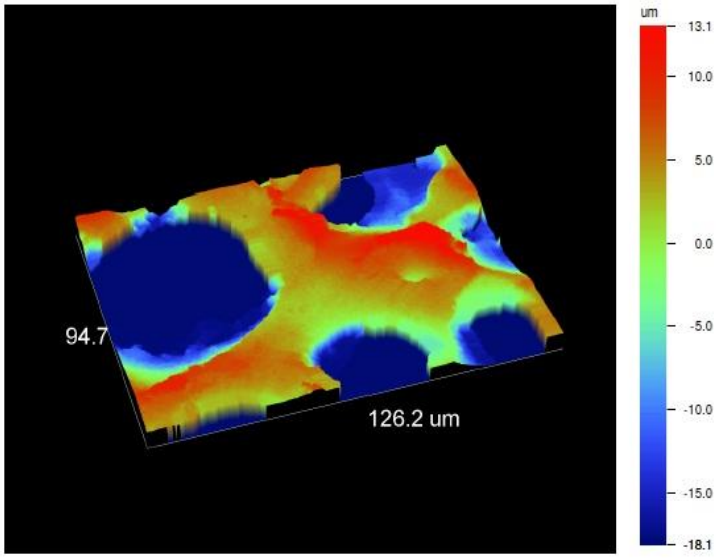

Figure B. 9 Pad 2 (40 polishes)

Surface Stats:

Ra: 6.89 um

Rq: 8.29 um

Rt: 36.26 um

Measurement Info:

Magnification: 50.20

Measurement Mode: VSI

Sampling: 197.22 nm

Array Size: 640 X 480

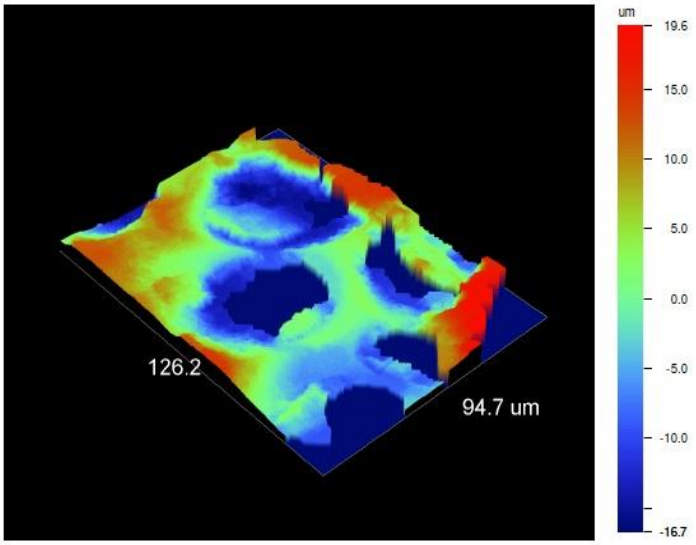

Figure B. 10 Pad 2 (50 polishes)

Surface Stats:

Ra: 5.14 um

Rq: 6.04 um

Rt: 37.42 um

Measurement Info:

Magnification: 50.20

Measurement Mode: VSI

Sampling: 197.22 nm

Array Size: 640 X 480

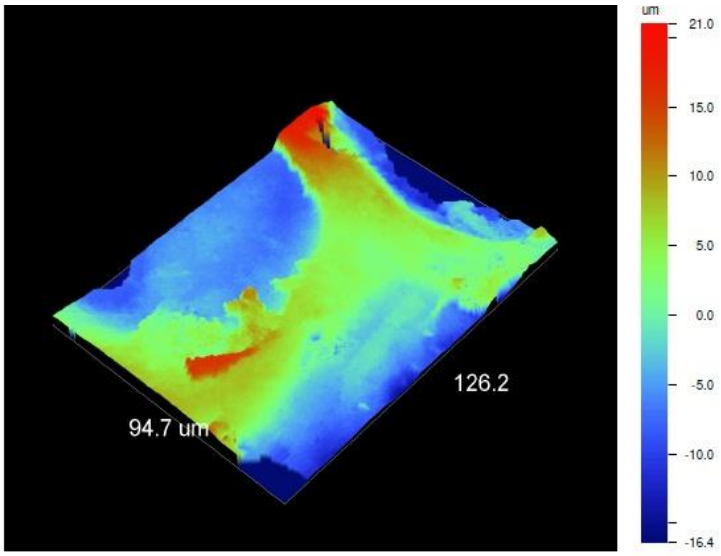

Figure B. 11 Pad 3 (10 polishes)

Surface Stats:

Ra: 5.62 um

Rq: 6.95 um

Rt: 40.50 um

Measurement Info:

Magnification: 50.20

Measurement Mode: VSI

Sampling: 197.22 nm

Array Size: 640 X 480

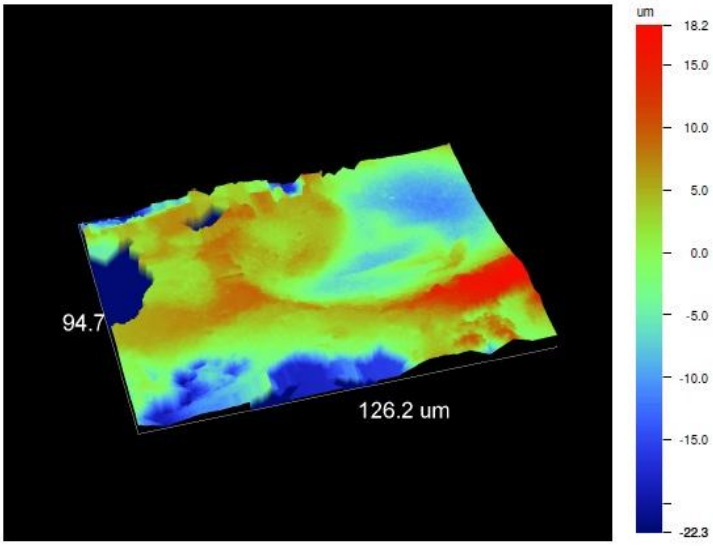

Figure B. 12 Pad 3 (20 polishes)

Surface Stats:

Ra: 6.82 um

Rq: 8.31 um

Rt: 33.53 um

Measurement Info:

Magnification: 50.20

Measurement Mode: VSI

Sampling: 197.22 nm

Array Size: 640 X 480

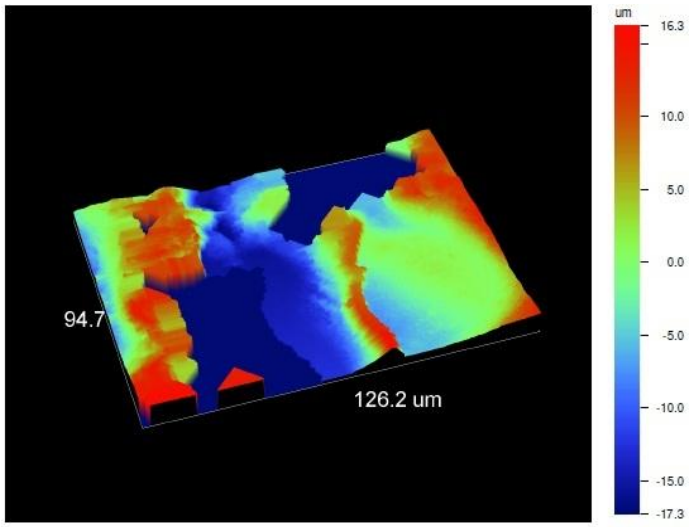

Figure B. 13 Pad 3 (30 polishes)

Surface Stats:

Ra: 6.82 um

Rq: 8.31 um

Rt: 33.53 um

Measurement Info:

Magnification: 50.20

Measurement Mode: VSI

Sampling: 197.22 nm

Array Size: 640 X 480

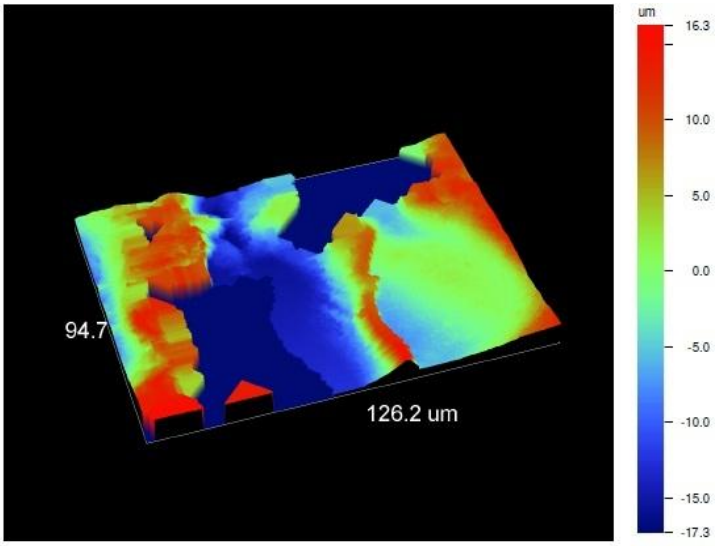

Figure B. 14 Pad 3 (40 polishes)

Surface Stats:

Ra: 3.89 um

Rq: 4.61 um

Rt: 21.84 um

Measurement Info:

Magnification: 50.20

Measurement Mode: VSI

Sampling: 197.22 nm

Array Size: 640 X 480

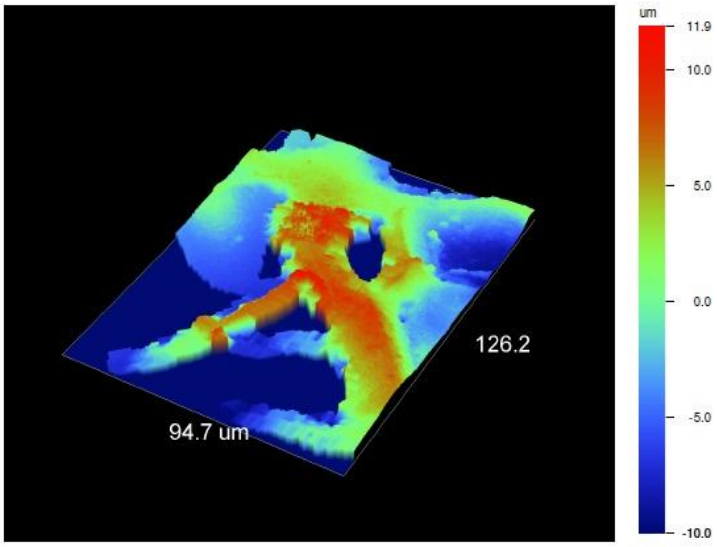

Figure B. 15 Pad 3 (50 polishes)

B.2 SEM Pad Characterization

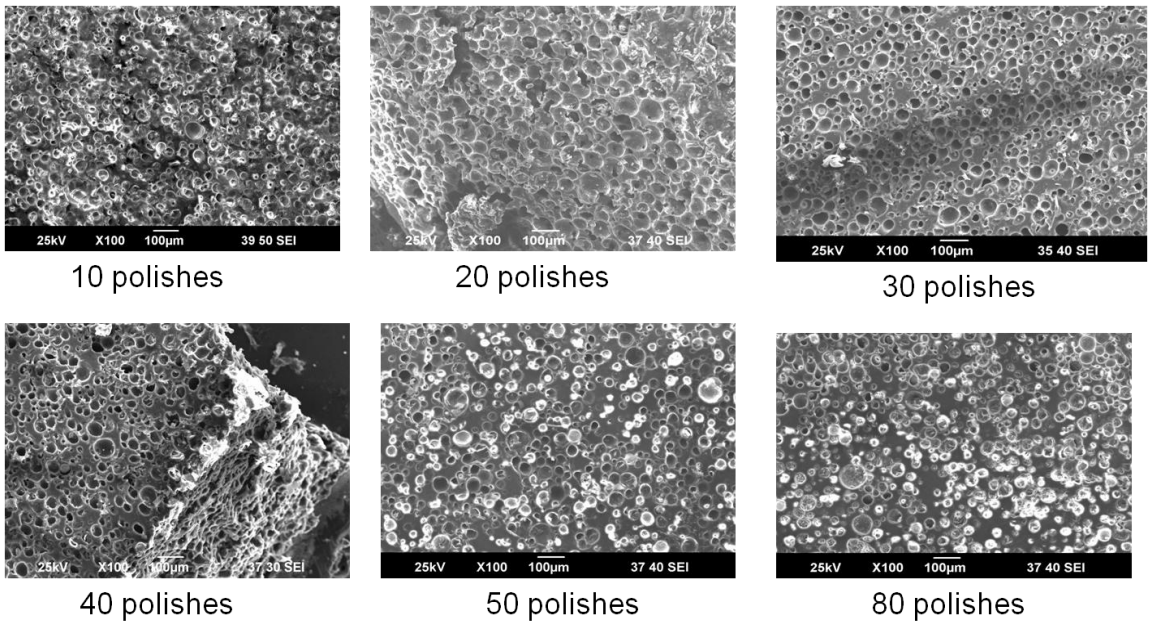

Figure B. 16 SEM morphology evolution

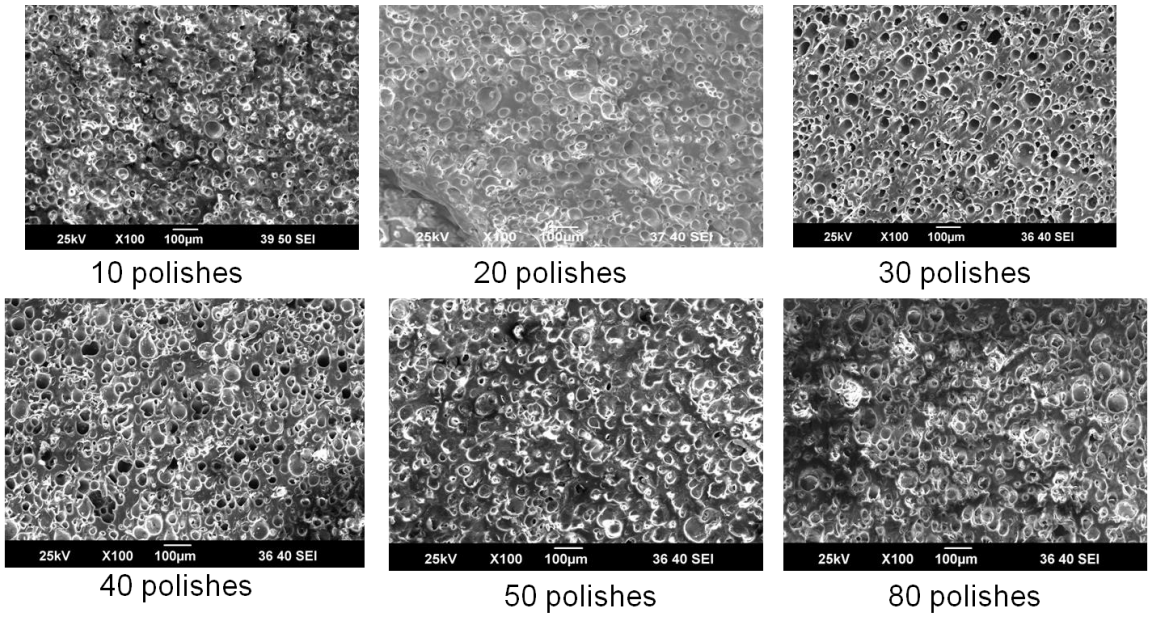

Figure B. 17 Pad (2) SEM morphology evolution

APPENDIX B (CONT)

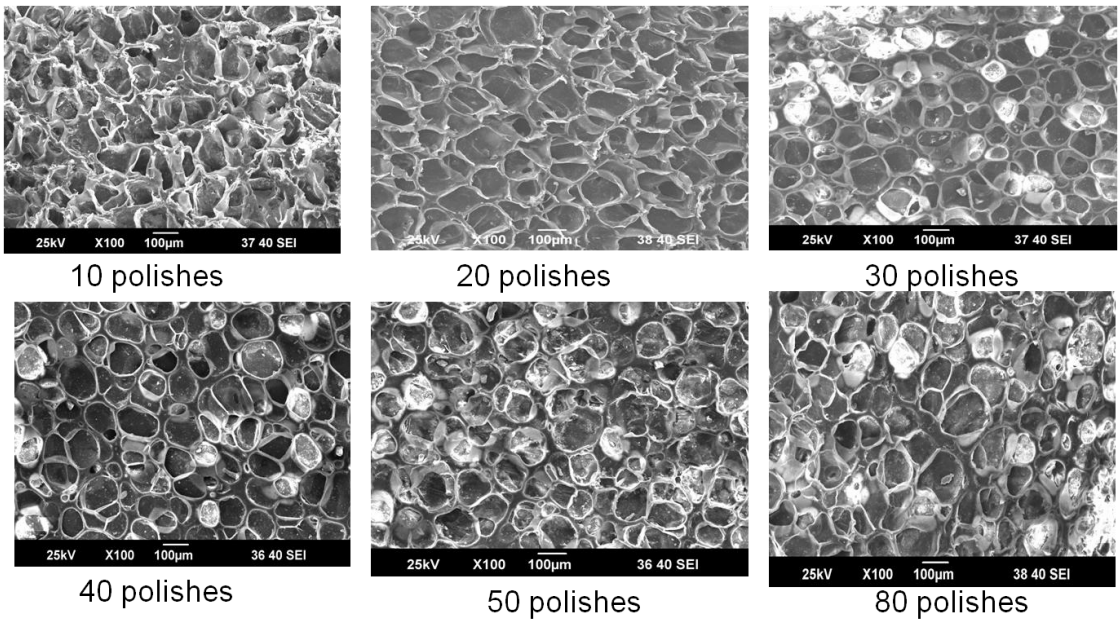

Figure B. 18 Pad (3) SEM morphology evolution

APPENDIX B (CONT)

B.3 UTS Characterization

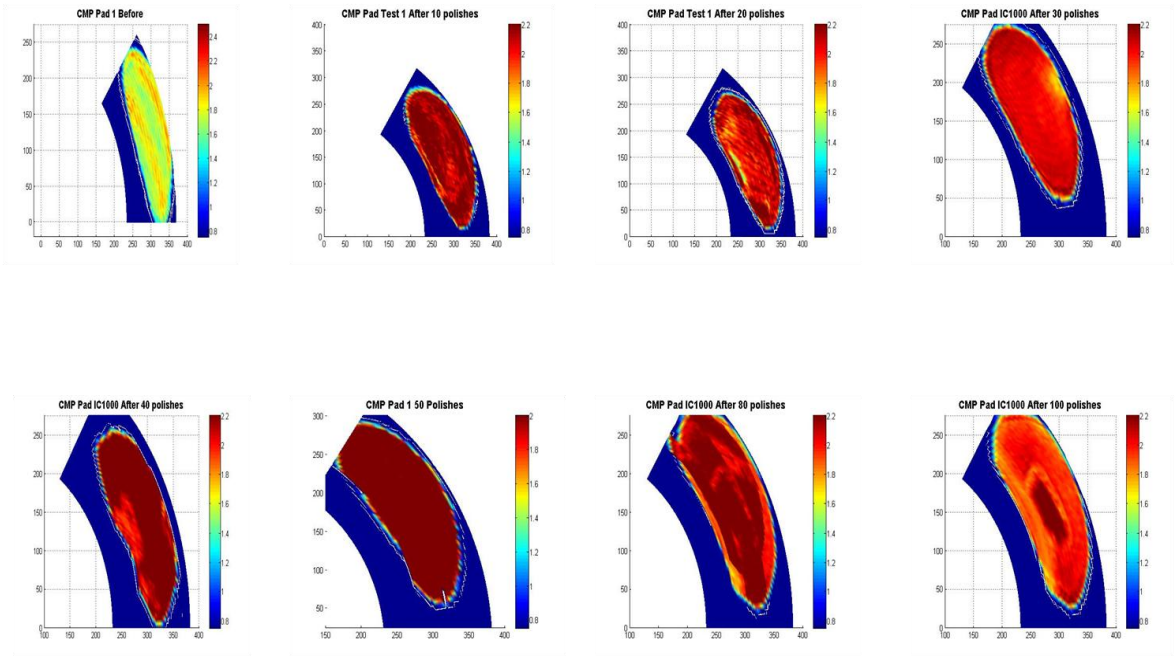

Figure B. 19 Pad (1) UTS characterization

APPENDIX B (CONT)

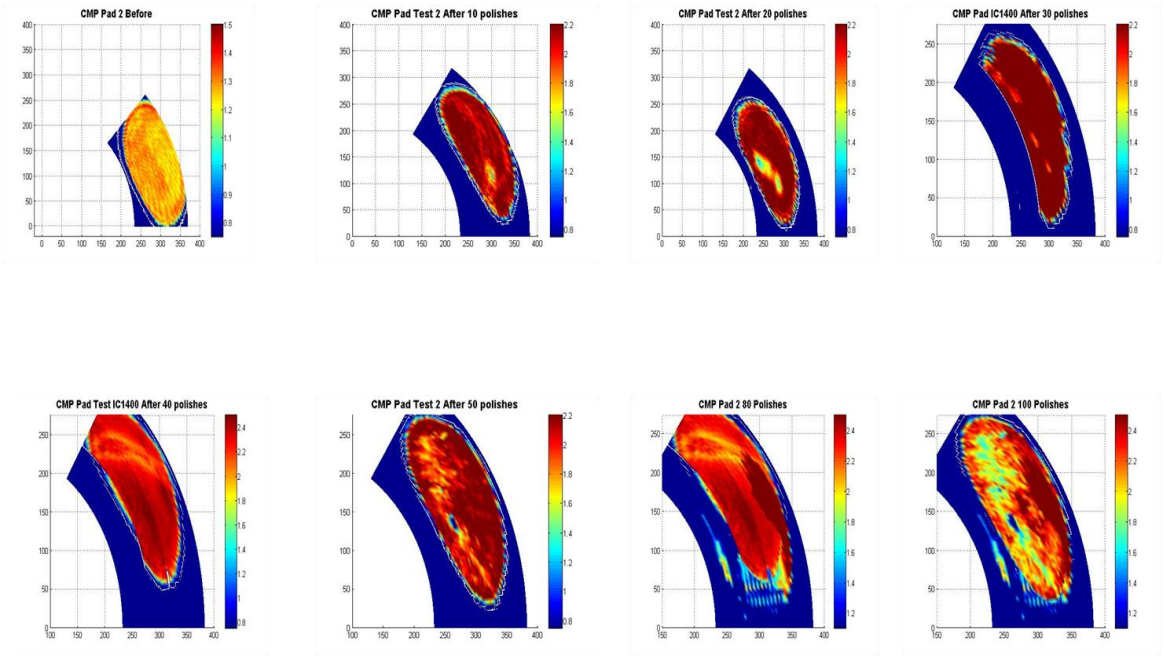

Figure B. 20 Pad (2) UTS characterization

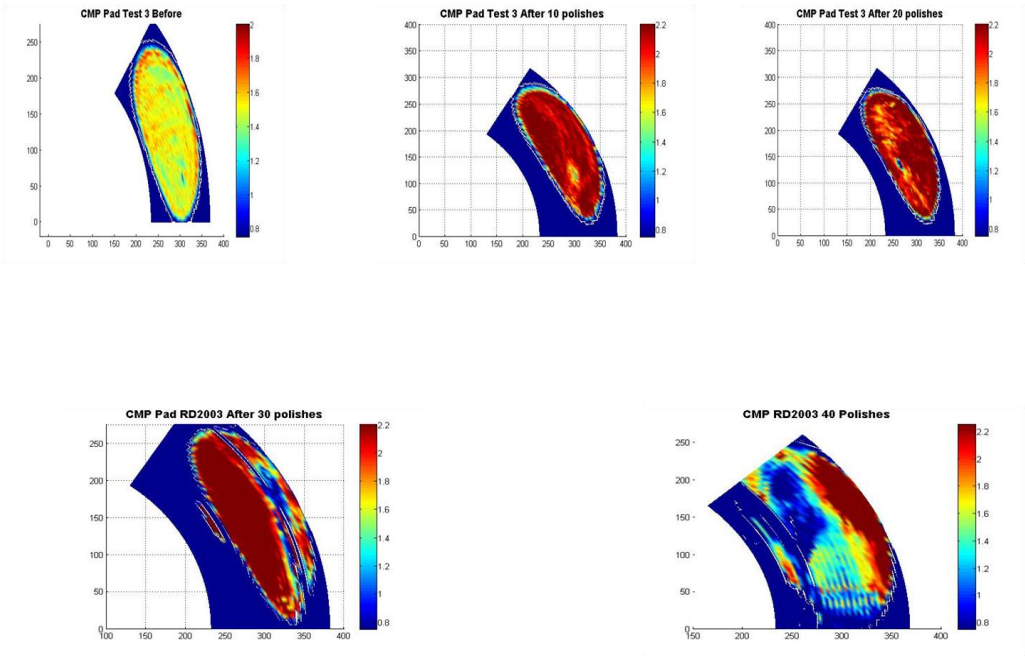

Figure B. 21 Pad (3) UST characterization

B.4 Pad Characterization Results

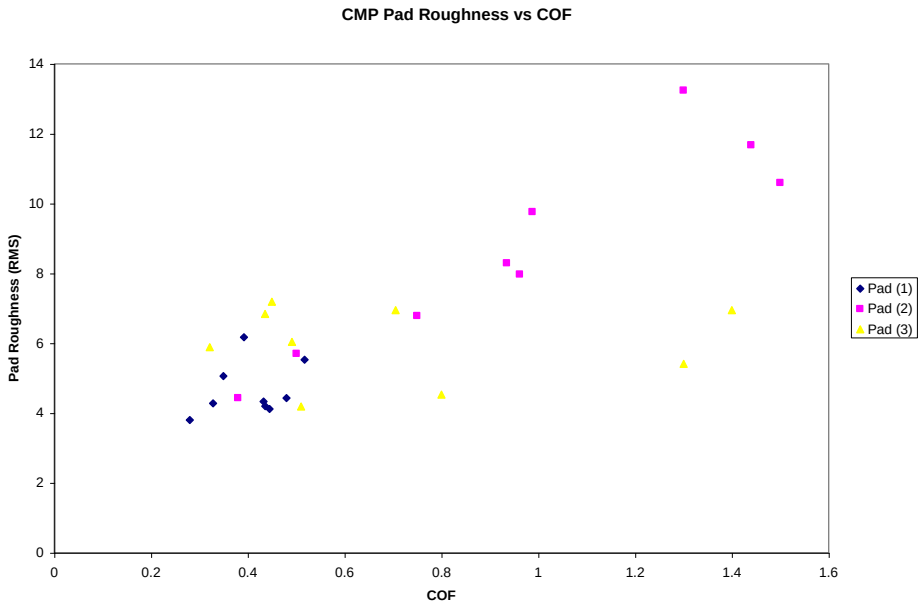

Figure B. 22 CMP pad roughness vs.COF

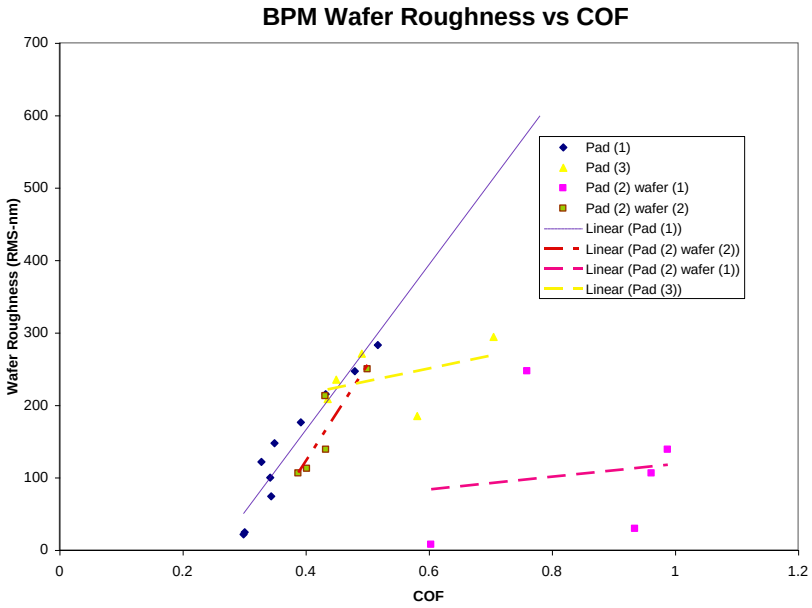

Figure B. 23 BPM wafer roughness vs. COF

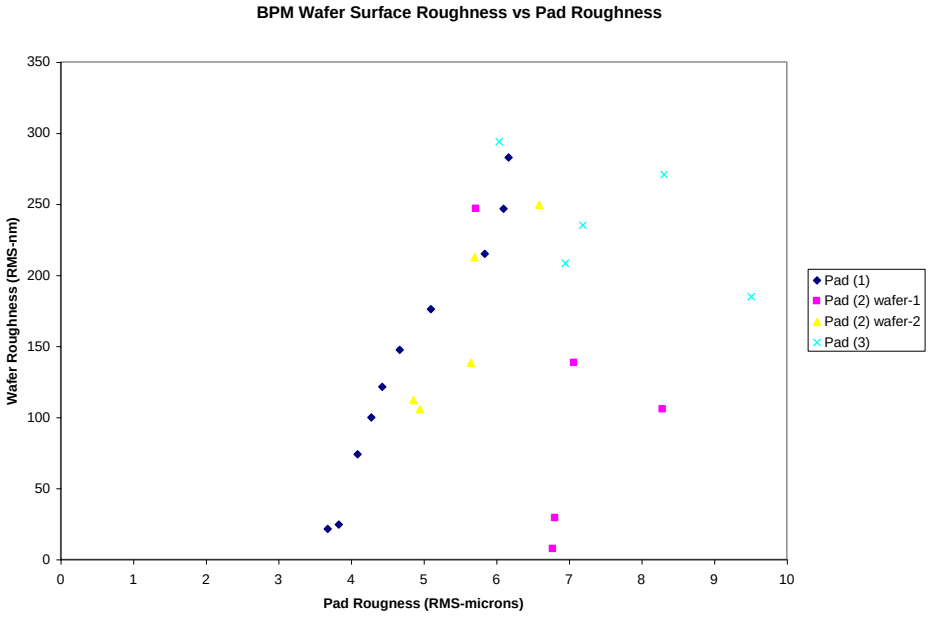

Figure B. 24 Wafer roughness vs. pad roughness

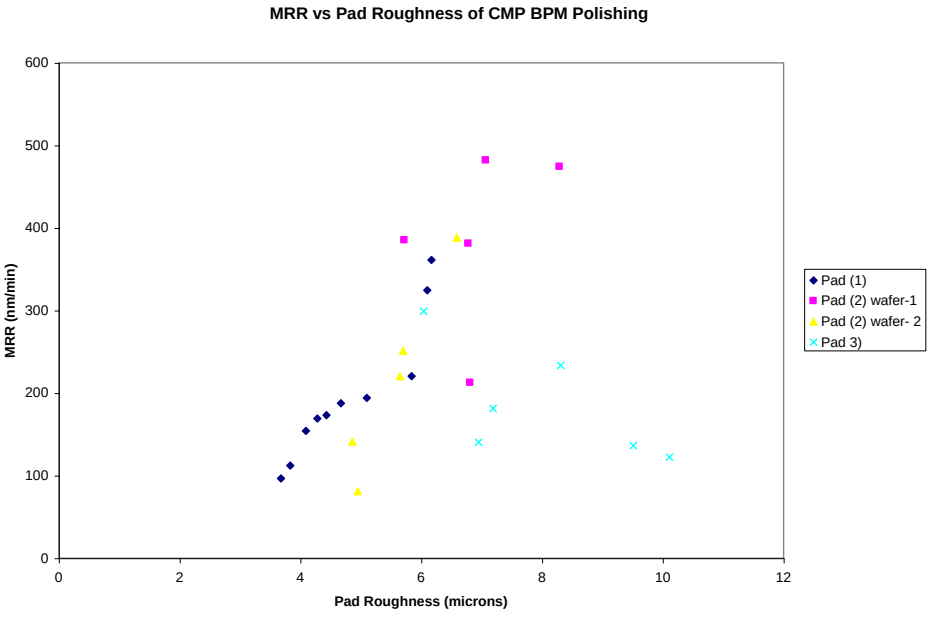

Figure B. 25 MRR vs. pad roughness

ABOUT THE AUTHOR

Joe completed his bachelors at University of South Carolina (USC) in mechanical engineering and he completed his Masters at USC in biomechanical engineering. Following USC, he switched his research interest and went to Carnegie Mellon University (CMU) to study CMP from a materials science aspect. At CMU he was a fellow of the material research and science engineering center (MRSEC). He obtained his 2nd Masters from Carnegie Mellon University (CMU) in 2008. He then joined Dr. Ashok Kumar's lab at the University of South Florida to conduct research on CMP and magnetic storage devices. He has received numerous awards and grants to travel to China and Brazil to present his research on CMP while publishing 2 journal papers with another 3 papers submitted at this time. He will accept a position in the department of defense upon graduation and looks to return to academia after gaining industry experience.